MODULATION OF CALCIUM ENTRY MECHANISMS AS A POTENTIAL THERAPY FOR ACUTE PANCREATITIS

Thesis submitted in accordance with the requirements of Cardiff University

for the degree of Doctor of Philosophy

Eloise Stapleton

September, 2016

DECLARATION

This work has not been submitted in substance for any other degree or award at this or any other university or place of learning, nor is being submitted concurrently in candidature for any degree or other award.

STATEMENT 1

This thesis is being submitted in partial fulfillment of the requirements for the degree of PhD

STATEMENT 2

This thesis is the result of my own independent work/investigation, except where otherwise stated, and the thesis has not been edited by a third party beyond what is permitted by Cardiff University's Policy on the Use of Third Party Editors by Research Degree Students. Other sources are acknowledged by explicit references. The views expressed are my own.

STATEMENT 3

I hereby give consent for my thesis, if accepted, to be available online in the University's Open Access repository and for inter-library loan, and for the title and summary to be made available to outside organisations.

STATEMENT 4: PREVIOUSLY APPROVED BAR ON ACCESS

I hereby give consent for my thesis, if accepted, to be available online in the University's Open Access repository and for inter-library loans **after expiry of a bar on access previously approved by the Academic Standards & Quality Committee**.

Summary

Acute pancreatitis is a human disease in which cytosolic Ca^{2+} overload and mitochondrial dysfunction have been implicated as the initial triggers. Sustained elevations in cytosolic Ca^{2+} result in intracellular activation of digestive enzymes, mitochondrial dysfunction and cellular necrosis. This leads to autodigestion of the pancreas and subsequent inflammation, which can prove fatal. Intracellular Ca^{2+} release from stores is coupled to the activation of store-operated Ca^{2+} entry (SOCE) channels such as the Ca^{2+} release activated Ca^{2+} (CRAC) channel or the canonical transient receptor potential (TRPC) 3 channels in the plasma membrane. These channels drive cytosolic Ca^{2+} overload. Targeting these channels is an appealing therapeutic strategy. One of aim of this study was to determine if there are any inhibitors, in addition to GSK-7975A, that can specifically block these channels and prevent cytosolic Ca^{2+} overload.

Analogues of 2-APB, a well know but problematic inhibitor of SOCE channels, DPB163-AE and DPB162-AE were found to inhibit SOCE channels efficiently at a low micromolar concentration. This was similar to the effect seen with the inhibitor GSK-7975A. However, increasing concentrations of DPB163 resulted in impaired clearance of Ca^{2+} from the cytosol, whereas DPB162 inhibited SOCE further. RO2959, another reported CRAC channel inhibitor, was found to be less effective at inhibiting SOCE in pancreatic acinar cells than in other cell types. This phenomenon was true for the DPB compounds. RO2959 was effective at inhibiting SOCE in dose dependent manner when applied acutely or when pre-incubated with cells. In addition, there were observed effects of RO2959 on Ca^{2+} clearance from the cytosol. This likely contributed to the observed finding that RO2959 also increased levels of necrosis, due to impaired Ca^{2+} clearance.

Targeting TRPC3 channels, the non-specific cation channels, has been difficult as it is lacking a specific inhibitor. Treatment with Pyr3, initially thought to be a specific TRPC3 inhibitor was particularly effective at inhibiting SOCE. However, during the time course of this work it came to light that TRPC3 at low micromolar concentration does not discriminate between TRPC3 and CRAC channels. Treatment with a reportedly specific inhibitor, Pyr10, resulted in a reduction in Ca^{2+} influx. However, in a similar manner to DPB163 and RO2959 there appeared to be an effect of Pyr10 on the Ca^{2+} clearance from the cell.

A second aim of this thesis was to investigate the role of calmodulin in SOCE in pancreatic acinar cells. Calmodulin is thought to regulate CRAC channels by mediating Ca^{2+}-dependent

inactivation of the channel. Inhibitors of calmodulin: calmidazolium and W-7 were used. Both inhibitors resulted in an inhibition of SOCE. However, this inhibition was not as remarkable as CRAC channel inhibition. This could have been because the calmodulin inhibitors were not directly inhibiting the Orai1 protein of the CRAC channel rather were targeting one of the channels regulating proteins - calmodulin. A cell permeable activator of calmodulin was also utilised in this study – CALP3. CALP3 had previously been shown to protect acinar cells from cytosolic Ca^{2+} overload and also to block non-specific cation channels in T cells. At the concentration found to protect against Ca^{2+} overload, no effect on SOCE was observed. Increasing the concentration resulted in significant inhibition, but it was likely due to a non-specific effect of a supramaximal concentration.

CRAC channel inhibition was the more effective as a target for reducing SOCE and subsequent Ca^{2+} overload than targeting calmodulin-regulation of CRAC channels or targeting TRPC3 channels. However, several of the "specific" inhibitors available to target this channel, including DPB163 and RO2959 had a multitude of off-target effects including a significant effect on the Ca^{2+} extrusion mechanism of pancreatic acinar cells. GSK-7975A had the fewest undesired effects and also inhibited SOCE more than any other inhibitor. It is an ideal candidate for future drug development.

When the work in this study is viewed in the context of the wider published work, the idea of focusing on CRAC channel inhibition as a potential therapeutic for acute pancreatitis is a promising future avenue.

Acknowledgements

Table of Contents

Table of Figures

Abbreviations

2-APB	2-aminoethyl diphenylborinate
ACh	Acetylcholine
ADP	Adenosine diphosphate
AM	Acetoxymethyl
ATP	Adenosine trisphosphate
BAPTA	1,2-bis(o-aminophenoxy)ethane-N,N,N',N'-tetraacetic acid
BTP2	3,5-bistrifluoromethyl pyrazole
Ca^{2+}	Calcium
CAD	CRAC activation domain
cADPR	Cyclic adenosine diphosphate ribose
CALP	Ca^{2+}-like peptide
CaM	Calmodulin
cAMP	Cyclic adenosine monophosphate
CCCP	Carbonyl cyanide m-chlorophenylhydrazone
CCK	Cholecystokinin
CHO	Chinese hamster ovary
CICR	Ca^{2+}-induced Ca^{2+} release
CPA	Cyclopiazonic acid
CRAC	Ca^{2+} release activated Ca^{2+}
CRACM	Orai1
CRACR2A	CRAC regulator 2A
CFP	Cyan fluorescent protein
DAG	Diacylglycerol
DMEM	Dulbecco's Modified Eagle's medium
DMSO	Dimethyl sulphoxide
DNA	Deoxyribonucleic acid
DPB	Diphenyl borinate
dsRNA	Double stranded ribonucleic acid
EDTA	Ethylenediaminetetraacetic acid
EF hand	Calcium binding helix-loop-helix structural domain
ER	Endoplasmic reticulum

ER/PM	Endoplasmic reticulum/plasma membrane
FAEE	Fatty acid ethyl ester
FBS	Foetal bovine serum
FRET	Förster resonance energy transfer
fS	Femtosiemens
Gd^{3+}	Gadolinium
GFP	Green fluorescent protein
GPCR	G-protein coupled receptor
GST	Glutathione S-transferase
HEK293	Human embryonic kidney 293 cells
HEPES	4-(2-Hydroxyethyl)piperazine-1-ethanesulfonic acid
I_{CRAC}	CRAC channel current
IL	Interleukin
IP_3	Inositol-3,4,5-trisphosphate
IP_3R	Inositol-3,4,5-trisphosphate receptor
K^+	Potassium
La^{3+}	Lanthanum
LED	Light emitting diode
mAChR	Muscarinic acetylcholine receptor
MCU	Mitochondrial Ca^{2+} uniporter
Mn^{2+}	Manganese
MPO	Myeloperoxidase
MPTP	Mitochondrial permeability transition pore
MW	Molecular weight
Na^+	Sodium
NAADP	Nicotinic acid adenine dinucleotide phosphate
NCX	Na^+-Ca^{2+} exchanger
NFAT	Nuclear factor of activated T cells
PBS	Phosphate buffered saline
PCR	Polymerase chain reaction
PIP_2	Phosphatidylinositol-4,5-bisphosphate
PLC	Phospholipase
PMCA	Plasma membrane Ca^{2+}-ATPase

POA	Palmitoleic acid
POAEE	Palmitoleic acid ethyl ester
R	Receptor
RBL	Rat basophilic leukaemia
RNA	Ribonucleic acid
RNAi	RNA interference
RyR	Ryanodine receptor
SCID	Severe combined immunodeficiency
SEM	Standard error of mean
SERCA	SR/ER Ca^{2+}-ATPase
siRNA	Small interrupting RNA
SMM	Small molecule microarray
SOCE	Store operated Ca^{2+} entry
SR	Sarcoplasmic reticulum
STIM1	Stromal interaction molecule 1
TAE	Tris base, acetic acid and EDTA
TG	Thapsigargin
TLC-S	Taurolithocholic acid 3-sulphate
TNF-α	Tumour necrosis factor-α
TRP	Transient receptor potential
TRPC	Transient receptor potential canonical
TRPM	Transient receptor potential melastatin
TRPML	Transient receptor potential mucolipin
TRPV	Transient receptor potential vanilloid
WT	Wild type
YFP	Yellow fluorescent protein

1 Introduction.

1.1 Calcium signalling in mammalian cells

The role of calcium (Ca^{2+}) as a signalling molecule dates back to 1882, when Sydney Ringer sought to determine the effect of different components of blood on the contraction of the ventricle (1). He found that saline solution, when used to perfuse the ventricle, induced contraction of the muscle. Ringer clarified his finding in a second paper, where he noted that the saline solution he had used was not made from distilled water, as he originally thought, but rather was made from "pipe water" or tap water; which in London at the time consisted of 38.3 parts per million of Ca^{2+} (2). When Ringer proceeded to add Ca^{2+} to his saline solution, made with distilled water, he was able to reproduce his findings from his original paper, indicating that Ca^{2+} was the key for contraction of the ventricles (2,3). This was the beginning of the discovery of the diverse role Ca^{2+} plays as an intracellular signalling molecule (3).

Ca^{2+} is a ubiquitous intracellular messenger molecule that is responsible for controlling a variety of cellular processes from fertilisation, gene transcription, neurotransmitter release, memory formation, muscular contraction to exocytosis. However, Ca^{2+} is also implicated in various pathologies such as cardiac arrhythmia (4), Alzheimer's disease (5), cancer (6) and the focus of this thesis: acute pancreatitis (7). Under resting conditions intracellular cytosolic Ca^{2+} levels are tightly regulated and remain at approximately 50 - 100 nM dependent on the cell type (8). Elevations in cytosolic Ca^{2+} levels, as a response to an external stimulus, can reach micromolar range. If these elevated levels of Ca^{2+} are sustained and not cleared from the cytosol, in a timely fashion, typically the outcome is cell death. This intracellular messenger is vital for physiology but an excess of Ca^{2+} is toxic for cells, therefore tightly regulated Ca^{2+} homeostasis is imperative for cell survival (9). Cytosolic Ca^{2+} levels are in constant flux and are an equilibrium between mechanisms that increase cytosolic Ca^{2+} concentrations and mechanisms that decrease cytosolic Ca^{2+} concentrations (10).

The Ca^{2+} required for these intracellular signals is derived from two major sources: an intracellular store or the extracellular medium. The major intracellular store is the endoplasmic reticulum (ER) or in muscle it is known as the sarcoplasmic reticulum (SR); on the membranes of both stores there are release channels that allow cells to liberate Ca^{2+} for signalling.
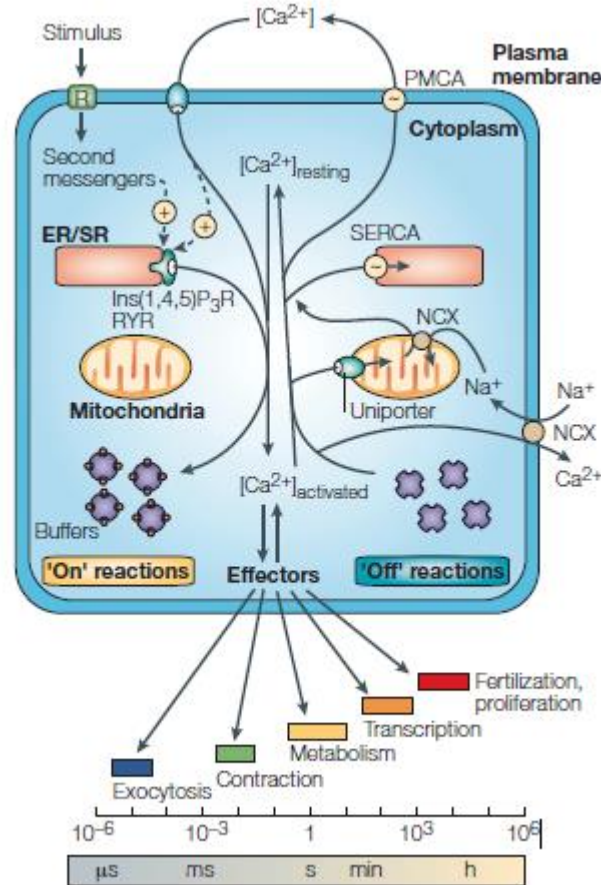
Figure 1.1 Intracellular Ca^{2+} signalling is broken down into "on" and "off" reactions

The left side of the schematic describes mechanisms by which mammalian cells increase cytosolic Ca^{2+} concentration from the stimulus of a receptor (R) at the plasma membrane, to the generation of a second messenger molecule that elicits Ca^{2+} release from intracellular stores and subsequent activation of store-operated Ca^{2+} entry. The right side of the schematic depicts the mechanisms by which mammalian cells clear Ca^{2+} from the cytoplasm, sequestration into ER stores, uptake into mitochondria and extrusion across the plasma membrane. The effector panel at the bottom of the schematic describes the physiological functions of increased cytosolic Ca^{2+} and the time scale over which these cytosolic Ca^{2+} signals persist. Schematic taken from a review (10).

There are a huge number of ways in which cells permit Ca^{2+} to cross the plasma membrane, which vary dependent on the nature of the cell in question, there are voltage-gated Ca^{2+} channels, store-operated Ca^{2+} channels, receptor-operated Ca^{2+} channels to mention but a few (10). Increases in cytosolic Ca^{2+} are therefore elicited by different mechanisms dependent on the cell type and function, there are several conserved receptors, channels and pumps across the spectrum of mammalian cells. These are detailed in the following sections, which are subdivided into: Plasma membrane receptors, plasma membrane channels, intracellular Ca^{2+} release channels and Ca^{2+} clearance mechanisms.

Generally, intracellular Ca^{2+} signals can be broken down into "on" reactions and "off" reactions as described in (10). Mechanisms that serve to increase cytosolic Ca^{2+} concentration are considered "on" reactions and mechanisms that serve to decrease cytosolic Ca^{2+} concentration are considered "off" reactions. The schematic, figure 1.1, depicts a summary of all the mechanisms by which it is possible to elevate cytosolic Ca^{2+} and remove cytosolic Ca^{2+} from the cell.

1.1.1 Plasma membrane receptors

The combination of plasma membrane receptors expressed by a cell varies depending on the cell type, for example pancreatic acinar cells are largely dependent on the activation of muscarinic acetylcholine receptors (mAChR) and cholecystokinin (CCK) receptors in order to mobilise Ca^{2+}(11), whereas cardiac myocytes express angiotensin II, endothelin and several subtypes of adrenoceptors (12). These are all examples of G-protein coupled receptors (GPCR) and they transduce their signals through different alpha subunits. Most GPCRs activate phospholipase C (PLC) and stimulate the hydrolysis of phosphatidylinositol-4,5-bisphosphate (PIP$_2$) to second messengers: diacylglycerol (DAG) and inositol-3,4,5-trisphosphate (IP$_3$). IP$_3$ is the ligand for the intracellular ER Ca^{2+} release channel the IP$_3$ receptor (IP$_3$R) (13). Other alpha subtypes of GPCRs are known to activate adenylyl cyclase, an enzyme that catalyses the conversion of adenosine trisphosphate (ATP) to the second messenger - cyclic adenosine monophosphate (cAMP).

1.1.2 Plasma membrane channels

In the extracellular medium Ca^{2+} is at a significantly higher concentration compared to in the cytosol and this maintains the potential difference across the cell membrane. Extracellular Ca^{2+} concentration is in the millimolar range (14). Generally, mammalian cells can be subdivided into electrically excitable and electrically non-excitable cells. These cells possess

different mechanisms that allow Ca^{2+} to cross the plasma membrane. In the plasma membrane of excitable cells, such as neurones and myocytes, are voltage-gated Ca^{2+} channels that upon depolarisation of the membrane by an action potential, open to allow Ca^{2+} to enter the cell, down its concentration gradient. This results in an elevation in the concentration of cytosolic Ca^{2+} which is often the stimulus for subsequent Ca^{2+} release that is described in section 1.1.3. In non-excitable cells, such as pancreatic acinar cells or more generally epithelial cells, the plasma membrane is not electrically excitable meaning that voltage-gated Ca^{2+} channels would be redundant, as there is not a change in the membrane potential to activate and open the channel. Such non-excitable cells possess store-operated Ca^{2+} channels that are activated upon the depletion of the intracellular Ca^{2+} store, the ER. There is a Ca^{2+} sensor that spans the ER membrane and detects the intra-luminal Ca^{2+} concentration, any depletion in luminal Ca^{2+} results in the activation of the closely apposed store-operated Ca^{2+} channel which opens and allows Ca^{2+} to enter the cytosol. The store-operated channels are thought to exist in both a Ca^{2+} selective form and a non-selective cation form.

1.1.3 Intracellular Ca^{2+} release channels

As previously mentioned the ER is the major intracellular Ca^{2+} store in cells, the ER luminal free Ca^{2+} concentration is in the region of $100 - 300$ μM (15). This again maintains the potential difference across the ER membrane and provides a concentration gradient for Ca^{2+} release from the ER when the channels are open. The IP_3R in the ER membrane is one such Ca^{2+} release channel, for activation of the IP_3R both its ligand IP_3 (16) and Ca^{2+} are required. Activation of the IP_3R occurs when a PLC-coupled cell surface receptor is stimulated, such as the mAChR activation by ACh, due to the production of IP_3. Once the IP_3R is activated Ca^{2+} is able to move from the ER lumen into the cytosol down the concentration gradient (17). In addition to the IP_3R the other major ER Ca^{2+} release channel is the ryanodine receptor (RyR). RyR, like IP_3R, is activated by Ca^{2+} and also by second messengers such as cyclic ADP ribose (cADPR), which is a cyclic adenine nucleotide like cAMP, and nicotinic acid adenine dinucleotide phosphate (NAADP) (18). Ca^{2+} is sufficient to activate RyR alone, as opposed to IP_3R that requires dual activation by both IP_3 and Ca^{2+}. The two-pore channels exists on the membrane of acidic Ca^{2+} stores, NAADP is the major ligand for activation of these channels and subsequent liberation of Ca^{2+}, which is thought to serve to activate RyR-mediated Ca^{2+} release through a process known as Ca^{2+} induced Ca^{2+} release (CICR) (19).

Both IP_3R and RyR have three isoforms, different cell types have differential expression of each isoform; furthermore, in some cells the major Ca^{2+} release channel is the RyR and in

others it is the IP_3R. In cardiac muscle the pre-dominant Ca^{2+} release channel is the RyR, specifically RyR2, which mediates CICR that provides the majority of the Ca^{2+} required for cardiac myocyte contraction, as opposed to the initial Ca^{2+} influx through the voltage-gated Ca^{2+} channels (20). Cardiac myocytes also express IP_3R, but Ca^{2+} released through IP_3R does not contribute the bulk Ca^{2+} required for a successful cardiac Ca^{2+} transient. Conversely, in pancreatic acinar cells IP_3Rs are the major release channel with IP_3R2 and IP_3R3 being the dominant isoforms (21). Pancreatic acinar cells also express RyR (18,22) but at a lower level than the expression of IP_3R. It is thought that the Ca^{2+} release mediated through the different release channels plays a role in the spatiotemporal dynamics of a cells Ca^{2+} signal, IP_3R release Ca^{2+} apically in pancreatic acinar cells (23), whereas RyR propagate the signal towards the basolateral pole of the cell, contributing to a global signal (24,25).

1.1.4 Ca^{2+} clearance mechanisms

Elevations in cytosolic Ca^{2+}, due to Ca^{2+} influx and Ca^{2+} release from intracellular stores, provides the necessary Ca^{2+} for physiological signalling; but as mentioned previously sustained elevations in cytosolic Ca^{2+} have severe consequences for cells (9). Therefore, mammalian cells have several mechanisms which they can employ to clear Ca^{2+} from the cytosol. The SR/ER Ca^{2+}-ATPase (SERCA) is found in the SR/ER membrane and actively pumps Ca^{2+} from the cytosol into the ER. The plasma membrane Ca^{2+}-ATPase (PMCA) is ubiquitously expressed in the plasma membrane of most eukaryotic cells and actively pumps Ca^{2+} from the cytosol across the cell membrane into the extracellular medium (26). These two Ca^{2+} clearance mechanisms are common to both excitable and non-excitable cells. Excitable cells also have a Na^+-Ca^{2+} exchanger (NCX), an ionic antiporter that in its forward-mode pumps Ca^{2+} out of the cell in exchange for Na^+ ions pumped into the cell. In cells where NCX is not expressed or is not functional then PMCA is the major pump that is responsible for clearing Ca^{2+} from the cytosol, across the plasma membrane. Further to these mechanisms it has long been known that mitochondria are capable of taking up Ca^{2+} from the cytosol (27), it is now known that this is via the mitochondrial Ca^{2+} uniporter (MCU) (28), which is localised on the inner mitochondrial membrane (29). Mitochondrial Ca^{2+} uptake is a rapid process, with the peak increase in mitochondrial Ca^{2+} concentration closely following the peak increase in cytosolic Ca^{2+} concentration (30), this increase in mitochondrial Ca^{2+} is dependent on ER Ca^{2+} release and subsequent Ca^{2+} influx into the cell to maintain high Ca^{2+} concentration within the ER/mitochondrial Ca^{2+} microdomain (30). Mitochondrial Ca^{2+}

uptake is a necessary physiological phenomenon (31) but can have pathological consequences when mitochondrial homeostasis is disrupted (32).

1.1.5 Cytosolic Ca^{2+} buffers

Cytosolic Ca^{2+} buffers are defined as molecules that chelate Ca^{2+} ions, they contain negatively charged groups that can trap the Ca^{2+} ion (33). Cytosolic Ca^{2+} buffers serve to reduce the concentration of free intracellular Ca^{2+}. Not all proteins that bind Ca^{2+} are considered to be cytosolic Ca^{2+} buffers. The EF hand family of proteins, proteins that possess an EF-hand which is a Ca^{2+} binding motif, are considered to be Ca^{2+} sensors. When EF-hand containing proteins bind Ca^{2+} there is a conformational change that is conducive to signal transduction; Ca^{2+} buffers do not undergo conformational changes when Ca^{2+} binds (34). Not all Ca^{2+} sensors are Ca^{2+} buffers, a Ca^{2+} sensor can serve as a Ca^{2+} buffer when it is at a sufficiently high concentration, calmodulin is an EF hand containing protein that is considered to be a Ca^{2+} sensor, as it binds Ca^{2+} and results in signal transduction, in turn it also buffers Ca^{2+} (33,35). Ca^{2+} buffers serve to modulate the spatiotemporal profile of Ca^{2+} signals by altering the amplitude and rate of increase or decrease of Ca^{2+} signals (10). Calbindin D-28 and calretinin are cytosolic Ca^{2+} buffers that served to chelate cytosolic Ca^{2+} ions, reducing cytosolic Ca^{2+} concentration (10,33). Calbindin and calretinin have fast buffering properties whereas parvalbumin, another cytosolic Ca^{2+} buffer, has much slower buffering kinetics (33). Parvalbumin is present in mouse fast twitch muscle fibres at approximately 1 mM (36), there is considerable heterogeneity in the concentration of this buffer present in other cell types, for example in dendritic cells it is present at approximately 80 μM (37). The importance of Ca^{2+} is highlighted by the altered Ca^{2+} signal dynamics observed in knock out animals (37,38).

1.2 Ca^{2+} signalling in non-excitable cells

There are clear distinctions between Ca^{2+} signalling in electrically excitable cells and non-electrically excitable cells. Typically in excitable cells there is a need for the Ca^{2+} signal to be rapid and short-lasting, consider the cardiac myocyte as an example: in order to activate the contractile machinery for a successful heart beat there must be a whole-cell Ca^{2+} transient, that is a global elevation in cytosolic Ca^{2+}. To achieve a heart rate of 60 beats per minute, the cardiac myocytes need to achieve one global Ca^{2+} transients per second, this includes both the increase and decrease in cytosolic Ca^{2+} back to pre-stimulation levels. This is achieved via membrane depolarisation of the cardiac myocytes plasma membrane (including the t-tubular network). The change in membrane potential opens voltage-gated Ca^{2+} channels and

allows for Ca^{2+} influx, down its concentration gradient, into the cell. RyRs are closely apposed to the plasma membrane in cardiac myocytes, as such in the ER/PM microdomain Ca^{2+} concentrations are high and this facilitates CICR. The primary Ca^{2+} influx is amplified by the Ca^{2+} release from the ER via the RyR. There is saltatory propagation of the Ca^{2+} signal from clusters of RyR to the next etc. This provides the Ca^{2+} to bind to troponin C and elicit contraction. This is known as excitation-contraction coupling (20).

In non-electrically excitable cells, it is not possible to depolarise the membrane and furthermore the cells do not possess voltage-gated Ca^{2+} channels (39). Rather the primary source of Ca^{2+} for intracellular Ca^{2+} signals is Ca^{2+} release from intracellular stores, primarily the ER. As there is no initiating Ca^{2+} signal via voltage-gated channels, there is a necessity for an alternative signal to liberate Ca^{2+} from the ER store. This comes in the form of a second messenger, which for the vast majority of non-excitable cells is likely to be IP_3 (13,40,41), it couples activation of cell surface receptors with an increase in cytosolic Ca^{2+} concentration. IP_3, as mentioned previously, is formed from the hydrolysis of PIP_2 catalysed by PLC, which is activated upstream by an alpha subunit of a GPCR (10,42).

1.2.1 IP_3 Receptor

The IP_3R is the major Ca^{2+} releasing channel in the ER of non-excitable cells expressing PLC-coupled cell surface receptors (43). Binding of IP_3 and Ca^{2+} are both required to activate the IP_3R (44). The IP_3R receptors form homotetramers (45), there are three isoforms of the IP_3R encoded by three genes, all three isoforms have different sensitivities to IP_3 (46,47). There is evidence suggesting that IP_3 must bind to more than one IP_3 binding site on the receptor before it can open (48,49), but not all IP_3 binding sites need to be occupied (50). IP_3R activation is biphasically dependent on cytosolic Ca^{2+}, 0.5 to 1 µM cytosolic Ca^{2+} will serve to co-activate the receptor, whereas cytosolic Ca^{2+} concentrations over 1 µM will inhibit IP_3R (17,44). Once activated, the channel allows for the permeation of Ca^{2+} and thus efflux of Ca^{2+} from the ER into the cytoplasm. In this way IP_3R mediates CICR, providing there is sufficient IP_3 available to bind to and co-activate receptors, this is the mechanism by which non-excitable cells can amplify the primary Ca^{2+} signal to give rise to global Ca^{2+} signals. IP_3R are susceptible to inhibition of Ca^{2+} release by the action of heparin (51,52) and caffeine (53). Dependent on the nature of the non-excitable cell in question will affect what the requirement is for the increase in cytosolic Ca^{2+} concentration for example stimulus-secretion coupling, similar in nature to excitation-coupling, is a phenomenon in secretory epithelia cells such as salivary glands and the exocrine pancreas, this initial phase of this

process is dependent on Ca^{2+} release from the ER via IP_3R whereas for continued secretion, Ca^{2+} influx from the extracellular medium is required (39).

1.2.2 Ryanodine Receptor

RyRs are another group of intracellular Ca^{2+} release channels closely related to IP_3R, there is approximately 17 % sequence homology between the two types of channels (54,55). RyRs have been most extensively studied in cardiac and skeletal muscle (56–58). There are three isoforms, with differential expression in different cell types, for example RyR2 is the pre-dominant isoform in cardiac tissue and RyR1 pre-dominant in skeletal muscle (59) In addition to the expression of RyRs in excitable cells, expression of RyRs has also been demonstrated in non-excitable cells such as hepatocytes (60,61). Caffeine treatment, in cardiac myocytes, has a potentiating effect on Ca^{2+} released from RyRs, but in hepatocytes caffeine treatment inhibited Ca^{2+} signals, as caffeine was found to inhibit IP_3 synthesis (62), thereby inhibiting IP_3-induced Ca^{2+} release (53). Kidney tissue was demonstrated to express RyR2, to exclude contamination from smooth muscle present due to blood vessels the results were confirmed in a kidney epithelial cell line (63). Further expression of different isoforms of RyR were identified in parotid acinar cells (64,65). RyRs are sensitive to inhibition by ryanodine, a plant alkaloid that inhibits its namesake receptor by binding to it in its open state and inhibiting the channel in a dose-dependent manner (59). Furthermore, RyRs are also sensitive to inhibition by ruthenium red (66). Generally, RyRs are much less abundant in non-excitable cells than in excitable cells, but they have a much larger conductance, as such they still contribute to CICR but are not the predominant channel through which Ca^{2+} permeates.

1.2.3 Store-operated Ca^{2+} entry

As seen in figure 1.1, the time scale over which certain Ca^{2+} signals are required to last can be quite prolonged, the signals required for fertilisation and proliferation last for hours, which is clearly very different to the time scale of the Ca^{2+} signal that initiates cardiac myocyte contraction. Even though in some cells like pancreatic acinar cells the ER Ca^{2+} store is quite large it is still finite, therefore an alternative source of Ca^{2+} is required to drive the prolonged signal and to refill the ER stores upon termination of the stimulus. The initial Ca^{2+} release from the ER results in a fall in ER luminal Ca^{2+} concentration, which is now known to be detected by Stromal interaction molecule 1 (STIM1), the recently discovered ER Ca^{2+} sensor (discussed in further detail in the section below). Studies have shown that upon store depletion this protein aggregates and translocates to parts of the ER membrane that are in

close apposition to the plasma membrane, more specifically closely apposed to the Ca^{2+} release activated Ca^{2+} (CRAC) channels, a type of store-operated Ca^{2+} entry channel. Aggregated and activated STIM1 activates CRAC channels, opening them and allowing the influx of Ca^{2+} into the cytosol from the extracellular medium. There is a large driving force for Ca^{2+} across the plasma membrane into the cell, as long as the channels remain open Ca^{2+} will enter the cell. Ca^{2+} influx via store-operated Ca^{2+} channels provides the Ca^{2+} required to drive the physiological process which is stimulated by a prolonged elevation in cytosolic Ca^{2+}.

1.2.4 Ca^{2+} extrusion

Once the stimulus at the cell surface receptor has terminated there will be no further hydrolysis of PIP_2 at the membrane by PLC and no subsequent production of IP_3. IP_3 is degraded by several enzymes, such as IP_3 3-kinase and inositol polyphosphatase 5-phosphatase (67), thereby can no longer bind to its receptor to elicit Ca^{2+} release from the ER. Whenever there is an elevation in cytosolic Ca^{2+} the extrusion mechanisms are activated in order to clear this elevated Ca^{2+}; during sustained stimulation the magnitude of the "on" reactions is greater than the magnitude of the "off" reactions and therefore cytosolic Ca^{2+} concentrations increase. Once the cell surface receptor stimulation ceases, the "on" mechanisms cease and therefore the magnitude of the "off" reactions is greater than the "on" mechanisms and cytosolic Ca^{2+} concentrations decrease (10,42).

During sustained cell surface receptor stimulation, SERCA pumps have very little effect on removing Ca^{2+} from the cytosol as the Ca^{2+} release channels are open, as such PMCA is primarily responsible for Ca^{2+} extrusion (68) and is the only mechanism in non-excitable cells to remove Ca^{2+} across the plasma membrane (69). In excitable cells the NCX is expressed and extrudes Ca^{2+} across the plasma membrane, in exchange for Na^+, it is a low-affinity extrusion mechanism compared to PMCA but has a higher conductance (69). There is some evidence for NCX in expression in some non-excitable cells (70), but it is likely to play only a minor role in maintenance of Ca^{2+} homeostasis. Conversely, PMCA is a high affinity pump and is activated at Ca^{2+} concentrations in the region of 100-300 nM, it therefore enables maintenance of cytosolic Ca^{2+} homeostasis when Ca^{2+} is not significantly elevated above resting concentrations (71,72). There is also evidence that PMCA alone is sufficient to maintain Ca^{2+} homeostasis in cardiac specific NCX knock-out mice (73). Once receptor stimulation has ceased, SERCA has more of an impact in Ca^{2+} uptake from the cytosol as the Ca^{2+} release channels of the ER will no longer be open. The activity of SERCA is largely

dependent on the concentration of Ca^{2+} within the ER as opposed to the concentration of Ca^{2+} in the cytosol (11). As PMCA extrudes all the Ca^{2+} across the membrane during sustained receptor stimulation, in order to refill the ER stores Ca^{2+} must re-enter the cell, this occurs through store-operated Ca^{2+} channels such as the CRAC channel and does not significantly change in cytosolic Ca^{2+} concentration (74).

1.3 Ca^{2+} signalling in exocrine cells

In exocrine cells Ca^{2+} signalling is primarily responsible for the regulation of exocytosis, fluid secretion and gene expression (75). Exocrine cells typically have highly polarised structures, which translates to a functional polarisation and thereby polarisation in the regulatory signal, in this case Ca^{2+} signalling. Both salivary glands and the exocrine pancreas have been extensively studied as models of non-excitable, exocrine cells (11,75,76). Due to the structural polarity of cells, organelles have distinct subcellular locations. The bulk of the ER is located in the basal region of exocrine cells, but IP_3R are localised in the apical region of both pancreatic acinar cells and salivary acinar cells (77–80), present on thin extensions of ER membrane that extend from the base of the cell towards the apical region (81). This structural data supported the previously determined spatial profile of Ca^{2+} signals seen in exocrine cells: in hepatocytes, pancreatic acinar cells, lacrimal acinar cells, submandibular gland acinar cell and submandibular gland duct cells; in which the Ca^{2+} signal is initiated in the apical pole of the cells and propagates around to the basolateral pole of the cell (75). Functionally, the purpose of Ca^{2+} release from the ER through IP_3R in the apical pole is to provide the stimulus required for secretion. In pancreatic acinar cells the secretory granules that contain the digestive proenzymes are located at the apical pole of the cell, fluid secretion in salivary gland cells and all ductal cells occurs across the apical membrane too. There is expression of IP_3R found at the basal pole of some exocrine cells, which likely aids in the propagation of the Ca^{2+} signal. Furthermore there is also expression of RyR at basolateral pole of cells this too allows for propagation of a whole cell Ca^{2+} wave via CICR (82).

PMCA is largely localised to the apical region of cells, in order to extrude Ca^{2+} from the region in which it is primarily liberated, to prevent the unnecessary propagation of Ca^{2+} signals. There is also expression on the basolateral membrane, but much less (79). As this is a high-affinity pump it is activated with each oscillation in cytosolic Ca^{2+} thus ensuring the tight regulation of cytosolic Ca^{2+} (68). Furthermore, it maintains the apical luminal Ca^{2+} concentration which maintaining the driving force of Ca^{2+} into the cell and provides Ca^{2+} required for endocytosis (83). SERCA is primarily located at the basal pole of exocrine cells

to allow for store refilling directly into the ER, of which the bulk is situated in the basal region of the cell (79,81).

1.4 Ca^{2+} signalling in pancreatic acinar cells

As previously discussed pancreatic acinar cells are one of the most extensively studied exocrine cells and as such largely match the description of exocrine cells given in section 1.3. A schematic diagram of a polarised pancreatic acinar cell is shown in figure 1.2. This schematic demonstrates that the bulk of ER is localised in the basal region of the cell, with projections into the apical region, where the bulk of the IP$_3$R are localised. IP$_3$R localisation in the apical region promotes local Ca^{2+} signals, these signals are largely restricted to the apical pole due to the perigranular mitochondria. Local Ca^{2+} signals promote the exocytosis of zymogen granules which are also localised in the apical pole of the cell. The store-operated Ca^{2+} channels are localised in the basal pole, as are SERCA pumps which serve to actively refill the ER Ca^{2+} store

These cells are responsible for the synthesis and the secretion of digestive proenzymes, predominantly trypsinogen, chymotrypsinogen and to a lesser extent pancreatic amylase and lipase (84,85). The sight, smell and taste of food are sufficient to stimulate pancreatic enzyme secretion, this is known as the cephalic phase of digestion and is mediated via the vagal cholinergic system (86,87). The gastric phase of digestion also stimulates secretion of pancreatic enzymes, mediated via the cholinergic system (88). The secretion of the digestive enzymes is stimulated by the ingestion of food, the duodenum is the most responsive part of the gastrointestinal tract in its response to nutrients and elicits high levels of enzyme secretion upon nutrient exposure (89), this comprises the intestinal phase of digestion. The entry of chyme into the duodenum initiates the release of neurotransmitters and hormones that activate the release of digestive enzymes from pancreatic acinar cells (87,89).

Digestive proenzymes are stored in zymogen granules, in pancreatic acinar cells (90) after their synthesis in the rough ER and packaging into vesicles in the Golgi. The pro-enzymes are inactive forms of the digestive enzymes, which are activated in the lumen after secretion (91). As the apical region of the cell is the closest to the duct of the exocrine pancreas, the apical pole is region in which the zymogen granules are stored (90,92), poised to begin the process of exocytosis upon receiving the Ca^{2+} signal.
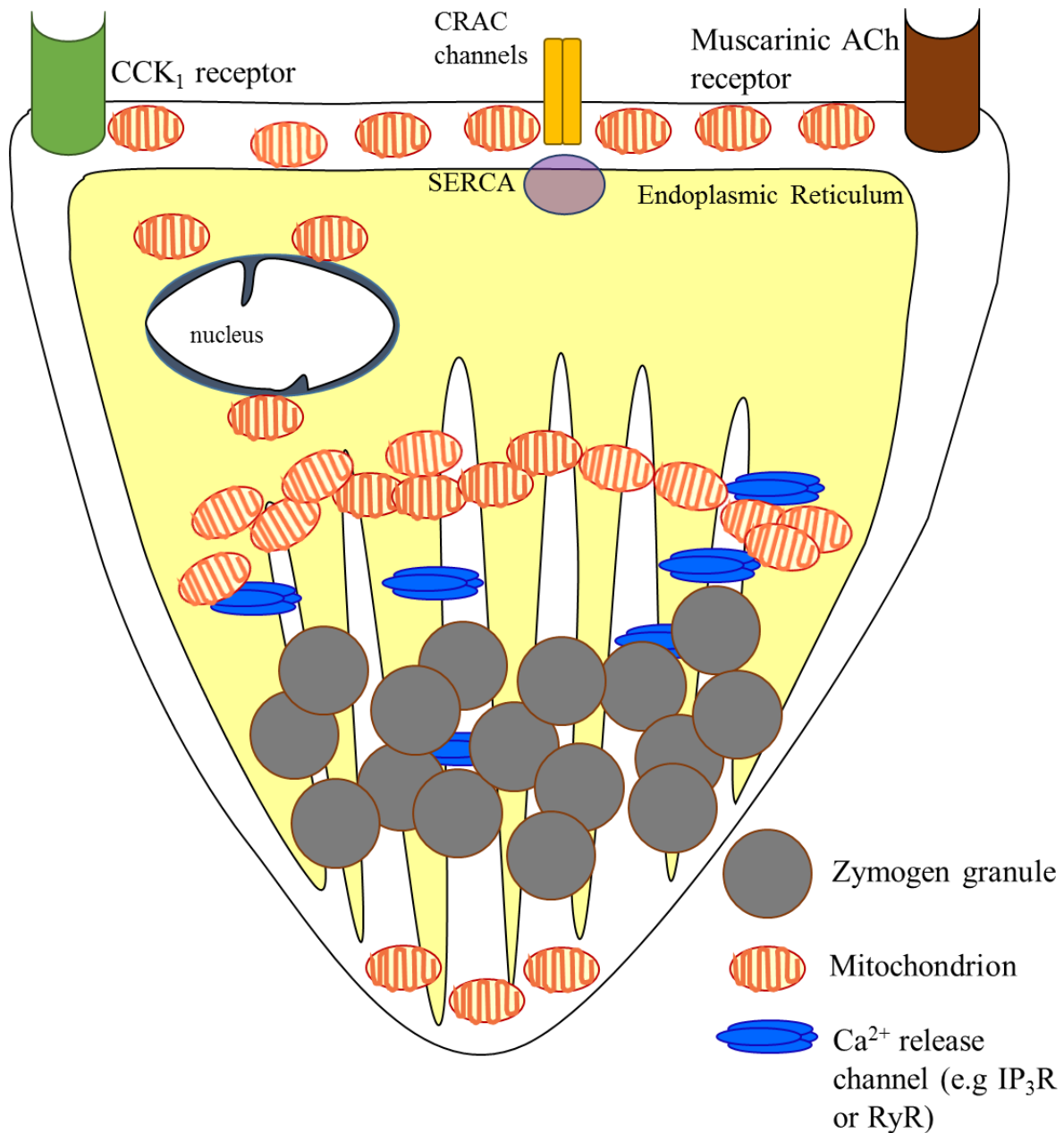
Figure 1.2 Schematic figure of a polarised pancreatic acinar cell

Pancreatic acinar cells are the prototypical exocrine cells and are highly polarised. The digestive proenzymes synthesised in these cells are stored in zymogen granules located in the apical pole. The bulk of the endoplasmic reticulum (ER) is localised in the basal region of the cell with thin projections that reach into the apical pole. The bulk of the Ca^{2+} release channels, predominantly IP_3R are localised in the apical pole. There are three major sub-cellular locations of mitochondria – sub-plasmalemmal, perigranular and perinuclear. The cell surface receptors are largely localised on the basal membrane of the cell with the SOCE channels. Ca^{2+} uptake pumps such as SERCA are found in the basal part of the cell ready to take up Ca^{2+} that enters the cell through SOCE channels.

The zymogen granules themselves are an intracellular store of Ca^{2+}, forming part of the acidic Ca^{2+} store, which to can liberate Ca^{2+} in response to agonists such as IP_3 (93) but this does not render ER Ca^{2+} release unnecessary (11).

It was established more than forty years ago that an increase in cytosolic Ca^{2+} was required for enzyme secretion from pancreatic acinar cells, it was first demonstrated in submandibular salivary glands; it was also known that physiological agents that induced pancreatic enzyme secretion, such as ACh, also released Ca^{2+} into the cytosol (94,95) – although the mechanism of this release was yet to be deduced (40). The increase in cytosolic Ca^{2+} due to Ca^{2+} release, induced by ACh application, always preceded the release of amylase (95). A later paper demonstrated that initial amylase release, stimulated by ACh, was independent of extracellular Ca^{2+} but could not be sustained in the absence of extracellular Ca^{2+}. Re-introduction of Ca^{2+} to the extracellular solution, during maintained ACh stimulation, resulted in amylase release once again (96). This is because sustained amylase release requires sustained elevation in cytosolic Ca^{2+} which is driven by Ca^{2+} entry from the extracellular solution (97). Increase in cytosolic Ca^{2+} upon CCK stimulation was later visualised using quin2 as a fluorescent Ca^{2+} probe (98). It was observed that the amplitude of the Ca^{2+} signal was directly proportional to the concentration of agonist used to stimulate said signal - until a peak in intracellular Ca^{2+} was attained; however, the magnitude of amylase released had a biphasic relationship with the concentrations of agonist applied to cells (98,99). The Ca^{2+} signal that is responsible for triggering the exocytosis of enzymes in acinar cells was demonstrated to be an oscillatory signal (100,101)

Pancreatic acinar cells express CCK receptors for which the ligand is the hormone CCK, the release of which is stimulated during the intestinal phase of digestion (102,103). In addition, acinar cells also express mAChR for which the ligand is the neurotransmitter acetylcholine (ACh), which is released during all stages of digestion (87,88,104). In addition, vasoactive intestinal peptide, substance P, gastrin-releasing peptide and secretin also regulate enzyme secretion by the acinar cells (105).

mAChR are GPCRs that are coupled to PLC (106), which hydrolyses PIP_2 resulting in the production of the second messenger IP_3 and the downstream liberation of Ca^{2+} from Ca^{2+} stores via the IP_3R. The CCK receptor type 1 has two different affinity states in pancreatic acinar cells (107,108), when activated by physiological concentrations of CCK it is thought that the high affinity binding site on the CCK receptor is occupied and coupled to an ADP-

ribosyl cyclase (109) – one of which is CD38(110). ADP-ribosyl cyclases, such as CD38 are responsible for the synthesis of two second messengers: cADPR and NAADP (111), at least in pancreatic acinar cells. NAADP was first demonstrated to release Ca^{2+} from intracellular stores in sea urchin eggs (112) and later in pancreatic acinar cells (113). It was also demonstrated that cADPR liberates Ca^{2+} from intracellular stores localised in the apical pole of pancreatic acinar cells (114). cADPR-induced Ca^{2+} released was demonstrated to be both heparin and ryanodine sensitive, indicating it liberated Ca^{2+} from both IP_3R and RyR (114). It is thought that NAADP releases Ca^{2+} from acidic organelles through two-pore channels (19) localised on lysosomes (115), the ER store directly via RyR (18) and indirectly through CICR from RyR (19,110,115). cADPR has also been demonstrated to liberate Ca^{2+} from other acidic stores such as zymogen granules (93). When supra-physiological concentrations of CCK are present, CCK is thought to bind to the low affinity binding site on the CCK receptor, PLC is activated and IP_3 is formed, liberating Ca^{2+} from the ER through the IP_3R (107,108). The cell surface receptors and the second messengers produced upon binding of the appropriate ligand is summarised in figure 1.3, detailing the intracellular receptors that are targeted by the second messengers.

Stimulation of cell surface receptors such as mAChR and CCK receptors, on the basolateral membrane, stimulates the formation of IP_3, NAADP and cADPR, which bind to their respective receptors on the membrane of intracellular Ca^{2+} stores, resulting in the release of Ca^{2+} into the apical region of the acinar cell. Ca^{2+} signals, both local and global signals, are always initiated in the apical region of pancreatic acinar cells, even if they are elicited differently (23,116). Stimulation of the cell surface receptors at physiological concentrations of an agonist results in a Ca^{2+} signal that is oscillatory and is restricted to the apical pole (23,117). Each oscillation in cytosolic Ca^{2+} has been shown to precede a wave of exocytosis of secretory granules, often measured by monitoring changes in membrane capacitance (118,119). The restriction of these oscillatory Ca^{2+} signals is due in large part to the Ca^{2+} buffering capacity of the cytosol (120). In pancreatic acinar cells there is a distinct feature that aids the restriction of Ca^{2+} signals to the apical pole, this is the perigranular belt of mitochondria around the granular region of the cell (121–123). This belt of mitochondria (figure 1.2) serves to increase the buffering capacity of this sub-cellular region, as mitochondria have the capacity to take up Ca^{2+} via the MCU; cytosolic Ca^{2+} signals in the apical pole are followed by mitochondrial Ca^{2+} signals in the perigranular mitochondria (122).
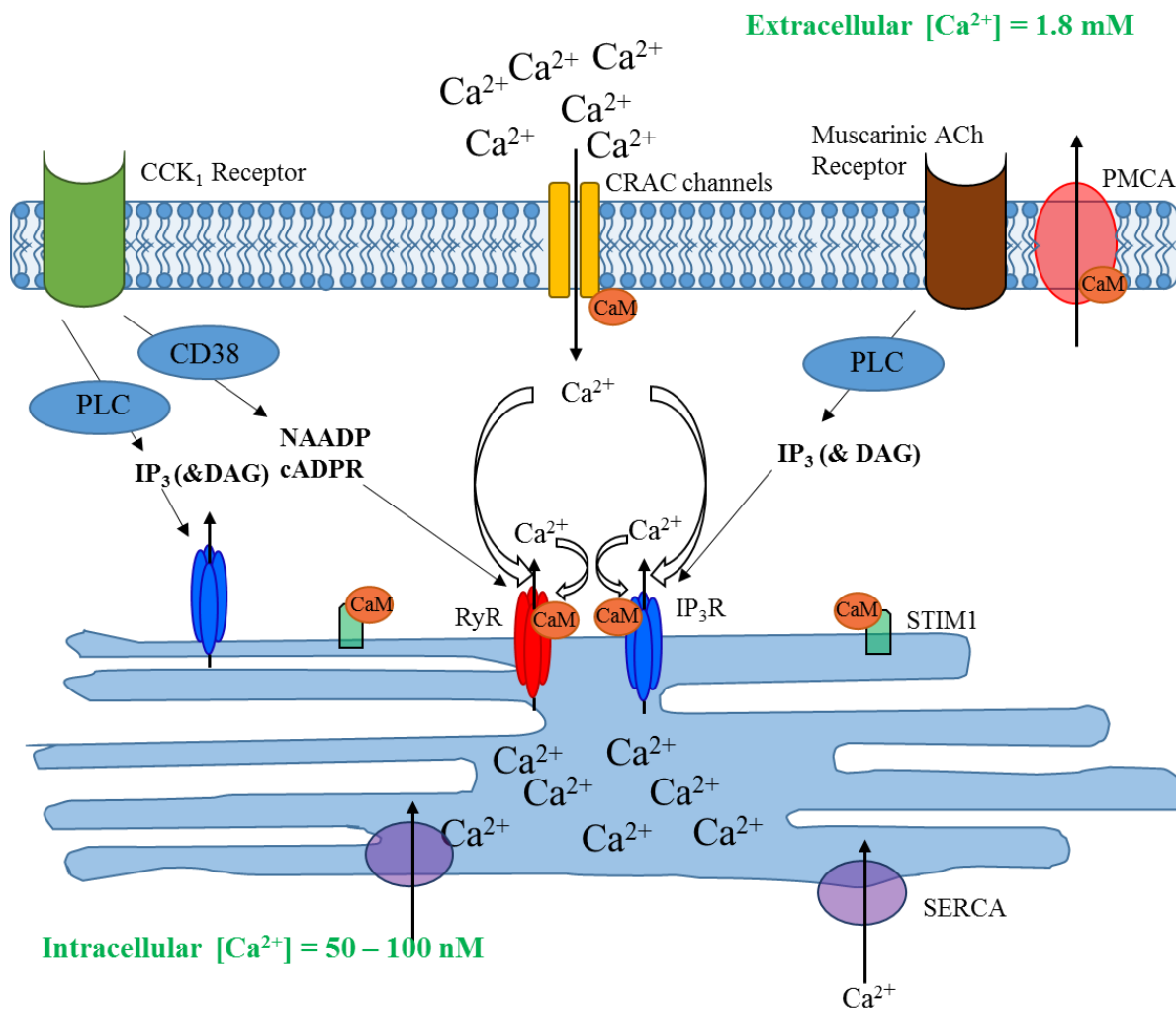
Figure 1.3 Schematic diagram of the Ca^{2+} signalling pathway in a pancreatic acinar cell

The two major cell surface receptors in pancreatic acinar cells are the muscarinic ACh receptors and the CCK_1 receptor. ACh is coupled to PLC which hydrolyses PIP_2 to give IP_3 and DAG. IP_3 binds to the IP_3R on the ER membrane and results in the release of Ca^{2+} from the ER store. The CCK_1 receptor has two affinity states, when CCK binds to the high affinity state CD38 is activated resulting in the production of NAADP and cADPR as second messengers. Which can liberate Ca^{2+} from RyR on the ER membrane (and other channels on lysosomes – not shown). If CCK binds to the low affinity binding site then PLC is activated and IP_3 is produced. Both IP_3R and RyR have calmodulin binding domains. Once Ca^{2+} is liberated from the ER STIM1, in the ER membrane, detects ER store Ca^{2+} content and oligomerises and translocates to ER-PM junctions to activate CRAC channels, allowing Ca^{2+} to enter the cell from the extracellular space. CRAC channels also possess calmodulin binding domains. STIM1 also has a calmodulin binding domain. SERCA is a Ca^{2+}-ATPase that actively pumps Ca^{2+} back into the ER and PMCA is another Ca^{2+}-ATPase that actively pumps Ca^{2+} out of the cell across the plasma membrane both are activated by increased cytosolic Ca^{2+} levels.

Furthermore, the proximity of the mitochondria to the granular region provides the ATP required by the secretory machinery of the cell (11), ATP production by mitochondria is also driven by Ca^{2+} (31).

The initial Ca^{2+} signal for exocytosis is primarily elicited by IP_3-induced Ca^{2+} release from the ER (23,124) and is independent of extracellular Ca^{2+} (125). However, for sustained release of enzymes, in order to digest a sizeable meal, continuous oscillations in intracellular Ca^{2+} for that duration of time would be required, thereby Ca^{2+} influx from the extracellular medium is also required (125). There is sufficient Ca^{2+} stored in the ER to respond to stimulation by a physiological concentration of ACh for 7-8 minutes in the absence of extracellular Ca^{2+}, after that the frequency and the amplitude of Ca^{2+} oscillations decreased until they ceased (126). Ca^{2+} influx across the membrane provides the necessary Ca^{2+} to drive prolonged intracellular Ca^{2+} signals, Ca^{2+} entry is through store-operated $^{Ca2+}$ entry channels located on the basal membrane of acinar cells (74). It is now known that the ER Ca^{2+} filled status is monitored by STIM1, which upon Ca^{2+} depletion, oligomerises and activates, leading to activation and opening of the CRAC channels found in the plasma membrane (for more extensive details on mechanism of store-operated Ca^{2+} entry, see section 1.5) (127). Both STIM1 and Orai1, the two key constituents of the CRAC channel are expressed in pancreatic acinar cells and functionally mediate store-operated Ca^{2+} entry (80,128–130). In instances where cell surface receptor stimulation is sufficiently high, due to high concentration of agonist, global Ca^{2+} signals are elicited (23,120). The signal is initiated apically and overwhelms the buffering capacity of the cytosol and the perigranular mitochondria (121), resulting in the propagation of the Ca^{2+} signal to the basolateral poles of the cell via CICR and the RyRs play a key role in this (25) (figure 1.3).

In addition to the ER intracellular Ca^{2+} store pancreatic acinar cells also possess an acidic Ca^{2+} store, localised in the apical region. Lysosomes contain a lot of Ca^{2+} creating an electrochemical gradient for release to the cytosol. In the lysosome membrane are channels known as two pore channels which release Ca^{2+} when stimulated by their agonist NAADP. This process contributes to elevations in cytosolic Ca^{2+} in response to agonist stimulation (18,131).
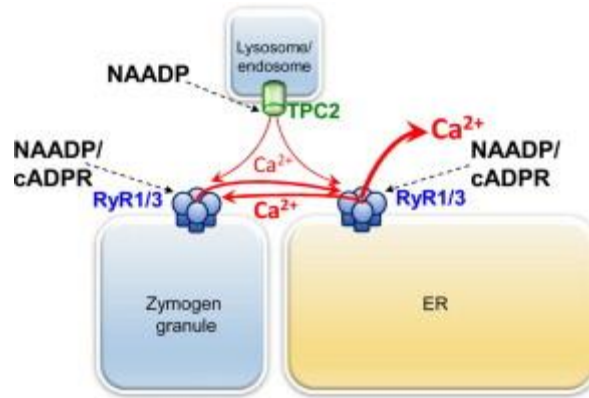
Figure 1.4 Schematic diagram demonstrating how NAADP-induced Ca^{2+} release can contribute to an elevation in cytosolic Ca^{2+}

NAADP stimulates Ca^{2+} release from lysosomes or endosomes through the two pore channels, which results in CICR through RyR located on zymogen granules and the ER. Figure from (18).

The PMCA is the major Ca^{2+} extrusion pathway in pancreatic acinar cells. Experiments indicated that Ca^{2+} extrusion in this cell type was not mediated by NCX (132). ACh stimulated an increase in cytosolic Ca^{2+} concentration, that resulted in an increase in extracellular Ca^{2+} concentration that was similar in amplitude (132,133), indicating that the majority of Ca^{2+} that was released by maximal stimulation by ACh was extruded across the plasma membrane (83), rather than taken back up into intracellular Ca^{2+} stores or into mitochondria. In addition to extruding Ca^{2+} released by maximal stimulation of the cell, the PMCA also pumps Ca^{2+} released by physiological stimulation of cells, in the form of oscillatory signals, across the membrane resulting in step-wise increase in extracellular Ca^{2+} concentration. This action of the PMCA enabled resting cytosolic Ca^{2+} concentrations to be restored (68). The PMCA is primarily localised at the apical membrane of the cell, where there is expression on the lateral membrane and much less expression on the basal membrane (83,134). It has a calmodulin-binding domain which facilitates its activation by intracellular Ca^{2+}, by increasing the affinity of the pump for Ca^{2+} and increasing the maximum pumping capacity. The PMCA was found to be saturated at cytosolic Ca^{2+} concentrations of approximately 400 nM, indicating its role in maintaining resting cytosolic Ca^{2+} concentrations (135).

The SERCA actively pumps Ca^{2+}back into the ER and provides another Ca^{2+} extrusion pathway in pancreatic acinar cells (136). Pancreatic acinar cells express SERCA2a and SERCA2b, SERCA2a was shown to be exclusively expressed at the apical pole of the cell,

whereas high levels of SERCA2b expression was detected primarily at the basal pole of the cell, with further staining noted on the nuclear envelope (134). Basal expression of SERCA allows for uptake of Ca^{2+} into the ER in the basal part of the cell, where the bulk of the ER is located in the polarised pancreatic acinar cell (137), store-operated Ca^{2+} influx through a focal point on the basal membrane resulted in reloading of the ER stores with Ca^{2+}, with no notable increase in cytosolic Ca^{2+} (74), due to local Ca^{2+} entry and local uptake. Of note, subsequent stimulation of the cells resulted in a Ca^{2+} signal initiated apically, indicating a tunnelling of the Ca^{2+} through the ER from the base of the cell to the apical region (74) demonstrating the lumen of the ER is continuous. There is further evidence suggesting that the movement of Ca^{2+} from the ER bulk in the basal region of the cell to the ER extensions in the apical region of the cell is rapid, once Ca^{2+} is released from the apical termini (137). The SERCA was found to be more than 20 times faster in resequestering Ca^{2+} into ER stores when cytosolic Ca^{2+} concentrations were elevated (350 nM) as opposed to closer to resting concentration (120 nM) suggesting the uptake of Ca^{2+} into ER stores is largely reserved for removing Ca^{2+} from the cytosol after global signalling events (135).

1.5 Store-operated Ca^{2+} entry.

Several cellular functions, not limited to exocytosis, are dependent on prolonged intracellular Ca^{2+} signals (138) and intracellular Ca^{2+} stores provide only a finite source of Ca^{2+}. Ca^{2+} entry across the plasma membrane down the huge concentration gradient for Ca^{2+} provides an almost limitless supply of Ca^{2+} to drive intracellular Ca^{2+} signalling needs. In non-excitable cells this Ca^{2+} entry is via store-operated channels in the plasma membrane rather than voltage-gated channels; the CRAC channel is the most well studied store operated Ca^{2+} channel, although the molecular identity of the channel components remained elusive for many decades. Gene expression is another cellular process that has a requirement for Ca^{2+} entry through CRAC channels. Nuclear factor of activated T cells (NFAT) is a downstream effector of increased cytosolic Ca^{2+}. The NFATs are a family of transcription factors that under resting conditions are localised in the cytosol of cells, in a highly phosphorylated state. Calcineurin is a Ca^{2+}/calmodulin-dependent phosphatase that is responsible for dephosphorylating NFAT resulting in its translocation from the cytosol to the nucleus, where it can regulate transcription of its associated genes. NFAT molecules provide the link between intracellular Ca^{2+} signals and gene expression (139). Translocation of NFAT to the nucleus can therefore be utilised as a read out for CRAC channel activity, as following even a short pulse of Ca^{2+} entry through CRAC channels NFAT translocates to the nucleus (140) – it

can be monitored using fluorescently tagged NFAT or utilising a GFP gene under NFAT promoter which will be expressed after NFAT has translocated.

The idea of capacitative Ca^{2+} entry was first introduced in 1981 (141) and then by Putney in 1986 (142). The idea proposed was that Ca^{2+} entry occurs in response to intracellular Ca^{2+} store depletion in order to refill intracellular store and that the activating feature, Ca^{2+} store depletion, is as a result of Ca^{2+} release. Putney attributes the hypothesis to two papers from the 1970s using lacrimal and parotid acinar cells respectively (143,144) where stores were shown to be refilled by Ca^{2+} entry and in one report this refilling was shown to be independent of cell surface receptor activation (143). His idea in identifying store-operated Ca^{2+} as "Capacitative Ca^{2+} entry" was due to continuous loading and release of Ca^{2+} into and fro, stores, like a capacitor in a circuit (145). It remained unclear where the Ca^{2+} that entered across the plasma membrane went, it was originally hypothesised that it directly entered the intracellular stores which were thought to be connected to the plasma membrane (145). A later study provided evidence that Ca^{2+} enters the cytosol before uptake into the intracellular stores (146), it also demonstrated that thapsigargin, which is now a known SERCA pump inhibitor, inhibited Ca^{2+} uptake into the intracellular store (146) - thapsigargin became a very useful tool to study store-operated Ca^{2+} entry.

Hoth and Penner undertook extensive electrophysiological recordings combined with Fura-2 measurements and demonstrated the existence of a Ca^{2+} selective ion channel which is known as the CRAC channel, through which Ca^{2+} enters the cell across the plasma membrane. Removal of extracellular Ca^{2+} resulted in loss of CRAC channel current (I_{CRAC}) (147). Chelation of divalent ions in the extracellular medium resulted in an increase in the permeability of monovalent ions, through CRAC channels, that did not exist in the presence of divalent ions (148); when conducted by monovalent ions I_{CRAC} is larger than when conducted by Ca^{2+} (149). The channel conductance is so small it could not be measured directly, it was indirectly measured by Zweifach and Lewis to be 24 fS. When current was carried by Na^+ (in the absence of divalent ions in the extracellular medium) it was approximated to be 2.6 pS (149). The channels also exhibited intracellular Ca^{2+} dependent inactivation (147) and extracellular Ca^{2+} dependent potentiation of the channel (148).

For many years it was clear that these channels were activated by the depletion of Ca^{2+} from the ER stores, rather than an increase in cytosolic Ca^{2+} levels. The mechanism by which store-depletion activated I_{CRAC} remained elusive until the identity of the components of the

CRAC channel were determined. Hypotheses ranged from a diffusible signal, which confers information on the depletion status of intracellular stores to activate Ca^{2+} entry, to a conformational change model similar to the one that occurs in skeletal muscle between ryanodine receptors and voltage gated Ca^{2+} channels. In the skeletal muscle conformational-change model the voltage gated Ca^{2+} channel, in the plasma membrane, is physically coupled to intracellular RyR found in the ER membrane situated at an ER-PM junction, where the ER and plasma membrane a within a few nanometres of one another. The idea was suggested that CRAC channel was somehow physically coupled to IP₃ receptors, which could convey ER Ca^{2+} store status to the plasma membrane channel, thus a fall in ER Ca^{2+} would result in a conformational change in the IP₃ receptor and activation of the CRAC channel and subsequent Ca^{2+} influx. However, there is a lack of evidence to support this particular hypothesis of a direct physical coupling, although the close spatial association of the ER and PM is now known. The formation of ER-PM junctions is now key to the accepted mechanism of store-depletion and CRAC channel activation.

The molecular identity of both the ER Ca^{2+} sensor (150,151) and the CRAC channel (152–154) were determined in 2005 and 2006 respectively. STIM1 and STIM2 were identified in a small interrupting RNA (siRNA) screen in HeLa cells (151); at the same time another group identified STIM1 in *Drosophila* S2 cells (150). The siRNA screens in which STIM1 or STIM2 had been knocked down demonstrated normal Ca^{2+} release dynamics, but the subsequent plateau in intracellular Ca^{2+} was markedly reduced in STIM1 knockdown, STIM2 knockdown and STIM1/2 knockdown experiments (151). Authors noted that in response to store depletion there was a rapid translocation of STIM1 from a disperse expression pattern across the ER at rest, to punctate structures located at sites of the ER that were juxtaposed to the plasma membrane. STIM1 was identified as being the ER Ca^{2+} sensor, it is a single transmembrane protein that spans the ER membrane with its amino terminus located inside the lumen of the ER. The luminal terminus of STIM1 contains a Ca^{2+} binding motif known as an EF-hand domain, this domain allows STIM1 to monitor the concentration of free Ca^{2+} within the lumen of the ER. Mutations of residues in the EF-hand that prevent Ca^{2+} from binding allow Ca^{2+} entry independent of ER store content (151,155). The second laboratory that identified STIM1 determined that it had a significant role in store-operated Ca^{2+} entry utilised a small scale RNA interference (RNAi) screen in *Drosophila* S2 cells and identified that *Stim* knockdown resulted in a reduction in store-operated Ca^{2+} influx in both Ca^{2+} imaging and electrophysiological experiments (150). Authors then moved to study the role of

STIM1 in Jurkat T cells, knockdown of STIM1 in these cells resulted in a dramatic reduction in Ca^{2+} entry, which was also seen in HEK293 cells where the pattern of STIM1 expression was confirmed to be the same as the other study(151) and was reduced upon STIM1 knockdown (150).

A year after the work identifying STIM1 several groups identified Orai1, a four transmembrane domain channel protein that is the pore forming subunit of the CRAC channel. The groups identified Orai1 using patients who had severe combined immunodeficiency (SCID) and their families, researchers identified mutations in a gene associated with SCID through genetic linkage analysis (152). A concurrent RNAi screen in *Drosophila* cells that sought to identify regulators of NFAT resulted in the identification of d*Stim* and d*Orai*. Knockdown of either d*Stim* or d*Orai* resulted in inhibition of thapsigargin-activated store operated Ca^{2+} entry (152). Expression of wild-type Orai1 rescued the CRAC current in T cells derived from SCID patients. Further siRNA studies were undertaken to identify other components involved in SOCE. A second laboratory also utilised *Drosophila* S2 cells for a high-throughput genome wide RNAi screen, where 23 000 genes were tested for their involvement in SOCE (154). Using STIM1 as a positive control two genes were identified as having an involvement in store-operated Ca^{2+} entry - CRACM1 and CRACM2. siRNA against CRACM1 in HEK293 and Jurkat T cells resulted in a significant reduction CRAC currents as stimulated by IP_3 mediated store depletion (154). The third laboratory to identify Orai1 also used *Drosophila* S2 cells in a genome wide RNAi screen, they identified Ca^{2+} entry inhibition when d*Orai* was knocked-down. The results of the screen were confirmed in individual patch-clamp experiments where CRAC currents were measured in cells pre-treated with d*Orai* dsRNA, current was almost completely inhibited compared to control (153).

Three separate groups determined that Orai1/CRACM1 was a component of the CRAC channel but it remained unclear exactly what its role was (152–154). Further studies utilised mutagenesis of two conserved acidic residues of Orai1 and found altered ion selectivity of Orai1 when the mutant protein was overexpressed in HEK293 cells, this provided strong evidence for the role of Orai1 as the pore forming subunit of the CRAC channel, rather than a plasma membrane bound accessory protein of the channel (156). The exquisite selectivity of Orai1 for Ca^{2+}, under physiological conditions, is because when Ca^{2+} is bound to the pore of the channel monovalent ions such as Na^+ cannot permeate, this is similar to channel selectivity of voltage-gated Ca^{2+} channels for Ca^{2+} (156,157). Furthermore, it was determined

that CRAC channels have a very low conductance, which lead to difficulties in the measurement of the current, the conductance of the CRAC channel is 100 times smaller than that of other Ca^{2+} permeable channels (158). It is now known the Orai1 has an intracellular calmodulin-binding domain that facilitates Ca^{2+}-dependent inactivation of the channel (159,160), which is similar to the mechanism by which voltage gated Ca^{2+} channels are inactivated (161).

A **Pre-stimulation, at rest:**   B **After stimulation and Ca^{2+} release:**
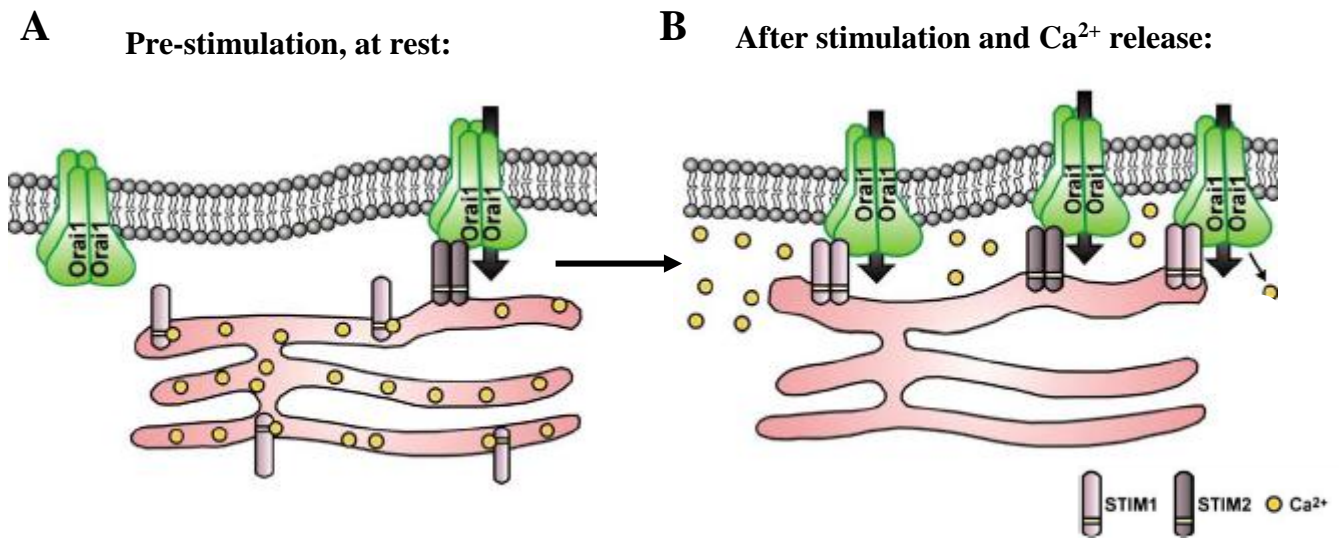
Figure 1.5 Schematic diagram demonstrating the dynamics of store operated Ca^{2+} entry and the key components involved: STIM1, STIM2 and Orai1

A - At rest, the ER is replete with Ca^{2+} which is sensed by the ER Ca^{2+} sensors STIM1 and STIM2, which are found dispersed throughout the ER membrane when they are bound to Ca^{2+}. Orai1 is localised in the plasma membrane and it thought to exist as a hexamer (shown here as a tetramer). STIM2 is responsible for maintaining resting levels of Ca^{2+} and so aggregates and activates Orai1 even at rest. **B-** In response to cell surface stimulation Ca^{2+} is released from the ER, this loss of Ca^{2+} from the ER is sense by STIM1, which aggregates and translocates to ER-PM junctions where it activates Orai1. Once activated Orai1 opens permit the influx of Ca^{2+} from the extracellular milieu.

Adapted from (162)

37

The mechanism by which STIM1 activated Orai1 was not clear immediately after the discovery of the two proteins. A simplified schematic diagram of the changes that occur to STIM1 and Orai1 during SOCE is shown in figure 1.4. It demonstrates the dispersed expression of STIM1in the ER membrane at rest and the translocation to ER-PM junctions, closely apposed to Orai1 after ER store depletion. It was known that the two proteins colocalised and were localised at ER-PM junctions (163,164). Whether the two proteins directly interacted or not was highly controversial for a period of time. Studies using confocal Förster resonance energy transfer (FRET) microscopy measured the interaction between fluorescently tagged Orai1 and STIM1. Orai1-CFP (cyan fluorescent protein) and STIM1-YFP (yellow fluorescent protein) were co-expressed in HEK293 cells and FRET measurements were made, FRET interactions dramatically increased upon depletion of ER stores by either thapsigargin or ionomycin (165). This supported the idea that STIM1 physically interacts with Orai1 (165,166). Upon store depletion, Ca^{2+} dissociates from the EF hand on STIM1 catalysing the oligomerisation of STIM1 (167); this step precedes the activation of Orai1 at the plasma membrane. STIM1 dimers can form without the cytosolic domain of STIM1 (168), in response to Ca^{2+} depletion. However aggregates of STIM1 are only stable when, in the very least, the CRAC activation domain (CAD) of STIM is present (169), meaning that the CAD domain of STIM1 mediates the oligomerisation of STIM1 but also binds to the N- and C-terminus of Orai1and activates it (170,171). STIM1 has a diffuse localisation in resting cells, with replete Ca^{2+} stores, which upon store depletion oligomerises before diffusing through the ER to the ER-PM junctions where they form puncta (172).

STIM1 and Orai1 form the minimal required constituents for CRAC channel activation and Ca^{2+} entry (163,171,173) but many other proteins have been found to play a role in the modulation of CRAC channel activity such as: the CRAC regulator 2A (CRACR2A) (174), SARAF (175) and calmodulin (176) are a few STIM1 binding proteins. In addition calmodulin also binds Orai1 (159,177) as does CRACR2A. Several other modulating proteins of CRAC channels have also been identified and are well reviewed by Prakriya and Lewis (127).

CRAC channels are highly conserved from yeast to humans (138,178) further emphasising the importance of store-operated Ca^{2+} entry to cells in physiology. Dysregulation in Ca^{2+} homeostasis is the precursor to many diseases as noted in section 1.1, more specifically dysregulation in store-operated Ca^{2+} entry has also been implicated in Alzheimer's disease (179), Cancer (180–182) and many diseases of the immune system (183–186). As early as

2000 (187) store-operated Ca^{2+} entry, which is now known to be mediated by the STIM1/Orai1 pathway, was identified as a potential therapeutic target for acute pancreatitis. It was noted by authors that supramaximal stimulation of cells resulted in a global and sustained increase in cytosolic Ca^{2+} that persisted until extracellular Ca^{2+} was removed, thus preventing further Ca^{2+} entry. By preventing Ca^{2+} re-entering cells, PMCA and SERCA can efficiently extrude elevated Ca^{2+} from the cytosol and reduce Ca^{2+} back to pre-stimulation levels. It was concluded that inhibiting Ca^{2+} entry would be an "attractive therapy for prevention of premature protease activation" (187). Orai1 and STIM1 expression in pancreatic acinar cells has since been reported (80). As seen in other cell types STIM1 has a dispersed localisation on the ER membrane of unstimulated pancreatic acinar cells, upon store depletion it translocates and forms puncta in sub-plasma membrane locations in the basolateral poles of the cells. The puncta formed by STIM1 colocalise with Orai1 (80). Ca^{2+} entry across the basolateral pole of the acinar cells serves to refill the ER stores after store depletion (74), the ER Ca^{2+} tunnel hypothesis indicates that Ca^{2+} uptake into the ER by SERCA in the basolateral region of the cell would then be tunnelled through the ER towards the apical region where it can be released through IP$_3$R and provide the signal for continued exocytosis (74). Once cell surface receptor stimulation has ceased, Ca^{2+} continues to enter the basolateral region of the cell to be taken up into the ER, store depletion status is still monitored by STIM1 and upon completion of refilling STIM1 is deactivated and re-translocates to a disperse expression across the ER membrane and Orai1 is no longer activated and open, as such Ca^{2+} influx also ceases.

1.5.1 Pharmacology of CRAC channels

As sustained activation of Orai1 and STIM1 mediated store-operated Ca^{2+} entry has been implicated in many different diseases, CRAC channels have been identified as a potential therapeutic target (183). The limiting factor has been and remains to be the lack of specific inhibitors of CRAC channels. Trivalent ions, such as lanthanum (La^{3+}) and gadolinium (Gd^{3+}), are very potent inhibitors of CRAC channel mediated Ca^{2+} entry, inhibiting at low nanomolar concentration. In addition to inhibiting Ca^{2+} entry mediated by CRAC channels the lanthanides also have non-specific effects on other Ca^{2+} entry channels like voltage-gated Ca^{2+} channels (188), non-specific cation channels (189) and potentially the PMCA (190), but at slightly higher concentrations. The mechanism by which Gd^{3+} ions block CRAC channels is by preventing Ca^{2+} from accessing the selectivity filter and pore of the channel, preventing

Ca^{2+} ion permeation (191). Due to the non-specific effects of the lanthanides their use in the development of further CRAC channel inhibitors is limited.

2-aminoethyl diphenylborinate (2-APB), originally developed as an IP_3R antagonist, was noted to inhibit CRAC channels (192). It was further noted that 2-APB had a biphasic action on CRAC channel currents (193); this is detailed further in chapter 3. Despite the ability of 2-APB to inhibit CRAC channel mediated Ca^{2+} entry, it was found to have numerous off-targets effects which rendered it unusable as a therapeutic agent, although it is a useful pharmacological tool in the laboratory, particularly due to its differential action on the different Orai isoforms. 2-APB it is capable of potentiating Ca^{2+} influx mediated by Orai1 and Orai2 at low doses and inhibit Orai1 and Orai2 at higher concentrations, whereas it can activate Orai3-mediated Ca^{2+} influx in a store-independent manner (193,194).

There are a plethora of pyrazole derived compounds that have been designed to target CRAC channels and these compounds have been used extensively *in vitro* (195,196). The pyrazole derivatives were originally developed as immunosuppressive agents, as those that were used clinically, such as cyclosporine A, were associated with nephrotoxicity and neurotoxicity (197). 3,5-bistrifluoromethyl pyrazole (BTP) compounds blocked the translocation of NFAT from the cytoplasm to the nucleus. When this was investigated further it was found to be due to an inhibitory effect on Ca^{2+} influx through CRAC channels. BTP2 or YM-58483 inhibited Ca^{2+} influx induced in Jurkat T cells in a dose-dependent manner, although used at doses of 10 nM only when it was used at doses of 1 µM was a remarkable inhibition of Ca^{2+} influx observed. When cells were pre-treated with BTP2 for one minute the observed IC_{50} was 100 ± 40 nM (198). In another experiment where peripheral blood lymphocytes were used, cells were pre-treated with 100 nM BTP2 for 24 hours before the experiment, however even this was not sufficient to entirely inhibit store operated Ca^{2+} entry (199). It was also shown to affect other channels that permit Ca^{2+} entry into the cell, BTP2 was shown to activate TRPM4 at low nanomolar concentration, a Ca^{2+} activated non-selective cation channel (200), this action rendered it unusable clinically, despite its preferential targeting of CRAC channels over inwardly rectifying K^+ channels, PMCA and voltage-gated Ca^{2+} channels (198,199).

Synta 66 is structurally very similar to BTP2 and was also demonstrated to be a CRAC channel inhibitor in RBL-1 cells (201) - a mast cell line, in Jurkat T cells and RBL-2H3 cells (202). The IC_{50} for Synta 66 in RBL-1 cells was 3 µM, and in RBL-2H3 cells it was measured to be 1.4 µM. Pre-treatment for 5 minutes with 10 µM Synta 66 was sufficient for

nearly complete inhibition of CRAC channel current (201). It was found that 10 μM Synta 66 had no effect on PMCA or inwardly rectifying K^+ currents, two major ion transport mechanisms in the plasma membrane of mast cells. However, in vascular smooth muscle cells Synta 66 was particularly potent at inhibiting CRAC channels between, the IC_{50} was between $26 - 43$ nM, however it appears that this study utilised 200 μM Ca^{2+} in the extracellular solution (203), which is 10 fold smaller than other experiments, thus resulting in a reduced driving force for Ca^{2+} to cross the membrane (201). Overall Synta 66 has a relatively high IC_{50} compared to BTP-2, so similarly would be of limited clinical use, but together the two compounds present ideal candidates from which chemists could develop new inhibitors (183).

Pyrazole derivatives have been particularly efficient as CRAC channel inhibitors but the specificity of the inhibitors for the CRAC channel only has always been limited. A novel compound GSK-7975A has been reported (130,204–207) to completely inhibit CRAC-mediated Ca^{2+} influx with a high degree of specificity within its therapeutic dose range (low micromolar) for further details see chapter 3.

1.5.2   AnCoA4 inhibition of Orai1

Using a technique known as a small molecule microarray (SMM) assay several drugs were identified as inhibitors of SOCE. SMM assays are a general binding assay that, compared to other assays used in high-throughput screens for drug development, requires little prior knowledge of protein structure or function (208). In SMM arrays nanolitres of organic compounds are arrayed onto glass slides and then incubated with the protein of interest. The protein of interest is conjugated to a fluorescent probe, in order that an interaction of the protein with the small molecule can be visualised (208).

In a SMM assay study the known minimal functional domains of STIM-1 and Orai1: the (CAD of STIM-1 and the N-terminal, the C-terminal and the 2-3 loop domains of Orai1 individually, were used to screen 12,000 small molecule compounds. STIM-1 CAD and Orai1 N-terminal, C-terminal and 2-3 loop were all conjugated to glutathione S-transferase (GST) and visualised using anti-GST fluorescent antibodies (209). Of the 12,000 compounds screened, 120 were found to bind to the Orai1 peptides and 51 of these compounds were commercially available and as such utilised in further testing. HEK293T cells were used to test the effects of the compounds in intact cells and an NFAT reporter gene assay was used. When SOCE occurs NFAT is dephosphorylated and is activated, as such an NFAT assay can

be used as readout of SOCE activity. The 51 commercially available compounds were applied to HEK293T cells at a concentration of 50 µM for 6 hours in the presence of 1 µM thapsigargin to activate SOCE, after which the NFAT-luciferase expression levels were measured. From the 51 compounds tested in intact cells four compounds were identified as having an inhibitory effect on the activation of the NFAT-luciferase reporter gene suggesting an inhibitory effect on Orai1. Of these four compounds AnCoA4 was identified as the most efficient inhibitor of Orai1 with an EC_{50} of 880 nM. AnCoA4 was found to bind directly to the C-terminal of Orai1 and prevented STIM1 binding. A fluorescence aggregation assay was used, in which mCherry constructs of the minimal functional domains of Orai1 were employed. Protein aggregation quenches the mCherry fluorescence, therefore compounds that bind the protein prevent aggregation and subsequent quenching, thereby increasing mCherry fluorescence. AnCoA4 is more efficient when pre-incubated with cells, before the recruitment of STIM1 to ER-PM junctions during store depletion, suggesting it is a competitive inhibitor of Orai1(209). This hypothesis was confirmed by an experiment in which an Orai1 mutant, that is constitutively active in the absence of STIM1, was inhibited by AnCoA4, confirming that AnCoA4 binds to the site of Orai1 responsible for channel gating and the interaction with STIM1.

1.5.3 Transient receptor potential channels

Transient receptor potential (TRP) channels is a large family of ion channels that are ubiquitously expressed by mammalian cell types. As a family they share a common primary structure and are all permeable to monovalent ions and/or Ca^{2+} (189). All TRP channels have six transmembrane domains that likely form tetramers, evolutionary they are from the same type of channel as voltage gated K^+ channels. The family is divided into sub-types based on sequence homology, the sub-types are: the canonical subtype - TPRC channels, the vanilloid subtype – TRPV channels, the melastatin subtype – TRPM channels and the mucolipin subtype – TRPML channels are some of the subtypes. TRP channels, specifically TRPC1, TRPC3 and TRPV6 channels were thought to be the plasma membrane component involved in store-operated Ca^{2+} entry (210–212), before the molecular identification of Orai1 was made. These three channels are all Ca^{2+} permeable.

Store-operated Ca^{2+} entry mediated through the Ca^{2+} selective CRAC channels is the major pathway through which Ca^{2+} enters non-excitable cells, however Ca^{2+} entry through non-selective cation channels still contributes towards an elevation in cytosolic Ca^{2+} and there is evidence of store-operated Ca^{2+} channels with biophysical properties distinct from that of

CRAC channels (138). TRPC channels typically generate non-selective cation currents. The TRPC channels are all activated in response to PIP_2 hydrolysis, due to stimulation of other cell surface receptors. Activation of TRPC channels by store-depletion is surrounded by a substantial amount of controversy in the field, some TRPC channels are activated in a store-independent manner, whereas evidence surrounding TRPC1 or TRPC3 channels is somewhat contradictory, with evidence indicating that TRPC1 and TRPC3 might serve as subunits in store-operated Ca^{2+} channels and are gated by STIM1 (213–215).

There is a lot of evidence supporting a role for TRPC1 and TRPC3 as subunits of store-operated Ca^{2+} channels, these papers utilise TRPC1 and TRPC3 channels in over-expression systems in many different cell types, from cell lines (216) to submandibular salivary gland cells (217). Knockdown of TRPC1 was performed utilising antisense oligonucleotides targeted against the protein, this knockdown resulted in a reduction in store-operated Ca^{2+} entry (217). It was found by knocking out TRPC1 in mice there was a reduction in store-operated Ca^{2+} entry induced by thapsigargin-mediated store depletion in salivary glands (218). Expression of the TRPC3 channel has been reported in pancreatic acinar cells (219). Knockout of TRPC3 in these cells or pharmacological inhibition of TRPC3 leads to a reduction in store-operated Ca^{2+} entry induced by thapsigargin-mediated store depletion (220,221).

The store-operated nature of TRPC channels is highly contested in the field (183), there is evidence that TRPC1 binds to and is activated by STIM1, in turn TRPC1 forms heteromultimers with TRPC3 and as such confers STIM1 dependence to TRPC3 (222), but this view is not held by all in the field.

1.6   Acute pancreatitis

Acute pancreatitis is a human disease characterised by inflammation, oedema and necrosis of pancreatic tissue (223). In England between 2013 and 2014 there were 25,000 hospital admissions for acute pancreatitis (224). In the United States acute pancreatitis was the most common gastrointestinal diagnosis with 275,000 admissions to hospital in 2009 (225). Patients admitted to hospital experience severe abdominal pain, nausea and vomiting and a fever (224). The major causes of acute pancreatitis are gallstones and excessive alcohol intake, there are some links to an increased incidence of acute pancreatitis including heavy smoking of cigarettes, hypertriglyceridemia and some drugs such as asparaginase.

Furthermore there are some genetic links to acute pancreatitis (226,227). In 10-20% of cases no known cause is found, despite recurrent attacks (228).

Most cases of acute pancreatitis resolve by themselves which is fortunate as there is no current specific therapy for acute pancreatitis. Typically the inflammation associated with acute pancreatitis is local but in some cases there is a systemic inflammatory response which impacts on the functioning of other organs (228). There is a 15 to 20 % risk of mortality due to organ failure, either the pancreas or a distant organ (228). One incidence of acute pancreatitis is linked to recurrent episodes of the acute form of the disease, recurrent episodes are linked with chronic pancreatitis, which has long term effects on the health of both the exocrine and endocrine pancreas, with implications in the development of diabetes and also pancreatic cancer (229).

As early as 1896 acute pancreatitis was attributed to the inappropriate, premature activation of pancreatic digestive proenzymes within pancreatic acinar cells (7), rather than after exocytosis from the cell and release from the pancreatic ducts into the duodenal lumen by enterokinase (84). The primary function of the exocrine pancreatic acinar cells is the synthesis of digestive proenzymes which are stored in the apical region of the cells in zymogen granules (230), however pathological stimuli can lead to intracellular activation of these enzymes, in the apical region of the cell, resulting in digestion of the acinar cell and surrounding tissue (231). The digestion results in cellular necrosis and release of the cell contents including digestive enzymes, resulting in further digestion of pancreatic acinar cells - this is known as autodigestion (223). Pancreatic injury results in inflammation, oedema, infiltration of leucocytes and necrosis (232). Pancreatic acinar cells themselves release inflammatory mediators in response to pancreatic injury such as tumour necrosis factor-α. (TNF-α) (233) and interleukin-6 (IL-6). The release of TNF-α results in the recruitment of more leucocytes to the site of injury, primarily these leucocytes are neutrophils and macrophages that, in turn, also release TNF-α which serves to amplify the inflammatory signal resulting in further recruitment of immune cells. Dendritic cells and T-cells are also recruited, but T-cells are recruited in much smaller numbers than the innate immune cells (232).

As noted, physiological secretion of digestive enzymes is coupled to an increase in cytosolic Ca^{2+} in an oscillatory pattern (100). The premature, intracellular activation of digestive enzymes, which ultimately leads to necrotic cell death of acinar cells, is also coupled to

intracellular Ca^{2+} release (234). The distinction between the physiological and pathophysiological outcomes is the spatio-temporal profile of the intracellular Ca^{2+} signal. Exocytosis of digestive enzymes is preceded by short-lasting, repetitive, transient oscillations in cytosolic Ca^{2+} localised to the apical pole of the acinar cell (23,100); whereas pathological intracellular activation of enzymes is preceded by a sustained global elevation in cytosolic Ca^{2+} due to emptying of intracellular stores and the subsequent Ca^{2+} entry from the extracellular space (7,187,235).

1.6.1 Alcoholic acute pancreatitis

Excessive alcohol intake has also been extensively implicated as a major cause of acute pancreatitis (231,236–239). A recent increase in hospital admissions for acute pancreatitis (239) has been positively correlated with an increase in chronic alcohol consumption and also binge drinking (239). Alcohol intake in excess of 4 drinks per day results in more than a doubling in the risk of developing pancreatitis (both acute and chronic forms) (240). Acute alcohol ingestion alone was insufficient to cause acute pancreatitis in a rat (241), further agents such as CCK were required to cause acute pancreatitis (242); suggesting that alcohol consumption may sensitise the pancreas to other triggers of acute pancreatitis (243). However, chronic administration of alcohol resulted in alterations to pancreatic morphology in animal model, such as lipid droplet accumulation, protein plugs in pancreatic ducts and sclerosis (244). Not all heavy drinkers develop acute pancreatitis, which is likely in part because when ethanol is applied to intact isolated pancreatic acinar cells, even in very high concentrations (850 mM), only a modest increase in cytosolic Ca^{2+} was elicited (237); in line with effects observed in rats fed with alcohol alone (241,242). There are evidently other factors involved in alcoholic acute pancreatitis.

There is evidence to suggest that excessive alcohol intake combined with a particularly fatty diet could be the most dangerous risk factor in developing acute pancreatitis (245). Pancreatic acinar cells express fatty acid ethyl ester (FAEE) synthases, which are enzymes that synthesise FAEE from ethanol and free fatty acids (246), which is the non-oxidative metabolism of alcohol in the pancreas. The oxidative metabolism of alcohol is mediated by alcohol dehydrogenase which produces acetaldehyde (247), there is evidence indicating that high concentrations of acetaldehyde can damage the pancreas of some species (248) but this does not appear to be the case in other experiments (248). Carboxylester lipase is a FAEE synthase that is synthesised in the acinar cell and stored in zymogen granules in the apical region of the cell (249). In autopsies of patients who have abused ethanol, FAEEs were found

45

in high concentrations in the pancreas and liver due to the high concentration of FAEE synthases in these organs (236).

The non-oxidative alcohol metabolites FAEEs have been implicated in mediating alcoholic acute pancreatitis by initiating a global, sustained increase in cytosolic Ca^{2+} concentration, that is responsible for prematurely activating digestive proenzymes; whereas the oxidative metabolite of alcohol, acetaldehyde, did not result in elevations in cytosolic Ca^{2+} (237). FAEEs when applied to pancreatic acinar cells induced significant cellular necrosis, but equivalent concentrations of acetaldehyde did not (237,250).

FAEEs have been shown to be toxic *in vivo*, in addition to the toxic effects that were observed during *in vitro* experiments. FAEE administration resulted in an increased trypsinogen activation, pancreatic oedema and vacuolisation of cytoplasm, indicating the presence of fats (251). It was demonstrated that it was the non-oxidative metabolite of ethanol and fats that was mediating the toxic effect of ethanol on pancreatic acinar cells as opposed to ethanol alone or its oxidative metabolite acetaldehyde (237). Palmitoleic acid (POA) ethyl ester (POAEE), one form of FAEE, when applied to pancreatic acinar cells gave rise to large and sustained increases in cytosolic Ca^{2+} concentration, that were concentration dependent in nature. This increase in cytosolic Ca^{2+} was due to IP_3R activation and Ca^{2+} release from the ER (252). Subsequent activation of store-operated Ca^{2+} entry mechanisms drove the sustained elevation in cytosolic Ca^{2+}, the increase was reversed when Ca^{2+} was removed from the extracellular solution (237) and when cells were treated with the CRAC channel inhibitor GSK7975-A *in vitro* (130) or *in vivo* application of GSK7975-A (253). POAEE was found to deplete the cell's ATP supply, resulting in the failure of the ATP-dependent pumps and ultimately necrosis of the cell (252).

The fatty acid, POA, itself elicited a substantial increase in cytosolic Ca^{2+} levels and induced cell death, the increase in cytosolic Ca^{2+} was slower than when elicited with POAEE (237). The cytosolic Ca^{2+} increase induced by POA was not reversed by the removal of extracellular Ca^{2+} unlike the Ca^{2+} rise elicited by POAEE (237) and furthermore was not inhibited by caffeine (252), suggesting that it is not driven by IP_3R-mediated Ca^{2+} release or store operated Ca^{2+} entry. The effects of POA and POAEE on cytosolic Ca^{2+} are likely due to their known uncoupling effect on oxidative phosphorylation (252,254), resulting in a decrease in mitochondrial ATP production and therefore impaired SERCA and PMCA activity. With an insufficient supply of ATP SERCA is unable to sequester Ca^{2+} back into the ER and balance

the passive leak; PMCA is unable to actively pump Ca^{2+} across the plasma membrane to counteract store-operated Ca^{2+} entry. In addition to impaired SERCA and PMCA activity, the vacuolar H^+-ATPase in no longer able to maintain the high concentration of Ca^{2+} in the acidic stores and so that store of Ca^{2+} is also released (238). In addition to the effect of POA and POAEE on mitochondrial ATP production, it has also been demonstrated that ethanol itself depolarises the mitochondrial membrane (255).

Application of low doses of ethanol and POA were demonstrated to elicit oscillatory increases in cytosolic Ca^{2+} that were converted to global sustained increases in cytosolic Ca^{2+} by using 4-MP to block oxidative metabolism of alcohol, preventing the formation of acetaldehyde. Further experiment in which the non-oxidative pathway was blocked using an inhibitor of carboxylester lipase, preventing the synthesis of FAEE, resulted in almost no increase in cytosolic Ca^{2+} (250). In the human disease it would appear the FAEE are responsible for mediating the toxic effects of alcohol in the development of acute pancreatitis (236,237,251–253) and as a model of acute pancreatitis administration of ethanol has minimal injurious effects on the pancreas (244) a model in which animals are administered free fatty acids and ethanol is a simple and elegant way to induce acute pancreatitis (250). Analysis of this model indicated that the treatment induced pancreatic damage, histological staining demonstrated pancreatic cell oedema, neutrophil invasion and pancreatic acinar cell necrosis, furthermore there was an increase in serum amylase and trypsin (250). *In vivo* inhibition of the oxidative metabolic pathway of alcohol worsened the damage to the pancreas, whereas inhibition of the non-oxidative metabolic pathway of alcohol ameliorated the damage to the pancreas.

1.6.2 Biliary acute pancreatitis

Gallstones form in the gallbladder and are a mixture of cholesterol and bile salts, they are often asymptomatic. Although they form in the gallbladder they may pass into the cystic duct which joins the common hepatic duct and drain into the common bile duct. Further down the common bile duct is the junction at which the pancreatic duct joins, this junction is known as the ampulla of Vater. This is one site of gallstone blockage and results in the reflux of bile into the pancreatic duct (256); because the opening from the common bile duct into the duodenum is blocked there is retrograde flow of bile up the common bile duct or along the pancreatic duct, this can be referred to as the "common channel theory" of acute pancreatitis (223). Another potential site for a gallstone to get lodged is in the pancreatic duct, this would not result in bile reflux into the pancreatic duct as it is blocked but it would result in

pancreatic ductal hypertension which could result in acinar cell injury (231). There is evidence that this can cause necrotising pancreatitis in some species but not in others, it is unclear whether it can cause necrotising pancreatitis in humans (223). There is significantly more evidence to support the common channel or bile reflux theory as a cause of acute pancreatitis (257).

Bile salts are toxic to pancreatic acinar cells, they can be taken up by acinar cells by transporters localised on the basolateral membranes of cells (258). Bile acids such as taurolithocholic acid 3-sulfate (TLC-S) have been demonstrated to elicit increases in cytosolic Ca^{2+} that increased with increasing concentration of bile acid (259). Some cells responded to TLC-S application with oscillatory Ca^{2+} signals and others with sustained increases; the proportion of cells that responded with sustained increased in cytosolic Ca^{2+} increased with increasing concentration of bile acids (259). When used *in vitro* TLC-S as well as other bile acids such as: sodium taurocholate and taurochenodeoxycholate all elicited large sustained increases in cytosolic Ca^{2+}(258,259), in a concentration dependent manner. The initial Ca^{2+} signal was derived from ER Ca^{2+} release, the sustained elevation of cytosolic Ca^{2+} was sourced from the extracellular milieu, removal of Ca^{2+} from the extracellular solution resulted in a rapid reduction of intracellular Ca^{2+} and return to baseline values, in the continued presence of bile acids. When TLC-S was applied to cells in Ca^{2+} free extracellular solution oscillatory Ca^{2+} signals were observed, indicating that the source of Ca^{2+} for the initial signal is derived from an intracellular source that is IP_3 sensitive, highlighted by the lack of response to TLC-S in the presence of caffeine (259). Experiments demonstrating that the removal of extracellular Ca^{2+}, in the maintained presence of TLC-S, caused a decrease in intracellular Ca^{2+} concentration (259) were supported by experiments in which bile acid increased the rate of Mn^{2+} influx which is indicative of unidirectional Ca^{2+} influx (258,260,261). Elevated cytosolic Ca^{2+} gets taken up by mitochondria and cause mitochondrial dysfunction, resulting in impaired ATP production and in the long-term provides the trigger for apoptosis and necrosis (223).

As bile acids are known to have detergent properties (262), it is often thought that their toxic effects on acinar cells are mediated by permeabilisation of the plasma membrane and the lysis of the cell rather than an interference with the cell signalling pathway in intact cells (258). The retrograde flow of bile through the pancreatic duct was found to be at an insufficient pressure, which would result in bile acids being present at insufficiently high concentration to cause pancreatic damage through detergent properties (263). Extensive damage of the plasma

membrane of cells exposed to bile acids *in vitro* was not observed, no leakage of fluorescent indicators suggests that the membrane integrity of cells remained intact (264) except when used at concentrations more than 10 times higher than was found to activate store-operated Ca^{2+} influx (258).

The role of Ca^{2+} influx, specifically CRAC channel mediated Ca^{2+} influx, in driving the sustained plateau in cytosolic Ca^{2+} concentration induced by bile acids was recapitulated *in vivo* in a mouse model of biliary acute pancreatitis. In this mouse model retrograde perfusion of the pancreatic duct with TLC-S was used to induce acute pancreatitis (253,265), it was adapted from a similar model used in rat pancreas that had previously never been successful in mouse (257). Retrograde perfusion of the pancreatic ducts with TLC-S induced an increase in serum amylase and trypsin concentration, IL-6 concentration and concurrently increased pancreatic oedema, inflammation, necrosis, as observed by histological staining. Orai1 inhibitors GSK-7975A and CM128 were found to be successful in ameliorating several hallmarks of acute pancreatitis exhibited by this mouse model, including reducing the TLC-S induced increase in the aforementioned hallmarks of acute pancreatitis (253).

In addition to liberating Ca^{2+} from IP_3 sensitive intracellular stores, bile acids have also been demonstrated to reduce ER store content, due to bile acid inhibition of the SERCA pump (258). This was not due to an alteration in ATP concentration, as at this concentration bile acids did not affect the level of ATP production, at higher concentrations of bile acids however, ATP production was affected (258). The previous experiments, in this paragraph were undertaken using a mixture of bile acids, TLC-S alone, at even very low concentrations 10 μM such as were unlikely to cause any notable increase in cytosolic Ca^{2+} concentration, was found to depolarise the mitochondrial membrane. High concentrations of TLC-S resulted in incredibly large membrane depolarisation, to a similar extent to the positive control CCCP (carbonyl cyanide m-chlorophenylhydrazone). Buffering of cytosolic Ca^{2+} with the fast acting chelator 1,2-bis(*o*-aminophenoxy)ethane-*N*,*N*,*N'*,*N'*-tetraacetic acid (BAPTA) prevented the depolarisation of the mitochondrial membrane observed with low concentrations of TLC-S (266).

1.6.3 Therapeutic targets for AP

As there are no current specific therapies for the treatment of acute pancreatitis, and it is the single most diagnosed gastrointestinal disease for which patients are admitted to hospital (239,267) it is prudent to consider targets for drug development.

The CRAC channel has already been identified as an ideal target in the treatment of acute pancreatitis (187). It is the channel through which Ca^{2+} enters the cytosol from the extracellular milieu, the source of the Ca^{2+} that drives the cytosolic Ca^{2+} overload that activates digestive proenzymes intracellularly, resulting in the onset of acute pancreatitis. Some strides have been made in focusing on this target in the treatment of acute pancreatitis (130,253,268) but also there is a keen interest in the development of CRAC channel inhibitors, as CRAC channel activity has been implicated in other diseases such as asthma and cancer (183) (for more information see section 1.5.1 and chapter 3).

Store operated Ca^{2+} entry is preceded by Ca^{2+} release from ER via IP_3R and RyR, without the depletion of Ca^{2+} from the ER the CRAC channels would not be activated, as such one way of preventing cytosolic Ca^{2+} overload during acute pancreatitis is to prevent Ca^{2+} release from the ER stores in the first instance. Some success via this pathway has been seen, using the calmodulin activating peptide CALP3 (7), as calmodulin is involved in the regulating of several mechanisms by which Ca^{2+} can enter the cytosol through IP_3R (17,269) (for more information see chapter 4).

Mitochondrial dysfunction has been shown to be a key event in the pathology of acute pancreatitis induced by FAEE (252) and by bile acids such as TLC-S(270). Cytosolic Ca^{2+} overload leads to mitochondrial Ca^{2+} overload; mitochondrial Ca^{2+} overload results in the opening of the mitochondrial permeability transition pore (MPTP), which permits molecules up to 1.5 kDa to enter the mitochondria, resulting in the loss of mitochondrial membrane potential which drives ATP production (271). With insufficient ATP production the Ca^{2+} ATPases are inactive, SERCA and PMCA cannot actively pump Ca^{2+} into the ER and across the plasma membrane, respectively. Cyclophilin D is an important regulator of the MPTP, loss of cyclophilin D resulted in improved cell survival (272) due to protection from Ca^{2+} overload, cells were particularly protected from necrotic cell death (273). In the cyclophilin D knock out cells the MPTP was more resistant to opening, and therefore the mitochondrial membrane was not depolarised and the cell did not undergo necrosis due to ATP depletion (255). Pancreatic acinar cells from cyclophilin D knockout mice did not exhibit the dramatic mitochondrial membrane depolarisation after ethanol treatment that wild type acinar cells did. Wild type cells incubated with ethanol and CCK demonstrated high levels of necrosis; the necrosis levels were reduced to wild type control levels (in absence of ethanol and CCK) in the presence of ethanol and CCK in the cyclophilin D knockout acinar cells (255). These experiments highlight the importance of cyclophilin D as a target in

diseases in which a hallmark is cellular necrosis, such as acute pancreatitis. Ethanol and CCK were used to induce alcoholic acute pancreatitis in mice, and in cyclophilin D knockout mice, the levels of necrosis were reduced, ATP levels were higher, serum amylase and trypsin levels were reduced, indicating protection against the hallmarks of acute pancreatitis. Small molecule inhibitors of cyclophilin D have been developed and one molecule has been found to have promise, it protected the mitochondrial membrane potential that is depolarised upon the application of TLC-S, it also reduced necrosis in both murine and human pancreatic acinar cells (274).

Caffeine has been demonstrated to prevent IP$_3$R-mediated Ca^{2+} release in vitro (53,275). This is thought to be due to an inhibition of phospholipase C-mediated production of IP$_3$. Caffeine and some of its metabolites were tested for their efficacy in inhibiting signals induced by various agents, including TLC-s. Caffeine inhibited signals induced by 500 μM TLC-S in a dose dependent manner. *In vivo* treatment of mouse models of acute pancreatitis with caffeine ameliorated most hallmarks of acute pancreatitis. In these mouse models acute pancreatitis was induced by several different agents: Caerulin, TLC-S and ethanol and POA. Even when caffeine treatment was not started for 24 hours after acute pancreatitis is induced, it was still effective in preventing a lot of the biochemical hallmarks of acute pancreatitis (275). This makes it a promising agent as patients often do not receive treatment within 48 hours after the onset of the disease process.

As the cause of pancreatic necrosis is the activation of digestive proenzymes, one strategy for treating acute pancreatitis is to administer protease inhibitors (276), this was utilised in randomised controlled trials to treat patients with severe acute pancreatitis. It was found to be a promising intervention in observational studies, small trials (277) and one randomised controlled trial (278) but a meta-analysis of many trials involving the intravenous infusion of protease inhibitors found that there was no significant difference in the mortality rate of patients suffering from acute pancreatitis who were treated with protease inhibitors compared to those patients who were not treated (279). This could be due to the fact that inhibiting activated proteases is too far downstream of the initial cellular mechanism that triggered the chain of events, which would indicate trials involving pharmacological agents with actions at an early stage of the pathology are necessary, such as those that are targeted towards Ca^{2+} signalling (276).

As acute pancreatitis is an inflammatory disease, one strategy to treat it has been the use of anti-inflammatory and immune-modulating agents. The recruitment of leucocytes to the site of pancreatic injury has been positively correlated with the severity of acute pancreatitis (280–283). For example a TNF-α antibody was used successfully to reduce acinar cell necrosis by preventing trypsinogen activation by neutrophils (284). A further benefit to this strategy of intervention is that the recruitment of leucocytes to the pancreas has been implicated in the activation of pancreatic stellate cells which are involved in fibrosis of the pancreas, a hallmark of chronic pancreatitis (190). Despite the testing of many different inhibitors of pro and anti-inflammatory agents, no one agent has been successful in clinical trials (232,282).

1.7   Aims of thesis

It is known that store-operated Ca^{2+} entry plays a role in the onset of acute pancreatitis due to its contribution to elevating cytosolic Ca^{2+}, regardless of the initial stimulus that elicits ER Ca^{2+} release. By contributing to cytosolic Ca^{2+} elevation, store-operated Ca^{2+} entry sustains cytosolic Ca^{2+} overload which results in the activation of the digestive proenzymes inside the pancreatic acinar cells and resultant cellular necrosis. Inhibition of the channels that are activated by store depletion means that this mechanism of elevating cytosolic Ca^{2+} is also inhibited. One aim of this thesis was to determine if there are any inhibitors that can maximally inhibit store-operated Ca^{2+} at lower concentration than GSK-7975A which has already been demonstrated to inhibit CRAC channel mediated Ca^{2+} influx. Such an inhibitor should be effective at low concentrations, sub-micromolar ideally, with minimal off-target effects. A second aim of this thesis was to determine if modulating calmodulin would be an effective method in reducing store-operated Ca^{2+} entry. This will be achieved through the use of both pharmacological agents and overexpression on mutant calmodulin protein.

2   Materials and Methods

2.1   Buffers and Solutions

2.1.1   Preparation of NaHEPES solution.

NaHEPES based extracellular solution containing: 140 mM NaCl, 4.7 mM KCl, 10 mM HEPES (4-(2-Hydroxyethyl)piperazine-1-ethanesulfonic acid), 1 mM $MgCl_2$, 10 mM glucose (pH adjusted to 7.2 with NaOH). NaHEPES was supplemented with 1 mM $CaCl_2$ for pancreatic acinar cell isolation. All above reagents were obtained from Sigma-Aldrich.

2.1.2   Preparation of Collagenase solution.

Collagenase (Worthington Biochemical Corp, NJ, USA) was prepared using fresh NaHEPES solution supplemented with 1 mM $CaCl_2$. Collagenase (4000 U) is dissolved in 20ml of NaHEPES, stored in 1ml aliquots at -20°C.

2.1.3   Preparation of Fluorescent Ca^{2+}-indicators.

Both Fura-2 acetoxymethyl ester (AM) (cat. F-1201) was obtained from Molecular Probes, Life Technologies, Paisley UK. It was prepared in DMSO at stock concentrations of 2 mM, aliquoted and stored at -20°C and was protected from light.

2.1.4   Reagents.

GSK-7975A was initially obtained from GlaxoSmithKline, Stevenage, UK. It was prepared, in DMSO, at a stock concentration of 10 mM, aliquoted and stored at -20 ˚C.

RO2959 was obtained from Glixx Laboratories (cat. GLXC-01511), Southborough, MA, USA. It was prepared in DMSO at stock concentration of 10mM and was stored at -20 ˚C and was protected from light.

Pyr3 was obtained from Sigma-Aldrich (cat. P0032), Dorset, UK, as were Calmidazolium Chloride (cat. C3930) and Chymostatin (cat. C7268). These reagents were prepared in DMSO at stock concentration of 10 mM, aliquoted and stored at -20 ˚C for no more than three months. Soybean trypsin inhibitor was also obtained from Sigma-Aldrich. It was stored at +4 °C. It was prepared fresh at 0.01% concentration in NaHEPES and was used immediately.

Cyclopiazonic acid (CPA) was obtained from both Tocris (cat. 1235), Bristol, UK and Calbiochem (cat. 239805), Merck Millipore, Watford UK. It was prepared in DMSO at stock concentration of 20 mM and stored at -20 °C for no more than three months.

Thapsigargin (cat. 586005) was obtained from Calbiochem, Merck Millipore, Watford UK. In addition, Pyr6 and Pyr10 were also obtained from Calbiochem. These reagents were prepared, in DMSO, at stock concentration of 10 mM, it was aliquoted and stored at -20 °C for no more than three months. Calmodulin was also obtained from Calbiochem, it was prepared in NaHEPES buffer, at a stock concentration of 2mM. It was aliquoted and stored at -20 °C.

CALP-3 was obtained from both Tocris, Bristol, UK (cat. 2321) and Genscript, NJ, USA. It was prepared, in NaHEPES, at a stock concentration of 2mM, it was aliquoted and stored at -20 ˚C.

Protease inhibitor cocktail tablets (EDTA free) were obtained from Roche, Sigma-Aldrich, UK (cat. 11873580001) and were stored at +4 ˚C, it was prepared fresh using 1 tablet per 30ml NaHEPES and used immediately.

2.2   Isolation of primary pancreatic acinar cells

Wild-type C57BL/6 male mice (Charles River) aged 6 – 8 weeks old weighing 23 ± 3g were killed humanely by cervical dislocation, in accordance with the UK Schedule 1 of the Animals (Scientific Procedures) Act, 1986. The pancreas was immediately dissected, washed twice with NaHEPES (supplemented with 1 mM Ca^{2+}) and injected with collagenase solution (200 units/ml); it was then incubated in this solution at 37^0C for 15-17 minutes, depending on the activity of a particular batch of collagenase. After the incubation the pancreas was triturated, using a pipette, in NaHEPES solution (supplemented with 1 mM Ca^{2+}). Cells were collected in a tube and centrifuged for one minute at 1200 rpm. The supernatant was discarded and the cells were re-suspended in 2ml of NaHEPES solution (supplemented with 1 mM Ca^{2+}). Large pieces of tissue were allowed to settle to the bottom of the tube and then were discarded. Cells were centrifuged a second time as above, the supernatant discarded and the cells are re-suspended in 2ml of NaHEPES solution (supplemented with 1 mM Ca^{2+}).

2.3 Ca^{2+} measurements of intact cells

Intact, freshly isolated pancreatic cells were loaded with Fura-2, in AM form, at a final concentration of 3 μM for 45 minutes at room temperature. After incubation with dye, the cells were centrifuged as above, supernatant discarded and the cells were re-suspended in 2ml of NaHEPES (+1 mM Ca^{2+}) solution.

An inverted Nikon Diaphot 200 system, using a 40x oil objective was used for Fura-2 measurements. An LED imaging system was used to excite Fura-2 at 355nm and 385nm and

green emission at 510nm. In all experiments except figure 4.11 A to figure 4.19 A solutions used in experiments were perfused over cells. In the aforementioned experiments with calmodulin, the perfusion of solutions was stopped at the point that calmodulin was introduced to the chamber by hand addition. Perfusion was then restarted after the Ca^{2+} influx phase of the experiment.

Image Pro Plus software was used to collect data during real time Ca^{2+} imaging.

2.4 Culture of AR42J cells

AR42J cells are a rat pancreatic exocrine explanted tumour cell line that most closely mimic primary pancreatic acinar cells. They have a secretory phenotype and respond to the usual agonists of pancreatic acinar cells such as CCK and ACh.

The cells were maintained in DMEM medium (with glutamine and pyruvate) supplemented with 10% FBS, 10 mM HEPES, 2.5 µg/ml Fungizone and 50 µg/ml Gentamycin and were incubated at 37˚C, 5% CO_2.

2.4.1 Passaging

When cells had achieved confluency (usually 1 week after seeding 1:10). The old medium was removed from the flask and cells were washed with 10 ml PBS (warmed to 37 ˚C), PBS was removed and cells were incubated with 800 µl trypsin + EDTA for 1 minute and 30 seconds. Flask was gently tapped to remove cells that remained adhered to the culture surface. Cells were re-suspended in 10 ml DMEM (supplemented with FBS + antibiotics) and were well mixed to ensure that the clusters, that this cell type tend to form, were broken down into single cells. Cells were then re-seeded at 1:10 ratio into a new flask. Medium was refreshed once per week, in between passages.

Cells for experiments were seeded onto glass coverslips (washed in ethanol and dried under UV light), in 2 ml of supplemented DMEM medium, at the appropriate density for transfection after 48 hours, thus allowing sufficient time for cells to adhere.

2.4.2 Transfection

Cells were transfected using PromoFectin from PromoKine (cat. PK-CT-2000-50) Heidelberg, Germany. PromoFectin is a non-liposomal transfection re-agent and was used according to the manufacturer's instructions. Per 6 well plate:

Table 1 Reagents required for transfection

Medium (µl)	PromoFectin (µl)	Plasmid DNA (µg)
200	6	3

In one 1.5 ml tube, 100 µl of DMEM medium (without antibiotics or FBS) was thoroughly mixed with 6 µl PromoFectin. In another 1.5 ml tube 100 µl DMEM was thoroughly mixed with 3 µg of desired plasmid DNA. The two tubes were combined and vortexed and left at room temperature to incubate for 30 minutes. The transfection mixture was then added drop-by-drop to AR42J cells, previously seeded onto glass coverslips in a 6-well plate. Cells were incubated in the mixture for 6-8 hours at 37 ˚C and 5% CO_2, at which point the medium was exchanged for fresh supplemented DMEM and cells were left to express the plasmid for a further 72 hours, at 37 ˚C and 5% CO_2.

2.4.3 Ca^{2+} imaging experiments – AR42J cells.

Intracellular Ca^{2+} levels were measured using the ratiometric dye – Fura-2. Cells were plated on glass coverslips in 6-well plates 24-48 hours before experiments and were maintained as in section 2.4. Cells were incubated with Fura-2 in AM form (3 µM) for 30 minutes at 37˚C, 5% CO_2. Cells were then rinsed once with NaHEPES buffer and incubated in NaHEPES + 1 mM Ca^{2+} for 20 minutes at room temperature to allow for de-esterification of the dye. Coverslips were mounted onto an imaging chamber with high silicone grease, to allow for perfusion of cells.

Ca^{2+} imaging was undertaken using an imaging system (Scientifica) and images were recorded using WinFluor software (The University of Strathclyde, Glasgow, UK). Fura-2 was excited at 355nm and 380nm, every 2 seconds and emission was collected at 510nm.

Data represents normalised ratio values calculated as follows: $(\mathbf{F_{355}/F_{380}})/ \mathbf{F_0}$ which can be simplified to: $\mathbf{R/R_0}$. Data presented as mean ± standard error of the mean (SEM) number of cells (n) given.

2.4.4 Ca^{2+} imaging experiments – mCherry-CaM-AR42J cells

Cells were transfected according to the protocol in section 2.4.2, some cells were transfected with m-Cherry-CaM^{WT} and others were transfected with mCherry-CaM^{mut1,2,3,4}. On the day of experiments cells were incubated with Fura-2 according to the protocol in section 2.4.3. Ca^{2+} imaging experiments were undertaken on an inverted Leica SPE confocal microscope, Leica Microsystems, Heidelberg, GmBH. A 40x oil objective was used. mCherry was excited with 532 nm laser and emission collected at 580-610 nm. A single image of the mCherry-CaM

expression was taken prior to the experiment, to ensure Ca^{2+} imaging data was collected from cells expressing the plasmid. Fura-2 was excited using a single wavelength with the 405nm laser and emission collected at 510 nm, images were collected every 2 seconds.

As a single wavelength of Fura-2 was measured, when there was an increase in cytosolic Ca^{2+} the fluorescence of Fura-2 decreased (corresponding to the 380nm wavelength). Data represents normalised ratio values calculated as follows: **1/ (F/ F$_0$).** The reason the data was inverted was to avoid confusion upon data analysis, as an increase in cytosolic Ca^{2+} is by convention reflected by an upward deflection on a graph. Data presented as mean ± standard error of the mean (SEM) number of cells (n) given.

2.5   Store depletion protocols

2.5.1   Standard Store depletion protocol.

Cells were perfused in a nominally Ca^{2+} free solution for approximately five minutes before commencement of recording to allow them to establish an equilibrium. Store-operated Ca^{2+} entry channels the ER stores were depleted using SERCA inhibitors thapsigargin (1 µM) or CPA (10 µM) in nominally Ca^{2+} free solution. Ca^{2+} was released from the ER and cytosolic Ca^{2+} levels increased. In the continued presence of the SERCA inhibitors Ca^{2+} could not be actively transported into the ER via SERCA. Ca^{2+} was instead extruded from the cell across the plasma membrane by the PMCA. SOCE channels were activated by ER store depletion, there was no subsequent Ca^{2+} entry due to the nominally Ca^{2+} free extracellular solution. When resting levels of cytosolic Ca^{2+} were attained Ca^{2+} was re-admitted to the extracellular solution (10, 5 or 2 mM) and there was a subsequent increase in cytosolic Ca^{2+}. When maximal Ca^{2+} entry and the resultant plateau in cytosolic Ca^{2+} was attained extracellular Ca^{2+} was removed and cytosolic Ca^{2+} concentration returned to baseline levels.

2.5.2   Store depletion with pre-incubation of channel inhibitors.

Cells were treated as above, with stores depleted by either thapsigargin or CPA in nominally Ca^{2+} free solution. During this store depletion inhibitors of SOCE were applied to cells in the continued presence of either thapsigargin or CPA. Channel inhibitors such as GSK-7975A, Pyr3, RO2959, Pyr6, Pyr10, DPB162-AE and DPB163-AE were applied at the 600 second time point, during an elevation of cytosolic Ca^{2+} but during the extrusion phase of store depletion. Cells were incubated for 10 minutes with inhibitors before the subsequent re-admission of Ca^{2+} to the extracellular solution, in the continued presence of the inhibitor. As before, when maximal Ca^{2+}entry and the resultant plateau in cytosolic Ca^{2+} were attained

extracellular Ca^{2+} was removed from the extracellular solution whilst the inhibitor was maintained until the cytosolic Ca^{2+} levels returned to baseline.

2.5.3   Store depletion with acute application of channel inhibitors

Cells were treated as in 2.5.1, store were depleted by either thapsigargin or CPA in nominally Ca^{2+} free solution and Ca^{2+} was re-introduced at the appropriate time point. When a plateau in Ca^{2+} influx was attained inhibitors such GSK-7975A, Pyr compounds, etc were applied to the extracellular solution in the maintained presence of extracellular Ca^{2+}. Generally, the PMCA clears the elevated cytosolic Ca^{2+} levels and when a new plateau in cytosolic Ca^{2+} levels was attained then extracellular $Ca^{2+}$was removed with inhibitors and cells were left until resting levels of cytosolic levels were re-attained.

2.5.4   Store depletion with pre-incubation of calmodulin modulators.

Ca^{2+}itself is an activator of calmodulin. Therefore, it was necessary to deplete stores of Ca^{2+} as slowly as possible in order to not activate calmodulin due to the efflux of Ca^{2+} from the ER. A two-step store-depletion protocol was employed. An initial 10-fold lower concentration of thapsigargin (200 nM) or CPA (1 µM) was applied to cells in a nominally Ca^{2+} free extracellular solution and was maintained until cytosolic Ca^{2+}levels had returned to baseline levels. A subsequent higher concentration of thapsigargin (2 µM) or CPA (10 µM) was applied to cells in order to ensure that stores has been fully depleted of Ca^{2+}. The modulators of calmodulin were then admitted to the extracellular solution and cells were pre-incubated in the continued presence of SERCA inhibitors before the re-admission of Ca^{2+} to the extracellular solution. Experiments then proceeded as in section 2.1.2 after maximal Ca^{2+} entry and the resultant plateau in cytosolic Ca^{2+} was attained.

2.5.5   Store depletion with inhibitors of proteases for calmodulin pre-incubation.

Experiments undertaken with calmodulin pre-incubation were undertaken in a similar manner as in section **2.5.4,** with the admission of varying protease inhibitors in tandem with the second high concentration of CPA. 0.01% trypsin inhibitors, protease inhibitor cocktail, 10 µM chymostatin and 100 µM EDTA were used to inhibit the various different proteases present in pancreatic acinar cell preparations, such as trypsin, chymotrypsin, metalloproteases and a multitude of other proteases.

2.6   Cellular necrosis measurements

Cells were isolated according to the protocol in section 2.2. The final cell suspension in 2 ml NaHEPES (1mM Ca^{2+}) was split into 0.5 ml aliquots into four separate 15 ml tubes. Up to

four conditions were measured during each experiment: 1) control 2) necrosis-inducing agent 3) necrosis-inducing agent + protective agent alone. 1) Control cells were incubated in the absence of any necrosis inducing agent or protective agent, with suitable vehicle control. 2) Cells were incubated with a necrosis-inducing agent such as POAEE or TLC-S, with suitable vehicle control. 3) Cells were incubated with either POAEE or TLC-s plus a protective agent such as a CRAC channel inhibitor. All cells were incubated for one hour at room temperature, in order to allow sufficient time to capture images of cells, the intervals at which the incubations were started was staggered, with each incubation time starting fifteen minutes after the previous. At the end of the hour incubation cells were stained with propidium iodide (final concentration 1 µg/ml). Images of the cells stained with propidium iodide were then captured using an inverted Zeiss (Zeiss UK, Cambridge, UK) spinning disc confocal microscope (20 x air objective), propidium iodide was excited using the 535 nm laser and collecting emission between 585 – 705 nm. 20 to 30 images were captured per condition and the number of viable cells and necrotic cells (propidium iodide positive staining) were counted. Data presented as the number of necrotic cells as a percentage of the total number of cells ± SEM.

2.7   Plasmid DNA amplification

2.7.1   Polymerase Chain Reaction (PCR)

PCRs were performed using Phusion High Fidelity master-mix (Fisher-Scientific) according to the conditions outlined in tables 1.1, 1.2 and 1.3 below.

Table 2 PCR components

Phusion Master-Mix	25µl
Forward Primer	0.5µM
Reverse Primer	0.5µM
Template	10ng
Sterile Deionised Water	to 50µl

Table 3 Primers

mCherryF	5'-TGCC<u>GGATCC</u>ATGGTGAGCAAGGGCGAGGAGG-3'
mCherryR	5'-TGCC<u>GATATC</u>TTGTACAGCTCGTCCATGCCGCCG-3'
RCaMF	5'-TGCC<u>GATATC</u>GCTGCAGCTATGGCTGATCAGCTGACTGAAGAACAG-3'
RCaMR	5'-GGTT<u>GCGGCCGC</u>TCATTTTGCAGTCATCATCTGTACG-3'

Table 4 PCR programme

	Reaction Conditions		
	Temp(°C)	Time	Cycles
Initial Denaturation	98	30 sec	1
Denaturation	98	5 sec	33
Primer annealing	72	8-12 sec	
Extension	72	7 min	1
Machine cool down	4	-	-

2.7.2 Agarose gel electrophoresis

The gel tray was set-up in accordance with the BioRad manufacturer's instructions. The appropriate amount of agarose was added to 1 X TAE (TAE, 50 X stock - 2M Tris, 2M acetic acid, 50mM EDTA) buffer to make the % agarose gel required. The mixture was heated in a microwave oven with occasional gentle shaking until the agarose had dissolved and the solution was clear. Ethidium bromide was added to achieve a final concentration of 0.2µg/ml. The solution was then poured into the gel tray and a comb inserted in order to form the wells. Once set, the gel tray was submerged in a gel tank containing fresh 1X TAE buffer. The comb was removed and the DNA samples in 1X DNA loading buffer were loaded on the gel with a DNA molecular weight (MW) marker. The voltage used for the electrophoresis was typically 80V and was stopped when the dye front had travelled three-quarters of the way through the gel. Visualisation of the gel was carried out on a UV transluminator and the image developed using a BioRad documentation system and BioRad Quantity One software.

2.7.3   Cloning of mCherry-CaM^{WT} and mCherry-CaM^{mut1,2,3,4} into the pCR3 vector

mCherry was amplified by PCR from the appropriate plasmid using the conditions described in section 2.7.1 and the primers listed in table 1.2 in order to incorporate a 5'-BamHI site and a 3'-EcoRV site for digestion of plasmid DNA. The appropriate buffers were used according to the manufacturer's instructions and generally 1.5 μg of DNA (plasmid and insert) was used in a 100μl reaction for 3 hours at 37°C. The DNA digests were then purified using the QIquick PCR purification kit. Separation of double digested linear plasmid and insert DNA was achieved via agarose gel electrophoresis as described in section 2.7.2. Ligation of the DNA fragment into the pCR3 vector was carried out in a molar ratio of 5:1 of DNA insert to vector. 2U T4 DNA ligase was used for performing the ligation and was carried out in the 1X reaction buffer supplied followed by incubation at 16 °C overnight. This ligation mixture was then stored at 4°C prior to transformation into competent *E.coli* TOP10 bacterial cells. After confirmation of successful cloning of pCR3-mCherry, CaM^{WT} and CaM^{mut1,2,3,4} were amplified by PCR from the appropriate plasmids and cloned in a similar fashion using EcoRV and NotI restriction enzymes into the pCR3-mCherry plasmid.

2.7.4   Quantification of DNA

The concentration of DNA was deduced by spectrophotometric quantification of duplicate 1:100 dilution samples. The absorbance of the duplicates was measured at 260nm (A_{260}) in a 1.5ml quartz cuvette using a Perkin-Elmer MBA2000 spectrophotometer. The concentration was calculated automatically by using the equation 1unit A_{260} = 50μg/ml of double stranded DNA.

2.7.5   Transformation into competent E.coli bacteria cells

Frozen 100μl aliquots of chemically competent TOP10 *E.coli* cells were allowed to thaw on ice. Ligation mixture was added to these cells and mixed before incubation on ice for 30 minutes. The mixture was then heat shocked at 42°C for 45 seconds before returning to ice for a further 5 minutes. 900μl of sterile antibiotic-free L.B. Lennox broth was added to the mixture followed by incubation with shaking for 1 hour at 37°C and 225rpm. Typically 200μl of the mixture was plated out on L.B. Lennox agar plates containing a 1:1000 dilution of the appropriate antibiotic. Agar plates were inverted and incubated overnight at 37°C.

Results

2.7.6 Cloning of mCherry-CaM^{WT} and mCherry-CaM^{mut1,2,3,4} into pCR3 vector.

A two-step cloning strategy was used to create the mCherry-CaM^{WT} and mCherry-CaM^{mut1,2,3,4} constructs. mCherry was amplified by PCR from its plasmid using the appropriate primers to incorporate a 5'-BamHI site and a 3'-EcoRV site, for cloning into the pCR3 vector. After confirmation of successful cloning of this construct (Figure 2.1), CaM^{WT} and CaM^{mut1,2,3,4} were amplified by PCR from their plasmids using the appropriate primers to incorporate 5'-EcoRV and 3'-NotI sites; and to provide an in-frame ligation point between mCherry and CaM constructs. Restriction digests with BamHI and NotI ensured successful ligations, confirming the presence of the inserts (Figure 2.2).
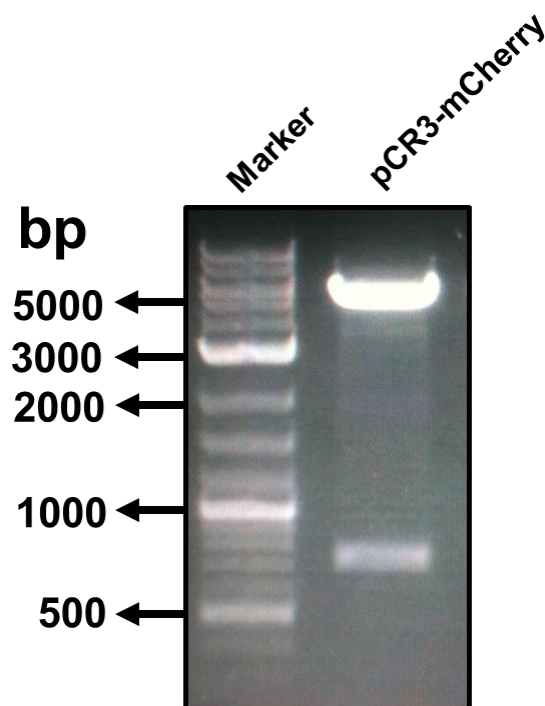
Figure 2.1 Agarose gel showing positive clone of pCR3-mCherry

1% agarose gel showing the products of enzymatic digestion of a DNA mini-prep corresponding to a positive clone of pCR3-mCherry, using BamHI and EcoRV restriction enzymes. The 5.1 kb band represents the pCR3 vector and the band between 500 and 1000 bp represents the mCherry insert.
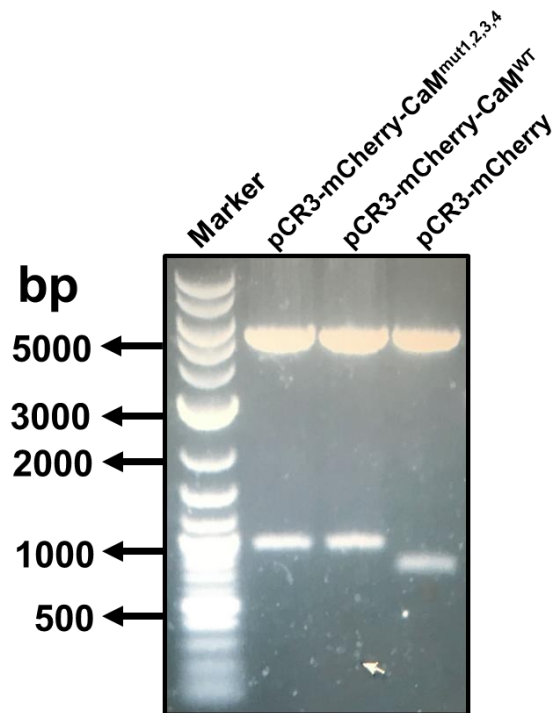
Figure 2.2 Agarose gel showing positive clones of pCR3-mCherry-CaM^{WT,} pCR3-mCherry-CaM^{mut1,2,3,4} and pCR3-mCherry

0.9% agarose gel showing the products of enzymatic digestion of DNA maxi-preps corresponding to positive clones of pCR3-mCherry-CaM^{WT} and pCR3-mCherry-CaM^{mut1,2,3,4} (lane 3 is the control pCR3-mCherry plasmid), using BamHI and NotI restriction enzymes. The 5.1 kb band represents the pCR3 vector, the bands at ~1.15 Kb represent the mCherry-CaM^{WT} and the mCherry-CaM^{mut1,2,3,4} inserts (lanes 2 and 3) and the band between 500 and 1000 bp (lane 4) represents the mCherry insert.
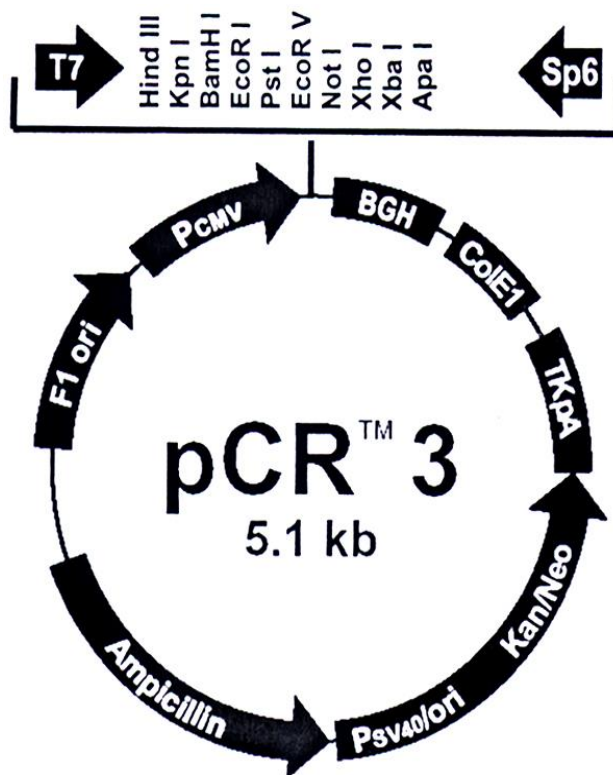
Figure 2.3 Vector map of pCR$^{\text{TM}}$ 3 (courtesy of Invitrogen)

2.8   Data handling and statistics

Ratio fluorescence values from Fura-2 loaded cells were normalised to 1 by dividing all values by an average value of resting fluorescence (R/R$_0$). All the Fura-2 traces are averages represented with the standard error of the mean as error bars.

The changes in Ca^{2+} entry were measured by calculating the change in amplitude from the baseline (after store depletion) to the peak of Ca^{2+} influx. Data represented as the average change in R/R$_o$ $\pm$ SEM. Where possible the rate of influx was measured as the time taken to reach half-maximal point of Ca^{2+} entry, data represented as mean t$_{1/2}$ $\pm$ SEM .

Data was tested for normal distribution using the D'Agostino and Pearson test for normality using GraphPad Prism. For data sets with two conditions in which the data points are normally distributed then a parametric test was used to test for statistical significance: unpaired T-test. For data that was not normally distributed a non-parametric test was used: a Mann-Whitney test was used, using GraphPad Prism. For data from more than two conditions, a one-way ANOVA was used for to test for significance from data that was normally distributed data. For data points, from more than two conditions, that are not normally distributed a Kruskal-Wallis test was used to test for significance.

64
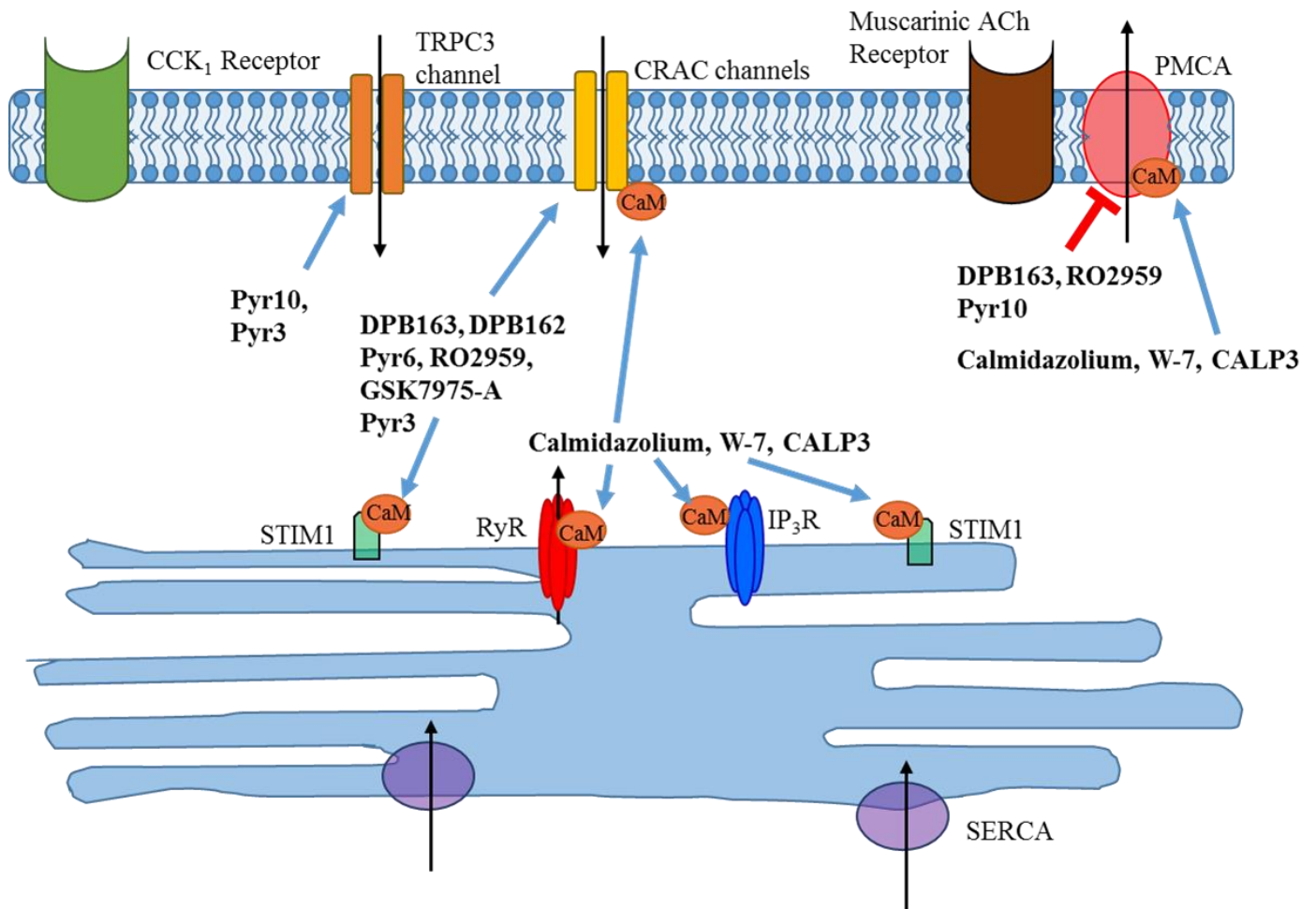
Figure 2.4 Schematic diagram of proposed site of action of the pharmacological agents

Blue arrows indicate the site of action that each pharmacological agent is reported to act upon. The red lines indicate the site of action it is hypothesised that the pharmacological agent also act upon.

3 Results - Pharmacological inhibition of Store-operated Calcium entry mechanisms in pancreatic acinar cells

3.1 Introduction

3.1.1 Orai1 inhibition

As previously described the hallmark of acute pancreatitis, the inappropriate intracellular activation of digestive proenzymes such as trypsinogen, is the result of a sustained elevation in cytosolic Ca^{2+} levels. Ca^{2+} release from intracellular stores, such as the ER, gives rise to the initial increase in cytosolic Ca^{2+} concentration. ER Ca^{2+} stores are a finite source of Ca^{2+}, once depleted cells are reliant on Ca^{2+} entry into the cell to drive sustained Ca^{2+} signalling. Elevated cytosolic Ca^{2+} is cleared via PMCA and mitochondrial Ca^{2+} uptake (234). Within the ER membrane and extending both into the cytosol and into the ER lumen is the ER Ca^{2+} sensor STIM-1. STIM-1 detects Ca^{2+} depletion from the ER, it oligomerises and activates store-operated Ca^{2+} entry channels in the plasma membrane. CRAC channels are the main type of store-operated channels found in pancreatic acinar cells, Orai1 is the pore forming subunit of these channels. Upon store depletion, STIM-1 activates Orai1 and Ca^{2+} enters the cell down its electrochemical gradient, thus sustaining cytosolic Ca^{2+} signalling in physiology (127) and Ca^{2+} overload in pathology (183).

The hypothesis that inhibiting store-operated calcium entry channels would be effective in reducing Ca^{2+} overload and as such trypsinogen activation (187) was suggested sixteen years ago. A non-physiological concentration of CCK (10 nM) was applied to cells and resulted in an initial release of Ca^{2+} from intracellular stores, after reaching a sharp peak Ca^{2+} was largely cleared from the cytosol. Ca^{2+} levels did not return to baseline levels and remained significantly elevated. This elevation persisted until extracellular Ca^{2+} was removed and then cytosolic Ca^{2+} levels returned to baseline. This treatment with CCK also resulted in intracellular trypsinogen activation. CCK application in Ca^{2+} free extracellular solution resulted in the preservation of the initial peak in cytosolic Ca^{2+} due to Ca^{2+} release from internal stores, but the sustained elevation in cytosolic Ca^{2+} was lost; further there was also no intracellular activation of trypsinogen. However, sixteen years ago there were no specific antagonists of store-operate Ca^{2+} channels, as such there was very little progress in testing this hypothesis.

Pancreatic acinar cells express Orai1 both apically and basolaterally (80) and it has been demonstrated to functionally mediate SOCE in these cells. Relatively recently

GlaxoSmithKline generated a compound that has been demonstrated, at low micromolar concentration, to yield near complete inhibition of CRAC channel mediated Ca^{2+} entry in human lung mast cells (204), RBL-2H3 cells (205) and mast and T-cells derived from human, mice rat and guinea pig (206). In collaboration with GlaxoSmithKline, utilising their novel Orai1 specific inhibitor –GSK-7975A(205), we sought to determine the effect of inhibiting Orai1 in pancreatic acinar cells. The ER store depletion protocol is described in section 2.5.1 and was utilised in the following study; store depletion was mediated by SERCA pump inhibitors in nominally Ca^{2+} free extracellular solution and resulted in the activation of CRAC channels. Upon re-addition of Ca^{2+} to the extracellular solution there was subsequent SOCE into the cell.

Figure 3.1 A is an example of the classic store-operated Ca^{2+} entry protocol utilised to study CRAC channel mediated Ca^{2+} entry. It can be manipulated to introduce pharmacological agents. In figure 3.1B cells were pre-treated with GSK-7975A for 5 minutes, according to section 2.5.2. Five minutes pre-incubation with this inhibitory compound was sufficient to significantly reduce the amplitude of Ca^{2+} entry by approximately 83%. A double-pulse re-introduction of Ca^{2+} was utilised in this figure and demonstrated that a subsequent re-introduction of Ca^{2+} resulted in a peak of Ca^{2+} entry of the same amplitude as the first peak of Ca^{2+} entry. When the time of pre-incubation was increased from five to ten minutes, there was a further significant reduction in the amplitude of Ca^{2+} entry (figure 3.1C), with entry inhibited by 93.4 ± 5 %. Upon re-introduction of 5 mM Ca^{2+} to extracellular solution, after ten minutes of washing with physiological buffer, there was no recovery of Ca^{2+} entry (figure 3.1D). This demonstrated that if GSK-7975A is reversible, 10 minutes was not sufficient time to see reversal of the inhibitory effects of the compound. The changes in Ca^{2+} entry due to the above interventions with GSK-7975A are summarised in Figure 3.1E as the change in F/F_0 due to Ca^{2+} influx. Figure 3.1 was taken from (130), an *in vitro* study on the effect of CRAC channel inhibition as a potential treatment for acute pancreatitis.
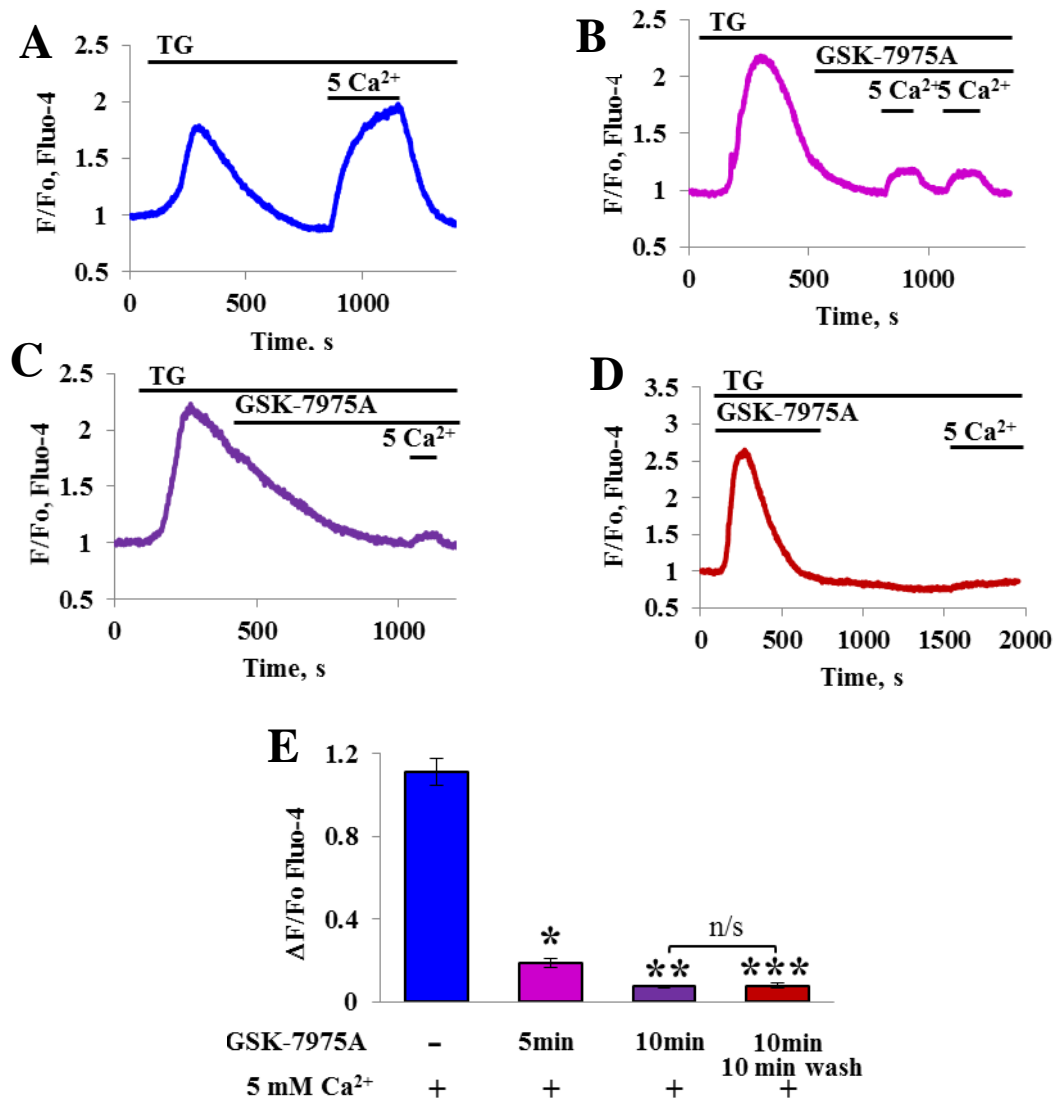
Figure 3.1 GSK-7975A inhibited Orai1 mediated store-operated Ca^{2+} influx in pancreatic acinar cells

Representative fluorescence traces of Fluo-4 loaded pancreatic acinar cells

A – Stores depleted according to protocol in section 2.5.1, 5 mM extracellular Ca^{2+} was reintroduced (n=5). **B** – Cells are pre-incubated with10 μM GSK-7975A for five minutes according to protocol in section 2.5.2. 5 mM extracellular Ca^{2+} was re-introduced (n=5) in two separate phases to induce Ca^{2+} influx . **C**- 10 μM GSK-7975A was pre-incubated with cells for 10 minutes before 5 mM extracellular Ca^{2+} was re-introduced (n = 14). **D**- After pre-incubation with 10 μM GSK-7975A ten minutes of washing in physiological buffer was not sufficient to prevent inhibition induced by 5 mM extracellular Ca^{2+}. **E**- Summary of the mean changes of Ca^{2+} influx (ΔF/F$_0$) in control cells (blue bar) and in cells pre-incubated with GSK-7975A for 5 minutes (fuscia bar) and ten minutes (Purple bar) cells washed after pre-incubation (red bar). Data presented as mean ± SEM. Adapted from (130)

Furthermore, GSK-7975A was found to inhibit sustained elevations in cytosolic Ca^{2+} induced by POAEE, a non-oxidative alcohol metabolite and prevented intracellular protease activation (130). In a paper published shortly after it was shown that 10 μM GSK-7975A was sufficient to inhibit sustained elevations in cytosolic Ca^{2+} induced by a high concentration of CCK and by acute pancreatitis inducing bile salt - TLC-S. Lastly, it was found to inhibit vacuolisation – another major hallmark of acute pancreatitis (268).

Another paper extended on the work of the two aforementioned papers, the authors sought to determine if inhibition of SOCE entry had translational potential. As such the researchers utilised GSK-7975A and another CRAC channel inhibitor CM_128 on isolated human pancreatic acinar cells; 50 μM GSK-7975A was sufficient to near maximally inhibit Ca^{2+} entry in human pancreatic acinar cells. CM_128 was more potent at inhibiting Ca^{2+} entry in human acinar cells than GSK-7975A, significantly inhibiting SOCE at 1 μM (253). In mouse pancreatic acinar cells, at 1 μM, CM_128 was significantly more effective than 1 μM GSK-7975A and had a striking inhibitory effect on Ca^{2+} entry (253). As with any potential therapeutic agent it was necessary for GSK-7975A to be tested *in vivo*, in an appropriate animal model for the human disease, before it could be considered for further trials. GSK-7975A was tested in 3 different mouse models of acute pancreatitis. The authors used a high dose (49.3 μM) and a low dose (8.9 μM) of GSK-7975A to protect against acute pancreatitis. The biochemical markers of acute pancreatitis that were measured were: serum amylase, IL-6, trypsin activity, pancreas and lung myeloperoxidase (MPO), all of which were reduced by GSK-7975A. Furthermore, oedema, necrosis and inflammation were all significantly reduced by both low and high doses of GSK-7975A (253). Together, these three papers provide strong evidence that CRAC channel inhibition is both sufficient and effective to ameliorate the hallmarks of this acute disease. In addition to GSK-7975A, CM_128 another novel inhibitor of Orai1, was also used and shown to be inhibitory at a lower concentration both *in vitro* and *in vivo*.

3.1.2 **2-APB as a CRAC channel blocker.**

Over recent years there have been a variety of CRAC channel inhibitors that have been utilised, with varying success and specificity. 2-aminoethyl diphenylborinate (2-APB), initially thought to be an IP$_3$R antagonist (286), is capable of potentiating CRAC channel mediated Ca^{2+} entry at low micromolar concentration (1-10 μM) and inhibiting the same channels at high micromolar concentration (30-100 μM) (287). 2-APB application inhibited SOCE induced by thapsigargin in a variety of cells including HeLa (288), rat basophilic

leukaemia (RBL) (289), primary hepatocytes (290) and Chinese hamster ovary (CHO) (291). 2-APB also has multiple off-target effects, it has been reported to target SERCA (292), PMCA (192) and non-specific cation channels in the plasma membrane (289). Further, it affects the structure of mitochondria and their ability to release the Ca^{2+} they have taken up during periods of elevated cytosolic Ca^{2+} (288).

In 2008, it was shown the 2-APB had differential effects on each of the Orai isoforms; it had a bimodal effect on Orai1 and 2, activating the two channels at lower concentrations and inhibiting them at higher concentrations, whereas Orai3 was only activated (194,293). At a high concentration of 50 µM 2-APB was shown to inhibit and reverse STIM-1 puncta formation (293). Another CRAC channel blocker Gd^{3+}, although effective in reducing Ca^{2+} influx via CRAC channels, did not alter STIM-1 puncta formation (293). STIM-1 puncta formation reversal by 2-APB is only a partial explanation for the inhibitory effect on CRAC channels, as it is not observed with other channel inhibitors, the potentiation of the channel seems to be independent of STIM1 puncta formation (293).

The laboratory of Dr Mikoshiba generated a database of 2-APB analogues in search of more potent inhibitors of CRAC channels, that had only a minimal effect on the IP_3R (294,295). DPB163-AE and DPB162-AE were identified in the screening process as being 100 times more potent than 2-APB at inhibiting CRAC channel mediated Ca^{2+} entry, with maximal inhibitory activity on store-operated Ca^{2+} entry at high nanomolar to low micromolar concentration in CHO cells, HeLa cells and DT40 cells (294,295).. DPB162-AE is a bona fide CRAC channel inhibitor, which unlike 2-APB it has no potentiating effects. On the other hand, DPB163-AE has similar bimodal effects to 2-APB, although not in CHO-K1 cells. The bimodal activity of DPB163-AE was surprising as the two analogues are structural isomers of each other (296). The efficacy of the two 2-APB analogues varied between the cells tested, the compounds were the most effective in DT40 cells, then CHO cells and least inhibitory in HeLa cells which the authors interpret to mean that the cells have different composition of channel constituents. Orai3 is activated by DPB163-AE at low concentrations. It can be hypothesised that if endogenous SOCE is potentiated by DPB163-AE at low concentrations it may functionally express the Orai3 isoform as part of its pore forming subunit. DPB162-AE was observed to reverse STIM1 puncta formation after store depletion. When DPB162-AE was pre-incubated with cells, before store depletion, it was able to inhibit STIM1 puncta formation, suggesting that DPB162-AE is more of a STIM inhibitor as opposed to a modulator of the CRAC channel pore (295).

3.1.3 TRPC3 mediated Ca^{2+} entry

Expression of the canonical transient receptor potential (TRPC) channel, TRPC3, has also been reported in pancreatic acinar cells (219–221). TRPC channels are non-selective cation channels (297) activated by stimulation of PLC-coupled receptors and the subsequent hydrolysis of PIP_2, in a manner similar to the whole TRPC sub-family (298). Before the identity of the CRAC channel was determined TRPC channels were considered as likely candidates as the main component of the CRAC channel. The store-operated nature of TRPC channels is still highly contested in the field (183). It is accepted that TRPC1, 4, and 5 all bind to STIM1 but TRPC3, 6 and 7 do not (299). However, it has been demonstrated that STIM1 regulates TRPC3, indirectly, via heteromultimerisation with TRPC1 (214). TRPC1 directly binds STIM1 via electrostatic interaction (215) via two STIM1 lysines and two conserved aspartates and glutamates in the C-terminus of TRPC1 (222). Heteromultimers of TRPC1 and TRPC3 are known to form in several cell types such as: hippocampal neuronal cells, human parotid gland ductal cells, HEK-293 and myoblast cells (214,300–303). Ca^{2+} signalling through TRPC1 and TRPC3 is known to play a pathophysiological role in Duchenne muscular dystrophy (300).

TRPC3 channels are expressed in the apical and lateral regions of pancreatic acinar cells (219–221) and therefore contribute to Ca^{2+} influx, likely of a store-operated nature. Studies utilising a TRPC3 knockout mouse found a significant reduction, of more than 50 %, in SOCE in pancreatic acinar cells and submandibular gland cells when using CPA to deplete ER stores (220). In addition to the effects on SOCE, the frequency of Ca^{2+} oscillations was reduced in TRPC3 knockout mice when compared with wild type, regardless of the nature of stimulation (CCK or carbachol). The study utilised a caerulin-induced model of acute pancreatitis in the TRPC3 knockout mice in which, when compared with wild type mice, there was an observed reduction in SOCE; this was correlated with a reduction in the severity of acute pancreatitis, as seen by a reduction in pancreatic oedema and reduced serum amylase (220).

The TRPC subclass of the TRP family has very few specific inhibitors (304). In a 2011 study Pyr3, a compound reported to be a specific antagonist of TRPC3 channels, was utilised alongside the TRPC3 knock out mouse to determine the effect on intracellular Ca^{2+} signalling. The study sought to determine the outcomes of TRPC3 pharmacological and genetic targeting in pancreatic acinar cells and submandibular gland acini, and the subsequent implications for severity of acute pancreatitis and indirectly for Sjögren's syndrome. The

frequency of Ca^{2+} oscillations, stimulated by CCK, was reduced in WT cells treated with 3 µM Pyr3, which was found to be in line with genetic deletion of TRPC3. Treatment of acini from TRPC3 knockout mice with Pyr3 did not result in a significant reduction in the frequency of Ca^{2+} oscillations compared with TRPC3 knockout acini in the absence of Pyr3. This was similar to the effects on SOCE, WT pancreatic acini treated with 3 µM Pyr3 exhibited a 50% reduction in SOCE, which was similar to the reduction in SOCE due to deletion of TRPC3. Treatment of TRPC3 knockout pancreatic acini with Pyr3 did not result in a further reduction of SOCE compared to TRPC3 knockout pancreatic acini in the absence of Pyr3. The caerulin-model of acute pancreatitis was utilised again in this study, 0.1 µg/g body weight of Pyr3 was administered to mice, these mice presented with a reduced serum amylase compared to caerulin treated mice in the absence of Pyr3, they also demonstrated a reduced oedema compared to the control (221).

3.2 Results - Inhibition of Orai1-mediated Ca^{2+} entry

3.2.1 2-APB analogues

In the concentration that 2-APB maximally inhibits store-operated calcium entry it also released Ca^{2+} from ER stores. 100 µM 2-APB when applied in the presence of 1 mM extracellular Ca^{2+} to pancreatic acinar cells elicited a dramatic increase in cytosolic Ca^{2+} levels that was sustained in the maintained presence of 2-APB (130). DPB163-AE when applied to cells at the maximal inhibitory concentration for store-operated Ca^{2+} entry of 1 µM, in the presence of 1 mM extracellular Ca^{2+}, did not give rise to a noticeable increase in cytosolic Ca^{2+} (figure 3.2 A and B), contrasting with the action of 2-APB at the relevant concentration for inhibiting Ca^{2+} entry. 1 µM ACh was applied to cells after the application of 1 µM DPB163-AE as a positive control in figure 3.2 B, to confirm that it was possible to mobilise Ca^{2+} from ER stores, confirming that the stores were not Ca^{2+} depleted and were metabolically capable of subsequently pumping Ca^{2+} from the cytosol, across the plasma membrane.

Unlike in CHO, HeLa and DT40 cells 1 µM DPB163-AE had no effect on SOCE in pancreatic acinar cells – figure 3.2 C. When applied in the presence of a sustained elevation in cytosolic Ca^{2+}, due to Ca^{2+}influx, 1 µM DPB163-AE did not decrease cytosolic Ca^{2+} levels. The sustained elevation in cytosolic Ca^{2+} persisted until Ca^{2+} was removed from the extracellular solution. Increasing the concentration of DPB163-AE to 3 µM resulted in a dramatic decrease in cytosolic Ca^{2+} levels. 3 µM DPB163-AE reduced cytosolic Ca^{2+} levels by $73 \pm 3.1\%$, when applied acutely in the presence of a sustained elevation in cytosolic Ca^{2+}.
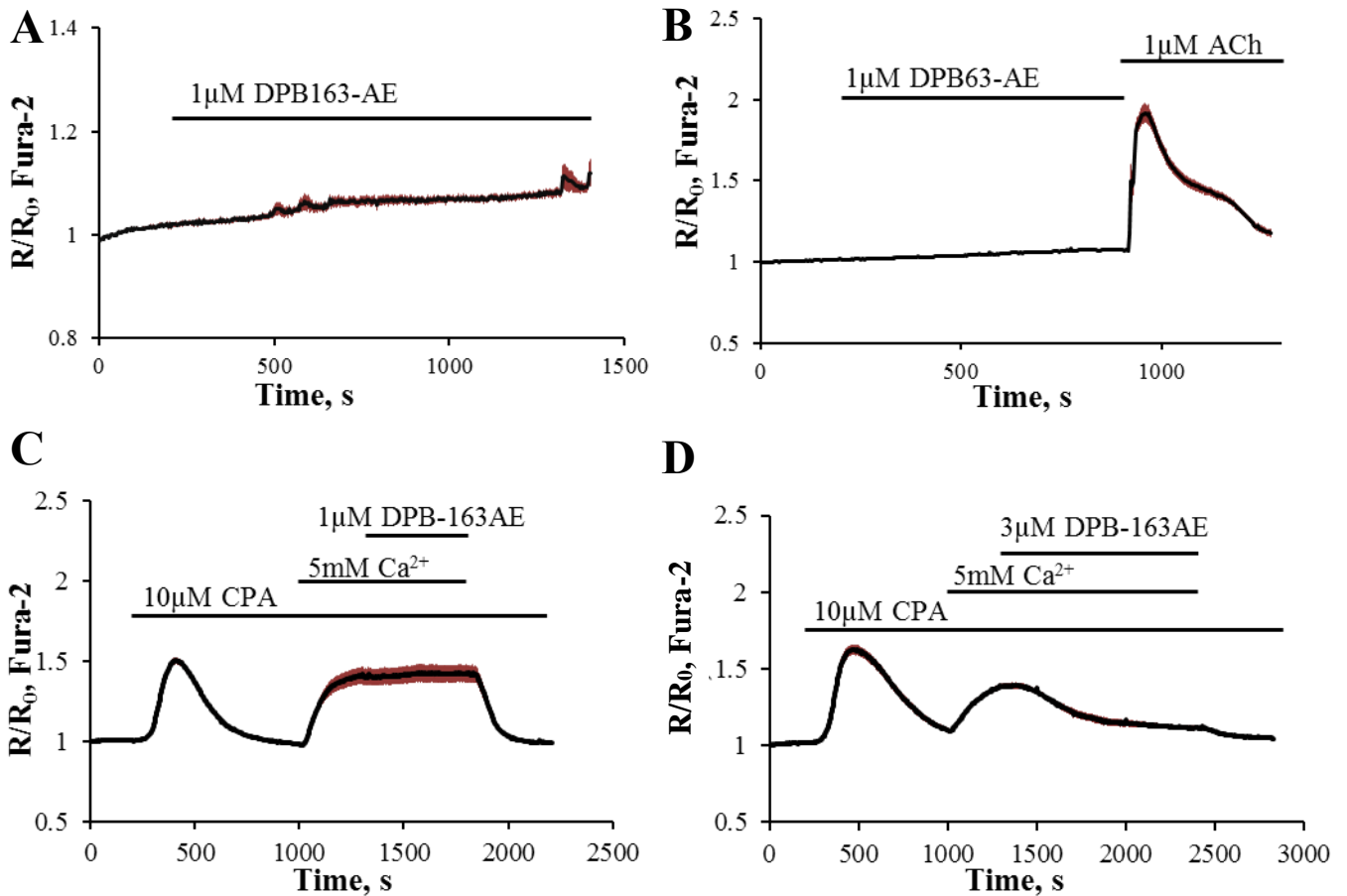
Figure 3.2- DPB163-AE did not release Ca²⁺ from ER stores but can inhibit store-operated Ca²⁺ entry in a concentration-dependent manner

Average traces ± SEM from Fura-2 loaded pancreatic acinar cells.

A – 1 μM DPB163-AE was applied to cells in presence of 1mM extracellular Ca^{2+} (n=17). **B** – 1 μM DPB163-AE was applied to cells in the presence of 1 mM extracellular Ca^{2+}. 1 μM Ach was then applied to cells as a positive control (n=32). **C-** Cells were treated according to the protocol in section 2.5.3, 1 μM DPB163-AE was applied on top of a sustained elevation in cytosolic Ca^{2+}, due to re-introduction of 5 mM extracellular Ca^{2+} (n=19) **D-** Cells were treated according to the protocol in section 2.5.3, 3 μM DPB163-AE was applied on top of a sustained elevation in cytosolic Ca^{2+}, due to the re-introduction of 5 mM extracellular Ca^{2+} (n=10).

Removal of Ca^{2+} and DPB63-AE from the extracellular solution resulted in a further decrease of cytosolic Ca^{2+} back to baseline levels.

As 1 μM DPB163-AE had no effect on reducing SOCE, this concentration was not utilised for further experiments. In a pre-incubation protocol, as described in section 2.5.2, cells were pre-incubated with 3 μM DPB163-AE during store-depletion for ten minutes, before the re-introduction of Ca^{2+} to the extracellular solution (figure 3.3 A). The subsequent amplitude of Ca^{2+} influx was significantly reduced by $51.1 \pm 4.9\%$ compared to the Ca^{2+} influx in control cells (p = 0.0005) (figures 3.3 B). The half time of Ca^{2+} influx in cells pre-treated with 3 μM DPB163-AE was significantly faster when compared with the half time of Ca^{2+} influx in control cells (p = 0.0335) (figure 3.3 C). In a similar manner, the half time of Ca^{2+} efflux was significantly faster in DPB163-AE pre-treated cells compared with control cells (p = 0.0017).

Other inhibitors of Orai1 such as GSK-7975A maximally inhibited Orai1-mediated SOCE in pancreatic acinar cells at 10 μM, so this concentration of DPB163-AE was also used on pancreatic acinar cells to determine if increasing the concentration of inhibitor would result in a further inhibition of Ca^{2+} influx. In figure 3.3 D cells were treated according to section 2.5.2, with a ten minute pre-incubation with 10 μM DPB163-AE during the store depletion phase. After approximately five minutes pre-incubation, a plateau in cytosolic Ca^{2+} was attained that was elevated above resting Ca^{2+} levels, cytosolic Ca^{2+} levels then slowly started to increase before the re-introduction of Ca^{2+} to the extracellular solution.
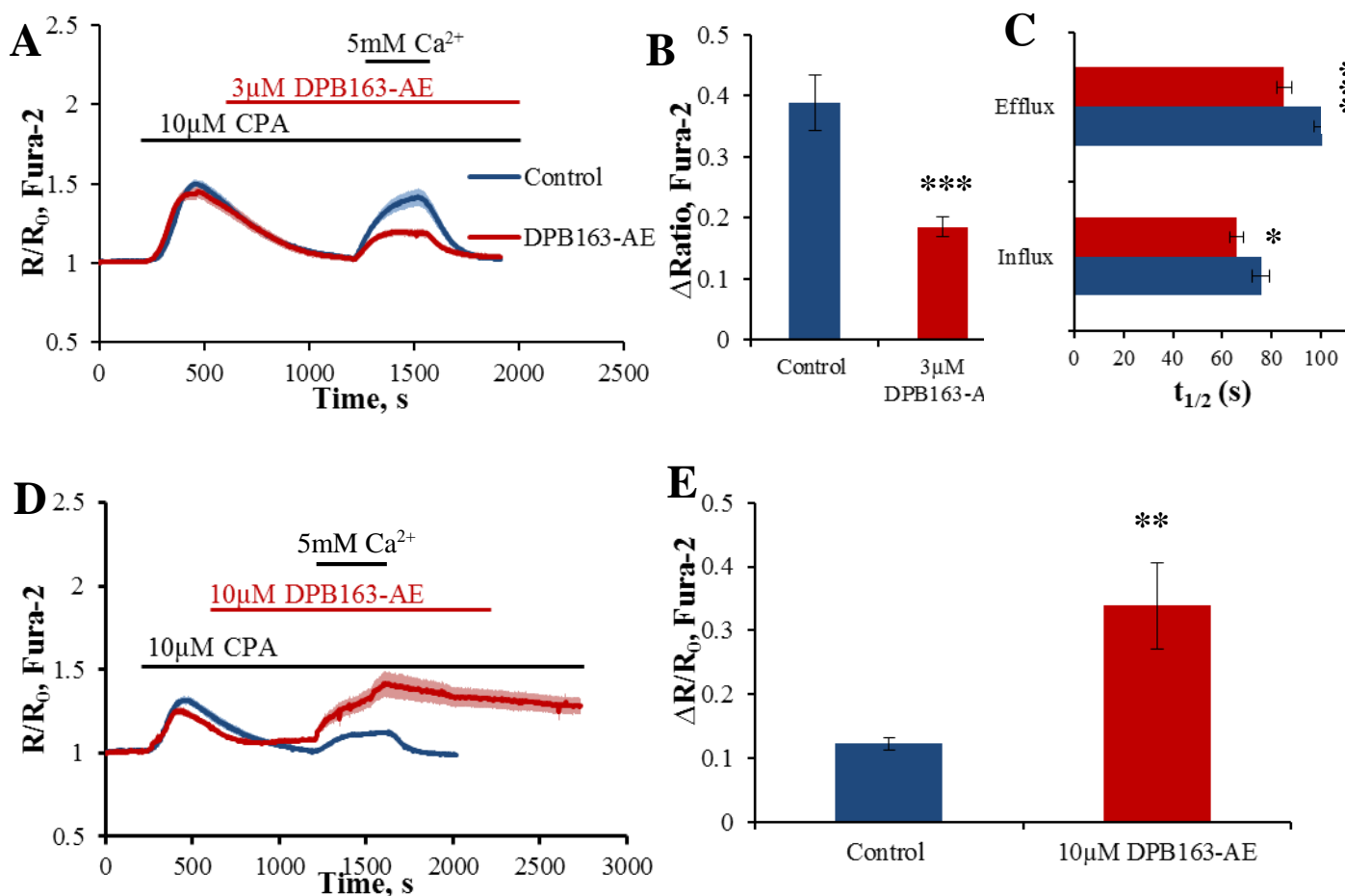
Figure 3.3 - Pre-incubation with DPB163-AE had a bimodal effect on Ca²⁺ influx

Average traces (± SEM) from Fura-2 loaded pancreatic acinar cells

A- Cells were treated according to the protocol in section 2.5.2, cells were pre-incubated with 3 μM DPB163-AE for 10 minutes before 5 mM Ca²⁺ was subsequently re-introduced to the extracellular solution. Blue trace represents control cells (n=16). Red trace represents 3uM DPB163-AE (n=22). **B-** graph summarising the changes in ratio amplitude due to Ca²⁺ influx (from **A**) from control cells (blue bar) and cells pre-incubated with 3 μM DPB163-AE (red bar) (p = 0.0005). **C-** Graph summarising the half time of influx (lower bars: blue bar–control cells and red bar – 3 μM pre-incubated cells) (p = 0.0335) and efflux (upper bars blue – control cells and red – 3 μM pre-incubated cells) (p = 0.0017). **D-** Cells were treated according to the protocol in section 2.5.2, cells were pre-incubated with 10 μM DPB163-AE before 2 mM Ca²⁺ was subsequently re-introduced to the extracellular solution. The blue trace represents control cells (n=25). Red trace represents cells pre-treated with 10 μM DPB163-AE (n=17.). **E-** Graph summarising the changes in ratio amplitude due to Ca²⁺ influx (from **D**) in control cells (blue bar) and cells pre-incubated with 10 μM DPB163-AE (red bar) (p = 0.0057).

75

The amplitude of Ca^{2+} influx in cells pre-incubated with 10 µM DPB163-AE was more than double the amplitude compared to control cells (figure 3.3 E). Furthermore, unlike in figure 3.3 A, when Ca^{2+} was removed from the extracellular solution, in figure 3.3 D, cytosolic Ca^{2+} levels continued to increase and remained significantly elevated above baseline levels, even when DPB163-AE was removed from the extracellular solution.

DPB162-AE, the structural isomer of DPB163-AE, was also used to inhibit Ca^{2+} entry in pancreatic acinar cells. 3 µM DPB162-AE was applied to cells according to the protocol in section 2.5.2 during store depletion for ten minutes before the re-introduction of 5 mM Ca^{2+} to the extracellular solution. This was sufficient to significantly inhibit the amplitude of Ca^{2+} influx by 83.9 ± 2.2 % compared to SOCE in control cells (figure 3.4 B). The half time of SOCE in cells pre-incubated with 3 µM DPB162-AE was significantly slower compared to control cells (figure 3.4 C), whereas the half time of Ca^{2+} efflux in the pre-treated cells was significantly faster than in control cells.

As with DPB163-AE, 10 µM DPB162-AE was also used on pancreatic acinar cells, figure 3.4 D demonstrates a ten minute pre-incubation with 10 µM DPB162-AE before the re-introduction of 5 mM Ca^{2+} to the extracellular solution. Conversely to pre-incubation with DPB163-AE, in which there was an increase in cytosolic Ca^{2+} levels and subsequent sustained elevation of cytosolic Ca^{2+} when compared with control cells, with DPB162-AE the amplitude of Ca^{2+} influx was significantly reduced when compared with control (figure 3.4 E). The half time of SOCE in cells pre-incubated with 10 µM DPB162-AE was significantly inhibited compared with control cells, as was the half time of Ca^{2+} efflux (figure 3.4 F). As with DPB163-AE in figure 3.2 D, 3 µM DPB162-AE was applied to cells according to the protocol in section 2.5.3, in figure 3.4 G; there was an immediate reduction in cytosolic Ca^{2+} levels and after five minutes a new lower plateau in cytosolic Ca^{2+} was established. This acute application of 3 µM DPB162-AE was sufficient to reduce Ca^{2+} entry by 62.9 ± 3.0. The acute application of DPB162-AE was less inhibitory when applied to cells in an acute protocol (figure 3.4 G) compared to when cells were pre-treated with the same concentration (figure 3.4 A), this is different to the data from cells treated acutely with DPB163-AE (figure 3.2 D) and cells pre-treated with the same concentration of DPB163-AE (3 µM in figure 3.3 A), where acute application was more effective.
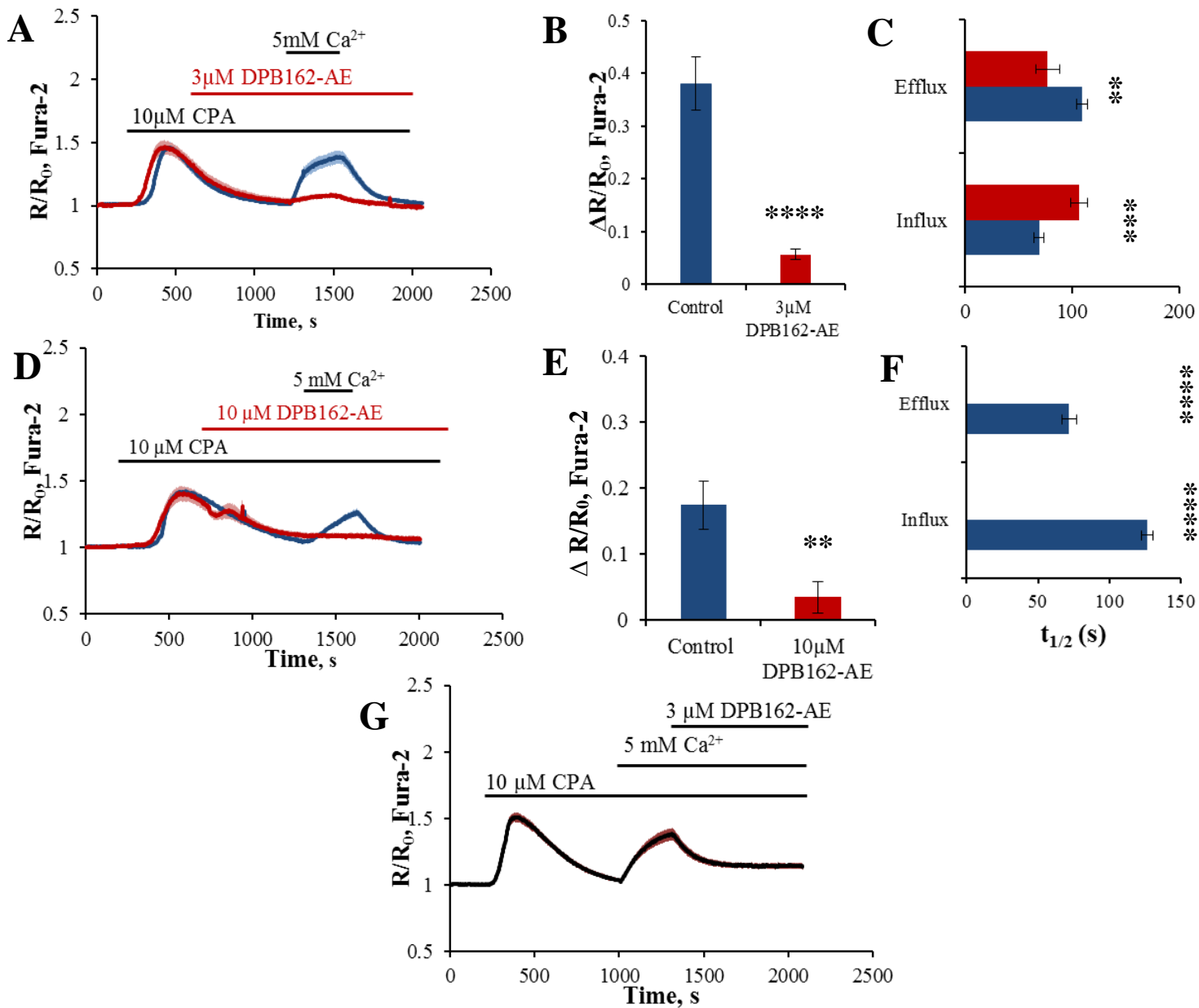
Figure 3.4 Pre-incubation with DPB162-AE had solely an inhibitory effect on Ca²⁺ influx

Average traces (±SEM) from Fura-2 loaded pancreatic acinar cells.

A - Cells were treated according to the protocol in section 2.5.2, cells were pre-incubated with 3 μM DPB162 for 10 minutes before 5 mM Ca²⁺ was subsequently re-introduced to the extracellular solution. Control – Blue (n=14). 3uM DPB162 - red (n=8.). **B-** Summary of ratio amplitude changes due to Ca²⁺ influx (from **A**) from control (blue bar) and DPB162 treated cells (red bar p<0.0001). **C-** Summary of the half time of influx (lower bars p=0.0006) and efflux (upper bars p=0.0151) blue – control cells and red – DPB162 treated cells. **D-** Cells were treated according to the protocol in section 2.5.2, cells were pre-incubated with 10 μM DPB162-AE before 5 mM Ca²⁺ was subsequently re-introduced to the extracellular solution. Control - blue (n=5). 10 μM DPB162 - red (n=10). **E-** Summary of ratio amplitude changes due to Ca²⁺ influx (from **D**) in control cells (blue bar) and DPB162-AE treated (red bar p = 0.0068). **F-** Summary of the half time of influx (lower bar p < 0.0001) and efflux (upper bar p < 0.0001) blue – control cells. **G-** Cells were treated according to the protocol in section 2.5.3, 3 μM DPB162 was applied on top of a sustained elevation in cytosolic Ca²⁺, as a result of the re-introduction of 5 mM extracellular Ca²⁺ (n=11)

77

1.1.1. Roche inhibitor - RO2959.

RO2959 is an Orai1 specific inhibitor developed by Roche and was initially shown to inhibit endogenous CRAC channel mediated SOCE in RBL-2H3 cells, a rat basophilic leukaemia cell line (305). In addition, RO20959 was shown to inhibit human Orai1, Orai2 and Orai3 mediated SOCE in a stable expression system in CHO cells (305). However, it was much less potent at inhibiting Orai2 and Orai3 in this system. An IC_{50} of 402 ± 129 nM in RBL-2H3 was obtained for RO2959 action on endogenous CRAC current. In order to achieve such low IC_{50} values, cells were pre-incubated with RO2959 for 30 to 60 minutes before the SOCE protocol was undertaken (209). One more recent study utilised RO2959 and found the IC_{50} to be much higher than the initial study for example in HEK293T; cells it was approximately 2.5 µM (306)

Figure 3.5 demonstrates the dose-dependent inhibitory effect RO2959 had on pancreatic acinar cells. In light of the IC_{50} obtained for RO2959 in the aforementioned study, 1 µM RO2959 was the first concentration to be tested on pancreatic acinar cells. Figure 3.5 A shows acute application of this concentration to pancreatic acinar cells according to the protocol in section 2.5.3 in the continued presence of 2 mM extracellular Ca^{2+}. In control cells, in the continued presence of extracellular Ca^{2+} and in the absence of inhibitor there is a decline of the plateau in cytosolic Ca^{2+} of $20.7 \pm 5.5\%$; in cells where 1 µM RO2959 was present in the extracellular solution the plateau in cytosolic Ca^{2+} slowly decreased by $38.3 \pm 2.1\%$. 1 µM RO2959 reduced cytosolic Ca^{2+} by 17.6% compared to control. The efficacy of this inhibitor in other cells was much greater, at the same concentration, than was demonstrated in pancreatic acinar cells, which is similar to the efficacy of inhibition observed with the 2-APB analogues.
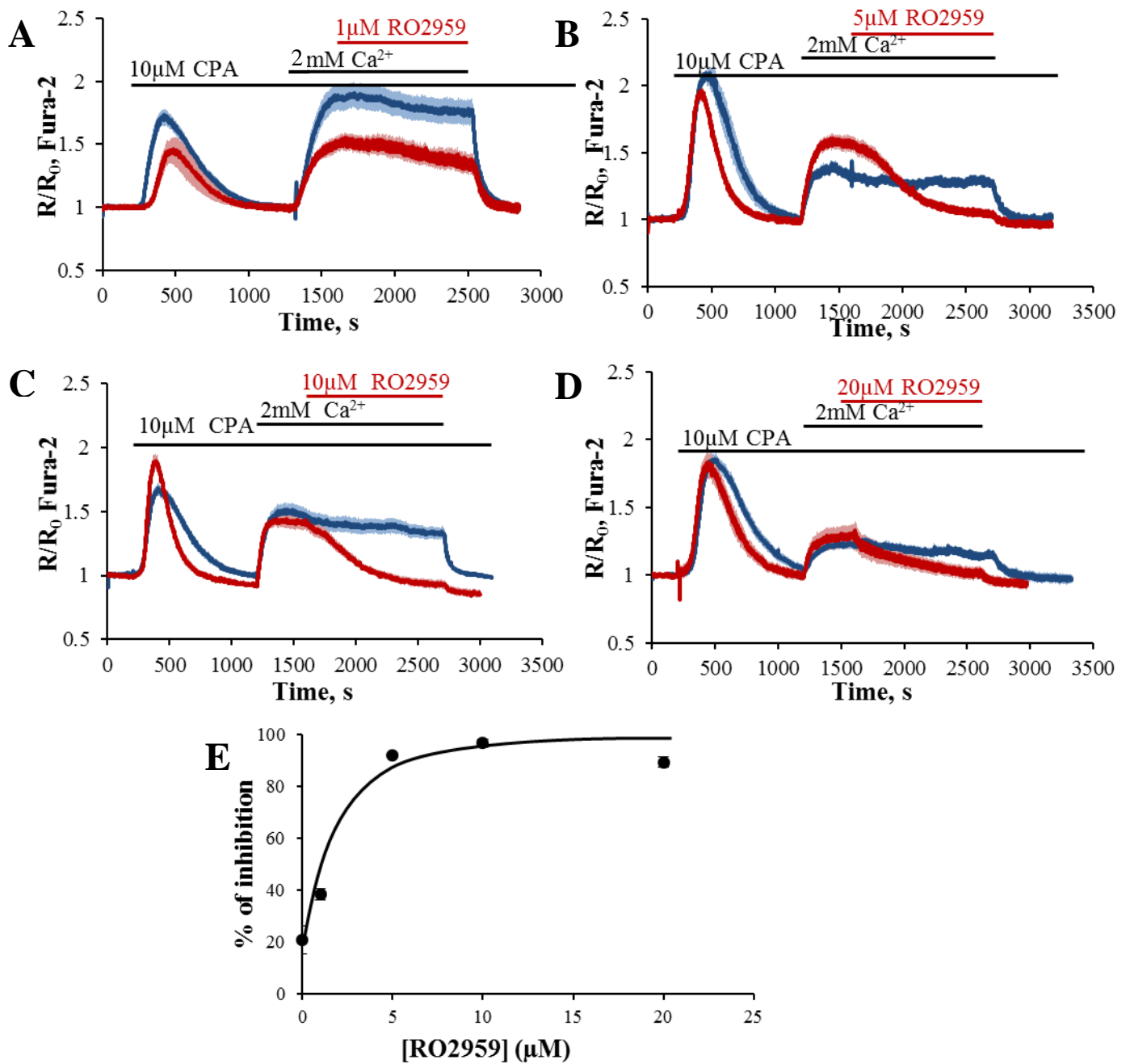
Figure 3.5 RO2959 had a dose-dependent inhibitory effect on Orai1-mediated Ca^{2+} influx, when applied to cells acutely.

Average traces (± SEM) from Fura-2 loaded pancreatic acinar cells.

A – 1 μM RO2959 was applied to cells according to the protocol in section 2.5.3, in the continued presence of 2 mM extracellular Ca^{2+} (control – blue n=9 1 μM RO2959 – red n=5.). **B** – 5 μM (control n=2. 5 μM RO2959 n=11); **C**- 10 μM (control = 15. 10 μM RO2959 n= 12) and **D**- 20 μM RO2959 (control = 8. 20 μM RO2959 n=7.) was applied to cells in an identical manner to panel **A. E** –Graph of percentage of inhibition against concentration of RO2959 (±SEM).

The concentration of RO2959 was increased to 5 µM (figure 3.5 B), this concentration was significantly more effective in inhibiting SOCE than 1 µM. When applied acutely, in exactly the same experimental protocol as in figure 3.5 A, 5 µM was sufficient to inhibit SOCE and as such reduce cytosolic Ca^{2+} by 91.9 ± 0.9 %. A further increase of inhibitor to 10 µM (figure 3.5 C) gave rise to a further inhibition of SOCE, and thereby reduced cytosolic Ca^{2+} by 96.6 ± 1.5 %. Increasing the concentration further to 20 µM (figure 3.5 D) did not further inhibit Ca^{2+}influx compared to 10 µM, when applied in an identical protocol, 20 µM reduced SOCE by 89.2 ±1.9 %. Figure 3.5 E summarises the percentage inhibition of RO2959 at 4 different concentrations when applied acutely to pancreatic acinar cells in the continued presence of 2 mM Ca^{2+} in the extracellular solution and an elevation in cytosolic Ca^{2+} levels. From this dose-response graph an IC_{50} of 2 µM RO2959 was obtained. This is more than double the IC_{50} for RO2959 in RBL-2H3 cells, inhibiting the endogenous CRAC current. However, the IC_{50} in that study was measured using whole-cell patch clamp as opposed to fluorescent Ca^{2+} imaging and as such is likely to be more sensitive.

The experiments undertaken in figure 3.5 provide additional vital evidence that CRAC channel inhibition is sufficient to decrease elevated cytosolic Ca^{2+} levels caused by store-operated Ca^{2+} influx, without any pre-incubation required. However, as in previous studies (130) and in line with other experiments in this chapter RO2959 was also utilised in a pre-incubation protocol according to section 2.5.2. Pancreatic acinar cells were pre-incubated with increasing concentrations of RO2959 for ten minutes before the re-introduction of 2 mM Ca^{2+} to the extracellular solution. Figure 3.6 A demonstrates the effect of pre-incubating cells with 1 µM RO2959 on Ca^{2+} influx. In those cells pre-incubated with RO2959, after store depletion with CPA, cytosolic Ca^{2+} levels dropped below baseline levels, which is sometimes seen during store depletion of pancreatic acinar cells. Pre-incubation with 1 µM did not significantly reduce the amplitude of Ca^{2+} influx compared with control cells (figure 3.6 B). In figure 3.6 C the time taken to reach both half maximal Ca^{2+} influx and half maximal Ca^{2+} efflux are shown, indicating the rate of influx and efflux. Pre-incubating cells with 1 µM RO2959, despite not reducing the amplitude of Ca^{2+}, resulted in a significant slowing in the rate of Ca^{2+} influx compared with control cells (p < 0.0001) but the rate of Ca^{2+} efflux was not significantly affected by this concentration of RO2959 (p = 0.1524). As the rate of Ca^{2+} influx is more influenced by Ca^{2+} influx mechanisms than efflux mechanisms, the half time of influx is a good indicator of inhibitors effect on Ca^{2+}influx.

Figure 3.6 Pre-incubation of cells with 1 μM RO2959 did not significantly inhibit the amplitude of Ca^{2+} influx but did significantly prolong the rate of Ca^{2+} influx

Average traces (± SEM) from Fura-2 loaded pancreatic acinar cells

A – 1 μM RO2959 was applied to cells according to the protocol in section 2.5.2 before the re-introduction of 2 mM Ca^{2+} to the extracellular solution (control – blue n=12 and 1 μM RO2959 – red n=9).**B - S**ummary of changes in ratio amplitude due to Ca^{2+} influx from figure **A** in control cells (blue) and cells pre-incubated with 1 μM RO22959 (red) (p = 0.4072). **C** – Summary of the changes in half time of Ca^{2+} influx in control – blue and RO2959 treated – red (lower bars) (p < 0.0001) and half time of Ca^{2+} efflux in control – blue and RO2959 treated cells – red (upper bars) (p = 0.1524).
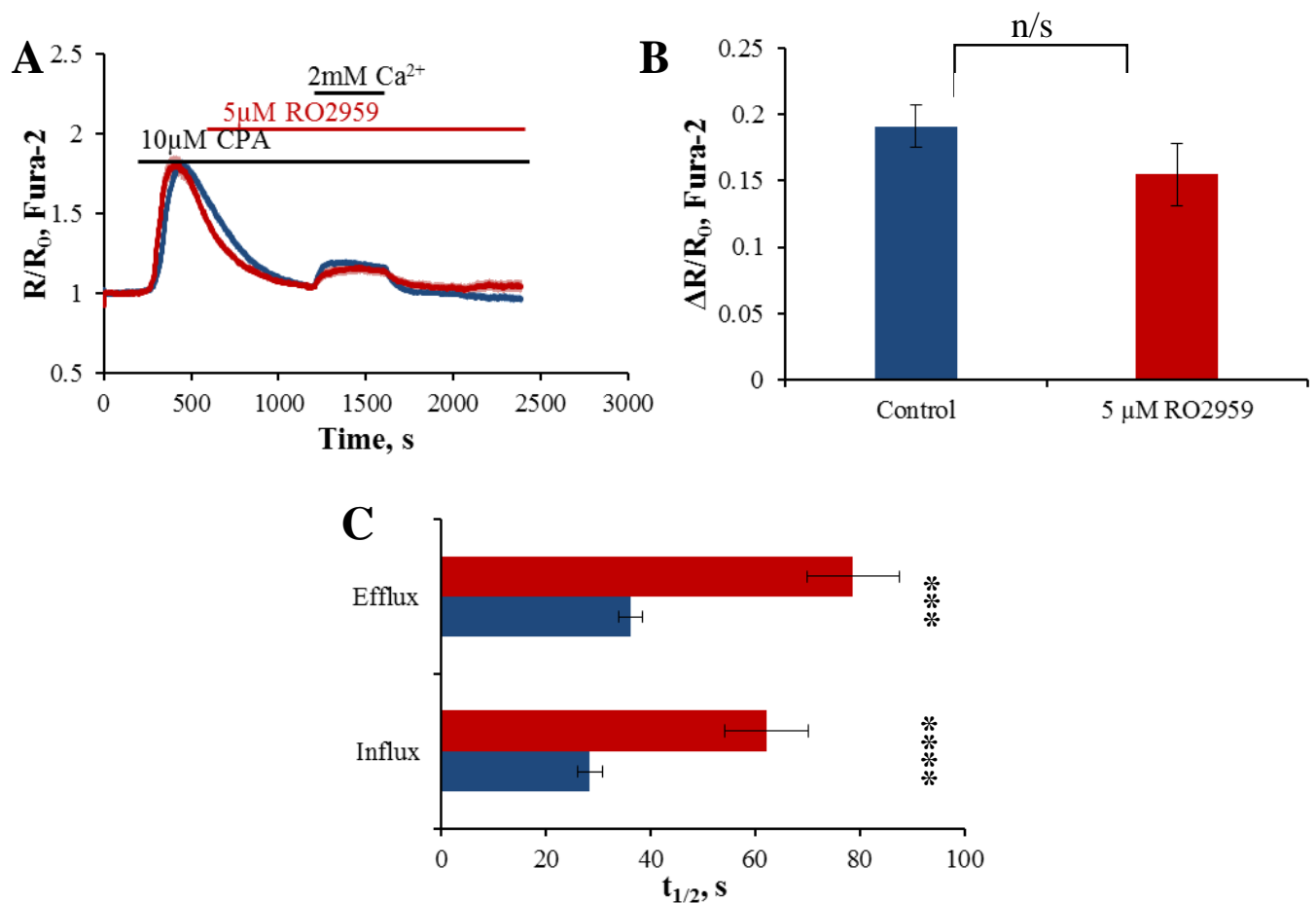
Figure 3.7 Pre-incubation of cells with 5 μM RO2959 resulted in a reduction in the amplitude of Ca²⁺ influx and the rate of Ca²⁺ influx

Average traces (± SEM) from Fura-2 loaded pancreatic acinar cells.

A- 5 μM RO2959 was applied to cells according to the protocol in section 2.5.2 before the re-introduction of 2 mM Ca^{2+} to the extracellular solution (control – blue n=21 and 5 μM RO2959 n= 16). **B -** Summary of changes in ratio amplitude due to Ca^{2+} influx from figure **A** in control cells (blue) and cells pre-incubated with 5 μM RO22959 (red) (p = 0.1964). **C –** Summary of the changes in half time of Ca^{2+} influx in control – blue and RO2959 treated – red (lower bars) (p < 0.0001) and half time of Ca^{2+} efflux in control – blue and RO2959 treated cells – red (upper bars) (p = 0.0002).

82

Figure 3.7 A shows that increasing the concentration of RO2959 to 5 µM and pre-incubating cells for the same duration still did not significantly decrease the amplitude of Ca^{2+} influx (p= 0.1964). The changes in ratio amplitude due to Ca^{2+} influx are summarised in figure 3.7 B. However, this is in contrast to the data in figure 3.5 B, where an acute application of 5 µM RO2959 resulted in a reduction of Ca^{2+} influx by 92%. Pre-incubation with 5 µM RO2959 was sufficient to significantly slow the rate of Ca^{2+} influx (p < 0.0001) compared with control cells and furthermore, this concentration resulted in a significantly slower rate of Ca^{2+} efflux (figure 3.7 C). The effect of 5 µM RO2959 pre-incubation on Ca^{2+} efflux was not observed with 1 µM RO2959 pre-incubation (figure 3.6 C).

The effect of further increasing the concentration of RO2959 to 10 µM and pre-incubating cells for the same duration as the previous two experiments is demonstrated in figure 3.8 A. This pre-incubation was sufficient to significantly reduce the amplitude of Ca^{2+} influx (p < 0.0001), compared to control cells. The changes in ratio amplitude due to Ca^{2+} influx are summarised in figure 3.8 B. When comparing acute application of RO2959 (figure 3.5 C) with pre-incubation with RO2959 (figure 3.8 C) 10 µM acutely reduced Ca^{2+} influx by 96.6 ± 1.5% whereas when it was applied in a pre-incubation experiment 10 µM reduced SOCE by 67.3 ± 2.7%.

Pre-incubation of cells with 20 µM RO2959 for the same duration as previous experiments, figure 3.9 A, was sufficient to significantly inhibit Ca^{2+} influx by 89.5 ± 2.9% (p=0.0095), compared with the amplitude of Ca^{2+} influx in control cells. The changes in ratio amplitude due to Ca^{2+} influx are summarised in figure 3.9 B. The same concentration of RO2959, when applied acutely resulted in a 89.2 ± 1.9% reduction in Ca^{2+} influx (figure 3.5 D). Although the amplitude of Ca^{2+} influx is significantly reduced by pre-incubation with 20 µM RO2959 the half time of Ca^{2+} influx between pre-incubation and control cells was not significantly changed (p = 0.1143). The time taken to reach half maximal Ca^{2+} efflux was significantly longer in RO2959 pre-incubated cells compared with control cells (p = 0.0095). The changes to the half time of Ca^{2+} influx and efflux are summarised in figure 3.9 C.
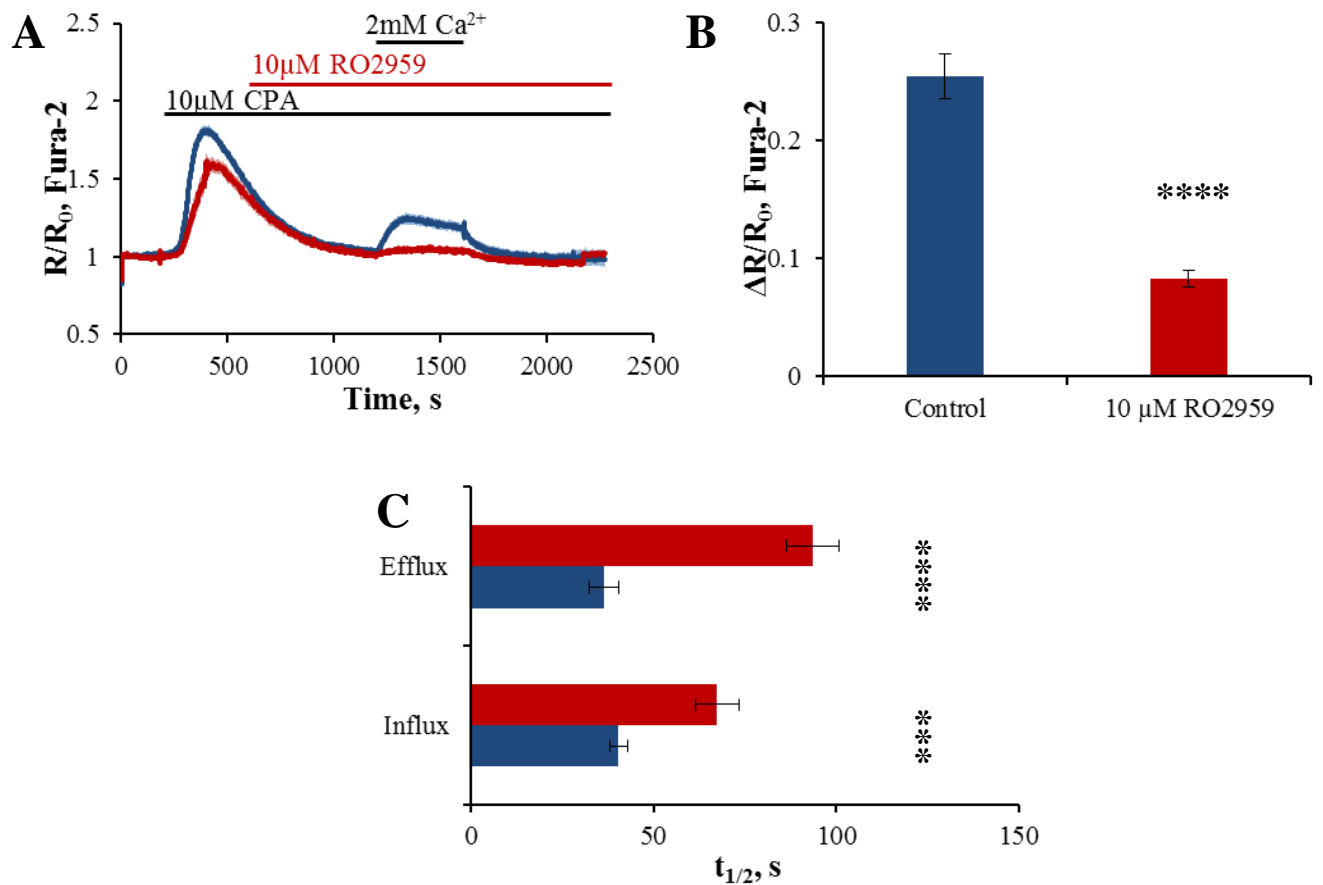
Figure 3.8 Pre-incubation of cells with 10 μM RO2959 significantly inhibited both the amplitude and rate of Ca^{2+} influx

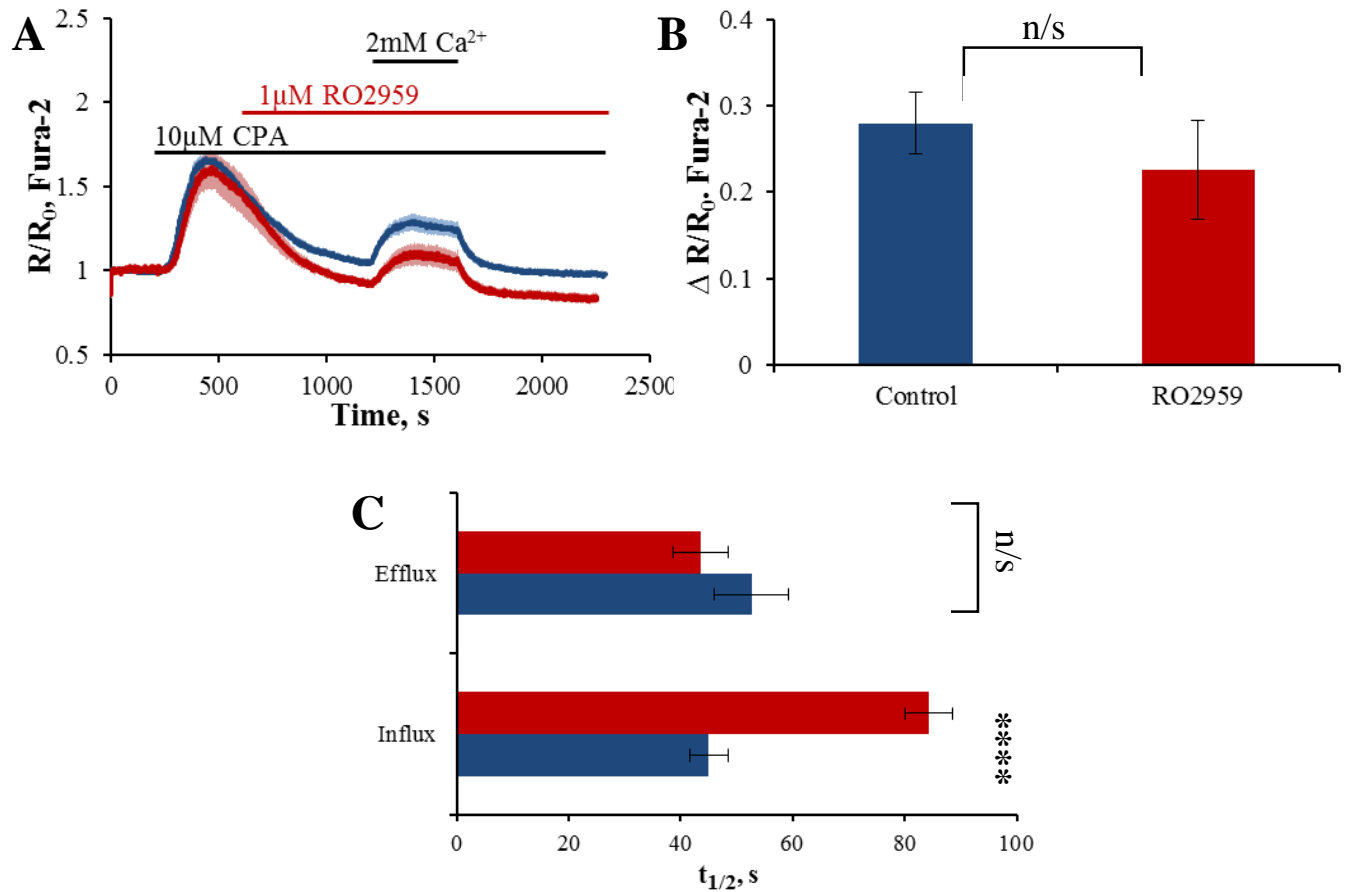Average traces (± SEM) from Fura-2 loaded pancreatic acinar cells.

A- 10 μM RO2959 was applied to cells according to the protocol in section 2.5.2 before the re-introduction of 2 mM Ca^{2+} to the extracellular solution (control – blue n=24 and 10 μM RO2959 n= 17). **B -** Summary of changes in ratio amplitude due to Ca^{2+} influx from figure **A** in control cells (blue) and cells pre-incubated with 10 μM RO22959 (red) (p < 0.0001). **C –** Summary of the changes in half time of Ca^{2+}influx in control – blue and RO2959 treated – red (lower bars) (p = 0.0004) and half time of Ca^{2+} efflux in control – blue and RO2959 treated cells – red (upper bars) (p < 0.0001).
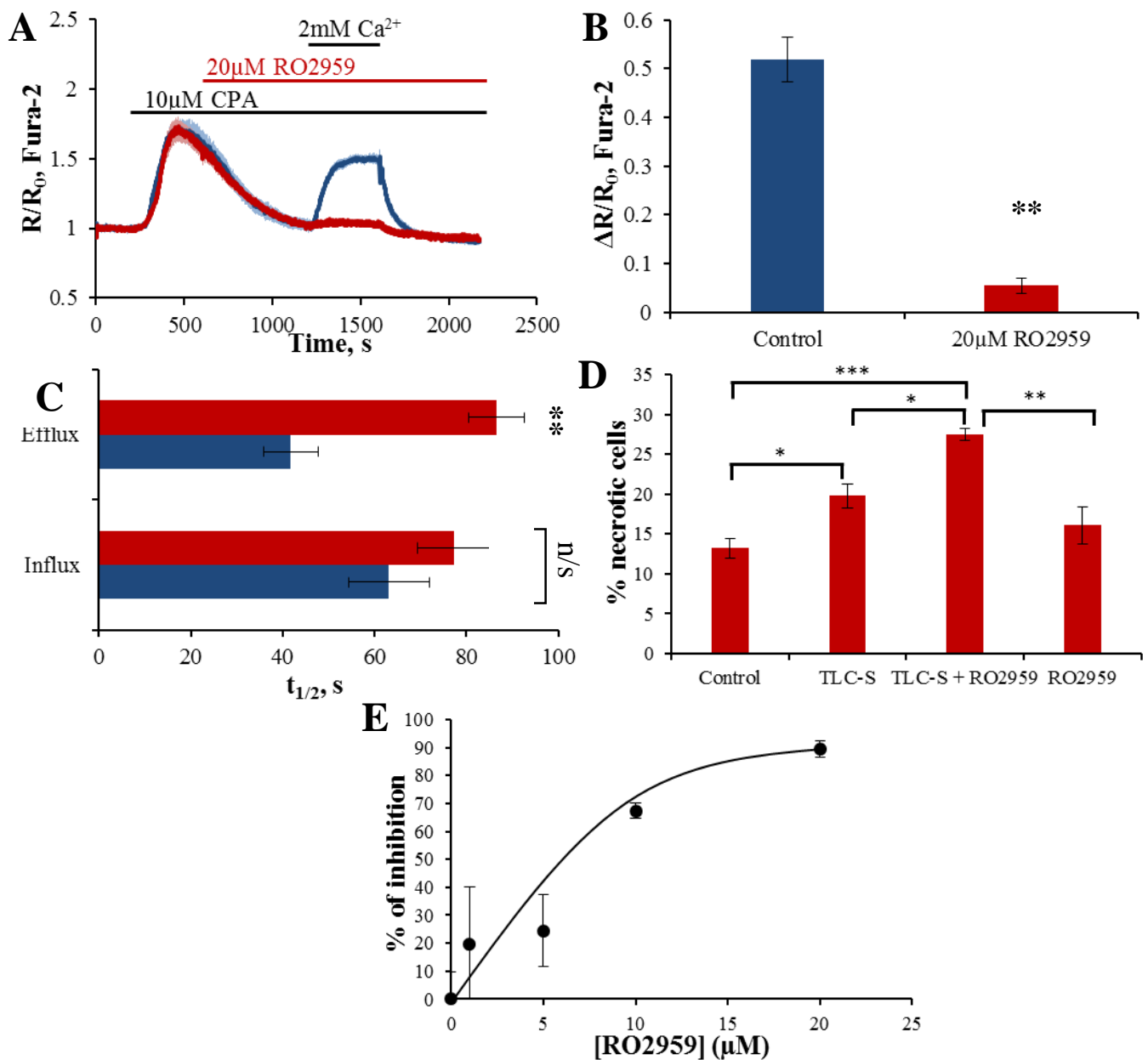
Figure 3.9 20 μM RO2959 significantly inhibited the amplitude of Ca²⁺ influx but resulted in an increase in cellular necrosis

Average traces (± SEM) from Fura-2 loaded pancreatic acinar cells.

A- 20 μM RO2959 was applied to cells according to the protocol in section 2.5.2 before the re-introduction of 2 mM Ca²⁺ to the extracellular solution (control – blue n=4 and 10 μM RO2959 n= 6). **B -** Summary of changes in ratio amplitude due to Ca²⁺ influx from figure **A** in control cells (blue) and cells pre-incubated with 20 μM RO22959 (red) (p = 0.0095). **C –** Summary of the changes in half time of Ca²⁺influx in control – blue and RO2959 treated – red (lower bars) (p = 0.1143) and half time of Ca²⁺ efflux in control – blue and RO2959 treated cells – red (upper bars) (p = 0.0095). **D-** Cellular necrosis measurements were made according to section 2.6, 1 hour incubation with 200 μM TLC-S resulted in an increase in cellular necrosis as measured by staining with propidium iodide. Cells were pre-incubated with 20 μM RO2959 before an hour long incubation with TLC-S, which resulted in a further increase in cellular necrosis (control = 79. TLC-S = 147. TLC-S + RO2959 = 214. **E –** Dose-response curve for % inhibition of Ca²⁺ influx for the above experiments

In order to be an effective treatment for acute pancreatitis a CRAC channel inhibitor is required to be effective at inhibiting Ca^{2+} influx, and thereby reducing cytosolic Ca^{2+} overload, as well as reducing the amount of cellular necrosis – two key hallmarks of acute pancreatitis. This is not always the case for agents known to inhibit CRAC channels; 2-APB has been demonstrated to cause cellular necrosis (130). Figure 3.9 D demonstrates the effect of an RO2959 cell death assay undertaken according to the protocol in section 2.6. Cells were incubated with the bile salt TLC-S for one hour, as a method of causing cellular necrosis mimicking biliary acute pancreatitis. In order to protect cells from cellular necrosis, cells were pre-incubated with 20 µM RO2959 for ten minutes before the hour long incubation with TLC-S. The results in figure 3.9 D demonstrate that the combined incubation with TLC-S significantly increased the percentage of necrosis compared with control (p = 0.05) and combined incubation of RO2959 and TLC-S resulted in a further increase in percentage of necrosis compared with TLC-S treatment alone (p = 0.05). RO2959 treatment alone did not significantly increase necrosis compared to control, but perhaps sensitised cells making them more vulnerable to cell death.

1.1.2. Pyr6

A recent paper described tools that were generated to distinguish between TRPC3-mediated Ca^{2+} entry and Orai1-mediated Ca^{2+} entry pharmacologically (195). The specificity of Pyr3 as a TRPC3 specific antagonist has been questioned. The authors tested Pyr2/BTP2, Pyr3, Pyr6 and newly generated Pyr10 for their ability to inhibit TRPC3 or Orai1. Pyr6 (307,308) was determined to be Orai1 specific inhibitor. Pyr10 was determined to be a TRPC3 inhibitor and is discussed in the TRPC3 section of this chapter (section 3.3).

Pyr6 had a maximal inhibitory effect in native RBL-2H3 cells at 10 µM. These cells were utilised in this paper to study endogenous SOCE, similar to other studies in this field (195). In pancreatic acinar cells, in a pre-incubation protocol (according to section 2.5.3) 10 µM Pyr6 (figure 3.10 A) was applied to cells for ten minutes before the re-introduction of 2 mM Ca^{2+} to the extracellular solution, this concentration was sufficient to significantly inhibit SOCE by $83.3 \pm 1.1\%$ compared to control (figure 3.10 B). The pre-incubation of cells with Pyr6 did not significantly reduce the time taken to reach half maximal Ca^{2+} influx but did significantly slow the time to half maximal Ca^{2+} efflux (figure 3.10 C). Figure 3.10 D shows the effect of acute application of 10 µM Pyr6 in the continued presence of 2 mM extracellular Ca^{2+} during a sustained plateau in cytosolic Ca^{2+}, this concentration was sufficient to reduce

SOCE by $83.3 \pm 5.4\%$, a significant reduction. Upon removal of Ca^{2+} and Pyr6 from the extracellular solution, cytosolic Ca^{2+} levels returned to baseline levels. Both the pre-incubation protocol and acute application protocol with 10 µM Pyr6 inhibited SOCE by the same percentage.

When Pyr6 was pre-incubated with AR42J cells, a pancreatic acinar cell-like cell line, the resultant Ca^{2+} influx was of a different magnitude compared with the same length pre-incubation, with the same concentration of Pyr6, in primary pancreatic acinar cells (figure 3.7). Figure 3.11 A demonstrates that pre-incubation of AR42J cells with 10 µM Pyr6 pre-incubation for ten minutes resulted in a reduction in the amplitude of Ca^{2+} influx, compared with control cells (figure 3.11 B). The time taken to reach half maximal Ca^{2+} influx was significantly slowed in cells pre-incubated with Pyr6 compared with control cells ($p = 0.0001$) but the time taken to reach half maximal Ca^{2+} efflux was significantly faster in cells pre-incubated with Pyr6 compared with control cells; the changes in half time of Ca^{2+} influx and efflux are summarised in figure 3.11 C. The difference in the magnitude of the inhibition in primary acinar cells compared with the pancreatic cell line was marked, in acinar cells Pyr6 reduced Ca^{2+} influx by 83.3 ± 1.6 % (figure 3.10), whereas in AR42J cells Ca^{2+} influx was reduced by 49.4 ± 5.0 % under identical conditions (figure 3.11). Functionally, this suggests a difference in expression levels of Orai1 in pancreatic acinar cells compared with AR42J cells, due to the difference in the magnitude of inhibition seen between the two cell types.
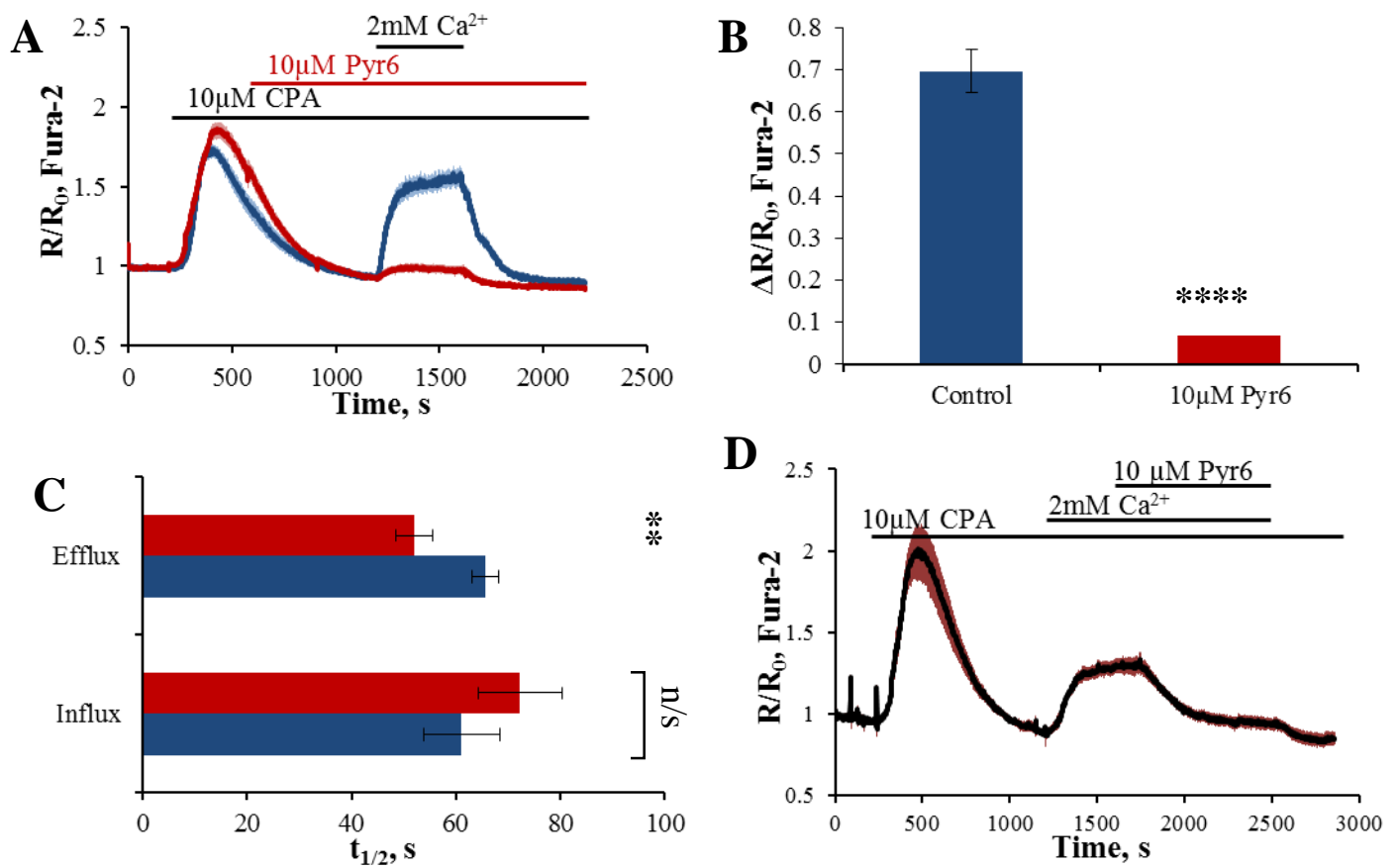
Figure 3.10 Pyr6 inhibited Orai1 mediated SOCE in both pre-incubation and acute treatments

Average traces (±SEM) from Fura-2 loaded pancreatic acinar cells

A- 10 μM Pyr6 was pre-incubated with cells according to the protocol in section 2.5.2, before the re-introduction of 2mM Ca^{2+} to the extracellular solution (control – blue n=28. 10 μM Pyr6 – red n=33.). **B- S**ummary of changes in ratio amplitude due to Ca^{2+} influx from figure **A** in control cells (blue) and cells pre-incubated with 10 μM Pyr6 (red) (p < 0.0001). **C –** Summary of the changes in half time of Ca^{2+}influx in control – blue and Pyr6 treated – red (lower bars) (p = 0.2108)and half time of Ca^{2+} efflux in control – blue and Pyr6 treated cells – red (upper bars) (p = 0.003). **D -** 10 μM Pyr6 was acutely applied to cells, according to the protocol in section 2.5.3, in the continued presence of 2 mM extracellular Ca^{2+} (n=11).
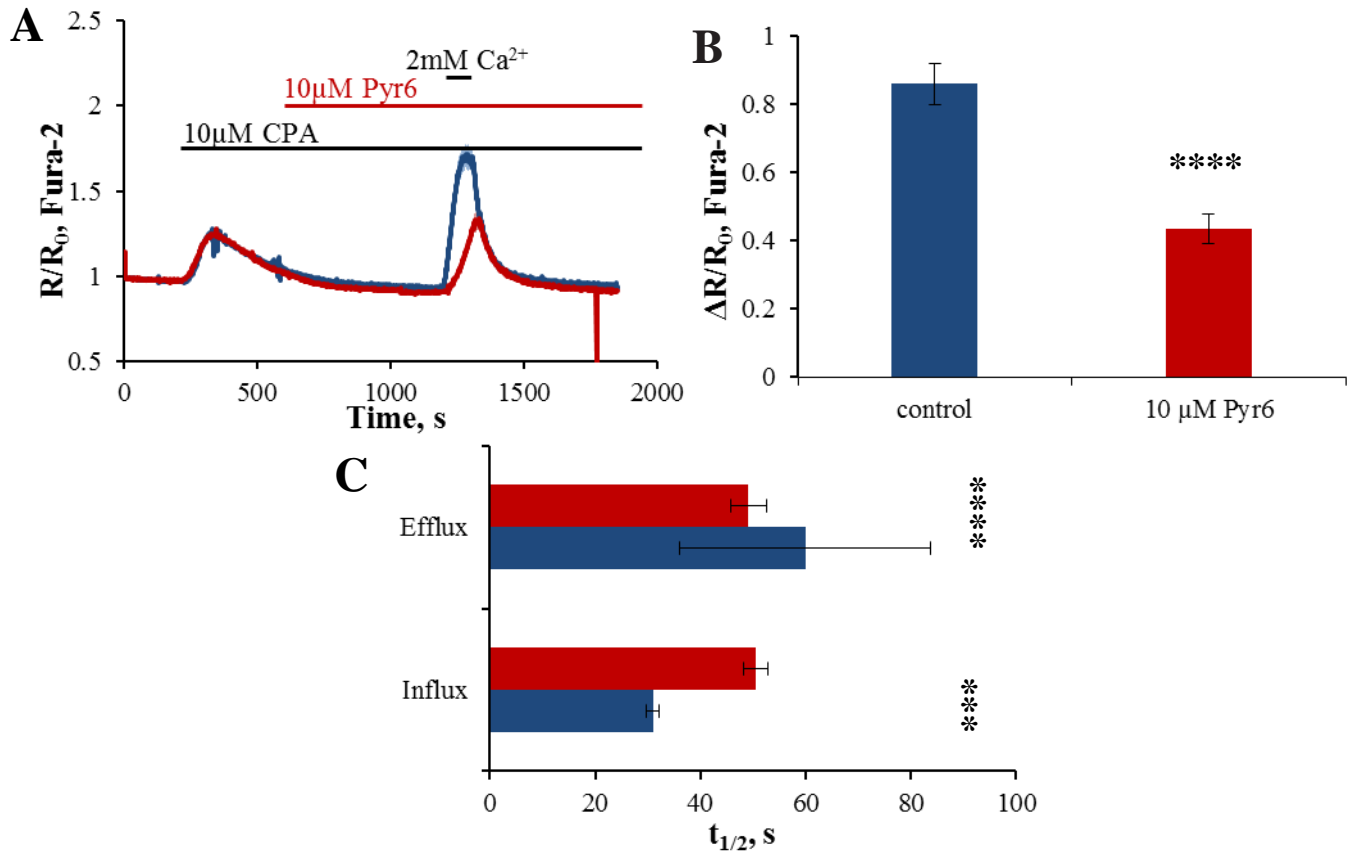
Figure 3.11 Pyr6 an Orai1 channel inhibitor, reduced store-operated Ca²⁺ influx in AR42J cells

Average traces (±SEM) from Fura-2 loaded AR42J cells

A- ER stores were depleted according to the protocol in section 2.5.2 and then cells were pre-incubated with 10 μM Pyr6 for ten minutes before 2 mM Ca^{2+} was subsequently re-introduced to the extracellular solution. Blue trace represents control cells (n = 52). Red trace represents 10 μM Pyr6 (n = 41). **B-** Summary of the changes in the ratio amplitude due to Ca^{2+} influx (from cells in figure **A**) control (blue bar) and Pyr6 treated (red bar) (p = 0.0001). **C-** Summary of the changes in the half time of Ca^{2+} influx (bottom bars) control – blue, Pyr6 treated – red (p = 0.0001). Half time of Ca^{2+} efflux (upper bars) control – blue, Pyr6 treated – red (p = 0.0005).

1.2. Inhibition of TRPC3 mediated Ca^{2+} entry

1.2.1. Pyr3

Pancreatic acinar cells also express TRPC3 channels, non-specific cation channels that contribute to Ca^{2+} influx but whether this Ca^{2+} influx channel is store-dependent is still debated in the field. In all instances application of Orai1 inhibitors, GSK-7975A (130), DPB163-AE, DPB162-AE, RO2959 and Pyr6, was effective at inhibiting Ca^{2+} entry, . However, concerns have been raised over the remaining small percentage of Ca^{2+} influx observed, a possible explanation is that there is contribution by other channels, such as TRPC3, to Ca^{2+} influx. Pyr3 was reported to be specific for TRPC3 but not for other members of the TRPC subfamily (309). Further to the study on pancreatic acinar cells isolated from TRPC3 knock out mice (220), Pyr3 was utilised in identical experiments also on pancreatic acinar cells in a later paper, where the authors saw a similar magnitude of inhibition on Ca^{2+} entry in cells treated with Pyr3 and cells deficient in TRPC3 (221). The reported maximal inhibitory effect seen with Pyr3 in pancreatic acinar cells was at 3 μM (221), resulted in approximately 50% reduction in SOCE.

In order to ensure maximal inhibition of TRPC3 channels in pancreatic acinar cells 10 μM Pyr3 was used in a pre-incubation protocol according to section 2.5.2, cells were pre-incubated for ten minutes before the re-introduction of 5 mM Ca^{2+} to the extracellular solution, as seen in figure 3.12 A. Figure 3.12 B demonstrates the effect of acute application of 10 μM Pyr3 on Ca^{2+} influx when applied to cells in the continued presence of 5 mM Ca^{2+}. The initial phase of Ca^{2+} influx from figure 3.12 B can be used as a control for Ca^{2+} influx in pre-incubation protocol (figure 3.12 A) as the experiments were undertaken on the same day. The changes in Ca^{2+} influx for figure 3.12 A and B are summarised in figure 3.12 E, on the left the blue bar represents the change in ratio amplitude due to Ca^{2+} influx in figure 3.12 B (acute application) and the red bar represents the change in ratio amplitude due to Ca^{2+} influx in figure 3.12 A (pre-incubation). Pre-incubation with 10 μM Pyr3 for ten minutes significantly inhibited Ca^{2+} influx by 86.3 ± 14.8 % compared to Ca^{2+} influx in control cells (p= 0.0007) (figure 3.12 A).

Figure 3.12 Pyr3, inhibitor of TRPC3 channels, inhibits Ca²⁺ entry in pancreatic acinar cells

Average traces (± SEM) from Fura-2 loaded pancreatic acinar cells.

A- Cells were treated according to the protocol in section 2.5.2 and pre-incubated with 10 μM for ten minutes before the re-introduction of 5 mM of Ca^{2+} to the extracellular solution (n = 9). **B-** Cells were treated according to the protocol in section 2.5.3, 10 μM Pyr3 was applied to cells in the continued presence of 5 mM extracellular Ca^{2+} on top of a sustained plateau in cytosolic Ca^{2+} (n = 10). **C-** Cells were treated identically to **A** with the exception of the re-introduction of 2 mM Ca^{2+} to the extracellular solution (n = 8). **D-** Cells were treated identically to **B** with the exception that 10 μM Pyr3 was applied in the continued presence of 2 mM extracellular Ca^{2+}(n = 9). **E-** Summary of the changes in ratio amplitude in acute application experiments (blue bars) with 5 mM extracellular Ca^{2+} (right) and 2 mM Ca^{2+}(left) and in pre-incubation experiments (red bars) with 5mM extracellular Ca^{2} (right, p = 0.0007) and 2mM extracellular Ca^{2+}(left, p < 0.0001).

The experiments were repeated using 2 mM Ca^{2+} extracellular calcium, in line with experiments undertaken in (221). Figure 3.12 C utilised an identical protocol to figure 3.12 A using 2 mM Ca^{2+} in the extracellular solution, the same concentration of Pyr3 was able to inhibit Ca^{2+} influx presumably due to the somewhat reduced driving force for Ca^{2+} into the cell. Figure 3.12 D utilised an identical protocol to figure 3.12 B, again substituting 5 mM for 2 mM extracellular Ca^{2+}. The effect of the same concentration of Pyr3 in the continued presence of a reduced extracellular Ca^{2+} concentration was greater than in figure 3.12 B. Pre-incubation with 10 μM Pyr3 for ten minutes inhibited Ca^{2+} influx, induced by 2 mM extracellular Ca^{2+}, by 96.3 ± 15.9 % compared to Ca^{2+} influx in control cells (figure 3.12 D). In both acute and pre-incubation protocols 10 μM Pyr3 had a more inhibitory effect on Ca^{2+} influx and therefore reduced cytosolic Ca^{2+} levels more in protocols in which Ca^{2+} influx was driven by 2 mM Ca^{2+} in the extracellular solution.

Ba^{2+} is often used to study SOCE, as it gives rise to a unidirectional flux of ions. Ba^{2+} binds Fura-2 much the same as Ca^{2+} and can enter cells across the plasma membrane, through Ca^{2+} permeable channels such as CRAC channels. However, it is not possible for Ba^{2+} to be sequestered into stores or extruded back across the plasma membrane, as it cannot be actively transported by ATP-dependent pumps (310–312). In figure 3.13 unidirectional Ba^{2+} flux was used to study the efficacy of Pyr3 in inhibiting Ba^{2+} influx in cells after store depletion. In figure 3.13 A, cells were treated according to the protocol in section 2.5.2 and were pre-incubated with 10 μM Pyr3 for 400 seconds before the introduction of 10 mM Ba^{2+} to the extracellular solution, in order to maximally activate Ba^{2+} entry through channels. The pre-incubation with Pyr3 significantly inhibited Ba^{2+} entry by 54.5 ± 4.6% compared to control cells (figure 3.13 B). The half time of influx was significantly slowed in Pyr3 pre-incubated cells compared to control cells (figure 3.13 C).
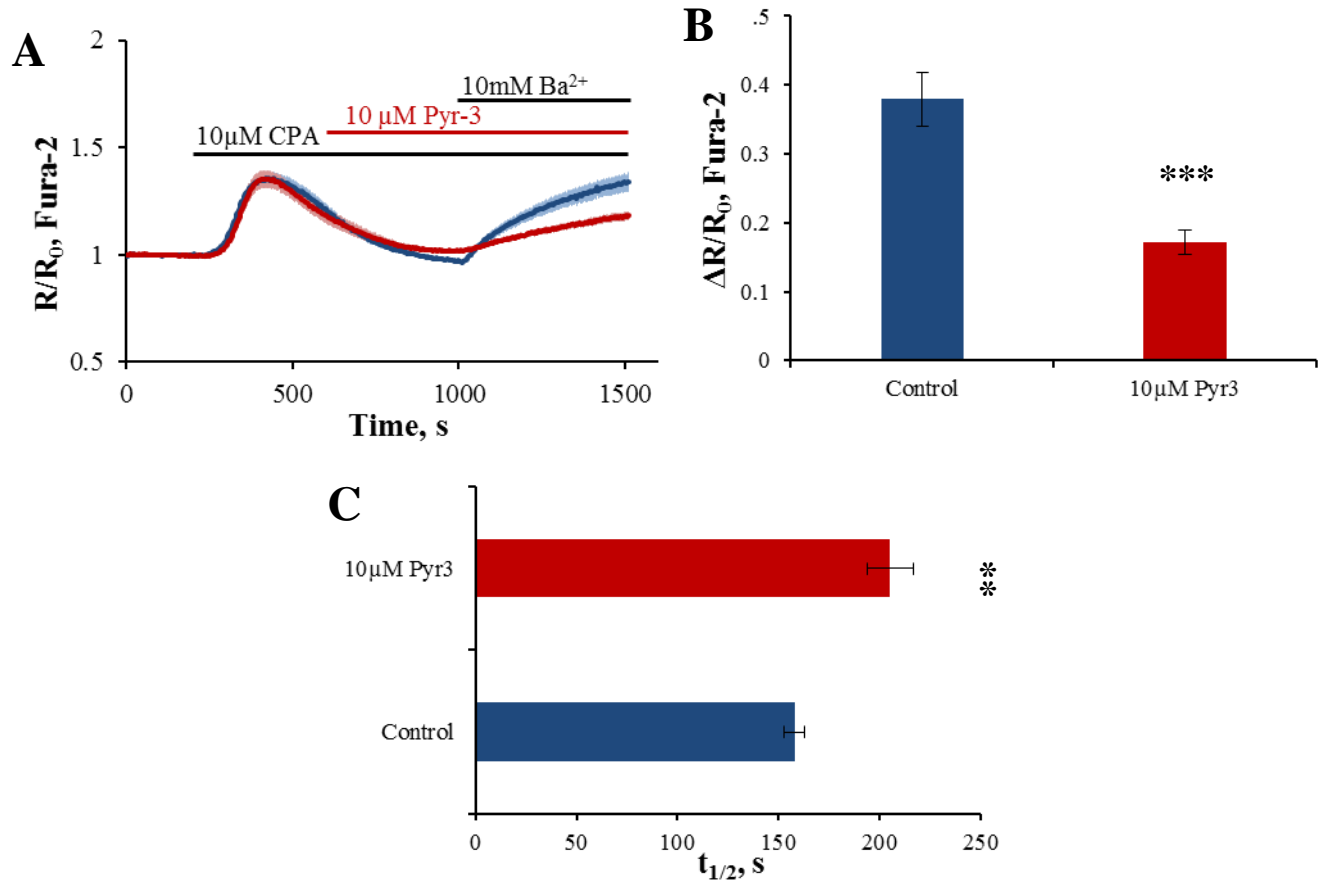
Figure 3.13 Pyr3 inhibited Ba^{2+} influx

Average traces (± SEM) from Fura-2 loaded pancreatic acinar cells.

A- Cells were treated according to the protocol in section 2.5.2, cells were pre-incubated with 10 μM Pyr3 for 400 seconds before the re-introduction of 10 mM Ba$^{2=}$ to the extracellular solution. Control-blue n=12. 10 μM Pyr3 – red n=13. **B-** Summary of the changes in ratio amplitude due to Ba^{2+}influx in control (blue) and 10 μM Pyr3 (red p = 0.0002). **C-** Summary of the changes in the half time of Ba^{2+} influx in control cells (blue) and 10 μM Pyr3 pre-incubated cells (red p= 0.0016)

1.2.2. Pyr10

As mentioned in section 3.2.3, a novel TRPC3 channel inhibitor was developed and utilised in experiments to determine the specificity of Pyr6 and Pyr3 for TRPC3 and Orai1 channels. Alongside Pyr3, Pyr10 was used to specifically inhibit TRPC3 channels (195). Pyr10 was found to be 18 times more specific for TRPC3 channels than for native CRAC channels, largely thought to mediate Ca^{2+} entry through Orai1. Pyr10 was able to inhibit Orai1 but was demonstrated to less effective at inhibiting Orai1-mediated Ca^{2+} influx and needed to be used at much greater concentrations than were effective to inhibit TRPC3 channels (195).

In HEK293 cells expressing YFP-TRPC3, 10 μM Pyr10 was sufficient to near maximally inhibit Ca^{2+} entry as measured by Fura-2 in Ca^{2+} imaging experiments, as such this concentration was used in the experiment in figure 3.14 A. Cells were pre-incubated with 10 μM Pyr10 for ten minutes before the re-introduction of 2 mM Ca^{2+} to the extracellular solution, according to the protocol in section 2.5.2. When applied to cells during the store depletion part of the protocol, 10 μM Pyr10 affected the Ca^{2+} clearance from the cytosol. In control cells the application of CPA in the absence of extracellular Ca^{2+} resulted in a transient increase in cytosolic Ca^{2+} that was rapidly extruded across the plasma membrane by the PMCA, ensuring that cytosolic Ca^{2+} levels return to baseline. However, cytosolic Ca^{2+} levels in cells pre-incubated with 10 μM Pyr10 did not return to baseline levels during the same time course as control cells. It is possible that if the time course of store depletion and pre-incubation were extended, cytosolic Ca^{2+} levels would have returned to baseline. As such, at the time point at which extracellular Ca^{2+} was re-introduced cytosolic Ca^{2+} level were significantly different compared to control (p= 0.0025). Despite this, the pre-incubation of cells with Pyr10 significantly inhibited the amplitude of Ca^{2+} entry (p= 0.012), as summarised in figure 3.14 B. The rate of Ca^{2+} influx in cells pre-incubated with 10 μM Pyr10 was significantly slower (p= 0.0075) compared to in control cells. The time take to reach half maximal Ca^{2+} efflux not significantly different in cells pre-incubated with Pyr10 compared to control cells (p= 0.1373).

Figure 3.14 The novel TRPC3 inhibitor Pyr10 had an inhibitory effect on Ca²⁺ influx

Average traces (± SEM) from Fura-2 loaded pancreatic acinar cells

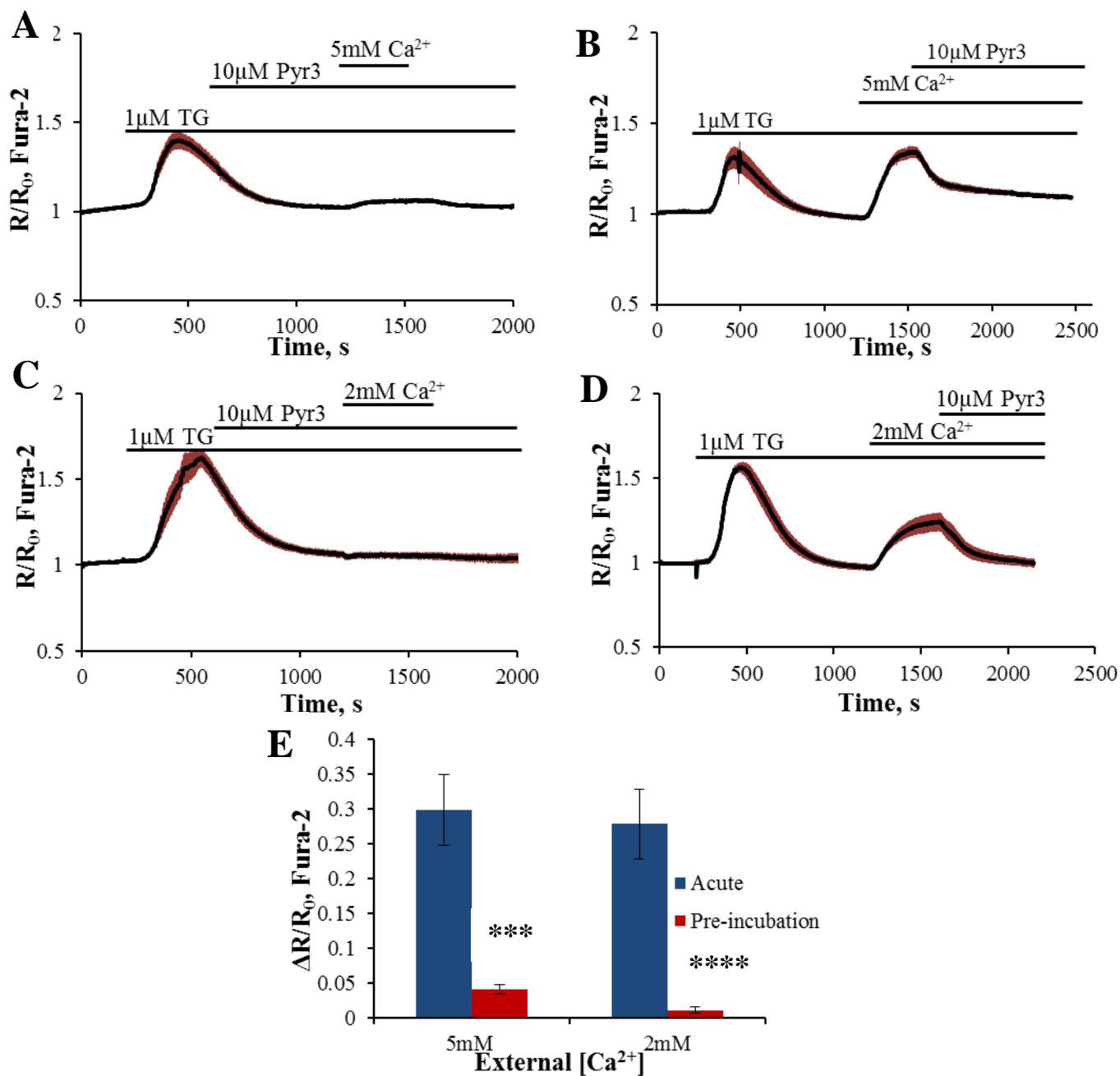**A-** Cells were treated according to the protocol in section 2.5.2, cells were pre-incubated with 10 μM Pyr10 for ten minutes before the re-introduction of 2 mM Ca^{2+} to the extracellular solution. Control – blue (n= 20) 10 μM pre-incubated – red (n=17). **B-** Summary of the change in ratio amplitude due to Ca^{2+} influx, from **A,** in control (blue) and 10 μM Pyr10 treated cells (red p= 0.012). **C-** Summary of half time of influx in control -blue and Pyr10 treated cells - red (lower bars p= 0.0075) and the half time of Ca^{2+} efflux in control – blue and Pyr10 treated cells – red (upper bars).

The Ca^{2+} influx and efflux half times are summarised in figure 3.14 C. Upon removal of Ca^{2+} from the extracellular solution cytosolic Ca^{2+} levels returned to baseline levels in control cells, however, in cells pre-incubated with Pyr10, cytosolic Ca^{2+} levels did not return to baseline levels, nor did they return to the level of pre-Ca^{2+} re-introduction. It is likely that this concentration of Pyr10 has non-specific and off-target effects. Based on the impaired clearance of Ca^{2+} from the cytosol in all repeats of the experiment in figure 3.14 A one of these non-specific targets is PMCA.

When AR42J cells were pre-incubated with Pyr6 the reduction in Ca^{2+} influx observed was significantly smaller than the same pre-incubation in primary acinar cells, therefore, it was sought to determine if this was the same case with Pyr10, which is reported to be more specific for Orai1 over TRPC3. When applied to AR42J cells, 10 μM Pyr10 incubation for 10 minutes (figure 3.15 A) resulted in a significant inhibition of Ca^{2+} influx compared with control cells ($p < 0.0001$). Furthermore, the magnitude of inhibition in AR42J cells due to Pyr10 pre-incubation (figure 3.15 A) was different to the magnitude of inhibition demonstrated in pancreatic acinar cells (figure 3.14 A). Pyr10 resulted in a 36.9 ± 9.1 % decrease in Ca^{2+} influx in pancreatic acinar cells, whereas in AR42J cells there was a decrease of 76.8 ± 5.1 % in Ca^{2+} influx. Figure 3.15 B summarises the changes in ratio amplitude due to Ca^{2+} influx in AR42J cells. The rate of Ca^{2+} influx was significantly slowed in cells pre-incubated with Pyr10 compared with control cells ($p < 0.0001$) and in addition rate of Ca^{2+} efflux was also significantly slowed in cells pre-incubated with Pyr10 ($p < 0.0001$) compared with control cells (figure 3.15 C).

Figure 3.15 Pyr10, a TRPC3 channel inhibitor, reduced store-operated Ca2+ influx in AR42J cells

Average traces (±SEM) from Fura-2 loaded AR42J cells

A- ER stores were depleted according to the protocol in section 2.5.2 and then cells were pre-incubated with 10 μM Pyr10 for ten minutes before 2 mM Ca^{2+} was subsequently re-introduced to the extracellular solution. The blue trace represents control cells (n = 55). The red trace represents 10 μM Pyr10 (n = 45). **B-** Summary of the changes in the ratio amplitude due to Ca^{2+} influx (from cells in figure **A**) control (blue bar) and Pyr10 treated (red bar) (p = 0.0001). **C-** Summary of the changes in the half time of Ca^{2+} influx (bottom bars) control – blue, Pyr10 treated – red (p = 0.0001). Half time of Ca^{2+} efflux (upper bars) control – blue, Pyr10 treated – red (p = 0.0001).

1.3. Inhibition of Orai1 and TRPC3-mediated Ca^{2+} entry

Although the application of Orai1 channel inhibitors alone and TRPC3 channel inhibitors alone was particularly effective at inhibiting Ca^{2+} influx, in each instance there was always a small percentage of Ca^{2+} influx that remained; presumably because the other entry channel remained uninhibited. At the time it seemed pragmatic to inhibit both entry channels simultaneously.

1.3.1. GSK-7975A and Pyr3

The use of both an Orai1 channel inhibitor and a TRPC3 channel inhibitor should be sufficient to inhibit Ca^{2+} entry entirely, as these are the major entry pathways in pancreatic acinar cells. As 10 µM GSK-7975A (130) and 10 µM Pyr3 (section 3.3.1) were used in single application experiments, they were the concentrations utilised in this dual inhibitor application experiment. Figure 3.16 A demonstrates the pre-incubation of cells with 10 µM GSK-7975A and Pyr3, according to the protocol in section 2.5.2, for ten minutes before the re-introduction of 10 mM Ca^{2+} to the extracellular solution. Figure 3.16 B shows the effect of acute application of 10 µM GSK-7975A and Pyr3 in the continued presence of 10 mM Ca^{2+} to the extracellular solution, on top of an elevation in cytosolic Ca^{2+} levels. In a similar manner to figure 3.12, the initial phase of Ca^{2+} influx from figure 3.16 B was used as a control in order to compare the pre-incubation of inhibitors from figure 3.16 A; this pre-incubation was sufficient to significantly inhibit Ca^{2+} influx and thereby reduce cytosolic Ca^{2+} levels by $81.3 \pm 5.8\%$ (figure 3.16 C). In figure 3.16 B the acute application of inhibitors was sufficient to significantly reduce Ca^{2+} influx and cytosolic Ca^{2+} levels by $76.8 \pm 1.8 \%$ (p< 0.0001). Removal of extracellular Ca^{2+} and inhibitors from the extracellular solution resulted in a further decrease in cytosolic Ca^{2+} levels back to baseline levels.

Experiments using GSK-7975A (130) used 5 mM Ca^{2+} in the extracellular solution in the re-introduction protocol; in experiments using Pyr3, figure 3.12 A, 5 mM Ca^{2+} was also used. Figure 3.17 A shows the effect of pre-incubating cells with 10 µM GSK-7975A and 10 µM Pyr3 before the re-introduction of 5 mM Ca^{2+} to the extracellular solution. This pre-incubation was sufficient to significantly inhibit Ca^{2+} influx by $78.1 \pm 4.2 \%$ (figure 3.17 B). Figure 3.17 C shows the acute application of 10 µM Pyr3 and GSK-7975A in the continued presence of 5 mM extracellular Ca^{2+}, during a sustained elevation in cytosolic Ca^2 levels.
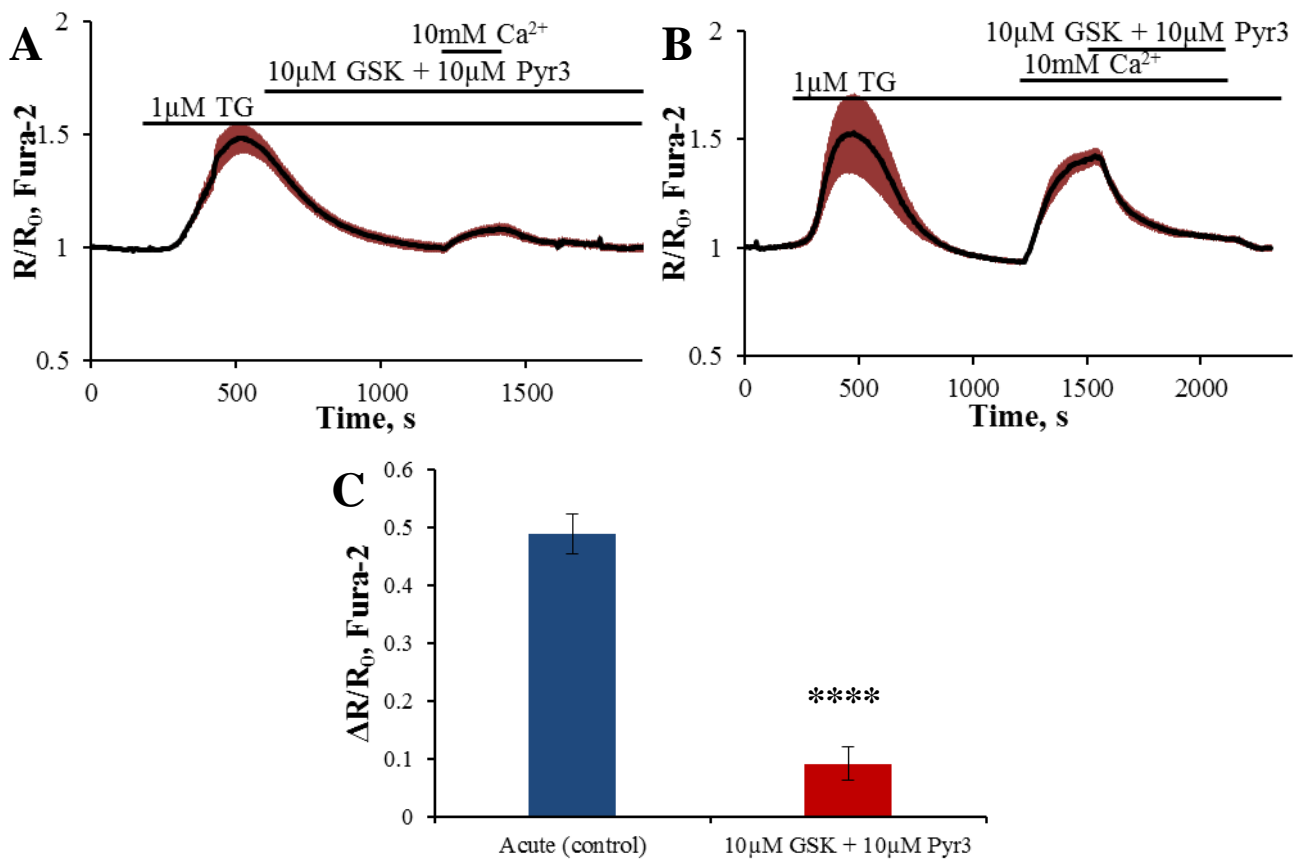
Figure 3.16 GSK-7975A and Pyr3 applied together to inhibited Orai1 and TRPC3-mediated Ca²⁺ entry
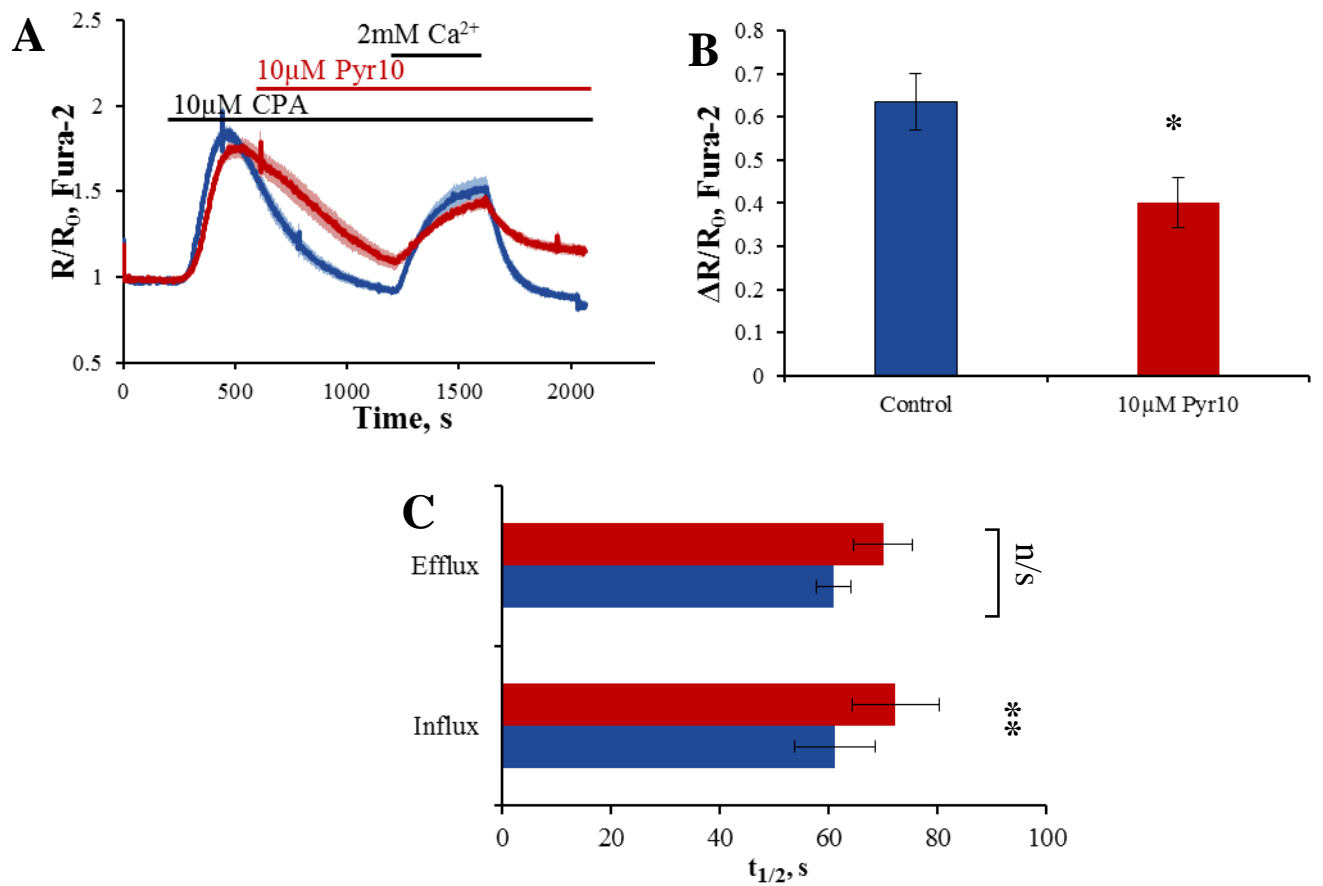
Average traces (± SEM) from Fura-2 loaded pancreatic acinar cells.

A- Cells were treated according to the protocol in section 2.5.2, cells were pre-incubated with 10 μM GSK-7975A and 10 μM Pyr3 for ten minutes before the re-introduction of 10 mM Ca^{2+} to the extracellular solution (n=13.). **B-** Cells were treated according to the protocol in section 2.5.3, 10 μM GSK-7975A and 10 μM Pyr3 was applied in the continued in presence of 10 mM extracellular Ca^{2+} on top of an increase in cytosolic Ca^{2+} levels (n = 4. p= 0.0008). **C-** Summary of the changes in ratio amplitude due to Ca^{2+} influx from acute application (used as control influx **B** blue bar₎ and from cells pre-incubated with GSK-7975A and Pyr3 (red bar p< 0.0001).
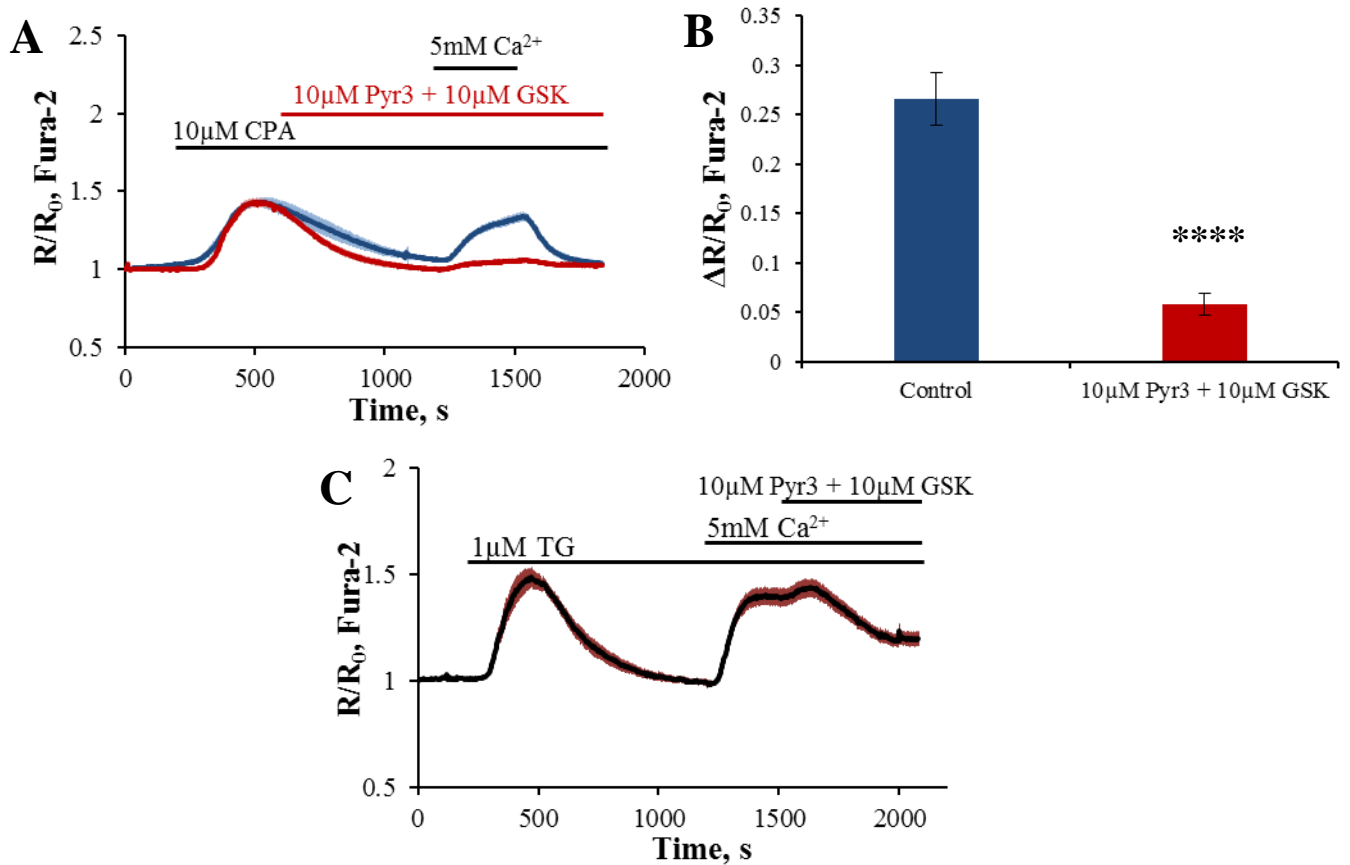
Figure 3.17 GSK-7975A and Pyr3 inhibited Orai1 and TRPC3 mediated Ca^{2+} influx induced by 5 mM Ca^{2+}
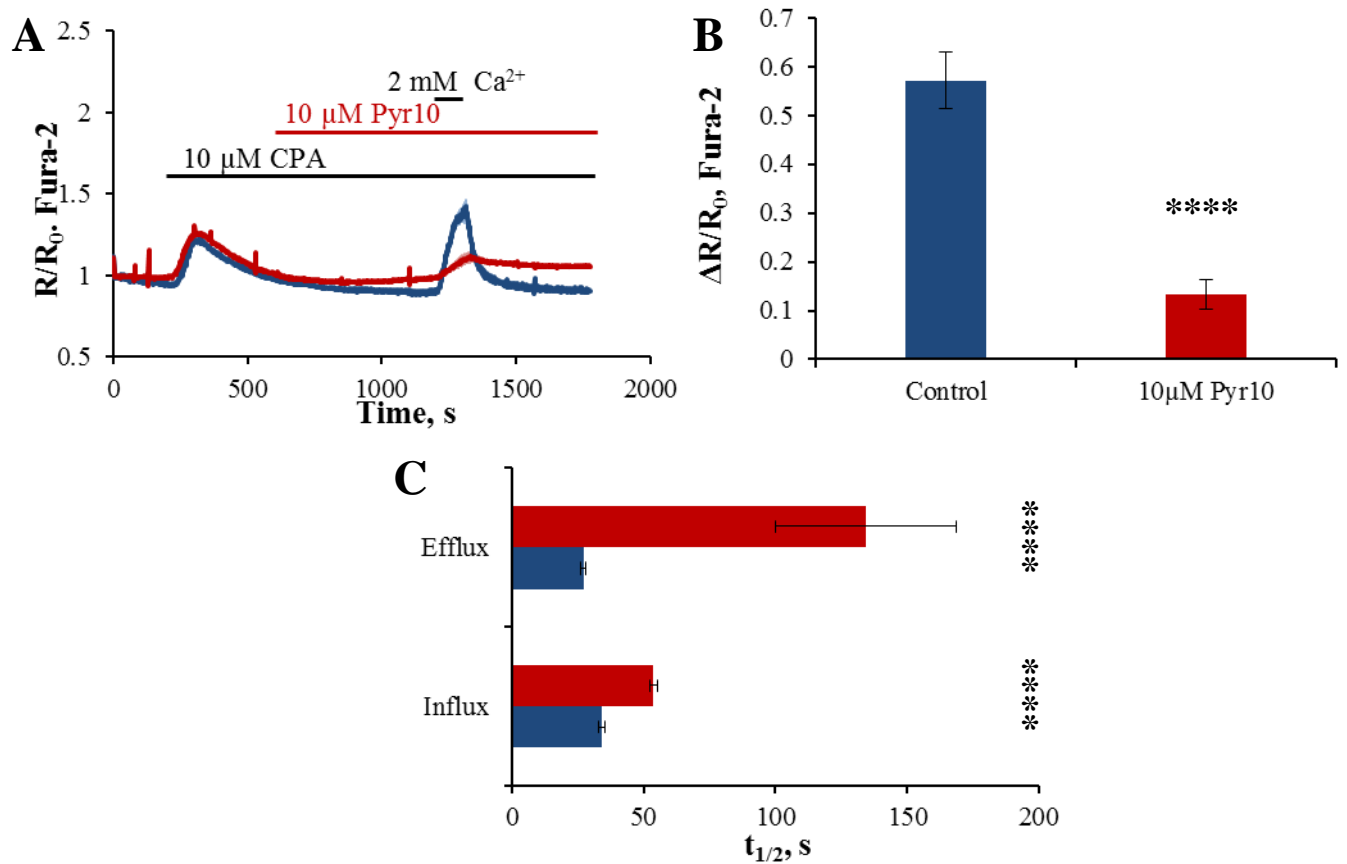
Average traces (± SEM) from Fura-2 loaded cells

A – Cells were treated according to the protocol in section 2.5.2. they were pre-incubated with 10 μM Pyr3 and 10 μM GSK-7975A for ten minutes before the re-introduction of 5 mM Ca^{2+} to the extracellular solution (control – blue n=5. 10 μM Pyr3 + 10 μM GSK-7975A – red n= 16.). **B-** Graph summarising the changes in ratio amplitude due to Ca$^{2\backslash=}$ influx from **A** in control cells (blue bar) and cells pre-incubated with Pyr10 and GSK-7975A (red bar, p < 0.0001). **C-** Cells were treated according to the protocol in section 2.5.3, 10 μM Pyr3 and 10 μM GSK-7975A was applied to cells in the continued presence of 5 mM Ca^{2+}, on top of an elevation in cytosolic Ca^{2+} levels (n= 8 p = 0.0018).

Upon addition of inhibitors to the extracellular solution, there was an initial small increase in cytosolic Ca^{2+} levels followed by a gradual decrease in cytosolic Ca^{2+} until a new plateau was reached. This acute application of GSK-7975A and Pyr3 was sufficient to significantly inhibit Ca^{2+} entry, and thereby to reduced cytosolic Ca^{2+} by 50.8 ± 6.1 % (p= 0.0018).

In figure 3.12 C and D, 2 mM extracellular Ca^{2+} was used to induce Ca^{2+} influx in order to study the inhibitory effect of Pyr3 alone , in figure 3.18 2 mM extracellular Ca^{2+} was also used to induce Ca^{2+} influx. Figure 3.18 A shows the effect of pre-incubating cells with 10 μM GSK-7975A and 10 μM Pyr3 for ten minutes before the re-introduction of 2 mM Ca^{2+} to the extracellular solution. This pre-incubation was sufficient to significantly inhibit Ca^{2+} entry by 87.9 ± 2.0 % (figure 3.13 B). Figure 3.18 C demonstrates the effect of acute application of 10 μM of both GSK-7975A and Pyr3 in the continued presence of 2 mM extracellular Ca^{2+}, on top of an elevation in cytosolic Ca^{2+}. Unlike in figure 3.17 C there was no increase in cytosolic Ca^{2+} after the addition of inhibitors, but rather a decrease in cytosolic Ca^{2+}, this continued until a new and lower plateau in cytosolic Ca^{2+} was attained. Ca^{2+} influx, and thereby cytosolic Ca^{2+}, was significantly inhibited by 65.0 ± 3.3% (p= 0.0002).

Pyr6 and Pyr10, inhibitors of Orai1 channels and TRPC3 channels respectively, were both used at 10 μM in a pre-incubation protocol (as described in section 2.5.2) for ten minutes before the re-introduction of 2 mM Ca^{2+} to the extracellular solution, as demonstrated in figure 3.18 D. The application of these two inhibitors during the store depletion step of the protocol resulted in incomplete clearance of Ca^{2+} from the cytosol after release from the ER. Ca^{2+}levels did not return to baseline levels and began to increase before Ca^{2+} was even re-introduced to the extracellular solution. Upon re-introduction of Ca^{2+} to the extracellular solution, the increase in cytosolic Ca^{2+} continued, the removal of extracellular Ca^{2+}did little to prevent the increase. The removal of Pyr6 and Pyr10 from the extracellular solution did result in the start of a declining phase of cytosolic Ca^{2+}. The effect of 10 μM Pyr10, in figure 3.14, was somewhat similar to that observed in figure 3.18 D. The cell's ability to clear Ca^{2+} from the cytosol was impaired during the store depletion by incubation with Pyr10, likely due to off-target effects on PMCA. This impaired clearance was exaggerated in experiments where Pyr6 and Pyr10 were incubated with cells together, in the absence of extracellular Ca^{2+}, cytosolic Ca^{2+} started to increase.
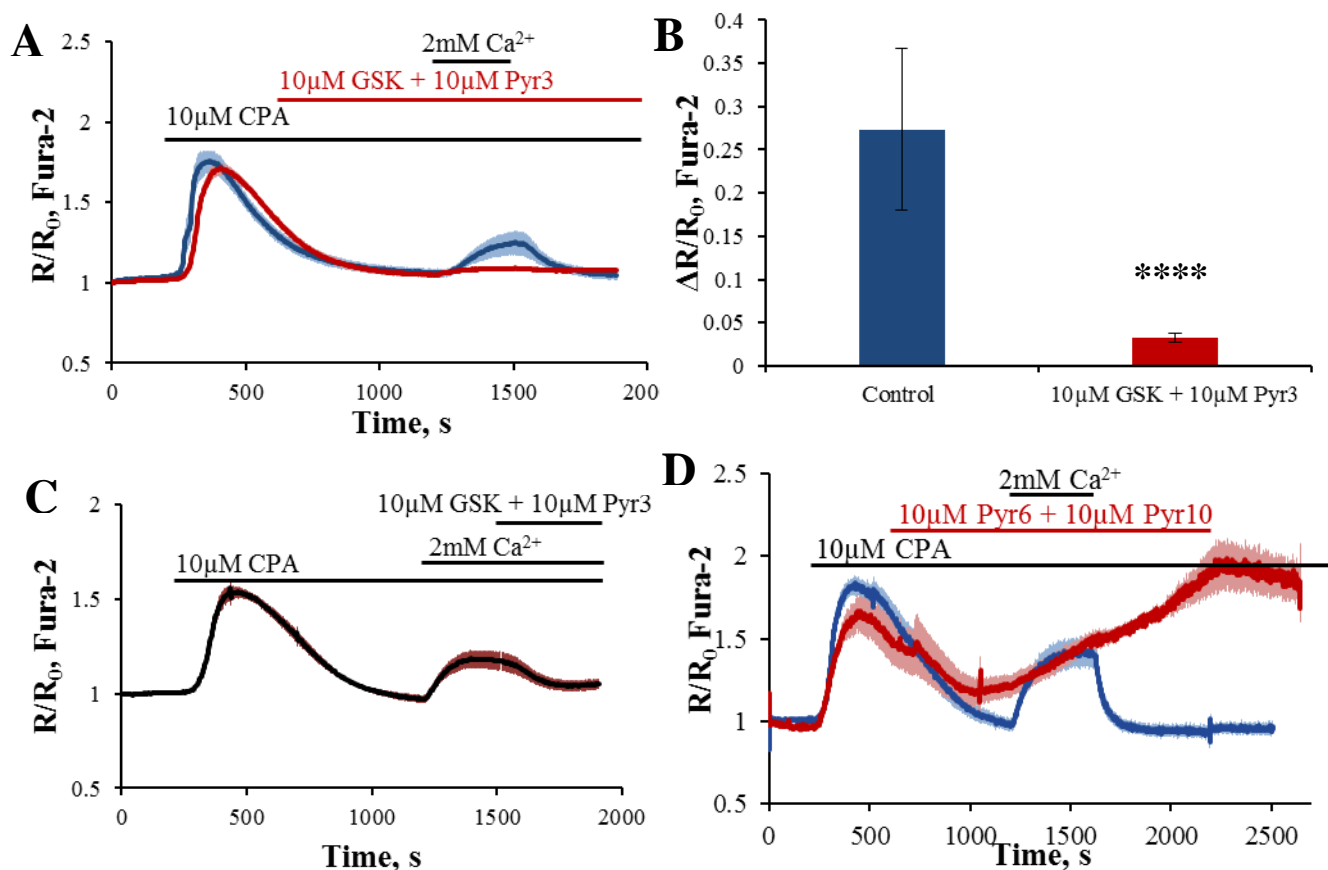
Figure 3.18 The inhibition of Orai1 and TRPC3 mediated Ca^{2+} influx induced by 2mM Ca^{2+}

Average traces (± SEM) from Fura-2 loaded pancreatic acinar cells.

A- Cells were treated according to the protocol in section 2.5.2, pre-incubated with 10 μM GSK-7975A and 10 μM Pyr3 before the re-introduction of 2 mM Ca^{2+} to the extracellular solution (control – blue n= 4. GSK-7975A + Pyr3 – red n= 1). **B-** Graph summarising the changes in ratio amplitude due to Ca^{2+} influx in control cells (blue bar) and cells pre-incubated with GSK-7975A + Pyr3 (red bar p= 0.0007). **C –** Cells were treated according to the protocol in section 2.5.3, 10 μM of both GSK-7975A and Pyr3 was applied to cells in the continued presence of 2 mM Ca^{2+} in the extracellular solution. (n= 5 p= 0.0002). **D –** Cells were treated according to the protocol in section 2.5.2, pre-incubated with 10 μM Pyr6 and 10 μM Pyr10 for ten minutes before the re-introduction of 2 mM to the extracellular solution (control – blue n = 9. 10 μM Pyr6 and Pyr10 – red n=8).

In figure 3.14 A the re-introduction of Ca^{2+} to the extracellular solution resulted in Ca^{2+} influx of a similar dynamic to that of control, although smaller in amplitude; unlike in figure 3.18 D. The removal of extracellular Ca^{2+} in figure 3.14 A resulted in a subsequent decrease in cytosolic Ca^{2+}, this was not the case in figure 3.18 D, in which it was necessary to remove Ca^{2+} and inhibitors from the extracellular solution in order to start to reduce cytosolic Ca^{2+} levels.

1.4. Discussion

During the time course of publication of the second two papers, the work in this chapter was undertaken using the various different inhibitors of Orai1 - DPB162-AE, DPB163-AE, RO2959 and Pyr6. The pharmacology in this chapter contributes towards the acceptance of CRAC channels as a drug target for acute pancreatitis. The use of Orai1 inhibitors in human pancreatic acinar cells and clinically relevant mouse models of acute pancreatitis confirms the viability of targeting these channels therapeutically (253).

There are undoubtedly wider therapeutic advantages to the inhibition of Orai1-mediated Ca^{2+} entry in this inflammatory disease, as SOCE plays a role in immune cells such as mast cells, macrophages and T-cells. If immune cells have a diminished ability to launch an immune response, due to inhibition of Orai1-mediated Ca^{2+} entry, there would be a resultant reduction in the severity of inflammation and therefore a reduced chance of the disease progressing to a more severe form (253,281,282). A recent report indicates that phagocytosis and cytokine production by macrophages, known to be recruited to the site of pancreatic acinar cell injury (313), is dependent on Ca^{2+} signalling in general but not specifically dependent on SOCE (314). This supports the point made in (253) that the principal effect of CRAC channel inhibition is due to the effect of the inhibitor on pancreatic acinar cells, which express the Orai11 isoform (80,129); as although inhibition of SOCE in innate immune cells prevents some of their functionality, neutrophils and macrophages are not entirely inhibited and can still launch an immune response thus contributing towards the severity of acute pancreatitis. T-cells would be inhibited by CRAC channel inhibition, although they are recruited to the site of pancreatic injury in significantly smaller numbers (282).

1.4.1. 2-APB analogues

2-APB, originally thought to be an IP_3R antagonist, is now known to have a biphasic action on CRAC channel mediated-Ca^{2+}entry. When 2-APB was applied to pancreatic acinar cells at 100-300 μM it gave rise to an increase in intracellular Ca^{2+} (130,315). As the 2-APB

analogues are reported to be 100 times more potent, the analogous concentration of the DPB compounds that would elicit an increase in intracellular Ca^{2+} would be 1 µM. However, at least in pancreatic acinar cells there was no noticeable increase in Ca^{2+} observed (figure 3.2A and B) when DPB163-AE was applied at this concentration, in the presence of extracellular calcium. 3 µM DPB163 and DPB162 was shown to be effective in markedly reducing Ca^{2+} influx, as such this concentration should have been tested to determine if there were any effects on Ca^{2+} release.

DPB163-AE and DPB162-AE, are structural isomers that are analogues of 2-APB developed by Dr Mikoshiba's group, they were not found to be as potent in inhibiting SOCE in pancreatic acinar cells as they were in their study (295). 1 µM of both analogues was found to completely inhibit Orai1-STIM1 mediated Ca^{2+} entry in HEK293 cells within 3 minutes, however in this chapter 1 µM was found to be largely ineffective. 3 µM of DPB162-AE and DPB163-AE was found to be more inhibitory than 1 µM, similar to the effect seen on HEK293 cells expressing STIM1-Orai2. This result, the authors might suggest, indicates that in pancreatic acinar cells the native CRAC current is mediated by Orai2, though not necessarily as a homomeric channel. DPB163-AE was found to potentiate Ca^{2+} entry in HeLa cells when used at lower concentrations (10-300 nM), this effect was not investigated in pancreatic acinar cells as 1 µM was not inhibitory as it was reported to be in (295).

When applied in a store-depletion protocol to activate SOCE, high concentrations of DPB163-AE (10 µM) resulted in incomplete clearance of Ca^{2+} from the cytosol (figure 3.3). It is likely that DPB163-AE interferes with a Ca^{2+} clearance mechanism, such as the PMCA, which during store depletion protocols is the predominant Ca^{2+} extrusion pathway. DPB163-AE at 10 µM potentiated Orai3 mediated Ca^{2+} entry initially, this was followed by 100 seconds of decreased current, however the current slowly increased towards the end of the recording (295). However, this seems to be a less than likely explanation for the observed effect of DPB163-AE in figure 3.3.

1.4.2. RO2959

It is known the pancreatic acinar cells express Orai1, but there is no evidence indicating if this is the only Orai isoform expressed in these cells (2,55,56). If in pancreatic acinar cells Orai1 forms heteromultimers with Orai2 and Orai3, as it is known to do in other cell types (317–319) then this would provide an explanation for why all the variety of Orai1 specific inhibitors are less potent in pancreatic acinar cells than in CHO, HeLa, RBL cells and

HEK293 (305). It is still unclear if heteromultimers of Orai form endogenously or just in an overexpression system (317–319). Orai1-Orai2 or Orai1-Orai3 heteromultimer formation has been suggested as a hypothesis for why the IC_{50} for RO2959 in CD4 T cells is much lower than the IC_{50} of RO2959 in RBL-2H3 cells, as potentially heteromultimers of Orai form in RBL-2H3 cells. The IC_{50} for RO2959 is lower for endogenous CRAC currents than for STIM1 and Orai1 overexpression systems (127,296,305). The same concentration of RO2959 (200 nM) inhibited Orai1 by 88%, Orai2 by 14% and Orai3 by 32%. If native CRAC channels can be formed of Orai1-Orai2 or Orai1-Orai3 heteromultimers then RO2959 will be a less potent inhibitor than in cells where the CRAC channels are formed from Orai1 homomultimers.

There were reported solubility issues with RO2959 (305). The authors of this study used RO2959 at a maximal concentration of 1 μM for this reason. In this chapter there was no notable effect of 1 μM RO2959 on SOCE when applied acutely (figure 3.5A) or when pre-incubated with cells during store depletion (figure 3.6 A). Furthermore, there were no noticeable solubility issues upon dissolving RO2959 in DMSO, therefore this would not be a contributing factor to the lack of efficacy observed with 1 μM RO2959 in the aforementioned figures. The authors in this study utilised a pre-incubation protocol, similar to the protocol in section 2.5.2; RBL-2H3 cells were pre-incubated with RO2959 for thirty minutes before activation of CRAC channels to allow for the compound to reach equilibrium, which they stated was important particularly for the low concentrations used (305); as acute pancreatitis is by its very nature an acute disease, any therapy needs to be effective when applied to cells already undergoing cytosolic Ca^{2+} overload and necrosis and not in advance.

An IC_{50} of approximately 2 μM was obtained from the graph in figure 3.5. Notably there is a steep concentration dependence of inhibition observed between 1 μM RO2959 and 5 μM RO2959. Further intermediate concentrations should be tested and added to the dose response curve to more accurately determine the IC_{50}. Calculating the IC_{50} of inhibitors using data generated by fluorescent Ca^{2+} imaging is likely not the most accurate method, as it is not a direct measurement of channel conductance; using patch clamp would result in more accurate measurements of the extent to which each concentration inhibits the channel current. Lastly, data demonstrated in figure 3.9 D indicates that rather than protecting cells from necrosis induced by bile salts, mimicking biliary acute pancreatitis, RO2959 increased the percentage of cell death. There is evidence that the balance between necrosis and apoptosis influences the severity of acute pancreatitis (320–322). RO2959 when pre-incubated with cells affected

the half time of Ca^{2+} efflux, which is dependent on the PMCA. If RO2959 impairs the clearance capacity of the PMCA, then cytosolic Ca^{2+} overload is likely. Cytosolic Ca^{2+} overload is one of the key causes of cellular necrosis. 200 µM TLC-s results in high levels of apoptosis, due to the production of reactive oxygen species (270), it is possible that RO2959 tilts the delicate balance between apoptosis and necrosis more towards the necrosis end of the scale.

1.4.3. Pyr6

Pyr6 is an Orai1 specific inhibitor of Ca^{2+}entry that preferentially inhibits Orai1 over TRPC3 (195); it was reported to have a 37-fold higher potency for Orai1 mediated Ca^{2+} entry over TRPC3 mediated Ca^{2+} entry. The work in this chapter utilised 10 µM Pyr6 to inhibit SOCE in pancreatic acinar cells, as this was the maximal inhibitory concentration used in RBL-2H3 cells (195). Ca^{2+} entry was significantly inhibited by this concentration of Pyr6 when it was pre-incubated with cells before the re-introduction of extracellular Ca^{2+} and furthermore when acutely applied to cells in the presence of elevated cytosolic Ca^{2+} levels (figure 3.10 A and C). When compared with GSK-7975A, which when pre-incubated with cells for ten minutes at 10 µM inhibited Ca^{2+} entry by $93.4 \pm 5\%$, Pyr6 was less effective at inhibiting Ca^{2+} entry; when used for the same duration of pre-incubation and the same concentration, it inhibited Ca^{2+} entry by $83.3 \pm 1.1\%$. Pyr6 was more effective at inhibiting Orai1-mediated Ca^{2+} entry than TRPC3-mediated Ca^{2+} entry (195) but GSK-7975A was more effective at inhibiting Ca^{2+}entry in pancreatic acinar cells than Pyr6, which is thought to be mediated by Orai1 (80,129,316). If in acinar cells the native CRAC channel is only formed by Orai1 homomultimers, this data then indicates that GSK-7975A is a more potent inhibitor of Orai1 than Pyr6. Data from experiments on AR42J cells, in which GSK-7975A was ineffective at inhibiting Ca^{2+} influx (130) contrasted with experiments using Pyr6 on AR42J cells. Pyr6 significantly inhibited Ca^{2+} influx. It is unlikely that they are targeting the same protein, there may be a possibility that Pyr6 indirectly inhibits Orai1. The isoform specific molecular identity of the Ca^{2+} influx in AR42J cells has yet to be determined, but from the work in this chapter it

1.4.4. Pyr3

TRPC3 channels are non-specific cation channels that are ubiquitously expressed in almost all tissues including pancreatic acinar cells. Although the store-operated nature of TRPC3 channels is still somewhat debated, TRPC3 has now been shown to bind to STIM1 (222,323).

The STIM1 Orai1-activating region (SOAR) domain of STIM1 binds to the coiled-coil domain in the C-terminus of TRPC3. Whereas previously it was shown that TRPC1 directly binds STIM1 and it is known to form heteromultimers with TRPC3, it was thought that in this way TRPC1 conveyed STIM1 dependence to TRPC3 (214). The binding of the channel to STIM1 meets one of the criteria of a store-operated channel (222).

Deletion of TRPC3 from pancreatic acinar cells resulted in a 50% reduction in the amplitude of SOCE (220) and pharmacological inhibition using Pyr3 resulted in a reduction of SOCE of a similar amplitude (with no further reduction in SOCE seen when Pyr3 was applied to TRPC3-deficient acinar cells) (221). This previously published study used Pyr3 at 3 µM and stated that this concentration had near maximal inhibition, with no further inhibition of SOCE seen at higher concentrations such as 10 or 50 µM, however, no dose-response in pancreatic acinar cells was demonstrated. In figure 3.12 and 3.13 Pyr3 was applied to acinar cells at 10 µM, the maximal inhibitory concentration as reported previously (309). The effect of increasing Pyr3 concentration from 3 µM (221) to 10 µM was a stronger inhibition of Ca^{2+} influx (96%) in pancreatic acinar cells. This is similar to the percentage of inhibition seen when CRAC channel inhibitor GSK-7975A was used to inhibit Ca^{2+} entry in pancreatic acinar cells (130). The specificity of Pyr3 for the inhibition of TRPC3-mediated Ca^{2+} entry over Orai1-mediated Ca^{2+} entry was tested using HEK293 cells overexpressing TRPC3 and RBL-2H3 cells, which endogenously express Orai1 (195). Pyr3 was found to lack specificity for TRPC3 over Orai1, the IC_{50} of Pyr3 for TRPC3 and Orai1 was 0.54 µM in both instances. Whereas the SOCE inhibitor Pyr2 (BTP2) had a lower IC_{50} for Orai1 (0.59 µM) over TRPC3 (4.21 µM). At the concentration used in this study it is likely that both TRPC3-mediated and Orai1-mediated Ca^{2+} entry are inhibited, thus resulting in a 96% inhibition of the Ca^{2+} influx into pancreatic acinar cells via both channels. Even at 3 µM used previously (221) there would have been no discrimination between Orai1 and TRPC3 channels using Pyr3. In order to specifically target TRPC3 and not Orai1 Pyr3 is not a suitable tool, but it may be useful if it is experimentally necessary to indiscriminately target Ca^{2+} entry.

1.4.5. Pyr10

Pyr10 was designed by the authors of the aforementioned paper and was found to more potently inhibit TRPC3 (195). The maximal inhibitory effect on TRPC3 was observed at approximately 50 µM, whereas for Orai1 it was approximately 500 µM, as measured in Fura-2 loaded YFP-TRPC3 expressing HEK293 cells. In figure 3.14, 10 µM Pyr10 was used in

similar experiments to those utilising Pyr3 and Pyr6. Pre-incubation with this concentration (figure 3.14 A) resulted in an altered and incomplete Ca^{2+} clearance from the cytosol during the store-depletion phase of the protocol. Typically upon CPA or thapsigargin application, in nominally Ca^{2+} free extracellular solution, Ca^{2+} is released from ER stores giving rise to a transient increase in cytosolic Ca^{2+} concentration; this is followed by Ca^{2+} extrusion across the plasma membrane via PMCA and therefore there is a subsequent decrease in cytosolic Ca^{2+} concentration back to pre-stimulation levels. In figure 3.14 A cytosolic Ca^{2+} concentration did not return to pre-stimulation levels after the addition of Pyr10 to the extracellular solution, in the maintained absence of extracellular Ca^{2+}. Cytosolic Ca^{2+} concentrations remained significantly elevated compared with control cells at the point at which Ca^{2+} was re-introduced to the extracellular solution, this is likely due to non-specific effects of Pyr10 on Ca^{2+} clearance mechanisms, such as the PMCA.

Pyr10 has been used recently in a paper investigating the role of TRPC3 in human coronary artery endothelial cells. The slight elevation in cytosolic Ca^{2+} levels after store depletion observed in figure 3.14 was also observed in their store-depletion protocol, but to a lesser extent, despite using 2 μM Pyr10 and not 10 μM (324). A second recent paper studying the contribution of TRPC3 to SOCE in primary nociceptors also utilised Pyr10 at 10 μM, the authors did not demonstrate any obvious changes in the dynamics of Ca^{2+} handling by dorsal root ganglion cells (325). If Pyr10 has off-target effects on the PMCA then it is less likely to negatively impact the Ca^{2+} handling in an excitable cell, which also possess the NCX that can remove Ca^{2+} from the cytosol.

2 μM Pyr10 had no inhibitory effect on SOCE in human coronary artery endothelial cells and 10 μM Pyr10 had no effect on SOCE in dorsal root ganglion cells, when measured using Fura-2 loaded cells in both instances. There is a full dose response curve for the effect of Pyr10 on RBL-2H3 cells in (195), with 10 μM inhibiting Ca^{2+} entry by approximately 40%. In pancreatic acinar cells 10 μM Pyr10 inhibited Ca^{2+} entry by $36.9 \pm 5.7\%$ despite the disturbances in cytosolic Ca^{2+} clearance. There is insufficient data to determine whether Pyr10 can specifically inhibit TRPC3 in pancreatic acinar cells.

1.4.6. GSK-7975A and Pyr3

As both Orai1 and TRPC3 contribute to Ca^{2+} entry in pancreatic acinar cells (80,129,130,220,221) an inhibitor that blocks both channels would be useful as a potential therapeutic to treat acute pancreatitis. At the point the experiments in figure 3.16 and 3.17

were conducted, the lack of specificity of Pyr3 for TRPC3 was not known (195). The aim of these figures when the experiments were performed was to use Pyr3 to target TRPC3 mediated Ca^{2+} entry and GSK-7975A to target Orai1-mediated Ca^{2+} entry. The combined pre-incubation of 10 µM Pyr3 and GSK-7975A for ten minutes reduced Ca^{2+} entry by 78.3 ± 1.1 % (in the presence of 5mM extracellular Ca^{2+}, figure 3.17) and by 81.3 ± 2.9 % (in the presence of 10 mM extracellular Ca^{2+}. Figure 3.16). There was no further inhibition of Ca^{2+} entry compared to the inhibition of Orai1 alone, this could be due to the lack of specificity of Pyr3 for TRPC3 and therefore non-specific inhibition of Orai1. The trend is true for experiments in which Pyr3 and GSK-7975A were applied acutely, in the presence of a sustained elevation in cytosolic Ca^{2+} levels, there was no further inhibition of Ca^{2+} entry compared to cells where only Orai1 was inhibited; a 50.8 ± 6.2 % reduction in the presence of 5 mM extracellular Ca^{2+} and 76.8 ± 1.8 % reduction in the presence of 10 mM extracellular Ca^{2+}.

One of the discrepancies between experiments studying SOCE is that different labs use slightly different concentrations of Ca^{2+} in their extracellular solutions to re-admit Ca^{2+} to the cell, by increasing the extracellular concentration the extent of inhibition by a particular inhibitor is reduced (183). In figure 3.16 10 mM extracellular Ca^{2+} is used to re-admit Ca^{2+} to the cells and in figure 3.17 5 mM Ca^{2+} is used, therefore it would be expected that the combined application of Pyr3 and GSK-7975A to be less effective in figure 3.16 than in figure 3.17, but the converse is observed. In pre-incubation experiments utilising 2 mM extracellular Ca^{2+}, Pyr3 and GSK-7975A were the most effective at inhibiting Ca^{2+} entry (88.0 ± 6.5 %) although in acute application the results did not follow the expected trend and Ca^{2+} entry was only reduced by 65 ± 3.2 %.

The motivation behind the experiment shown in Figure 3.18 D was to utilise Pyr6 and Pyr10 in an attempt to more specifically target Orai1 and TRPC3. However, the application of 10 µM of both inhibitors resulted in a disturbance in the clearance of Ca^{2+} from the cytosol, likely due to an effect on PMCA activity, similar to that seen in figure 3.14 A with Pyr10 application alone. In figure 3.18 D cytosolic Ca^{2+} levels had already increased to levels comparable with peak Ca^{2+} influx in control cells at the time point when Ca^{2+} was re-admitted to the extracellular solution. Only when both the inhibitors were removed from the extracellular solution did cytosolic Ca^{2+} levels begin to decrease, suggesting that the effects of Pyr6 and Pyr10 may be reversible.

The theory behind an attempt at dual inhibition of the two Ca^{2+} influx channels was based on a study in which two inhibitors of two targets implicated in nasal polyps – the leukotriene receptor and CRAC channels. The authors of the study utilised the two inhibitors at individual submaximal concentrations and found that this combination was as effective as using either inhibitor at their maximal concentration (326). The benefit of using submaximal concentration of any agent is that there is an improved therapeutic index of that agent and therefore a reduction in side effects. However, the combined treatment of acinar cells with both Orai1 inhibitors and TRPC3 inhibitors was not at submaximal concentrations, as such was not very well designed and no conclusions can be drawn from the data. It would be very interesting to observe the effects of submaximal concentrations of both inhibitors on both the amplitude of Ca^{2+} influx when treated in an acute manner, but also their effects on cellular necrosis and apoptosis.

1.4.7. Pancreatic acinar cells vs AR42J cells

The difference in the magnitude of inhibition observed in both pancreatic acinar cells and AR42J cells when exposed to the Orai1 specific inhibitor - Pyr6 and the TRPC3 channel specific inhibitor - Pyr10 could be due to different levels of expression of Orai1 and TRPC3 channels in the two different cell types. AR42J cells are used as a model pancreatic acinar cell line as they are the most similar cells to primary acinar cells that are commercially available. Primary pancreatic acinar cells are viable for several hours after isolation, but the more time they are left after isolation the higher the levels of cellular necrosis observed. Primary acinar cells are notoriously difficult to culture, although newer methods have been developed that report successful culture of pancreatic acinar cells for up to 10 days *in vitro* (327). Due to the difficulty in culturing primary acinar cells researchers have tended to look towards model cell lines, such as AR42J cells to do experiments that require extensive incubations such as transfections of plasmid DNA or knockdown with siRNA (328). From the functional data generated in this chapter, from primary acinar cells and AR42J cells, it can be hypothesised that the expression levels of Orai1 and TRPC3 are very different between the two cell types, with Ca^{2+} influx in pancreatic acinar cells primarily mediated by Orai1 channels and to a lesser extent TRPC3 channels; with the converse true in AR42J cells as TRPC3 inhibition resulted in a greater magnitude of inhibition than Orai1 inhibition. In order to quantitatively assess if the functional difference observed with pharmacological agents is due to a difference in expression levels of channels it would be prudent to run a

qPCR to determine the expression levels of mRNA for each channel and a western blot to determine relative protein levels.

AR42J cells are derived from a pancreatic exocrine tumour taken from a rat. AR42J cells are non-polarised cells that unless differentiated, by dexamethasone treatment, do not have substantial number of zymogen granules (329,330) and are not secretory in response to physiological stimuli of pancreatic acinar cells such as CCK (331). Although a useful tool to have, AR42J cells should not be studied in isolation from pancreatic acinar cells due to these differences, thereby a difference in which ion channels are primarily responsible for mediating Ca^{2+} influx in response to store depletion is highly likely. There is a lot of evidence for the role of TRP channels in tumorigenesis, with members of the TRPC, TRPM and TRPV family of channels implicated in proliferation and apoptosis (332). Targeting TRPC3 channels could provide a way of differentially targeting pancreatic cancer cells over normal acinar cells as a potential therapeutic strategy, as normal acinar cells seem to be more dependent on Orai1 for SOCE.

Future work

It remains to be determined whether there is expression of the Orai2 and Orai3 isoforms in pancreatic acinar cells. Such information could possibly provide an explanation for the different efficacy of CRAC channel inhibitors when used in pancreatic acinar cells as compared to cell lines or other primary cell types, such as with inhibitors including 2-APB analogues, RO2959 (295,305). This data should be obtained by running PCR experiments to determine the presence of Orai2 or Orai3 isoform mRNA. Western blots and immunostaining techniques should then be undertaken to confirm expression of the Orai2 and Orai3 protein, antibodies for both proteins are commercially available. Co-immunoprecipitation experiments can be done to determine if Orai2 and Orai3 do form heteromultimers with Orai1 endogenously, similar to the experiments undertaken studying TRPC channel heteromultimerisation in (214) and FRET based experiments such as those studying Orai heteromultimerisation (317). Confirmation of the formation of Orai heteromultimers would give rise to an explantion for altered channel kinetics and pharmacological response to antagonists (317).

A full dose-response study of Pyr10 is currently lacking in pancreatic acinar cells and would be necessary in order to determine a usable concentration to discriminate between Orai1 and TRPC3 mediated Ca^{2+} signals. Furthermore, as it is necessary for a therapeutic for acute

pancreatitis to have the capacity to reduce Ca^{2+} entry when applied in the presence of a sustained elevation in cytosolic Ca^{2+} levels, it is necessary to test whether Pyr10 is effective in inhibiting TRPC3-mediated Ca^{2+} entry in an acute manner. The same is true of Pyr6, a full dose-response study in pancreatic acinar cells is also lacking. However, at the same concentration as GSK-7975A (10 µM), Pyr6 is less effective in reducing cytosolic Ca^{2+} overload, due to Ca^{2+} influx; as such it may not be worthwhile investing more time investigating such an agent. The levels of apoptosis and necrosis measurements should be undertaken to determine the effect of Pyr6 and Pyr10 on cell fate. It is worthwhile noting, that in order to produce meaningful necrosis measurements all cell counting ought to be double-blinded to prevent inherent experimenter bias.

The development of specific CRAC channel inhibitors have been a focus in the field for many years (127,183) and binding site and mechanism of action of most SOCE inhibitors is largely unknown (127). Improving the specificity and potency of an inhibitor for a particular channel by making new analogues and undertaking structure-function studies becomes problematic when the binding site of the drug is unknown. Improved channel specificity of a drug is necessary, as is an improved potency of the drug, in order to be able to reduce the therapeutically viable concentrations delivered to patients and reduce the concentration of unbound drug found in plasma, as this unbound drug is available to bind non-specifically to other proteins resulting in off-target effects(333). In order to improve these factors it is important to know whether an inhibitor binds directly to the channel in question, or indirectly via an accessory protein. A recent study using minimal functional domains of channels in order to determine binding of inhibitors to functional channel domains provides a high-throughput way to test compounds and thereby improve drug design (209).

Once a new inhibitor has been identified, that is potent and specific for Orai1, it will be necessary to ensure it will target all hallmarks of acute pancreatitis. An ideal therapeutic for acute pancreatitis will need to: inhibit SOCE, prevent premature intracellular trypsinogen activation, reduce vacuolisation, reduce release of cytokines and recruitment inflammatory cells to the injured pancreas and ultimately reduce the extent of cellular necrosis. All hallmarks of acute pancreatitis need to be ameliorated and ideally the potential therapeutic candidate needs to be tested in multiple models of acute pancreatitis.

4   Modulation of Calmodulin to reduce cytosolic Ca2+ overload

4.1   Introduction

There is a superfamily of Ca^{2+} binding proteins called the Calmodulin superfamily, in which there are over 600 proteins that can sense or buffer intracellular Ca^{2+} (334). Calmodulin itself is part of this superfamily, it is a Ca^{2+} binding protein found at micromolar concentration (335) and is dispersed throughout the cytosol (336) of most eukaryotic cells (335). There is further evidence for the expression of calmodulin in the nucleus of cells (35,337). The amino acid sequence of calmodulin is highly conserved from yeast to humans, the only proteins more highly conserved are histones, β-actin and ubiquitin (338). A feature that all members of the calmodulin superfamily have in common is that they all possess a Ca^{2+} binding motif known as an EF hand (334).

Calmodulin is a protein of 148 amino acids, it has four EF-hands, allowing one molecule of calmodulin to bind with four molecules of Ca^{2+} (35,335). The first two EF hands are located in the N-terminal domain of calmodulin and the third and fourth EF hands make up the C-terminal domain; the two domains are separated by a short but flexible linker region (35). The EF-hands contain a 12 amino acid acidic group in the centre of a helix-loop-helix region and two alpha helices linked by a short loop region, and are known to bind to Ca^{2+} ions (35,334). The Ca^{2+} affinity for calmodulin makes it an efficient cytosolic Ca^{2+} sensor, as its affinity for Ca^{2+} falls within the intracellular free Ca^{2+} concentration range. Furthermore, the two separate domains of calmodulin have two different Ca^{2+} affinities, the C-terminus has a three to five fold higher affinity for Ca^{2+} than the N-terminus, and thereby the C-terminus binds Ca^{2+} before the N-terminus. Within each terminus Ca^{2+} ions will bind co-operatively to the EF hands, whereas the two domains bind Ca^{2+} independently of each other (35). The different domains of calmodulin have different conformational states depending whether Ca^{2+} is bound or unbound (apo-calmodulin). When no Ca^{2+} is bound the N-terminal EF hands are inaccessible and are tightly packed in a closed conformation, whereas the C-terminal is in a semi-open conformation; this may enable the C-terminal domain to bind to target proteins (339), such as the calmodulin binding sites on ion channels e.g. voltage gated Ca^{2+} channels (161).

Calmodulin mediates many Ca^{2+} dependent processes in cells, such as protein phosphorylation, cell proliferation and ion transport. It does this through binding with the many target proteins that it regulates. There are so many targets that scientists created a

database of them (340). A few examples of calmodulin targets are: calmodulin Kinase I (CaMKI), phosphatases such as calcineurin (CaN) (35,335), voltage gated Ca^{2+} channels (161), the PMCA pump (341), IP_3R, RyR (342) and lastly STIM (176) and Orai proteins (159). Calmodulin has been demonstrated to regulate all the above proteins in both negative and positive feedback loops, meaning it can activate or inactivate certain targets. This can depend on the target protein in question, and whether or not calmodulin is in its Ca^{2+}-bound or Ca^{2+}-free/apo-calmodulin state (343).

4.1.1   Inhibition of Calmodulin

Calmidazolium is a well characterised inhibitor of calmodulin. It was synthesised in 1981 (344) and was found to be more potent and selective for calmodulin than drugs at the time that had antagonistic effects on calmodulin, such as fungicides and insecticides (345). W-7 is also an inhibitor of calmodulin (346,347) which is reported to be less specific and less potent than calmidazolium (348).

W-7 was shown to inhibit amylase secretion from pancreatic acinar cells (349,350), which is known to be stimulated by local elevations in cytosolic Ca^{2+} concentrations. Furthermore, calmodulin antagonism, achieved using W-7 and other inhibitors, inhibited the volume of bile flow in isolated liver and also inhibited bile acid secretion (351).

Calmidazolium has been demonstrated to induce cytosolic Ca^{2+} signals in cells when applied in low micromolar concentration (2-5 µM) to Madin Darby Canine Kidney (MDCK) cells (352). W-7 has also been shown to induce Ca^{2+} signals in MDCK cells (353). It was found that removing extracellular Ca^{2+} only partially reduced the increase in cytosolic Ca^{2+} induced by both calmidazolium and W-7 (352,353), suggesting that in part this elevation in cytosolic Ca^{2+} is mediated by Ca^{2+} influx but part of the Ca^{2+} signal that is mediated by release from intracellular Ca^{2+} stores.

It was demonstrated that the binding of calmodulin to PMCA resulted in the sensitisation of PMCA to increased cytosolic Ca^{2+} concentrations (354) allowing for enhanced extrusion of Ca^{2+} from the cytosol across the plasma membrane. In pancreatic acinar cells it was demonstrated that inhibiting calmodulin prevented Ca^{2+} efflux by PMCA (355). This was replicated in RBL-1 cells, where calmidazolium slowed the rate of Ca^{2+} clearance from the cytosol as mediated by PMCA (177). In addition to its effects on PMCA pumps calmidazolium has also been reported to inhibit Ca^{2+} entry in cells such as cardiac myocytes (356) and smooth muscle cells (357). Ca^{2+} influx in these two cell types is largely mediated

114

by voltage gated Ca^{2+} cells. Calmodulin binds the C-terminus of voltage gated Ca^{2+} channels and regulates facilitation of the channel and mediates the fast Ca^{2+}-dependent inactivation of the channel (161,358). For further information on the role of calmodulin in the Ca^{2+} dependent inactivation of CRAC channels see section 4.1.3.

4.1.2   Activation of CaM

In pancreatic acinar cells there has been some success in targeting cytosolic Ca^{2+} overload by utilising activators of calmodulin (359). Ca^{2+}-like peptides (CALP) are activators of calmodulin that bind to EF hands and activate calmodulin in much the same way as Ca^{2+}. They are Ca^{2+} like mimetics that were designed to competitively bind to Ca^{2+} binding sites on target proteins to allow for modulation of the downstream cellular functions of Ca^{2+} signalling, such as excitation-contraction coupling (360). The EF hands found on troponin C and calmodulin have very similar amino acid sequences, as they are believed to have evolved from one common ancestral Ca^{2+} binding site. The ancestral Ca^{2+} binding site was used as a template to create a peptide with an amino acid sequence that has an opposite hydropathy score, in an attempt to design a final peptide with affinity for the Ca^{2+} binding sites of proteins such as calmodulin and troponin C (360). This method of peptide design is based on the idea that the shape of a protein, e.g. a receptor, is in part determined by the location of its hydrophobic and hydrophilic residues in the sequence rather than the actual amino acid identity, this can be referred to as the hydropathy pattern. By exactly inverting this hydropathy pattern a peptide should be generated with a complementary surface with which it can bind to the receptor or protein in question (361). This was the method use to generate the CALP peptide (360).

In order to test the efficacy of CALP in activating calmodulin, a phosphodiesterase activation assay was employed, cAMP hydrolysis was measured in the presence of calmodulin and CALP. Application of CALP increased the percentage of cAMP hydrolysed by phosphodiesterase, but did not have an effect in the absence of calmodulin; indicating that CALP was not directly interacting with phosphodiesterase but rather mediating its effects via calmodulin. This effect was not lost upon chelating of cytosolic Ca^{2+} with EGTA. Furthermore, CALP increased resting and ACh-induced tension in bladder smooth muscle cells. As experiments were undertaken at a low Ca^{2+} concentration, it was unlikely that CALP facilitated Ca^{2+} binding to calmodulin but rather, the effect on smooth muscle cells tension was due to CALP mediated activation of calmodulin directly (360). The CALP peptide used was 8 amino acids in length, which was designated CALP1 in subsequent studies; in spite of

strong evidence for it binding to the EF hand of calmodulin and activating the protein, this had not been directly demonstrated at that point. CALP1 had been designed to be complementary to the ancestral Ca^{2+} binding site but not specifically for the EF hand of calmodulin, as such a further three complementary peptides were developed with a similar sequence and of varying lengths (361). CALP2 was designed as a more specific peptide for the EF hand of calmodulin, with an inverted hydropathic pattern and was twelve amino acids in length. The CALP peptides were shown to bind to calmodulin and induce conformational changes in a similar manner to conformational changes induced by Ca^{2+} (361). CALP3 is the same length as CALP1, 8 amino acids and is the first eight amino acid residues of CALP2. CALP2 had a higher affinity for the EF hand of calmodulin than CALP1 and a similar affinity to Ca^{2+}. CALP3, the most similar in structure to CALP2, had a higher affinity for the calmodulin EF hand than CALP1, by two fold. Researchers observed nuclear magnetic resonance (NMR) spectra from calmodulin bound to Ca^{2+} and calmodulin bound to CALP1 and found peaks in common, and additional peaks in the calmodulin/CALP1 spectrum, indicating that CALP1 has conformational changes in common with Ca^{2+} but also had some additional changes. These were largely similar to conformational changes induce by Ca^{2+} binding with the C-terminus of calmodulin, indicating the location of CALP binding was an EF hand on the C-terminus, with no evidence that CALP1 or CALP3 bound the N-terminus EF hands of calmodulin (361).

As the CALP peptides only bound the C-terminus of calmodulin, whereas Ca^{2+} binds all four EF hands on both N- and C-terminal domains of calmodulin, it was necessary for the researchers to determine if the conformational changes elicited by CALP/Calmodulin complexes were functional or not. CALP2 did not elicit any changes in the cGMP hydrolysis, and was found to entirely inhibit cGMP hydrolysis under conditions where both Ca^{2+} and calmodulin were present; this was reversible when the concentration of Ca^{2+} present was increased (361). The opposite was true for CALP3.

Calmodulin localises primarily in the cytosol in cells, in order to activate calmodulin the CALP peptides must have been cell permeable, but this had not been demonstrated at this point. A fluorescent form of CALP1 was generated - F-CALP; F-CALP1 was visualised, using confocal microscopy, being rapidly taken up into neocortical neurones and Jurkat T cells (362). Furthermore, it was observed that both CALP1 and CALP3 were able to block Ca^{2+} channels. The neurones were stimulated with glutamate, which elicited a sustained increase in cytosolic Ca^{2+} levels, this increase in cytosolic Ca^{2+} was inhibited by CALP1 and

CALP3 in a dose dependent manner. The NMDA receptor, to which glutamate binds and initiates intracellular signalling pathways, was inhibited with its specific antagonist – MK801 to inhibit glutamate-induced cytosolic Ca^{2+} signals, acting as a positive control. Pre-treating cells with W-7, thus inhibiting calmodulin, before CALP3 was applied restored the elevation in cytosolic Ca^{2+} in response to glutamate. The data suggests the CALP3 was inhibiting the NMDA receptor activity, via calmodulin (362). In electrophysiological recordings CALP1 reversibly inhibited glutamate-induced NMDA currents. The peptide was used to inhibit non-selective cation channel currents in Jurkat T cells, this inhibition was due to a reduction in the open probability of the channel rather than an inhibition of the channel conductance, with evidence indicating that CALP1 was acting from the cytoplasmic side of the channel. Glutamate is an excitatory stimulus to neurones and at high concentrations it can cause cytotoxicity. CALP1 and CALP3 reduced the extent of cell death caused by glutamate, as measured by propipidium iodide, in a dose-dependent manner with IC_{50} of 52.48 and 50.97 µM respectively. More specifically, apoptosis measurements were made and both CALP peptides were found to inhibit apoptosis in the neuronal culture. It was concluded that this amelioration in cell death and apoptosis were due to inhibition of Ca^{2+} influx pathways by CALP peptides (362).

Excessive alcohol intake is a primary cause of acute pancreatitis, largely mediated by the non-oxidative alcohol metabolites fatty acid ethyl esters such as palmitoleic acid ethyl ester (POAEE) (237,252,363). Fatty acid ethyl esters, such as POAEE, act on pancreatic acinar cells and result in the release of Ca^{2+} from the intracellular stores, and subsequent activation of trypsinogen intracellularly (363). Ethanol itself can also have somewhat toxic effects on pancreatic acinar cells, however these are only at extremely high concentrations (237), it was found that 200 mM ethanol, when applied to intact pancreatic acinar cells, resulted in cytosolic Ca^{2+} elevations (359). However, in permeabilised cells 10 mM ethanol was sufficient to liberate Ca^{2+} from the intracellular stores (359). The addition of 2.5 µM full-length calmodulin to the extracellular solution of permeabilised cells had free access to the intracellular compartment of the cell, this addition was observed to dramatically reduced the amplitude of cytosolic Ca^{2+} increase. The Ca^{2+} signals in intact cells exposed to 200 mM ethanol were somewhat varied in their dynamics, typically in response to such high concentrations of ethanol there was a remarkably small but sustained increase in cytosolic Ca^{2+}. Further there were a subset of cells in which the cytosolic Ca^{2+} signal was oscillatory in nature. In the presence of CALP3, 200 mM ethanol application resulted in a sustained

increase in cytosolic Ca^{2+} in significantly fewer cells and significantly more cells that did not respond to ethanol. This result was amplified when higher concentrations of CALP were utilised (359). There was an increase in the number of cells that responded in an oscillatory manner when treated with ethanol in the presence of CALP compared with ethanol treatment alone, although in the presence of CALP-3 the amplitude of the oscillations was dramatically reduced. This data indicated that there was a shift in the dynamic of the Ca^{2+} signal from a sustained elevation in cytosolic Ca^{2+} concentration to a signal that was short lasting and local in nature, which was unlikely to result in the intracellular activation of digestive enzymes (359). 10 mM ethanol treatment in permeabilised cells was sufficient to activate intracellular trypsinogen and 100 mM ethanol further increased the levels of trypsinogen activation. Ethanol induced trypsinogen activation was calmodulin sensitive, incubating cells with calmodulin alone significantly inhibited enzyme activation and incubating cells with calmodulin and CALP3 further inhibited enzyme activation, achieving almost complete inhibition (363).

The mechanism of this protective effect is hypothesised to be mediated by the calmodulin dependent inhibition of IP_3R, due to the binding of calmodulin to the IP_3R (269). It has previously been demonstrated that 10 μM calmodulin markedly reduced the open probability of the IP_3R and 20 μM completely inhibited the IP_3R channel opening, even at high cytoplasmic Ca^{2+} levels. In order to remove the calmodulin inhibition on IP_3R channel currents, high micromolar concentrations of 400 μM or more of the calmodulin antagonist, W-7, were required to restore the current (269).

Research in Jurkat T cells indicated that the inhibition of the non-selective cation channels by CALP1 was thought to be through its interaction with calmodulin, rather than blocking the pore of the channel (362). Further evidence indicated that CALP1 was able to block the CRAC channel in RBL-2H3 mast cells (364). With this data in mind, in addition to the proposed mechanism that CALP3 modulates Ca^{2+} release from the ER through IP_3R in response to ethanol (359), the protective effects of CALP3 against ethanol induced Ca^{2+} elevations could be mediated through inhibition of store-operated Ca^{2+} pathways, which are largely mediated by STIM1/Orai1 CRAC channels in pancreatic acinar cells. Section 4.1.3 details the role of calmodulin in store-operated Ca^{2+} entry further.

4.1.3 Calmodulin and CRAC channels

In addition to being a cytoplasmic Ca^{2+} binding protein, calmodulin also associates with certain ion channels and pumps and aids their regulation. It has been known for some time that calmodulin binds to and regulates the PMCA and also voltage gated Ca^{2+} channels (161,358); of late is has been determined that there is a Ca^{2+} binding domain present in the CRAC channel structure. It is thought that the association of calmodulin to the CRAC channel mediates the Ca^{2+}-dependent negative feedback of the channel (159), similarly to the manner in which the Ca^{2+} dependent inactivation of voltage gated Ca^{2+} channels is mediated by calmodulin (161).

Section 1.5 extensively details the constituent components of the CRAC channel, with Orai1 as the pore-forming subunit that resides in the plasma membrane (152–154) and STIM1 as the ER Ca^{2+} sensor with an EF hand on the luminal side of the ER (150,151,155). Ca^{2+} dependent inactivation of the CRAC channel comes in two forms, fast Ca^{2+}-dependent inactivation and slow Ca^{2+}-dependent inactivation. The fast Ca^{2+}-dependent inactivation is thought to be mediated by calmodulin binding to a calmodulin binding domain on Orai1, and also a cytoplasmic domain of STIM1, adjacent to Orai1. Several years ago a putative calmodulin binding site was identified in the N-terminus of Orai1, amino acid residues 68-91 (159). The researchers searched for hydrophobic amino acid residues within this region, as hydrophobic residues are known to be a target for calmodulin binding (365). Several residues were identified in the N-terminal calmodulin binding domain of Orai1 and a series of mutated constructs were generated. Five of the mutations resulted in a loss of calmodulin binding to Orai1 and subsequent loss of Ca^{2+}-dependent inactivation; in two further mutations the calmodulin binding domain of Orai1 retained the ability to bind calmodulin and thereby Ca^{2+}-dependent inactivation was also retained (159). The activation of Orai1, however, appeared to be largely unaffected by the mutation of the calmodulin binding domain.

The nature of the interaction between the Orai1 and calmodulin was still not entirely clear until a crystal structure confirmed that the C-terminal domain of calmodulin binds to the N-terminal Orai1 calmodulin binding domain (160). The N-terminal domain of calmodulin also has the capacity to bind Orai1 but it has a much lower affinity for the calmodulin binding domain on Orai1; furthermore, the shape of the calmodulin N-terminal domain is less complementary to the calmodulin binding domain of Orai1 than that of the C-terminal domain surface. When bound to the calmodulin binding domain, calmodulin is in a Ca^{2+} bound state (160).

A group studying the selective activation of NFAT, a downstream event of local Ca^{2+} influx through Orai1 channels which can be used as a read out of Orai1 activity, found that whilst Ca^{2+} influx through Orai1 channels activated NFAT translocation to the nucleus, Ca^{2+} influx through Orai3 channels (pre-activated by 2-APB) failed to activate NFAT translocation to the nucleus (177). The N-terminal calmodulin binding domain of Orai3 was found to have several conserved residues in common with the N-terminal calmodulin binding domain of Orai1, but overall the N-terminal domain of Orai3 was much shorter. It was thought that if the calmodulin binding domain is functional it would be less effective in binding calmodulin, when compared with its Orai1 counterpart. Two chimeras of Orai1 and Orai3 were formed, the first in which Orai1 was combined with the N-terminal domain of Orai3 (N3-Orai1) and the second in which Orai3 was combined with the N-terminal domain of Orai1 (N1-Orai3). In cells expressing the N1-Orai3 protein NFAT was successfully activated, albeit to a lesser extent than in cells expressing STIM1/Orai1; indicating that the N-terminal domain of Orai1 and the calmodulin binding domain were sufficient to allow for downstream NFAT activation following local Ca^{2+} influx. Furthermore, utilising a Ca^{2+} insensitive calmodulin mutant (Calmodulin[mut1,2,3,4]), in which there was a point mutation of aspartate to alanine in all four EF hands that resulted in a mutant that could no longer bind Ca^{2+}, the researchers observed a reduction in the fast inactivation of the CRAC current compared with control cells (177). This recapitulated the findings of a previous study that found that the fast Ca^{2+}-dependent inactivation of the CRAC channel was reduced utilising a Ca^{2+} insensitive mutant form of calmodulin (366). The reduction in fast Ca^{2+}-dependent inactivation observed with the Ca^{2+} insensitive mutant was not observed using calmidazolium (177), which was similar to the opposing effects of observed when using the calmodulin insensitive mutant (358) and calmidazolium (367) on cells expressing voltage operated Ca^{2+} channels. Researchers did not observe any effect of calmidazolium on the Ca^{2+}-dependent inactivation and facilitation of voltage gated Ca^{2+} channels (367), instead of ruling out a role for calmodulin in these processes they employed a mutant form of calmodulin in which three of the EF hands were mutated and so were no longer able to bind Ca^{2+}. Using this mutant a strong inhibition of Ca^{2+} dependent inactivation and facilitation of the channel was observed, that was not observed when calmidazolium was used (358). A hypothesis has been developed that because the calmodulin is associated with the channel and not a free molecule it is somehow protected from the action of calmidazolium (358), this is used to explain why calmidazolium does not dramatically affect NFAT translocation to the nucleus, as calmodulin associated with Orai1 is shielded (177).

Conversely to the previous studies, calmidazolium and W-7 were found to potentiate SOCE in pulmonary artery smooth muscle cells when applied at 10 μM to the extracellular solution (368). The same potentiating effect of W-7 and calmidazolium on Ca^{2+} influx induced by thapsigargin was observed in MDCK cells (352,353). This concentration of calmidazolium also resulted in a dramatic increase in cytosolic Ca^{2+} levels when applied to cells in which Ca^{2+} stores were replete, in the presence of extracellular Ca^{2+}; such an effect was not observed in the absence of extracellular Ca^{2+} (368). Further to these studies, calmidazolium also potentiated Ca^{2+} entry induced by thapsigargin in HEK293 cells (369). To contradict these studies, there is evidence from experiments in hepatocytes that pre-incubating cells in the presence of calmidazolium was sufficient to inhibit store-operated Ca^{2+} influx induced by thapsigargin store depletion (370).

A calmodulin binding domain was also discovered in the polybasic region of STIM1, part of the cytoplasmic domain, which was found to have lots of hydrophobic residues, known calmodulin binding targets (176,365). A putative calmodulin binding site was identified (371). Further experiments provided biochemical analyses that demonstrated that both STIM1 and STIM2 bind calmodulin with high affinity, in a Ca^{2+}-dependent manner (176). Residues 667 − 685 of STIM1 bind calmodulin and residues 730-746 of STIM2 bind calmodulin. These regions of STIM1 and STIM2 were subsequently found to overlap with the lysine rich domain which is known to interact with the phosphoinositides in the plasma membrane, mediating the interaction of the ER Ca^{2+} sensor with the plasma membrane and thereby CRAC channels (372). Deleting the lysine-rich domain dramatically reduced the calmodulin binding ability of STIM1 and STIM2 C-terminal domain peptides (372).

4.2 Results

4.2.1 Inhibition of calmodulin

Calmodulin is known as a cytosolic Ca^{2+} buffer and has been demonstrated to protect pancreatic acinar cells from ethanol induced trypsinogen activation *in vitro* (359). Furthermore, in intact cells the addition of CALP3 reduced the increase in cytosolic Ca^{2+} elicited by ethanol. However, it was unclear whether this reduction in cytosolic Ca^{2+} levels was solely due to a reduction in intracellular Ca^{2+} release or a reduction in Ca^{2+} influx across the plasma membrane. As both Orai1 (159,160), STIM1(176,371) and PMCA (341) have calmodulin binding domains, modulation of calmodulin has the potential to alter Ca^{2+} influx via store-operated Ca^{2+} entry mechanisms and also clearance of cytosolic Ca^{2+} by the PMCA both of which serve to reduce cytosolic Ca^{2+} levels.

Calmidazolium is an inhibitor of calmodulin (344), it has been shown to elicit Ca^{2+} release when applied to cells, this release is similar in dynamics to Ca^{2+} release elicited by IP_3 (373); further it has been shown to activate store independent Ca^{2+} influx (368,373,374). In order to determine the effect of calmodulin inhibition on SOCE in pancreatic acinar cells, CPA was used to deplete intracellular stores, which was applied to cells in nominally Ca^{2+} free extracellular solution; as such Ca^{2+} was unable to re-enter the cell until it was re-admitted to the extracellular solution. Figure 4.1 A demonstrates the effect of 10 µM calmidazolium application to cells after store depletion (according to the protocol in section 2.5.2). In the previous chapter when inhibitors were added to the extracellular solution it was during store depletion with either CPA or thapsigargin, however due to the potential for calmidazolium to increase cytosolic Ca^{2+} concentration it was was added once cytosolic Ca^{2+} levels had returned to baseline levels after store depletion. Cells pre-incubated with calmidazolium exhibited a significant reduction in the amplitude of Ca^{2+} influx, the amplitude was reduced by 22.4 ± 2.5 % compared with control cells (figure 4.1 B). Furthermore, the half time of Ca^{2+} influx was significantly increased (40.9 ± 6.0%) in the presence of calmidazolium compared to control cells. The half time of Ca^{2+} efflux was not significantly affected by pre-incubation Calmidazolium (31.6 ± 6.8 % increase (figure 4.1 C). In this experiment Ca^{2+} influx was induced by the addition of 10 mM Ca^{2+} to the extracellular solution.
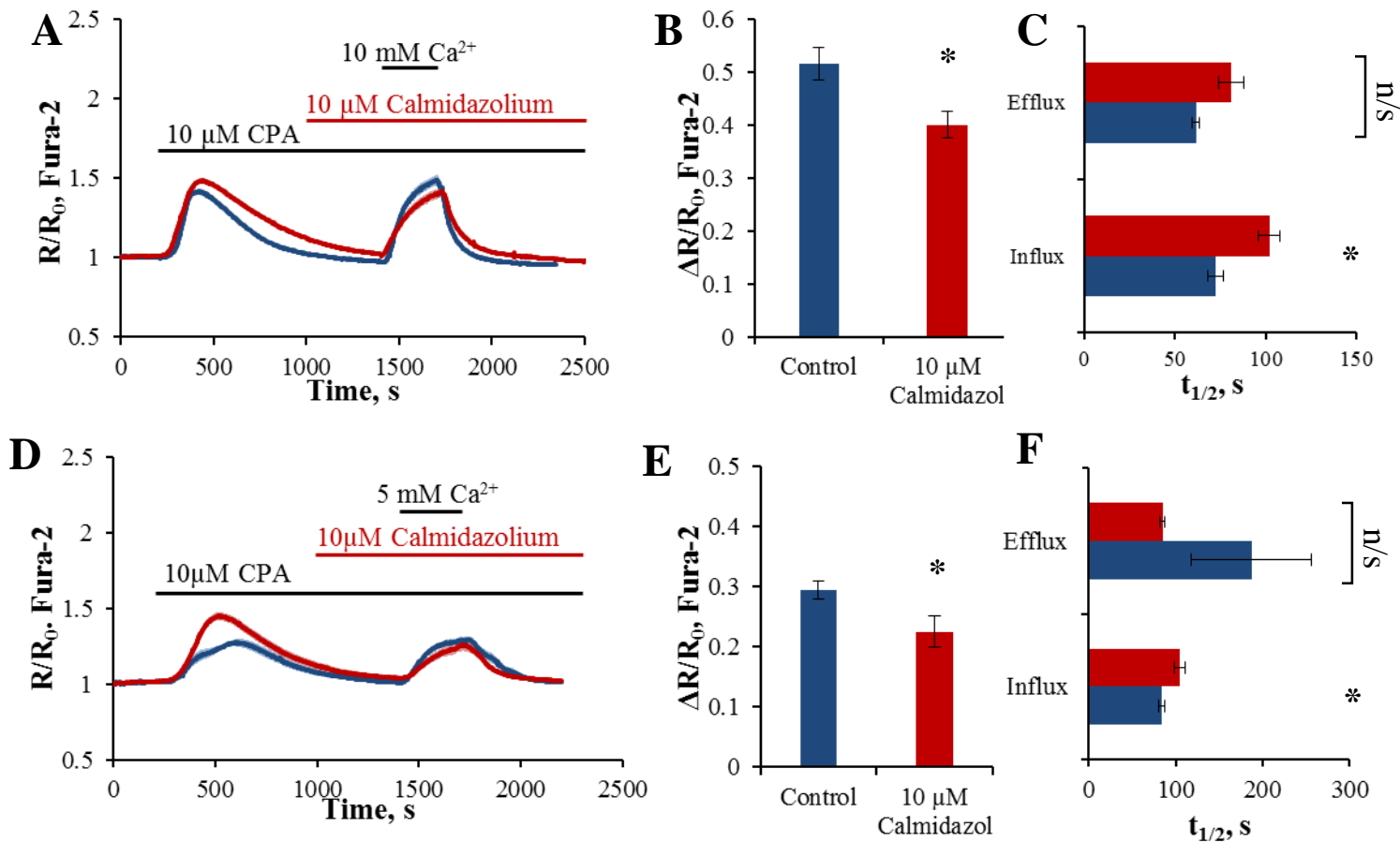
Figure 4.1 calmidazolium, a calmodulin inhibitor, inhibited store-operated Ca2+ entry in pancreatic acinar cells

Average traces (±SEM) from Fura-2 loaded pancreatic acinar cells

A - ER stores were depleted according to the protocol in section 2.5.2 and then cells were pre-incubated with 10 μM Calmidazolium for 400 seconds before 10 mM Ca^{2+} was subsequently re-introduced to the extracellular solution. Blue trace represents control cells (n = 10). Red trace represents 10 μM Calmidazolium (n = 29). **B-** Summary of the changes in ratio amplitude due to Ca^{2+} influx (from cells in figure **A**) control (blue bar) and calmidazolium treated (red bar) (p = 0.0186). **C-** Summary of the changes in the half time of Ca^{2+} influx (bottom bars p = 0.0085.) control - blue, calmidazolium treated - red. Half time of Ca^{2+} efflux (upper bars p = 0.3779) control – blue, calmidazolium treated - red. **D-** 10 μM Calmidazolium was applied to cells according to the protocol in section 2.5.2 and pre-incubated with cells for 400 seconds before the re-introduction of 5 mM Ca^{2+} to the extracellular solution, blue trace – control (n = 26) and red trace – 10 μM Calmidazolium (n = 17). **E-** Summary of changes in ratio amplitude due to Ca^{2+} influx in control (blue bar) and calmidazolium treated (red bar p = 0.0172). **F-** Summary of the changes in half time of Ca^{2+} influx (bottom bars p = 0.0190) control –blue. Calmidazolium treated – red. Half time of Ca^{2+} efflux (upper bars p = 0.2099) control – blue, calmidazolium treated – red.

123

In figure 4.1 D 10 µM calmidazolium was used to inhibit calmodulin in cells where Ca^{2+} influx was initiated by addition of 5 mM Ca^{2+} to the extracellular solution. The experiment was performed identically to that in figure 4.1 A, calmidazolium was introduced to the extracellular medium once cytosolic Ca^{2+} levels returned to baseline levels. Pre-incubation for 400 seconds was sufficient to significantly decrease the amplitude of Ca^{2+} influx (23.5 ± 2.6%, figure 4.1 E). In addition to inhibiting the amplitude of Ca^{2+} influx, pre-incubation with calmidazolium was sufficient to increase the half time of Ca^{2+} influx compared to control cells (25.9 ± 6.8 %). Similarly to figure 4.1 C, 10 µM calmidazolium pre-incubation was insufficient to significantly affect the half time of Ca^{2+} efflux compared to control cells (54.6 ±2.9% decrease, figure 4.1 F).

As in chapter 3, 2 mM Ca^{2+} was introduced to the extracellular solution to permit Ca^{2+} to re-enter the cytosol, as it is closer to physiological concentrations of extracellular Ca^{2+}. In figure 4.2 A cells were pre-incubated with 10 µM calmidazolium, in an identical protocol to figure 4.1 A and D, before the re-introduction of 2 mM Ca^{2+} to the extracellular solution. Ca^{2+} influx in control cells was reduced compared to Ca^{2+} influx in control cells where 5 mM Ca^{2+} was re-admitted to the extracellular solution (figure 4.1 D), as there is a reduced driving force for Ca^{2+} into the cytosol. Furthermore, Ca^{2+} influx was significantly reduced in cells pre-incubated with calmidazolium, compared to control cells (61.6 ± 1.2 %, figure 4.2 B). In addition to reducing the amplitude of Ca^{2+} influx, calmidazolium also increased the time taken for Ca^{2+} influx to reach half maximal compared to control cells (18.1 ± 2.3 %). The time taken for Ca^{2+} efflux to reach half maximal was also prolonged compared to the time taken for control cells (115.2 ± 3.8 %, figure 4.2 C).

Another inhibitor of calmodulin was also utilised to confirm that inhibition of calmodulin results in a reduction of Ca^{2+} influx, as this finding contradicts some studies (368,374). W-7 is also a calmodulin antagonist that inhibits the Ca^{2+}/calmodulin complex (375,376). In figure 4.3 A 100 µM W-7 was pre-incubated with cells, in an identical protocol to calmidazolium in figure 4.1 A, C and figure 4.2 A, after cytosolic Ca^{2+} levels had returned to baseline levels after   store   depletion.

Figure 4.2- Calmidazolium inhibited Ca^{2+} entry activated by 2 mM extracellular Ca^{2+}

Average traces (±SEM) from Fura-2 loaded pancreatic acinar cells

A- ER stores were depleted according to protocol in section 2.5.2 and the cells were pre-incubated with 10 μM calmidazolium for 400 seconds before the re-introduction of 2 mM Ca^{2+} to the extracellular solution. Control - blue trace (n = 6) calmidazolium treated- red trace (n = 25). **B-** Summary of changes in ratio amplitude due to Ca^{2+} influx (from cells in figure **A**) in control (blue bar) and calmidazolium treated (red bar p = 0.0005). **C-** Summary of the changes in half time of Ca^{2+} influx (bottom bars p = 0.0102) control – blue, calmidazolium treated – red. Half time of Ca^{2+} efflux (upper bars p = 0.0002), control – blue, calmidazolium treated – red

After store-depletion and pre-incubation with W-7, 10 mM Ca^{2+} was introduced to the extracellular solution, cells pre-incubated with W-7 exhibited a qualitatively large reduction in the amplitude of Ca^{2+} influx compared to Ca^{2+} influx in control cells, however the change was not significant (43.4 ± 1.2 %, figure 4.3 B). The time taken for Ca^{2+} influx to reach half maximal was significantly prolonged by pre-incubation with 100 μM W-7 compared to control cells (57.0 ± 4.6 %). The time taken for Ca^{2+} efflux to reach half maximal however, was not significantly prolonged by pre-incubation with 100 μM W-7 (16.1 ± 3.3 %, figure 4.3 C). The data generated from the two inhibitors, assuming their specificity for calmodulin, indicates that the rate of Ca^{2+} influx is regulated by calmodulin.

The Ca^{2+} insensitive protein described in section 4.1.3, in which all four EF hands have been mutated so that it can no longer bind Ca^{2+} has been developed and used extensively (366,377,378). It was found the amplitude of Ca^{2+} influx in cells expressing the Ca^{2+} insensitive protein was not affected, but the fast Ca^{2+} dependent inactivation of CRAC channels was affected (177). The plan was to use Ca^{2+} insensitive protein in this chapter to determine the effects of inhibiting the Ca^{2+} binding ability of calmodulin on the dynamics of SOCE in pancreatic acinar cells. Initial pilot studies resulted in conflicting results as to what the effects of Calmodulin[mut1,2,3,4] on Ca^{2+} handling in pancreatic acinar cells were, this was mostly due to the fact it was not possible to visualise cells expressing the mutant protein. As pancreatic acinar cells cannot be cultured, AR42J cells were used and transfected with the mCherry tagged version of both wild-type (mCherry-Calmodulin[WT]) or mutant (mCherry-calmodulin[mut1,2,3,4]) for three days according to previous protocols (328). Cells were loaded with Fura-2 and imaged according to the protocols in section 2.4.3 and 2.4.4 respectively. The experiment shown in figure 4.4 A is one in which 10 μM ACh and 30μM CPA were used to release Ca^{2+} from the ER store, in the presence of 1 mM Ca^{2+} in the extracellular solution. Cells expressing the mutant calmodulin exhibited a reduction in the amplitude of the subsequent cytosolic Ca^{2+} transient observed compared with cells expressing WT calmodulin. The amplitude of Ca^{2+} transient observed in both Calmodulin[mut1,2,3,4] and calmodulin[WT] are reduced compared to neighbouring cells on the coverslips that were not expressing the fluorescently tagged calmodulin plasmids. The differences were not statistically significant, likely due to insufficient statistical power. This can be overcome by repeating the experiment. Figure 4.4 B is a summary of the changes in amplitude of cytosolic Ca^{2+} transient in WT and mutant calmodulin expressing cells.
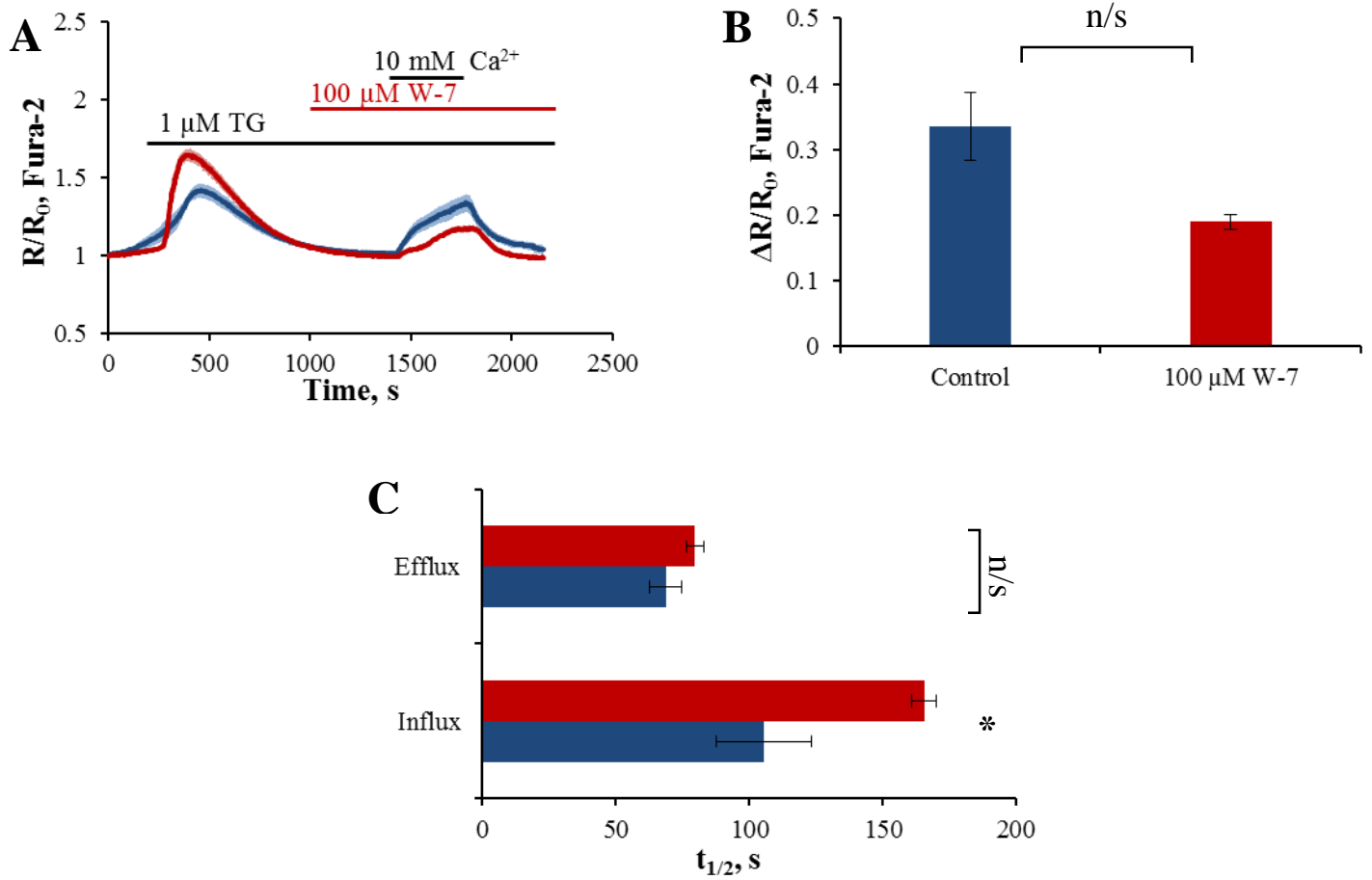
Figure 4.3 W-7, a calmodulin inhibitor, inhibited Ca^{2+} entry activated by 10 mM extracellular Ca^{2+}
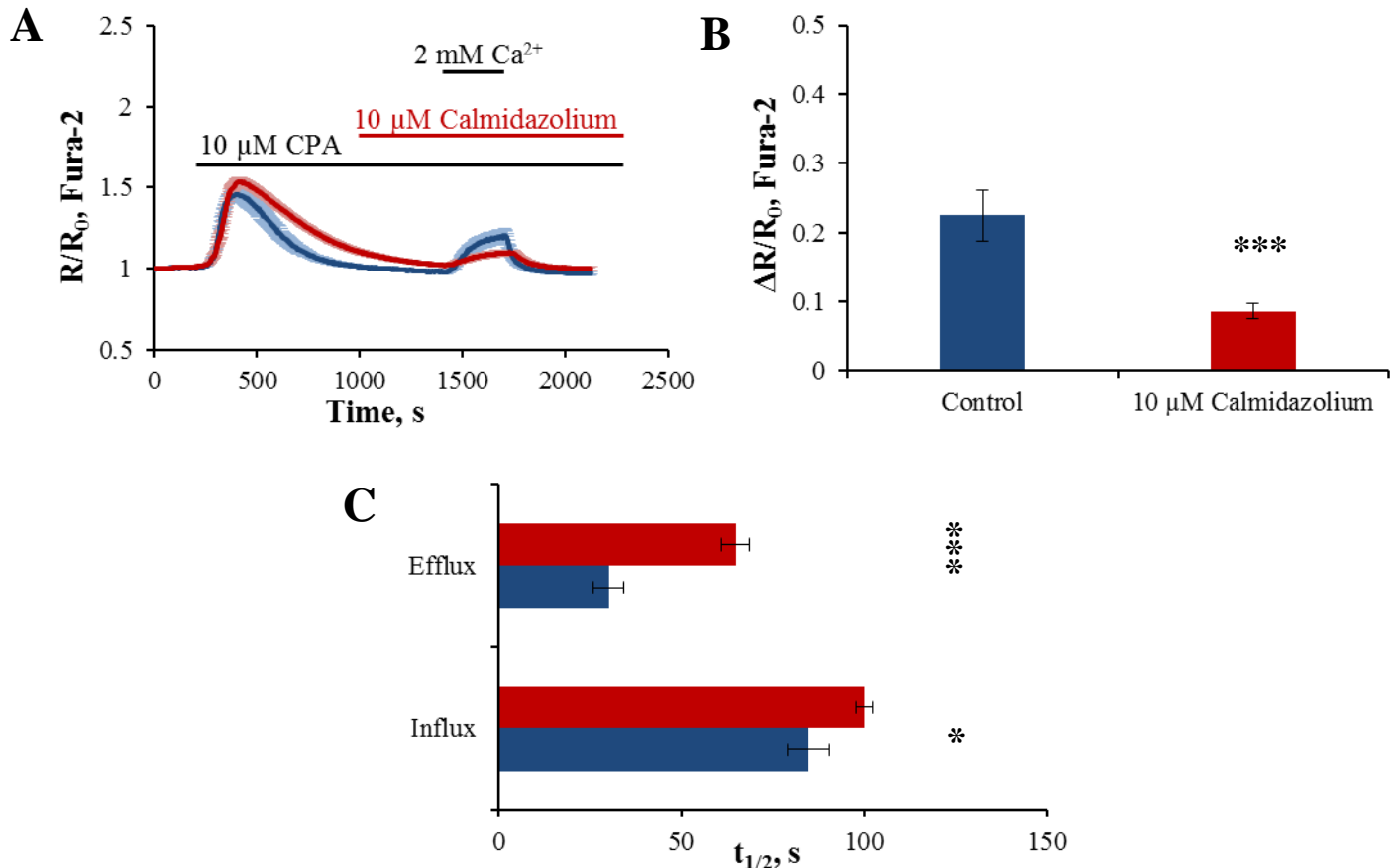
Average traces ($\pm$SEM) from Fura-2 loaded pancreatic acinar cells

A- ER stores were depleted using thapsigargin according to the protocol in section 2.5.2 and then cells were pre-incubated with 100 μM W-7 for 400 seconds before the re-introduction of 10 mM Ca^{2+} to the extracellular solution, blue trace – control (n = 10) and red trace – 100 μM W-7 treated (n = 4). **B-** Summary of changes in ratio amplitude due to Ca^{2+} influx (from cells in figure **A**) control – blue, W-7 treated – red (p = 0.1878). **C-** Summary of the changes in half time of Ca^{2+} influx (bottom bars p = 0.03) control – blue, W-7 treated – red. Half time of Ca^{2+} efflux (upper bars p = 0.0839) control –blue, calmidazolium treated – red.

A- 10 μM ACh + 30 μM CPA
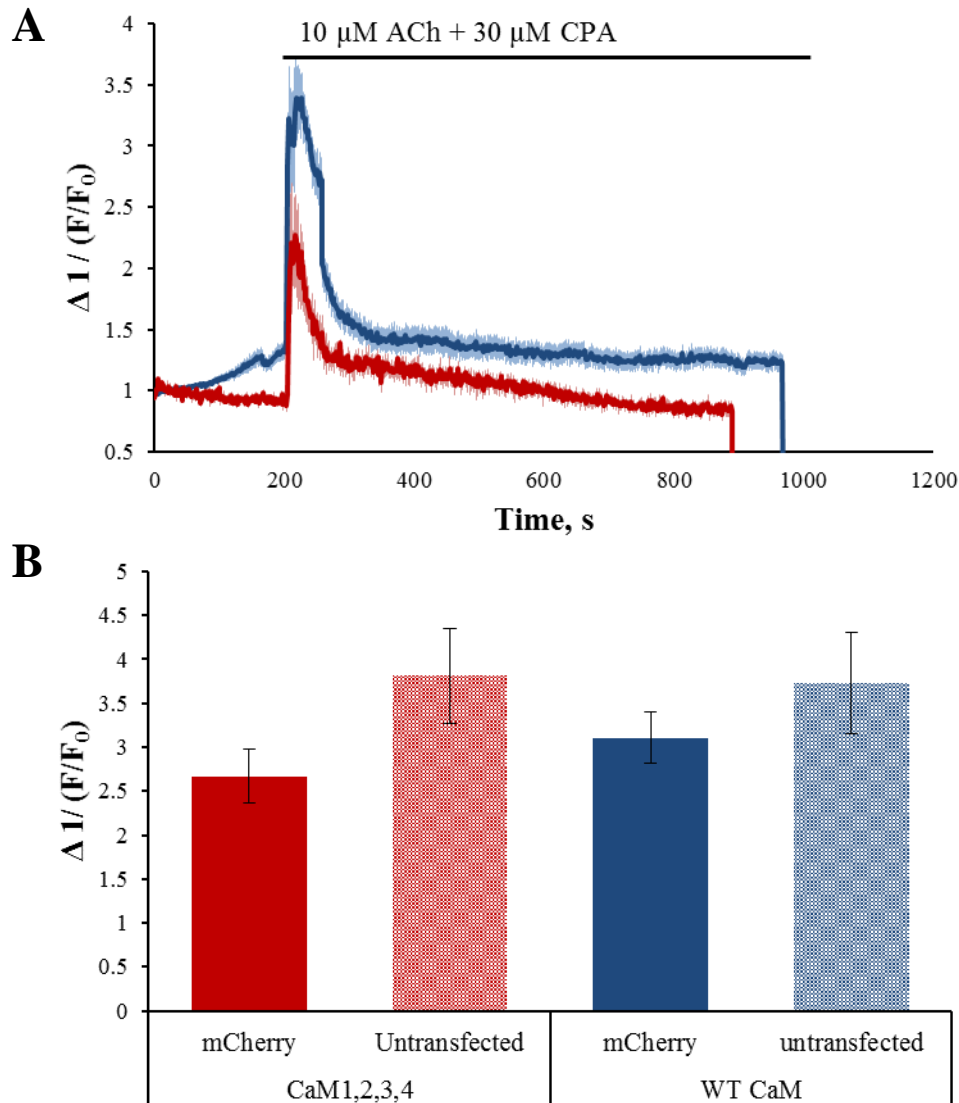
Figure 4.4 Expression of Ca^{2+} insensitive mutant calmodulin in AR42J cells resulted in a reduced amplitude of cytosolic Ca^{2+} signal

Averages traces (± SEM) of Fura-2 loaded AR42J cells

A- mCherry-Calmodulin^{WT} and mCherry-Calmodulin^{mut1,2,3,4} were generated according to the protocol in section 2.7 andwere expressed in AR42J cells according to the protocol in section 2.4. 2. Cells were loaded with Fura-2 according to the protocol in section 2.4.3. 10 μM ACh and 10μM CPA were applied to cells in the presence of 1 mM Ca^{2+} in the extracellular solution. **B-** summary of the overall changes in amplitude of cells expressing mCherry-Calmodulin^{mut1,2,3,4} (n =21) and untransfected cells (n = 20) and also the changes in amplitude of cytosolic Ca^{2+} in cells expressing mCherry-Calmodulin^{WT} (n = 45) and untransfected cells (n = 28).

4.2.2   Activation of calmodulin

CALP3, the calmodulin activator that inhibited ethanol induced elevation in cytosolic Ca^{2+} concentration, was utilised in figure 4.5 to determine if CALP3 had a dual effect of inhibiting Ca^{2+} release from intracellular stores and inhibiting Ca^{2+} entry. Based on data from a pilot experiment, in which 10 μM CALP3 was sufficient to significantly inhibit Ca^{2+} influx, in figure 4.5 A cells were exposed to a two-step store depletion (according to the protocol in section 2.5.4) and then were pre-incubated with 10 μM CALP3 for ten minutes before the re-introduction of 10 mM Ca^{2+} to the extracellular solution. This pre-incubation did not reduce the amplitude of Ca^{2+} influx in cells pre-incubated with CALP3 compared to Ca^{2+} influx in control cells (figure 4.5 B). In addition to having no significant effect on the amplitude of Ca^{2+} influx, 10 minutes pre-incubation with 10 μM CALP3 was insufficient to prolong the time taken for Ca^{2+} influx to reach half maximal compared with Ca^{2+} influx in control cells. Neither was there an effect on the time taken for Ca^{2+} efflux to reach half maximal compared with control cells (figure 4.5 C).

The pilot experimental data was obtained utilising 10 mM Ca^{2+} in the extracellular solution. this concentration of Ca^{2+} extracellularly would have provided a larger driving force for Ca^{2+} across the plasma membrane than 2 mM Ca^{2+}, thus resulting in a larger increase in cytosolic Ca^{2+} concentration. Higher concentrations of cytosolic Ca^{2+} are likely to be sufficient to completely activate calmodulin in the cytosol and associated with channels and pumps. Applying a calmodulin activating peptide is unlikely to have an additional effect. For the following experiments using CALP3, 2 mM Ca^{2+} was added to the extracellular solution instead of 10 mM Ca^{2+} in an attempt to avoid pre-activating calmodulin. Figure 4.5 D demonstrates the effect of increasing the CALP3 concentration to 100 μM, cells were pre-incubated with this concentration for 10 minutes before the re-introduction of 2 mM Ca^{2+} to the extracellular solution. This pre-incubation did not significantly affect the amplitude of Ca^{2+} influx compared to control cells (figure 4.5 E). The time taken for Ca^{2+} influx to reach half maximal was significantly shorter in cells pre-incubated with 100 μM compared to control cells (reduced by 22.0 ± 1.7 %). The time taken for Ca^{2+} efflux to reach half maximal however, was unaffected by the pre-incubation with 100 μM CALP3 compared with control cells (figure 4.5 F).

When ER stores are depleted using 10 μM CPA, although an efficient concentration for depleting the intracellular store of Ca^{2+}, the increase in cytosolic Ca^{2+} is rapid and substantial, sufficient to activate calmodulin in order to buffer increases in Ca^{2+}, to prevent the cytotoxic

effects of sustained elevation in cytosolic Ca^{2+} levels, such as intracellular activation of digestive proenzymes (234). As CALP3 is an activator of calmodulin, it would be ineffective if applied after calmodulin activation by elevated Ca^{2+} levels. A two-step store depletion protocol was employed, the first step a low concentration of CPA (1 μM) was applied to cells which induced a slower and more gradual passive leak of Ca^{2+} from ER. This was followed by the second step, in which cells were briefly exposed to 10 μM CPA to ensure the stores were entirely depleted. In addition to the two-step store depletion protocol the concentration of CALP3 was increased to 200 μM; pre-incubating cells with this concentration for ten minutes before the re-introduction of 2 mM Ca^{2+} to the extracellular solution, is shown in figure 4.6 A. This pre-incubation was sufficient to significantly inhibit Ca^{2+} influx compared to influx in control cells (figure 4.6 C). Figure 4.6 B depicts another experiment in which cells were pre-incubated with 200 μM CALP3 for 10 minutes before re-introduction of 2 mM Ca^{2+} to the extracellular solution, undertaken using the same experimental protocol as figure 4.6 A; however the store depletion phase with 1 μM CPA was shorter, as such as the experiments were not time locked they could not be combined to make one average trace. Despite this minor change, this pre-incubation was sufficient to significantly inhibit the amplitude of Ca^{2+} influx compared to influx in control cells (figure 4.6 C). The inhibition of Ca^{2+} influx in CALP3 pre-incubated cells was significant in both experiments (77.8 ± 1.8%).
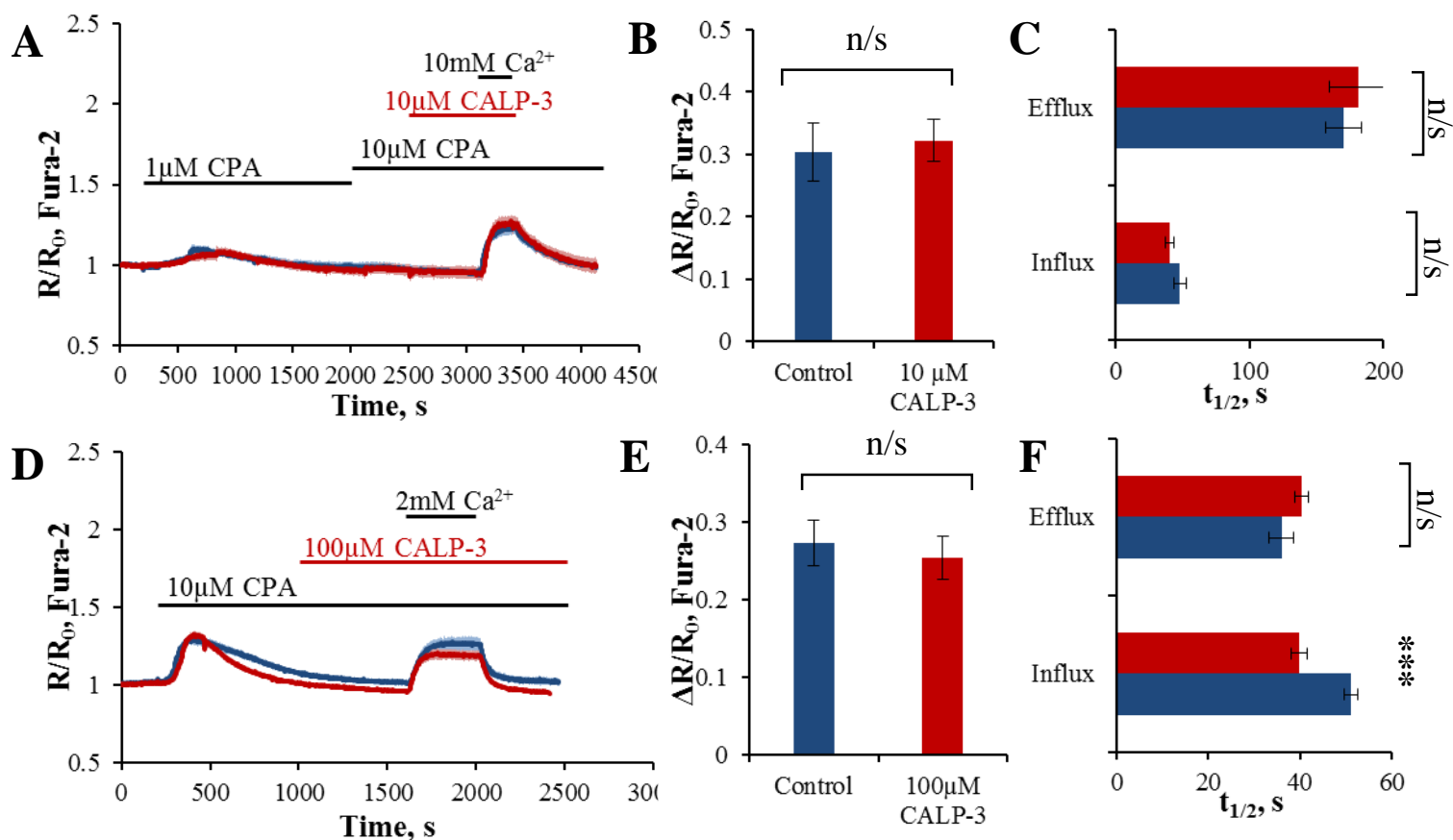
Figure 4.5 CALP3, a calmodulin activating peptide, had no effect on Ca^{2+} entry when pre-incubated with cells at 100 μM

Average traces (±SEM) from Fura-2 loaded pancreatic acinar cells

A- ER stores were depleted according to the protocol 2.5.4 and then cells were pre-incubated with 10 μM CALP3 for 10 minutes before the re-introduction of 10 mM Ca^{2+} to the extracellular solution. Blue trace – control (n = 8) and red trace – 10 μM CALP3 (n = 7). **B-** Summary of changes in ratio amplitude due to Ca^{2+} influx (from cells in Figure **A**) in control (blue bar) and CALP3 treated (red bar p = 0.7608). **C-** Summary of the changes in half time of Ca^{2+} influx (bottom bars p = 0.1810) control - blue CALP3treated – red.) Half time of Ca^{2+} efflux (upper bars p = 0.4563) control – blue, CALP3 treated – red. **D-** ER stores were depleted according to the protocol in section 2.5.2 and then cells were pre-incubated with 100 μM CALP3 for 10 minutes before the re-introduction of 2 mM Ca^{2+} to the extracellular solution, blue trace – control (n = 8) and red trace – 100 μM CALP3 (n = 15). **E-** Summary of changes in ratio amplitude due to Ca^{2+} influx (from cells in figure **D**) control (blue bar) and CALP3 treated (red bar p = 0.6779). **F-** Summary of the changes in half time of Ca^{2+} influx (bottom bars p = 0.0004) control – blue, CALP3 treated - red. Half time of Ca^{2+} efflux (upper bars p = 0.1125) control – blue, CALP3 treated – red.

131
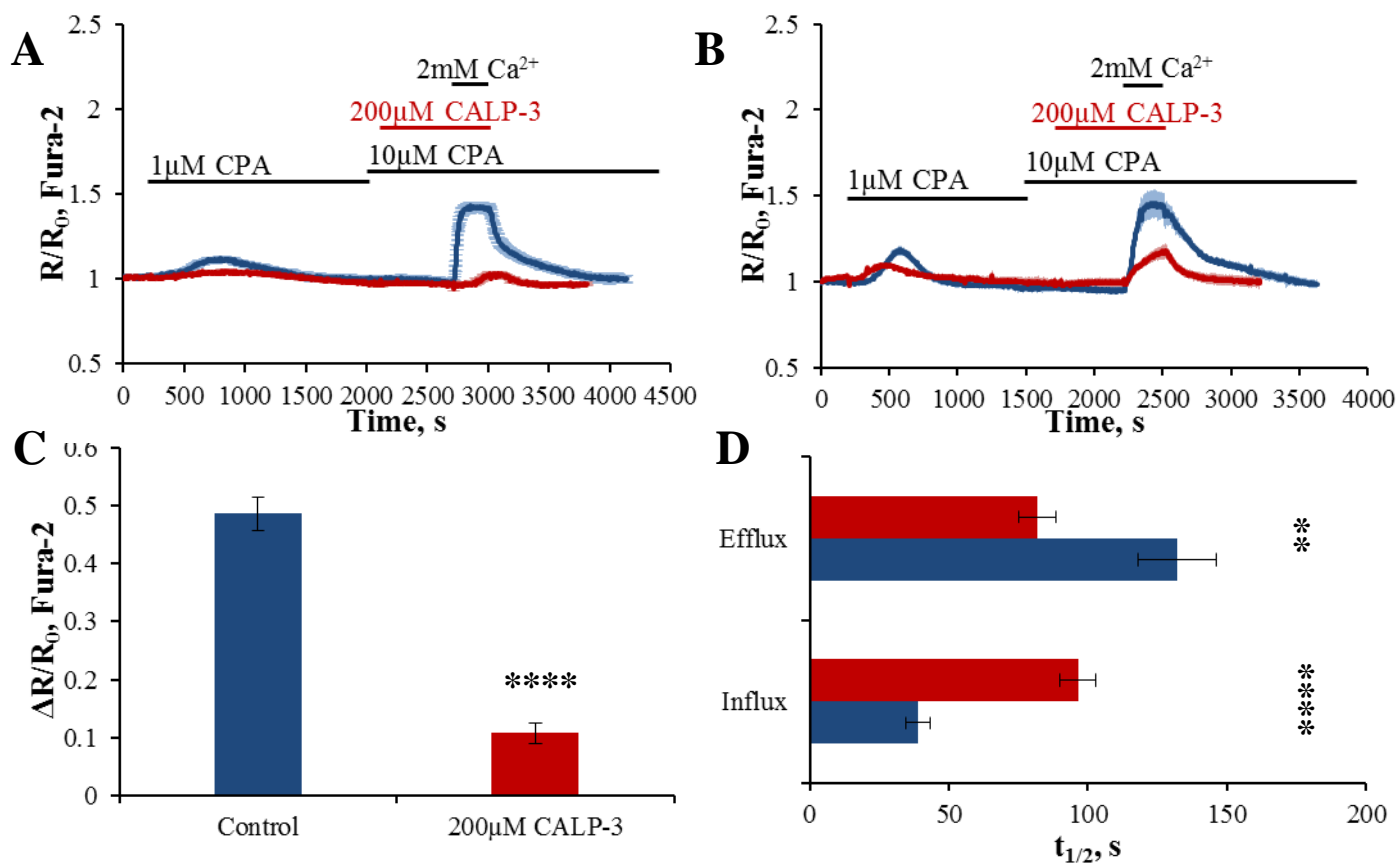
Figure 4.6 CALP3, a calmodulin activating peptide, inhibited Ca²⁺ influx when pre-incubated with cells at 200 μM

Average traces (± SEM) from Fura-2 loaded pancreatic acinar cells

A – Cells were treated according to the protocol in section 2.5.4, cells were pre-incubated with 200 μM CALP3 for 10 minutes before 2 mM Ca was subsequently re-introduced to the extracellular solution. Control cells – blue trace (n= 11) and 200 μM CALP3 – red trace (n = 15). **B** – a similar experiment to part A, on different time scale. 2 mM Ca²⁺ was re-introduced to the extracellular solution after pre-treatment with CALP-3. Control cells – blue trace (n = 5) and 200 μM CALP3 – red trace (n = 7). **C-** Summary of the changes in ratio amplitude due to Ca²⁺ influx, from **A** and **B**, in control cells (blue bar) and 200 μM CALP3 (red bar p < 0. 0001). **D**- Summary of the changes in the half time of Ca²⁺ influx, from **A** and **B** (bottom bars p < 0.0001) blue – control and red – 200 μM CALP3 and the half time of Ca²⁺ efflux (upper bars p = 0.004) control – blue and 200 μM CALP3 – red.

132

In addition, the time taken for Ca^{2+} influx to reach half maximal was significantly increased in cells pre-incubated with CALP3, compared to control cells (146.8 ± 6.3 %). Lastly, the time taken for Ca^{2+} efflux to reach half maximal was significantly decreased in cells pre-incubated with CALP3, compared to Ca^{2+} efflux in control cells (38.1 ± 6.8 %, figure 4.6 D).

As CALP3 is a cell permeable peptide (362), it likely does not need a prolonged pre-incubation period in order to access the cytosol and exert its action. When pre-incubated with cells for 100 seconds before the re-introduction of 2 mM Ca^{2+} to the extracellular solution, in figure 4.7 A 200 µM CALP3 was sufficient to significantly inhibit the ratio amplitude of Ca^{2+} influx in pre-treated cells compared to control cells in (35.1 ± 3.3 %, figure 4.7 B). The time taken for Ca^{2+} influx to reach half maximal in cells pre-incubated with 200 µM CALP3 was significantly prolonged compared to the time to half maximal Ca^{2+} influx in control cells (141.3 ± 1.6 %). The time taken to reach half maximal Ca^{2+} efflux was unchanged in cells pre-incubated with 200 µM CALP3 compared to that in control cells (decreased by 1.8 ± 14.2 %, figure 4.7 C).

As it is not possible to treat patients for an acute disease, such as acute pancreatitis, in advance it is necessary to find a treatment that is effective in ameliorating the pathological stimulus once it has been triggered and the disease has been set in motion, therefore any potential therapeutic needs to be effective when applied in an acute manner. Figure 4.7 E demonstrates the effect of applying 200 µM CALP3 in an acute protocol in the presence of a sustained increase in cytosolic Ca^{2+} due to the re-admittance of Ca^{2+} to the extracellular solution. In control cells, shown in figure 4.7 D, re-admittance of Ca^{2+} to the extracellular solution was followed by a rapid increase in cytosolic Ca^{2+}, upon reaching a peak there was a slight decrease and then an elevated plateau was established. This plateau remained significantly elevated compared to baseline and remained remarkably constant in the sustained presence of Ca^{2+} in the extracellular solution. The addition of 200 µM CALP3 to the extracellular solution, in figure 4.7 E, in the maintained presence of Ca^{2+} extracellularly and a sustained elevation in cytosolic Ca^{2+} resulted in a decrease in cytosolic Ca^{2+} levels, contrasting with control cells. The effect of this acute application of 200 µM CALP3 was to significantly reduce cytosolic Ca^{2+} levels by 57.2 ± 3.9 % ($p = 0.0357$).
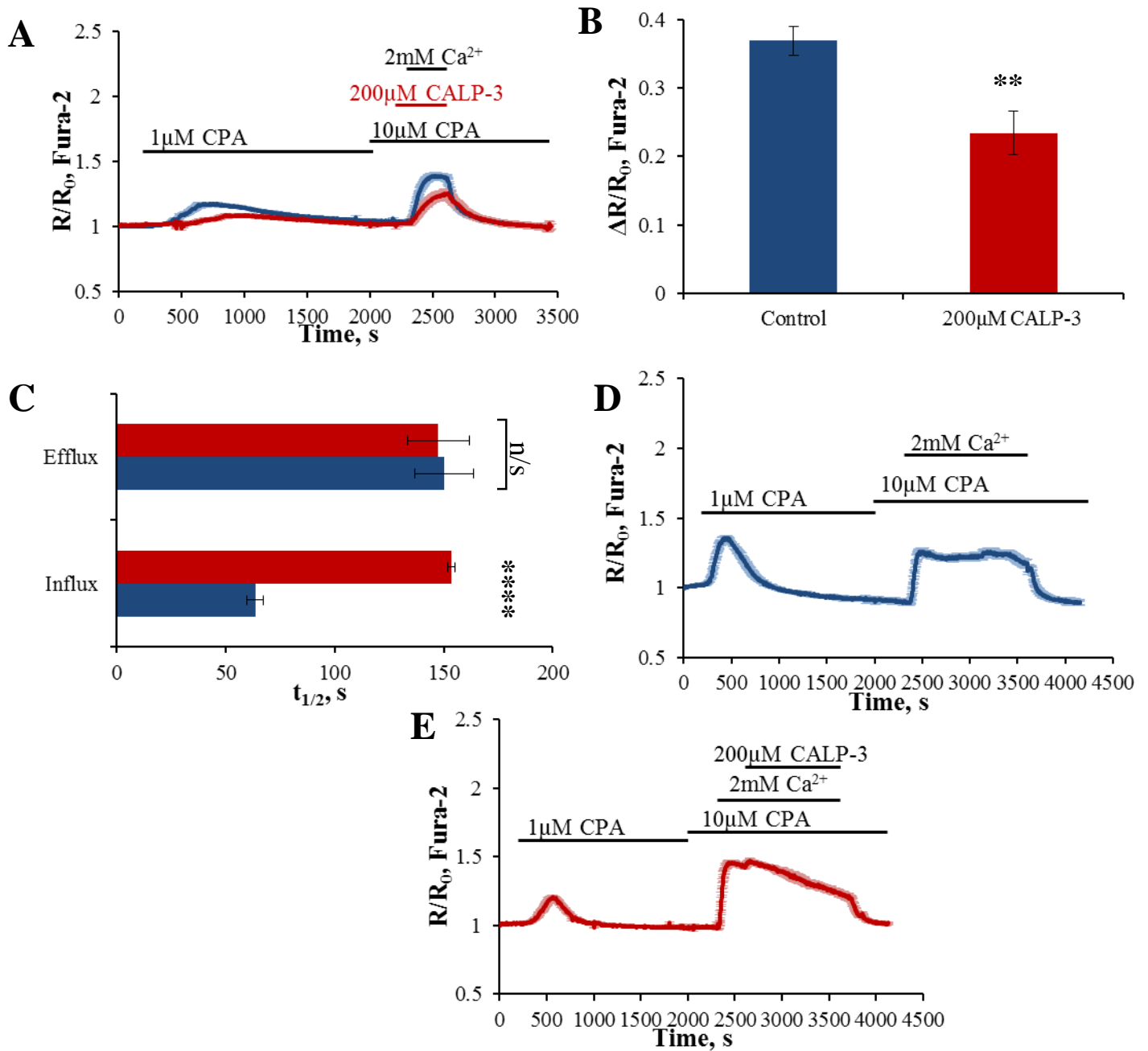
Figure 4.7 200 µM CALP3 inhibited Ca^{2+} entry when only briefly pre-incubated with cells and when applied acutely

Average traces (±SEM) from Fura-2 loaded pancreatic acinar cells

A- ER stores were depleted according to the protocol in section 2.5.4 and the cells were pre-incubated with 200 µM CALP3 for 100 seconds before the re-introduction of 2 mM Ca^{2+} to the extracellular solution. Blue trace – control (n = 25) and red trace – 200 µM CALP3 (n = 24). **B-** Summary of changes in ratio amplitude due to Ca^{2+} influx (from cells in figure **A**) control (blue bar) and CALP3 treated (red bar p = 0.0018). **C-** Summary of the changes in half time of Ca^{2+} influx (lower bars p = 0.0001) control – blue, CALP3 treated – red. Half time of Ca^{2+} efflux (upper bars p = 0.7928) control - blue, CALP3 treated – red. **D** & **E -** cells were treated according to the protocol in section 2.5.3, **D** is a control for **E**, in which 200 µM CALP3 was introduced to the extracellular solution in the continued presence of 2 mM Ca^{2+} on top of a sustained plateau in cytosolic Ca^{2+} (p = 0.0357).

Although significant, the reduction in cytosolic Ca^{2+} levels was incomplete; however, cytosolic Ca^{2+} was steadily decreasing and had the experiment been left for longer the reduction may have been more significant. Removal of Ca^{2+} from the extracellular solution resulted in a further reduction of cytosolic Ca^{2+} levels to baseline levels.

As AR42J cells are a model pancreatic acinar cell line, it was sought to determine if the effect of pre-incubating cells with 200 µM CALP3 was similar to that in primary pancreatic acinar cells, or if the differences that were observed with Pyr6 and Pyr10 treatment between AR42J cells and primary cells observed in chapter 3 were true for CALP3 treatment. AR42J cells were pre-incubated with 200 µM CALP3 for ten minutes before the re-introduction of 2 mM Ca^{2+} to the extracellular solution, figure 4.8 A. There was subsequent influx of Ca^{2+} in control cells and in cells pre-incubated with CALP3, the amplitudes of which were not significantly different from each other (figure 4.8 B). This was starkly in contrast with the results obtained in primary pancreatic acinar cells in which a ten minute pre-incubation resulted in a dramatic reduction in Ca^{2+} influx as observed in figure 4.6, a significant reduction in Ca^{2+} influx was observed with a short incubation with 200 µM CALP3 in figure 4.7, as well as the decrease in cytosolic Ca^{2+} observed after acute application with 200 µM CALP3. The half time of Ca^{2+} influx in AR42J cells pre-treated with CALP3 was significantly faster than in control and the time taken to reach half maximal Ca^{2+} efflux was also significantly slowed in AR42J cells pre-incubated with CALP3, compared with control (figure 4.8 C). The effect of CALP3 on the half-time of Ca^{2+} influx in AR42J cells was much more similar to pancreatic acinar cells than the effect of CALP3 on the amplitude of Ca^{2+}influx.
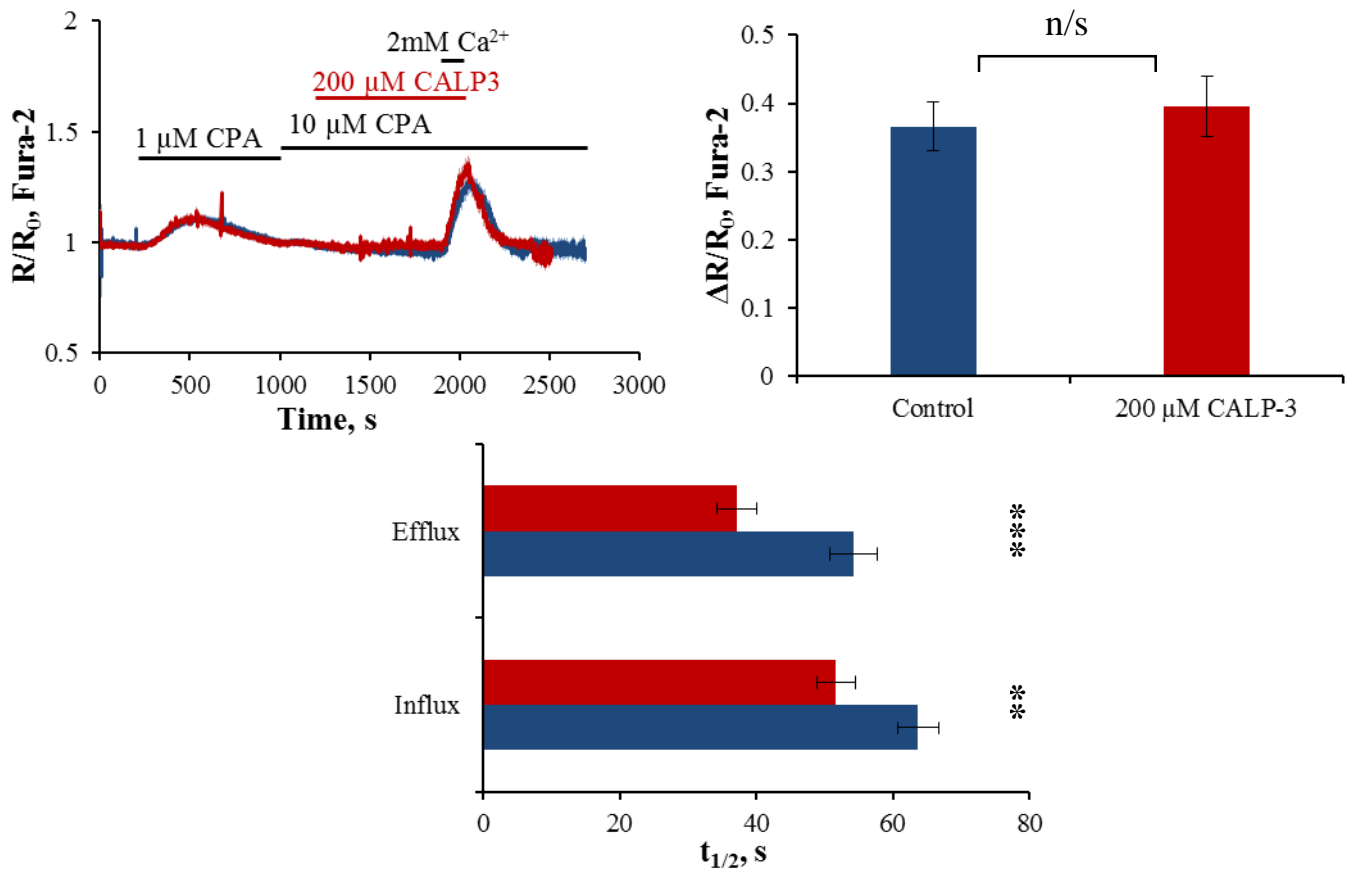
Figure 4.8 CALP3 significantly slowed the rate of store-operated Ca^{2+} influx and Ca^{2+} efflux in AR42J cells

Average traces ($\pm$SEM) from Fura-2 loaded AR42J cells

A- ER stores were depleted according to the protocol in section 2.5.4 and then cells were pre-incubated with 200 μM CALP3 for ten minutes before 2 mM Ca^{2+} was subsequently re-introduced to the extracellular solution. Blue trace represents control cells (n = 19). Red trace represents 200 μM CALP3 (n = 20). **B-** Summary of the changes in the ratio amplitude due to Ca^{2+} influx (from cells in figure **A**) control (blue bar) and CALP3 treated (red bar) (p = 0.8927). **C-** Summary of the changes in the half time of Ca^{2+} influx (bottom bars) control – blue, CALP3 treated – red (p = 0.0024). Half time of Ca^{2+} efflux (upper bars) control – blue, CALP3 treated – red (p = 0.0006).

4.2.3 Combined inhibition of Orai1 and Calmodulin

Inhibition of CRAC channels using several different inhibitors resulted in a significant reduction in store-operated Ca^{2+} entry (see chapter 3); furthermore, inhibition of calmodulin, using two different inhibitors also resulted in a decrease in store-operated Ca^{2+} entry. The aim of the following experiments was to determine the extent to which Ca^{2+} influx could be reduced when both CRAC channel inhibition and calmodulin inhibition were employed.

Figure 4.9 A demonstrates the effect of pre-incubating cells with 10 μM GSK7975-A and 10 μM calmidazolium for 10 minutes before the re-introduction of 10 mM Ca^{2+} to the extracellular solution, to maximally activate SOCE across the membrane. This pre-incubation was sufficient to significantly reduce the amplitude of Ca^{2+} entry compared to the amplitude of Ca^{2+} entry in control cells (49.9 ± 2.3 %, figure 4.9 B). In cells pre-incubated with 10 μM Calmidazolium and 10 μM GSK7975-A the elevated plateau in cytosolic Ca^{2+} did not remain constant; upon Ca^{2+} re-addition to the extracellular solution cytosolic Ca^{2+} levels rapidly reached a peak but almost immediately started to decline. This decrease in cytosolic Ca^{2+} continued at a steady rate until Ca^{2+} was removed from the extracellular solution, at which point the rate at which in cytosolic Ca^{2+} levels decreased became steeper until baseline levels in Ca^{2+} were re-attained. This decrease in cytosolic Ca^{2+} levels after the re-introduction of Ca^{2+} to the extracellular solution was not observed in control cells. In addition to reducing the amplitude of Ca^{2+} influx the pre-incubation with the calmodulin inhibitor and the CRAC channel inhibitor also significantly prolonged the half time to maximal Ca^{2+} influx in cells, compared with control cells (22.2 ± 4.7 %, p = 0.0129). The time taken to reach half maximal Ca^{2+} efflux was also prolonged in cells pre-incubated with 10 μM GSK7975-A and 10 μM calmidazolium compared with control cells (86.9 ± 4.2 %, figure 4.9 C.

Figure 4.9 Combined inhibition of Orai1 and calmodulin significantly inhibited Ca^{2+} influx

Average traces (±SEM) from Fura-2 loaded pancreatic acinar cells

A- ER stores were depleted according to the protocol in section 2.5.2 and then cells were pre-incubated with 10 μM calmidazolium and 10 μM GSK7975-A for 10 minutes before the re-introduction of 10 mM Ca^{2+} to the extracellular solution. Blue trace – control (n = 5) and red trace – 10 μM Calmidazolium and 10 μM GSK7975-A (n = 28). **B-** Summary of the changes in ratio amplitude due to Ca^{2+} influx in control (blue bar) and calmidazolium + GSK7975-A treated (red bar p = 0.0001). **C-** Summary of the changes in half time of Ca^{2+} influx (lower bars p = 0.0129) control – blue, calmidazolium + GSK7975-A – red. Half time of Ca^{2+} efflux (upper bars p = 0.0001) control – blue, calmidazolium + GSK7975-A treated – red.
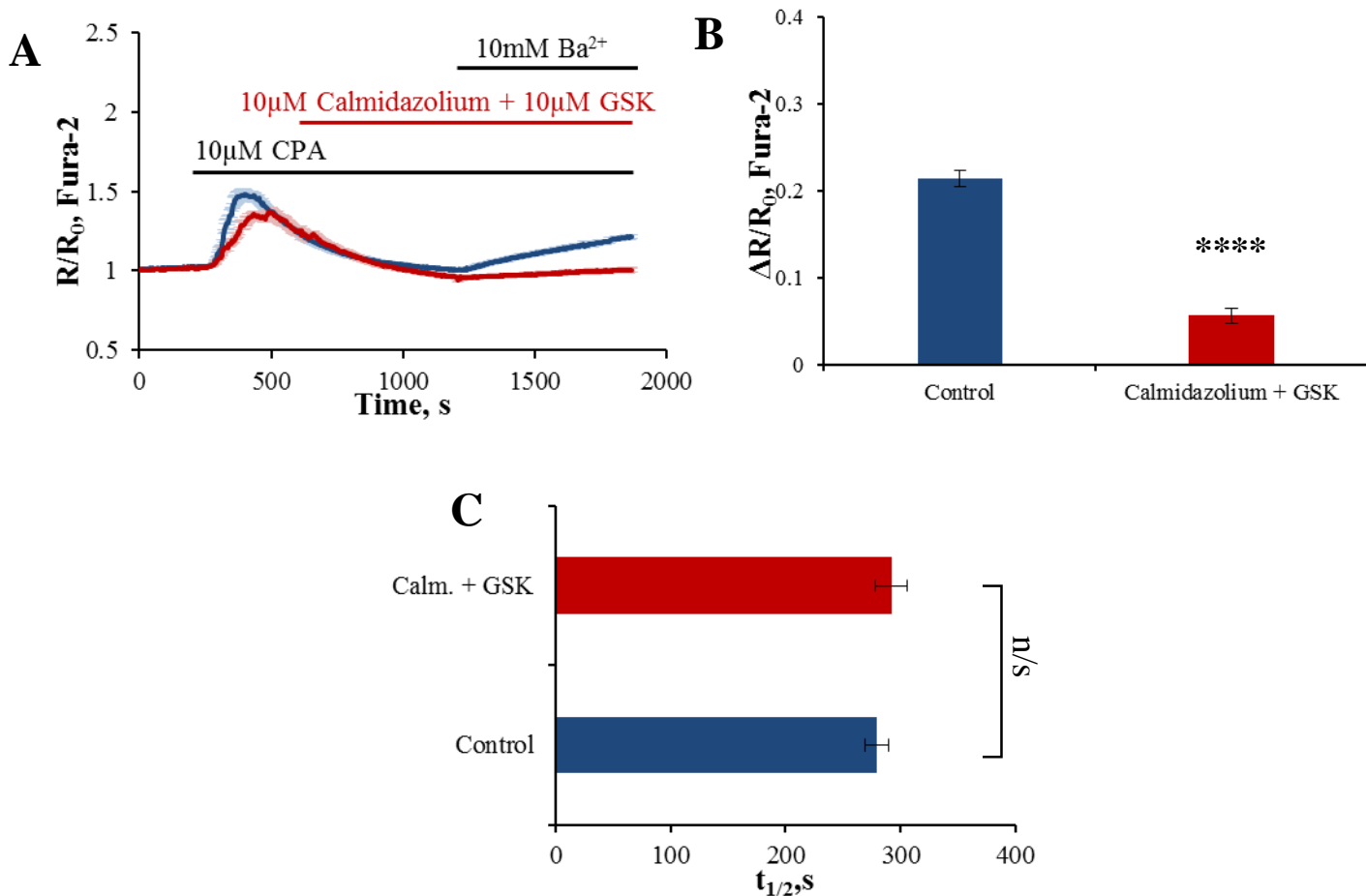
Figure 4.10 Combined calmodulin and Orai1 inhibition reduced Ba^{2+} entry activated by 10 mM extracellular Ba^{2+}

Average traces (± SEM) from Fura-2 loaded pancreatic acinar cells

A- ER stores were depleted according to the protocol in section 2.5.2 and then cells were pre-incubated with 10 µM Calmidazolium and 10 µM GSK7975-A for 10 minutes before the introduction of 10 mM Ba^{2+} to the extracellular solution, blue trace – control (n = 19) and red trace – 10 µM Calmidazolium and 10 µM GSK7975-A (n = 18). **B-** Summary of the changes in ratio amplitude due to Ca^{2+} influx in control (blue bar) and Calmidazolium + GSK7975-A treated (red bar p = 0.0001). **C-** Summary of the changes in half time of Ca^{2+} influx control – blue, calmidazolium + GSK7975-A treated – red. (p = 0.4613)

As described in chapter 3, Ba^{2+} can be used to assess the unidirectional flux of divalent ions into the cell, as CRAC channels are permeable to Ba^{2+} but PMCA and SERCA are incapable of actively pumping Ba^{2+} from the cytosol in the way they would pump Ca^{2+}. As in figure 3.13, in figure 4.10 A the ER Ca^{2+} stores were depleted using CPA, during the store depletion phase 10 µM GSK-7975A and 10 µM Calmidazolium were introduced to the extracellular solution and pre-incubated with the cells for 10 minutes before the introduction of 10 mM Ba^{2+} to the extracellular solution. In control cells there was an increase in cytosolic Ba^{2+} levels. There was also an increase in Ba^{2+} influx in cells pre-treated with the calmodulin inhibitor and CRAC channel inhibitor. The amplitude of Ba^{2+} influx in cells pre-treated with the calmodulin inhibitor and the CRAC channel inhibitor was significantly reduced compared with control cells (73.6 ± 4.0, figure 4.10 B). The time to half maximal Ba^{2+} influx was not significantly different in cells pre-incubated with calmidazolium and GSK-7975A compared to control cells (increase of 4.6 ± 5.0, figure 4.10 C). The gradients of the increase in Ca^{2+} influx from control cells and that from GSK-7975A and calmidazolium treated cells are clearly different. However, as a plateau in cytosolic Ba^{2+} concentration was not attained, the measurement of half time likely does not reflect this difference as accurately as measurement of the gradient might.

4.2.3 Effect of calmodulin and calmodulin-derived peptides on Ca^{2+} entry

CALP3, when applied to pancreatic acinar cells was able to inhibit SOCE in addition to its previously demonstrated capacity to reduce Ca^{2+} release in cells treated with ethanol (359). An additional finding of this paper was that the application of calmodulin to permeabilised cells resulted in decreased Ca^{2+} release from intracellular Ca^{2+} stores.

In figure 4.11 A a calmodulin containing extracellular solution was used to perfuse intact pancreatic acinar cells after store depletion using a two-step store depletion protocol described in section 2.5.4. Cells were pre-incubated with 10 µM calmodulin, derived from bovine brain, for ten minutes before the re-introduction of 2 mM Ca^{2+} to the extracellular solution. The amplitude of Ca^{2+} influx in cells pre-incubated with 10 µM calmodulin was significantly reduced compared to the amplitude of Ca^{2+} influx in control cells (18.0 ± 3.8 %, figure 4.11 B).

Figure 4.11 Pre-incubation with full length Calmodulin significantly inhibited Ca^{2+} entry

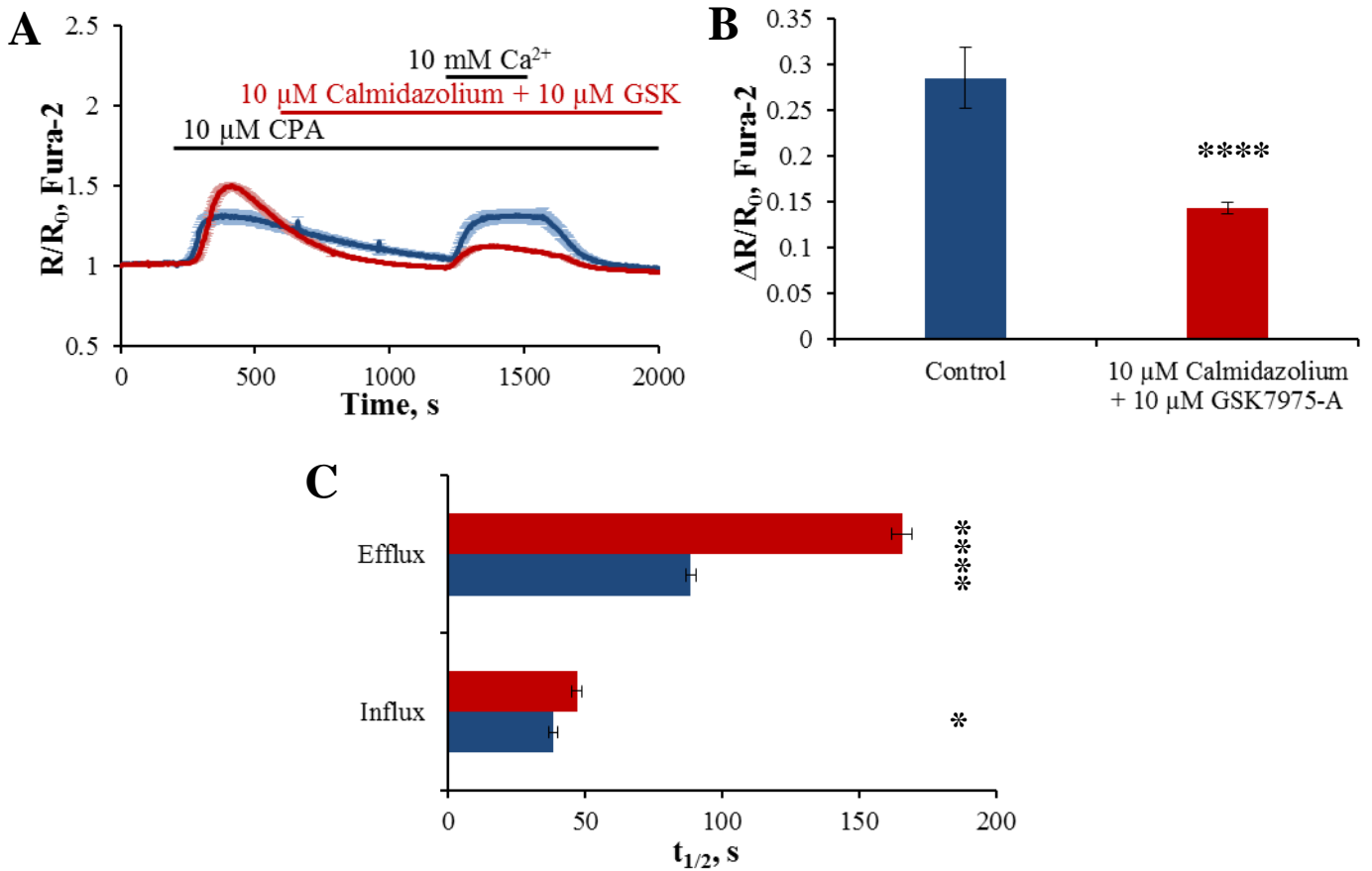Average traces (±SEM) from Fura-2 loaded pancreatic acinar cells

A- ER stores were depleted according to the protocol in section 2.5.4 and then cells were pre-incubated with 10 μM calmodulin for 10 minutes before the re-introduction of 2 mM Ca^{2+} to the extracellular solution. Blue trace – control (n = 19) and red trace – 10 μM Calmodulin (n = 14). **B-** Summary of the changes in ratio amplitude due to Ca^{2+} influx in control (blue bar) and calmodulin treated (red bar p = 0.0006). **C-** Summary of the changes in half time of Ca^{2+} influx (lower bars p = 0.0001) control – blue, calmodulin treated – red. Half time of Ca^{2+} efflux (upper bars p = 0.0001) control – blue, calmodulin treated – red.

Furthermore, the time taken to reach half maximal influx in cells pre-incubated with 10 µM calmodulin was significantly prolonged compared with the half time of Ca^{2+} influx in control cells (108.2 ± 17.3 %). The time taken to reach half maximal efflux in cells pre-incubated with 10 µM calmodulin was significantly shorter than in the half time of Ca^{2+} efflux in control cells (33.2 ± 4.1 %, figure 4.11 C.

It is highly unlikely that calmodulin, a 148 amino acid long protein, would be able to pass through the plasma membrane. In addition, there are not any known extracellular calmodulin binding domains through which calmodulin can bind and activate intracellular signal transduction pathways that have the ability to initiate intracellular calcium signalling and regulation of CRAC channels. A suspension of freshly isolated pancreatic acinar cells that have been partially digested from the whole tissue using collagenase is likely to contain cells that have undergone necrosis, which have released their cellular contents to the extracellular medium. The primary physiological function of pancreatic acinar cells is the synthesis of digestive pro-enzymes, which are stored in zymogen granules; ordinarily the proenzymes are activated after they are released from the cell via exocytosis. However, under necrotic conditions these proenzymes are released and are activated establishing a positive feedback cycle of digestion and necrosis. In addition to the release of digestive proenzymes other intracellular proteins would also be released. Proteases, such as trypsin and chymotrypsin, are the major class of digestive enzymes synthesised and stored harmlessly in zymogen granules as trypsinogen and chymotrypsinogen in the apical pole of acinar cells. In acute pancreatitis, once the proteases are activated extracellularly, the intracellular proteins that are released are highly vulnerable to proteolytic cleavage. There are many protease cleavage site on calmodulin, including several trypsin and chymotrypsin cleavage sites (see appendix Figure 1).

It was hypothesised that following cellular necrosis, once the cellular components have been released to the extracellular solution, the various proteases including trypsin and chymotrypsin cleave proteins such as calmodulin, forming smaller peptide products that are able to inhibit Ca^{2+} entry via SOCE channels. The mechanisms of the inhibition are to be determined. Interestingly, when AR42J cells, the pancreatic acinar like cell line, are pre-incubated with full length calmodulin at the same concentration for the same duration (figure 4.12 A), the inhibitory effect on the amplitude of Ca^{2+} entry observed in figure 4.11 A was not   observed.

142
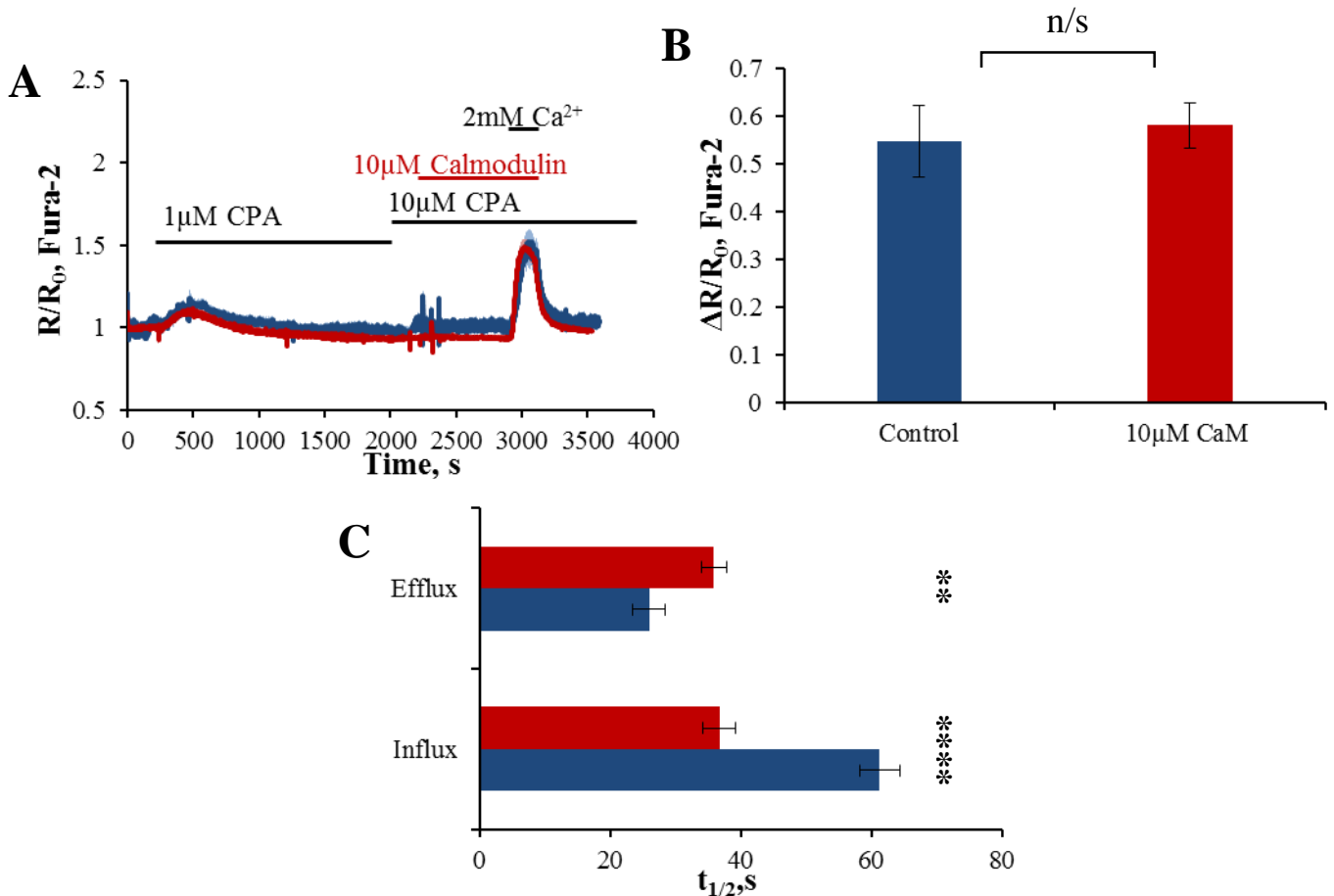
Figure 4.12 Calmodulin did not affect the amplitude of store-operated Ca²⁺ influx but significantly slowed the rate of store-operated Ca²⁺ influx and Ca²⁺ efflux in AR42J cells
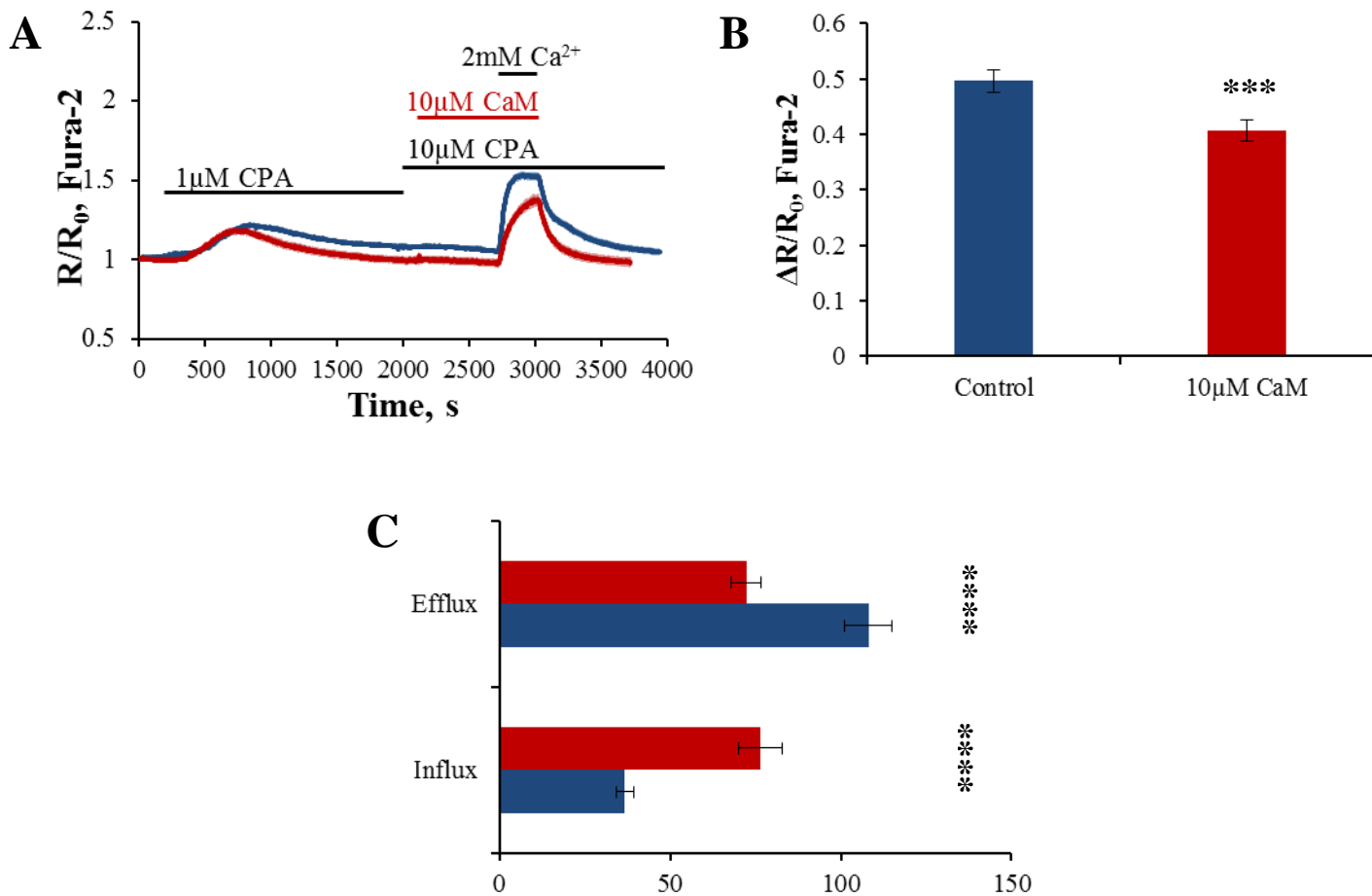
Average traces (±SEM) from Fura-2 loaded AR42J cells

A- ER stores were depleted according to the protocol in section 2.5.4 and then cells were pre-incubated with 10 µM calmodulin for ten minutes before 2 mM Ca^{2+} was subsequently re-introduced to the extracellular solution. Blue trace represents control cells (n = 10). Red trace represents 10 µM calmodulin (n = 13). **B-** Summary of the changes in the ratio amplitude due to Ca^{2+} influx (from cells in figure **A**) control (blue bar) and calmodulin treated (red bar) (p = 0.7027). **C-** Summary of the changes in the half time of Ca^{2+} influx (bottom bars) control – blue, calmodulin treated – red (p = 0.0001). Half time of Ca^{2+} efflux (upper bars) control – blue, calmodulin treated – red (p = 0.0026).

143

The change in ratio amplitude due to Ca^{2+} influx, summarised in figure 4.12 B, was not statistically significant. The time taken to reach half maximal Ca^{2+} influx was significantly faster in calmodulin pre-treated cells as was the time taken to reach half maximal Ca^{2+} efflux (figure 4.12 C). This data is surprising, as unless differentiated AR42J cells have not been reported to be secretory, these AR42J cells are not differentiated. This data suggests that this effect of calmodulin, by whatever mechanism, is non-specific.

Hypothetically, if the proteases released by acinar cells are inhibited, then calmodulin would not be cleaved and no smaller peptide fragments would be formed. Soybean trypsin inhibitor was used to inhibit trypsin in the extracellular solution and prevent its proteolytic action on calmodulin. Figure 4.13 A demonstrates the effect of pre-incubating cells with 0.01% trypsin inhibitor during the second step of store-depletion with 10 µM CPA (according to the protocol in section 2.5.5), both control cells and cells subsequently incubated with calmodulin were treated with trypsin inhibitor. After 400 seconds 10 µM calmodulin was introduced to the extracellular solution and pre-incubated with cells for ten minutes before the re-introduction of 2 mM Ca^{2+} to the extracellular solution. In control cells, in the presence of trypsin inhibitor but absence of calmodulin, after the re-introduction of Ca^{2+} to the extracellular solution there was an increase in cytosolic Ca^{2+} due to Ca^{2+} influx. This Ca^{2+} influx event was qualitatively no different in dynamics to Ca^{2+} influx in the absence of trypsin inhibitor, as seen in preceding experiments. In cells pre-incubated with calmodulin Ca^{2+} influx was significantly inhibited compared to control cells (63.5 ± 4.8 %, figure 4.13 B). Pre-incubation of cells with calmodulin in the presence of trypsin inhibitor significantly prolonged the time taken to reach half maximal Ca^{2+} influx (46.8 ± 7.6 %), whereas the time taken to reach half maximal Ca^{2+} efflux was not significantly affected by the calmodulin pre-incubation (decreased by 1.3 ± 5 %, figure 4.13 C). Evidently, inhibition of trypsin did not prevent cleavage of calmodulin, however there are other minor proteases that remain uninhibited.
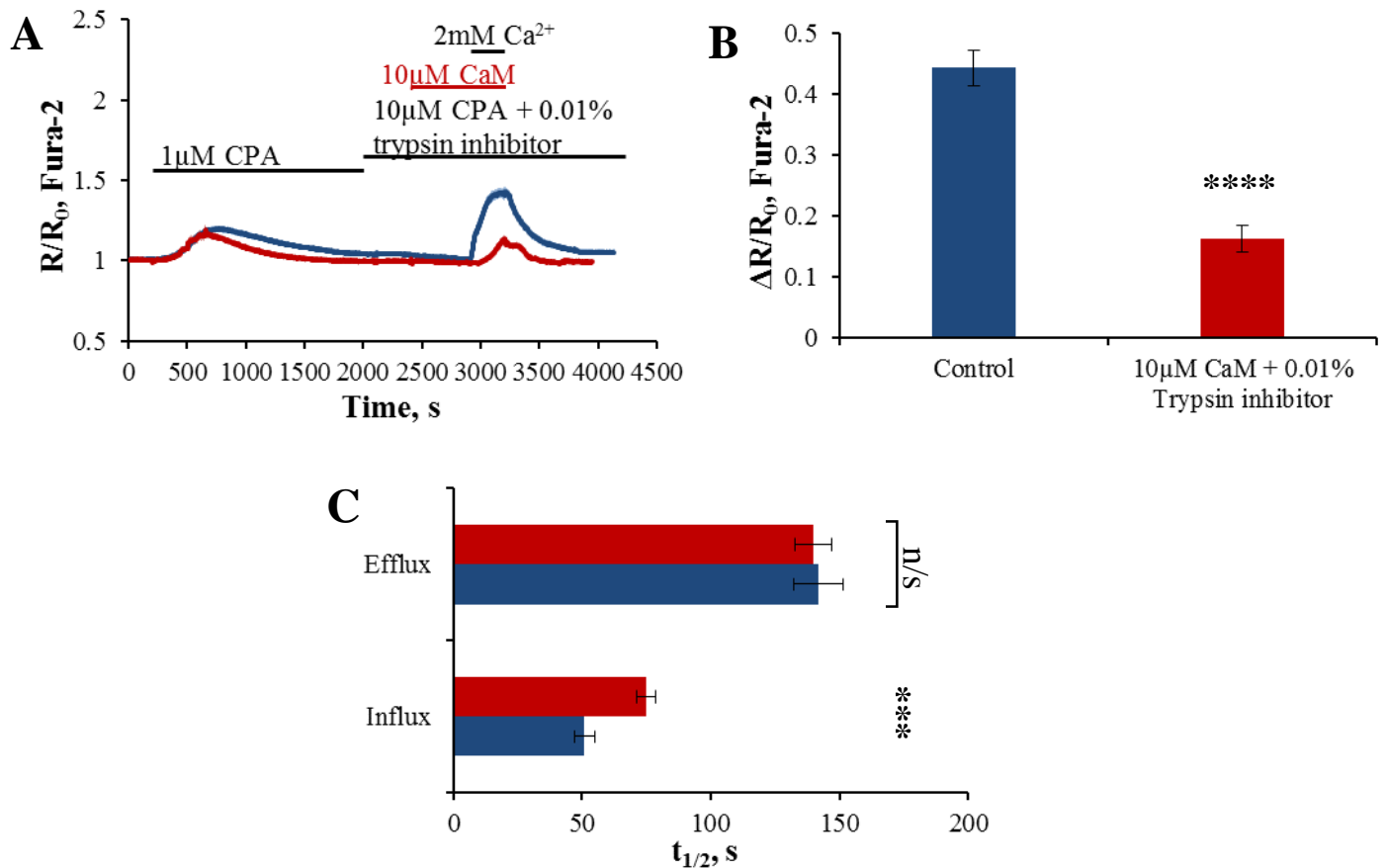
**Figure 4.13 Pre-incubation with trypsin inhibitor and full length Calmodulin significantly inhibited Ca^{2+} entry**

Average traces (±SEM) from Fura-2 loaded pancreatic acinar cells

A- ER stores were depleted according to the protocol in section 2.5.5, 0.01% trypsin inhibitor was added to the extracellular solution during the second step of store depletion in both conditions. After 400 seconds 10 μM calmodulin was introduced to the extracellular solution and pre-incubated with cells for 10 minutes before the re-introduction of 2 mM Ca^{2+} to the extracellular solution, blue trace – control (n = 37) and red trace – 10 μM calmodulin (n = 17). **B-** Summary of the changes in ratio amplitude due to Ca^{2+} influx (from cells in Figure **A**) in control (blue bar) and calmodulin treated (red bar p = 0.0001), both in the presence of 0.01% trypsin inhibitor. **C-** Summary of the changes in half time of Ca^{2+} influx (lower bars p = 0.0002) control – blue, calmodulin treated – red. Half time of Ca^{2+} efflux (upper bars p = 0.0968) control – blue, calmodulin treated – red.

Chymotrypsin in another protease that is synthesised and stored by the pancreatic acinar cells, this is also likely to be released and activated after cellular necrosis. Chymostatin is a chymotrypsin inhibitor and was used in a similar protocol to figure 4.13 A to inhibit chymotrypsin in the extracellular medium, thus preventing its proteolytic action on calmodulin. In figure 4. 4 A control cells and cells incubated with calmodulin were all pre-incubated in the presence of chymostatin, according to the protocol in section 2.5.5. After 400 seconds 10 μM calmodulin was introduced to the extracellular solution and pre-incubated with cells for ten minutes before the re-introduction of 2 mM Ca^{2+} to the extracellular solution. The amplitude of Ca^{2+} influx was not significantly different in cells pre-incubated with calmodulin compared with the amplitude of Ca^{2+}influx in control cells (increased by 17.5 ± 18.6 %, figure 4.14 B). However, the time taken to reach half maximal Ca^{2+} influx in cells pre-incubated with calmodulin was significantly less than the time taken to reach half maximal Ca^{2+} influx in control cells (30.2 ± 4.3 %) The time taken to reach half maximal Ca^{2+} efflux in cells pre-incubated with 10 μM calmodulin was significantly prolonged compared with the time taken to reach half-maximal Ca^{2+} efflux in control cells (41.9 ± 15.2 %, figure 4.14 C).

Although trypsin and chymotrypsin are the major proteases synthesised and stored in the pancreatic acinar cells, to a lesser extent acinar cells also synthesise and secrete other types of proteases. In order to inhibit as many proteases as possible, a protease inhibitor cocktail solution was applied to cells in the extracellular solution in both control and calmodulin treatment, according to the protocol in section 2.5.5, in figure 4.15 A. After 400 seconds 10 μM calmodulin was introduced to the extracellular solution and incubated with cells for 10 minutes before the re-addition of 2 mM Ca^{2+} to the extracellular solution. Cells pre-incubated with 10 μM calmodulin in the presence of the protease inhibitor cocktail exhibited a significantly larger amplitude in Ca^{2+} influx compared to cells in the presence of the protease inhibitor cocktail alone (61.6 ± 6.2 %, figure 4.15 B). The time taken to reach half maximal Ca^{2+} influx was unaffected by pre-incubation with calmodulin compared with control cells (increased by 8.6 ± 7.6%). The time taken to reach half maximal Ca^{2+} efflux was significantly prolonged in cells pre-incubated with calmodulin, compared with control cells (45.1 ± 10.4 %, figure 4.15 C).

146
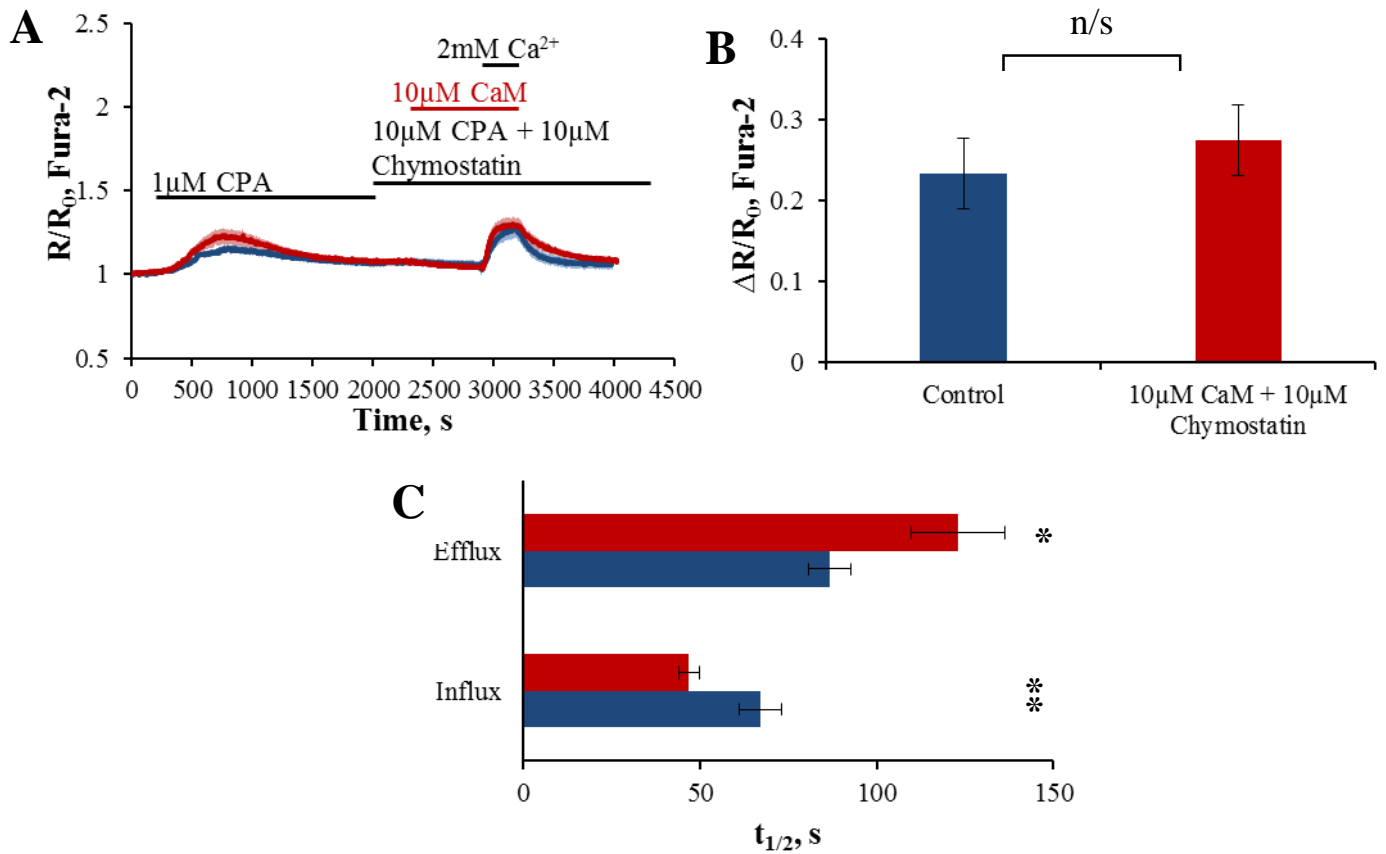
Figure 4.14 Pre-incubation with the chymotrypsin inhibitor, chymostatin and full length Calmodulin had no significant effect on Ca²⁺ entry

Average traces (±SEM) from Fura-2 loaded pancreatic acinar cells

A- ER stores were depleted according to the protocol in section 2.5.5, 10 μM chymostatin was added to the extracellular solution during the second step of store depletion in both conditions. After 400 seconds 10 μM Calmodulin was introduced to the extracellular solution and pre-incubated with cells for 10 minutes before the re-introduction of 2 mM Ca^{2+} to the extracellular solution, blue trace – control (n = 12) and red trace – 10 μM Calmodulin (n = 8). **B-** Summary of the changes in ratio amplitude due to Ca^{2+} influx (from cells in Figure **A**) in control (blue bar) and calmodulin treated (red bar p = 0.3813), both in the presence of 10 μM chymostatin. **C-** Summary of the changes in half time of Ca^{2+} influx (bottom bars p = 0.0076) control – blue, calmodulin treated – red. Half time of Ca^{2+} efflux (upper bars p = 0.0159) control – blue, calmodulin treated – red.

147
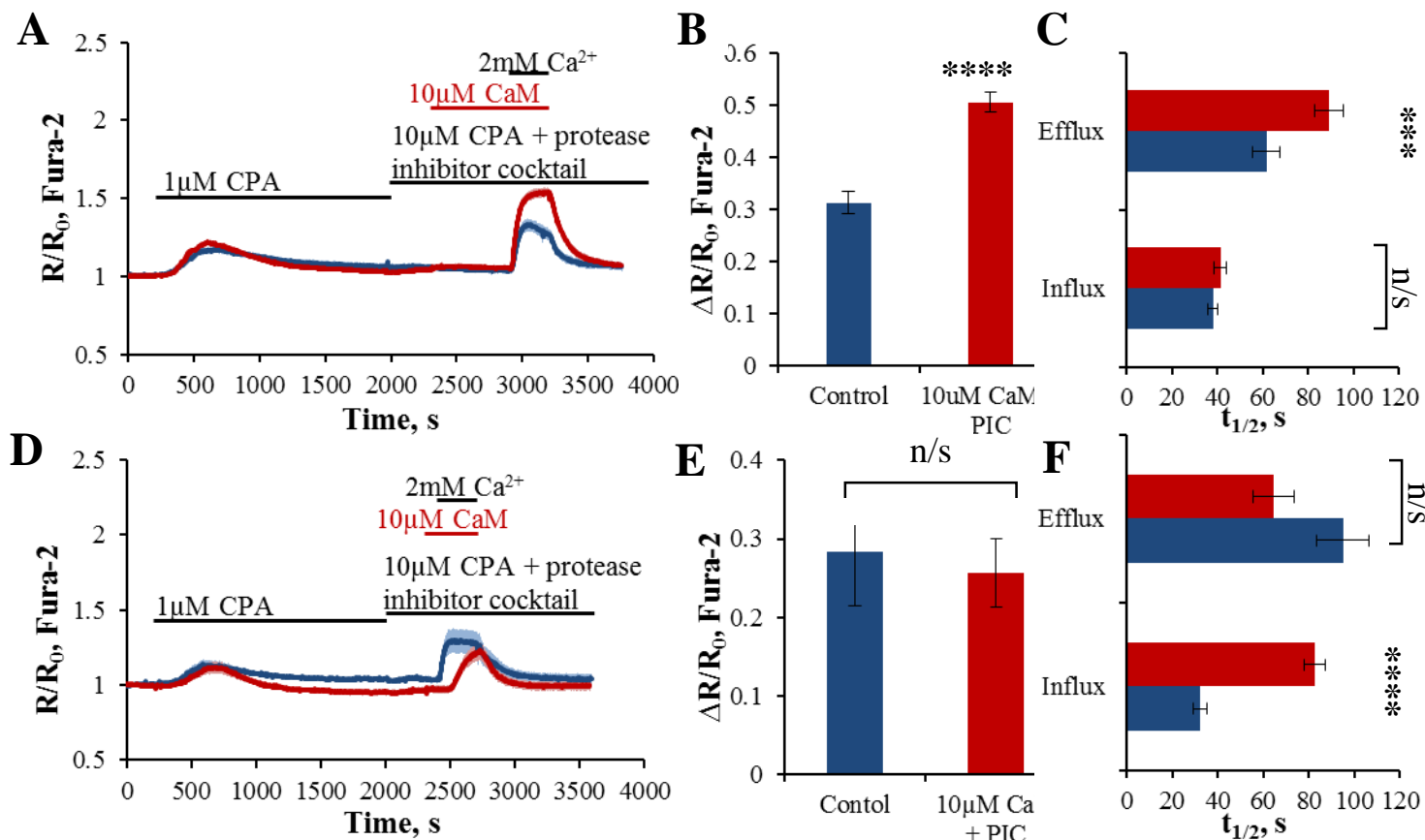
Figure 4.15 Pre-incubation with a protease inhibitor cocktail and full length Calmodulin significantly potentiated Ca^{2+} entry

Average traces (±SEM) from Fura-2 loaded pancreatic acinar cells

A- ER stores were depleted according to the protocol in section 2.5.5, protease cocktail inhibitor solution was added to the extracellular solution during the second step of store depletion in both conditions. After 400 seconds 10 µM calmodulin was introduced to the extracellular solution and pre-incubated with cells for 10 minutes before the re-introduction of 2 mM Ca^{2+} to the extracellular solution, blue trace – control (n = 25) and red trace – 10 µM Calmodulin (n = 24). **B-** Summary of the changes in ratio amplitude due to Ca^{2+} influx (from cells in figure **A**) in control (blue bar) and calmodulin treated (red bar p = 0.0001), both in the presence of the protease inhibitor cocktail. **C-** Summary of the changes in half time of Ca^{2+} influx (bottom bars p = 0.3822), control – blue, calmodulin treated. Half time of Ca^{2+} efflux (upper bars p = 0.0004). **D-** in a similar experiment to figure **A**, protease inhibitor cocktail solution was added to the extracellular solution during store depletion, after 400 seconds 10 µM calmodulin was introduced to the extracellular solution and incubated for a shorter time of 100 seconds before the re-introduction of 2 mM Ca^{2+} to the extracellular solution. **E-** Summary of the changes in ratio amplitude due to Ca^{2+}influx (from cells in figure **D**) in control cells (blue) and cells pre-incubated with calmodulin (red p = 0.7507). **F-** Summary of changes in half time of Ca^{2+} influx (lower bars p = 0.0001) control – blue, calmodulin treated – red. Half time of Ca^{2+} efflux (upper bars p = 0.0557).

Although it is unlikely that full length calmodulin was exerting an effect on intracellular Ca^{2+} signalling from the extracellular side of the plasma membrane, in an attempt to functionally determine if the action of calmodulin, in the presence of a protease inhibitor cocktail, on Ca^{2+} entry was due to an extracellular action or an intracellular action a short pre-incubation period with calmodulin was utilised in figure 4.15 D. Cells were pre-incubated with calmodulin for 100 seconds before the re-introduction of 2 mM Ca^{2+} to the extracellular solution, this shorter duration of pre-incubation with calmodulin was insufficient to potentiate Ca^{2+} entry as it had in figure 4.15 A, there was no significant difference in the amplitude of Ca^{2+} entry in calmodulin pre-incubated cells compared with control cells (decreased by 9.4 ± 15.5 %, figure 4.15 E). However, in spite of the lack of effect of calmodulin pre-incubation on the amplitude of Ca^{2+} influx, the time taken to reach half maximal Ca^{2+} influx in cells pre-incubated with calmodulin was significantly prolonged compared to Ca^{2+} influx in control cells (155.4 ± 14.3 %,). The time taken to reach half maximal Ca^{2+} efflux was not significantly affected by the pre-incubation with calmodulin (decreased by 32.0 ± 9.5 %, p = 0.0557). Figure 4.15 F summarises the changes in Ca^{2+} influx and Ca^{2+} efflux. The differences in dynamics of Ca^{2+} influx in calmodulin treated cells from figure 4.15 A and 4.15 D could be due to the difference in time cells were incubated with calmodulin for and in theory the cleavage peptides. It could have been due to the difference in the incubation time of the protein with proteases in the extracellular medium, 100 seconds may have been insufficient time for substantial protein cleavage.

In addition to trypsin and chymotrypsin and other proteases, metalloproteases are also found in the pancreas, although it is not entirely clear if they are of acinar cell origin. Neutrophils also express matrix metalloproteases and have been implicated in activating trypsinogen in acute pancreatitis (379). Metalloproteases are not inhibited by the protease inhibitor cocktail used in figure 4.15. EDTA has been used extensively as a broad spectrum metalloprotease inhibitor. In figure 4.16 A EDTA was introduced to the extracellular solution during the second step of store depletion with 10 μM CPA, in both conditions. In cells pre-incubated with 10 μM calmodulin, EDTA and calmodulin were introduced to the extracellular solution simultaneously. In cells pre-incubated with calmodulin, calmodulin was applied to cells and incubated for ten minutes before the re-introduction of 2 mM Ca^{2+} to the extracellular solution, significantly reducing the amplitude of Ca^{2+} influx compared to control cells (46.0 ± 12.4 %, figure 4.16 B). The time taken to reach half maximal Ca^{2+} influx in cells pre-incubated with calmodulin was not statistically different (+65.3 ± 30.2 %). The time taken to

reach half maximal Ca^{2+} efflux was significantly prolonged in cells pre-incubated with calmodulin compared with control cells (52.4 ± 20.0 %, figure 4.16 C).

In figure 4.17 A combined protease inhibition approach was undertaken, both a protease inhibitor cocktail solution and 0.01% trypsin inhibitor were introduced to the extracellular solution during the second stage of store depletion with 10 μM CPA. After 400 seconds 10 μM calmodulin was introduced to the extracellular solution and incubated with cells for ten minutes before the re-introduction of 2 mM Ca^{2+} to the extracellular solution. The pre-incubation with calmodulin in the presence of the protease inhibitor cocktail and trypsin inhibitor resulted in a significant reduction in the amplitude in Ca^{2+} entry compared with control cells (71.8 ± 56 %, figure 4.17 B). The time taken to reach half maximal Ca^{2+} influx was significantly shorter in cells pre-incubated with calmodulin than in control cells (43.3 ± 10.8 %) and the time taken to reach half maximal Ca^{2+} efflux was also significantly shorter in cells pre-incubated with calmodulin compared with control cells (37.2 ± 4.0 %, figure 4.17 C).

Figure 4.16 Pre-incubation with a metalloprotease inhibitor, EDTA, and full length Calmodulin significantly inhibited Ca^{2+} entry

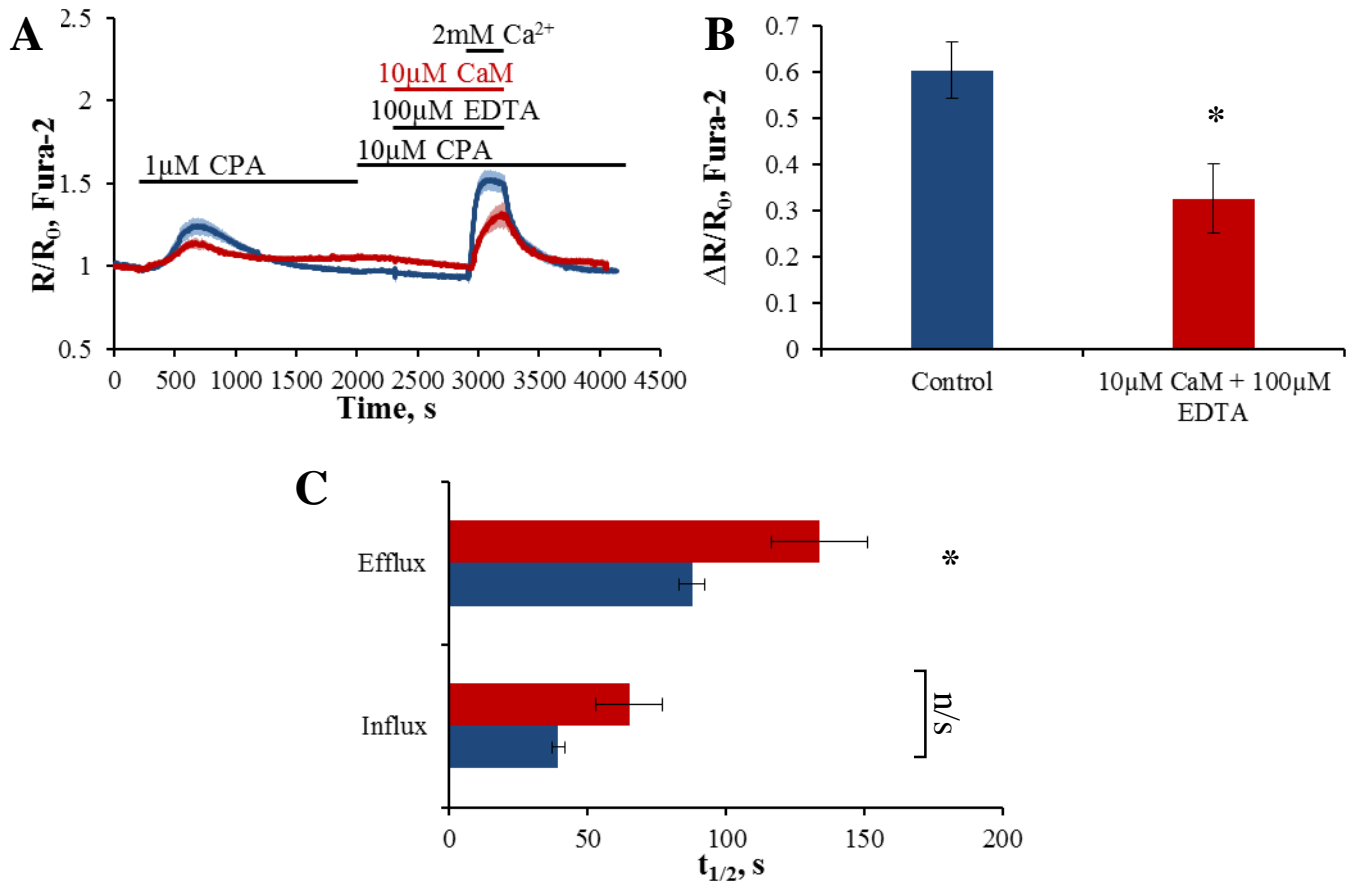Average traces (±SEM) from Fura-2 loaded pancreatic acinar cells

A- ER stores were depleted according to the protocol in section 2.5.5, EDTA was added to the extracellular solution during the second step of store depletion. In cells pre-incubated with 10 μM calmodulin, EDTA was added to the extracellular solution simultaneously with calmodulin. Cells were pre-incubated with calmodulin for ten minutes before the re-introduction of 2 mM Ca^{2+} to the extracellular solution, blue trace – control (n = 6) and red trace – 10 μM Calmodulin (n = 4). **B-** Summary of the changes in ratio amplitude due to Ca^{2+} influx(in cells from Figure **A**) in control (blue bar) and calmodulin treated (red bar p = 0.0381), both in the presence of EDTA. **C-** Summary of the changes in half time of Ca^{2+} influx (bottom bars, 0.2571) control – blue, calmodulin treated – red. Half time of Ca^{2+} efflux (upper bars p = 0.019) control – blue, calmodulin treated - red.
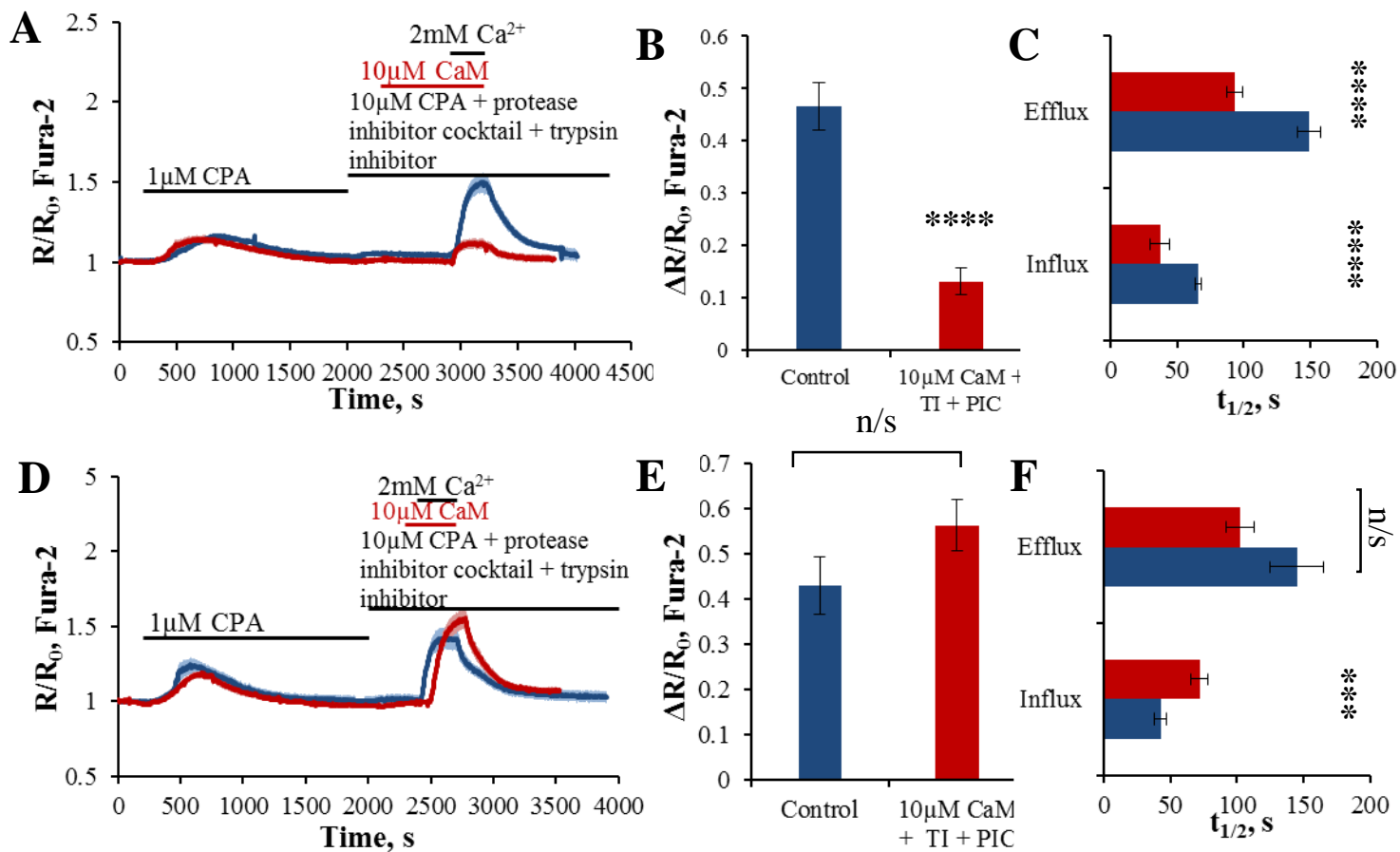
Figure 4.17 Contrasting effects of short and long pre-incubation with full-length calmodulin in the presence of with a protease inhibitor cocktail and trypsin inhibitor

Average traces (±SEM) from Fura-2 loaded pancreatic acinar cells

A- ER stores were depleted according to the protocol in section 2.5.5, a protease inhibitor cocktail and 0.01 % trypsin inhibitor were added to the extracellular solution during the second step of store depletion. After 400 seconds 10 μM calmodulin was introduced to the extracellular solution and pre-incubated with cells for 10 minutes before the re-introduction of 2 mM Ca^{2+} to the extracellular solution, blue trace – control (n = 27) and red trace – 10 μM calmodulin (n = 15). **B-** Summary of the changes in ratio amplitude due to Ca^{2+} influx (from cells in Figure **A**) in control (blue bar) and calmodulin treated (red bar p = 0.0001), both in the presence of a protease inhibitor cocktail and trypsin inhibitor. **C-** Summary of the changes in half time of Ca^{2+} influx (lower bars, p = 0.0001) control – blue, calmodulin treated – red. Half time of Ca^{2+} efflux (upper bars p = 0.0001). **D –** Similar experiment to figure **A,** a protease inhibitor cocktail and 0.01% trypsin inhibitor were added to the extracellular solution, and after 400 seconds 10 μM calmodulin was introduced to the extracellular solution and incubated with cells for 100 seconds before the re-introduction of 2 mM Ca^{2+} to the extracellular solution, blue trace – control (12) and red trace – 10 μM calmodulin (n = 12). **E-** Summary of the changes in ratio amplitude due to Ca^{2+} influx (from cells in Figure **D**) in control (blue) and calmodulin treated (red p = 0.1304). **F-** Summary of the changes in half time of Ca^{2+} influx (lower bars p = 0.001).) control – blue, calmodulin treated – red. Half time of Ca^{2+} efflux (upper bars p = 0.0756).

In a similar experiment to figure 4.17 D, a short pre-incubation of calmodulin with cells in the presence of the protease inhibitor cocktail solution and trypsin inhibitor was undertaken in figure 4.17 D. The amplitude of Ca^{2+} influx in cells pre-incubated with calmodulin was not significantly different to the amplitude of Ca^{2+} influx in control cells (increased by 30.9 ± 13.2 %, figure 4.17 E), which contrasted with the reduction in amplitude of Ca^{2+} influx in cells pre-incubated with calmodulin over a longer time course (figure 4.17 A). The time taken to reach half maximal Ca^{2+} influx was significantly prolonged in cells pre-incubated with calmodulin, compared with control cells (69.2 ± 14.8 %). However, there was no statistical difference in the time taken to reach half maximal Ca^{2+} efflux in cells pre-incubated with calmodulin compared with control cells (29.2 ± 7.2 %, figure 4.17 F).

Figure 4.17 demonstrates the effect of inhibiting proteases and trypsin on calmodulin induced inhibition of Ca^{2+} entry, however in this protocol neither chymotrypsin nor metalloproteases were inhibited. Figure 4.18 A demonstrates the effect of pre-incubating cells with 100 μM EDTA, a protease inhibitor cocktail and 0.01 % trypsin inhibitor during the second stage of the store-depletion protocol. Cells were then incubated with 10 μM calmodulin, in the maintained presence of inhibitors for ten minutes before the re-introduction of 2 mM Ca^{2+} to the extracellular solution. The change in ratio amplitude due to Ca^{2+} influx in cells pre-incubated with calmodulin was not significantly different to the amplitude of Ca^{2+} influx in control cells (increased by 25.6 ± 32.9 %, figure 4.18 B). The time taken to reach half maximal Ca^{2+} influx was significantly prolonged in cells pre-incubated with calmodulin compared with control cells (74.3 ± 16.7 %) and the time taken to reach half maximal Ca^{2+} efflux was significantly shortened in cells pre-incubated with calmodulin compared with control cells (40.0 ± 4.1 %, figure 4.18 C). From figure 4.11 A to figure 4.18 A calmodulin was introduced to the imaging chamber by hand addition rather than continuous perfusion of the solution over cells in the imaging chamber, which how experiments are typically performed.

Figure 4.18 Combined inhibition of trypsin, metalloproteases and generic proteases and the effect on calmodulin mediated inhibition on Ca²⁺ entry.

Average traces (±SEM) from Fura-2 loaded pancreatic acinar cells

A- ER stores were depleted according to the protocol in section 2.55, a protease inhibitor cocktail, 0.01 % trypsin inhibitor and 100 μM EDTA were added to the extracellular solution during the second step of store depletion. After 400 seconds 10 μM Calmodulin was introduced to the extracellular solution and pre-incubated with cells for 10 minutes before the re-introduction of 2 mM Ca²⁺ to the extracellular solution, blue trace – control (n = 9) and red trace – 10 μM Calmodulin (n = 7). **B-** Summary of the changes the in ratio amplitude due to Ca²⁺ influx (from cells in Figure **A**) in control (blue bar) and calmodulin treated (red bar p= 0.8217), both in the presence of a protease inhibitor cocktail, trypsin inhibitor and EDTA. **C-** Summary of the changes in half time of Ca²⁺ influx (lower bars p = 0.0007) control – blue, calmodulin treated- red. Half time of Ca²⁺ efflux (upper bars p = 0.0005). **D-**Identical to experiment in **A** except that Calmodulin was introduced to the extracellular solution, by perfusion rather than hand addition, and then pre-incubated with cells for 10 minutes before the re-introduction of 2 mM Ca²⁺ to the extracellular solution, blue trace – control (n = 5) and red trace – 10 μM Calmodulin (n = 4). **E-** Summary of the changes in ratio amplitude due to Ca²⁺ influx (from cells in Figure **D**) in control (blue bar) and calmodulin treated (red bar 0.0635), both in the presence of a protease inhibitor cocktail, trypsin inhibitor and EDTA. **F-** Summary of the changes in half time of Ca²⁺ influx (lower bars p = 0.999), control – blue, calmodulin treated – red, Half time of Ca²⁺ efflux (upper bars p = 0.2857).

Figure 4.18 D utilised the same combination of inhibitors as figure 4.18 A, EDTA, a protease inhibitor cocktail solution and trypsin inhibitor and the incubation with these inhibitors was for the same duration. 10 µM calmodulin was introduced to the extracellular solution by perfusion rather than hand addition, cells were again incubated for ten minutes before the re-introduction of 2 mM Ca^{2+} to the extracellular solution. There was not a statistically significant difference in the amplitude of Ca^{2+} entry in cells pre-incubated with calmodulin compared with control cells (decreased by 36.9 ± 14.6 %, figure 4.18 E). The time taken to reach half maximal Ca^{2+} influx was not significantly different in cells pre-incubated with calmodulin compared with control cells (increased by 1.4 ± 11.9 %, p = 0.999) and the time taken to reach half maximal Ca^{2+} efflux was not significantly different in cells pre-incubated with calmodulin compared with control cells (decreased by 19.3 ± 4.3 %, figure 4.18 F).

In the experiments in figure 4.18 A and D chymotrypsin was not inhibited and therefore was able to cleave calmodulin and potentially give rise to peptide fragments that could modulate Ca^{2+} influx. In figure 4.19 A the protease inhibitor cocktail was removed in attempt to determine the minimum inhibitor requirements to prevent the calmodulin-mediated inhibition of Ca^{2+} entry, and was replaced with chymostatin. Chymostatin, trypsin inhibitor and EDTA were all introduced to the extracellular solution and incubated with cells before the introduction of calmodulin to the extracellular solution, by perfusion. Cells were incubated with calmodulin and the inhibitors for ten minutes before the re-introduction of 2 mM Ca^2 to the extracellular solution. The amplitude of Ca^{2+} entry in cells pre-incubated with calmodulin was not significantly different to control cells (increased by 34.0 ± 9.7 %, figure 4.19 B). The time taken to reach half maximal Ca^{2+} influx in cells pre-incubated with calmodulin was significantly prolonged compared with control cells (20.2 ± 2.4 %) and the time taken to reach half maximal Ca^{2+} efflux was not statistically significant (14.0 ± 1.4 %, figure 4.19 C).
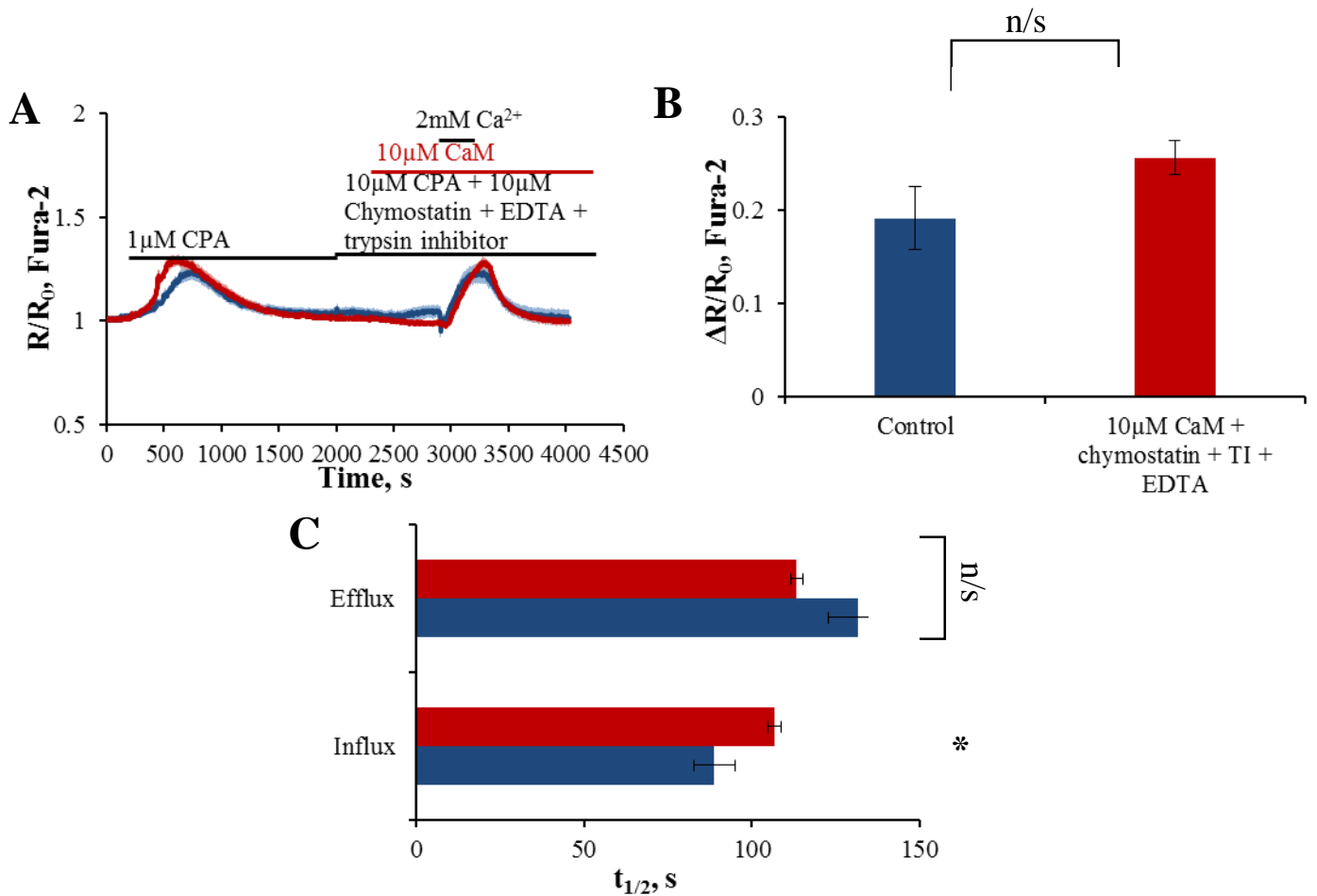
Figure 4.19 Combined inhibition of trypsin, metalloproteases and chymotrypsin prevents the calmodulin-mediated inhibition on Ca^{2+} entry.
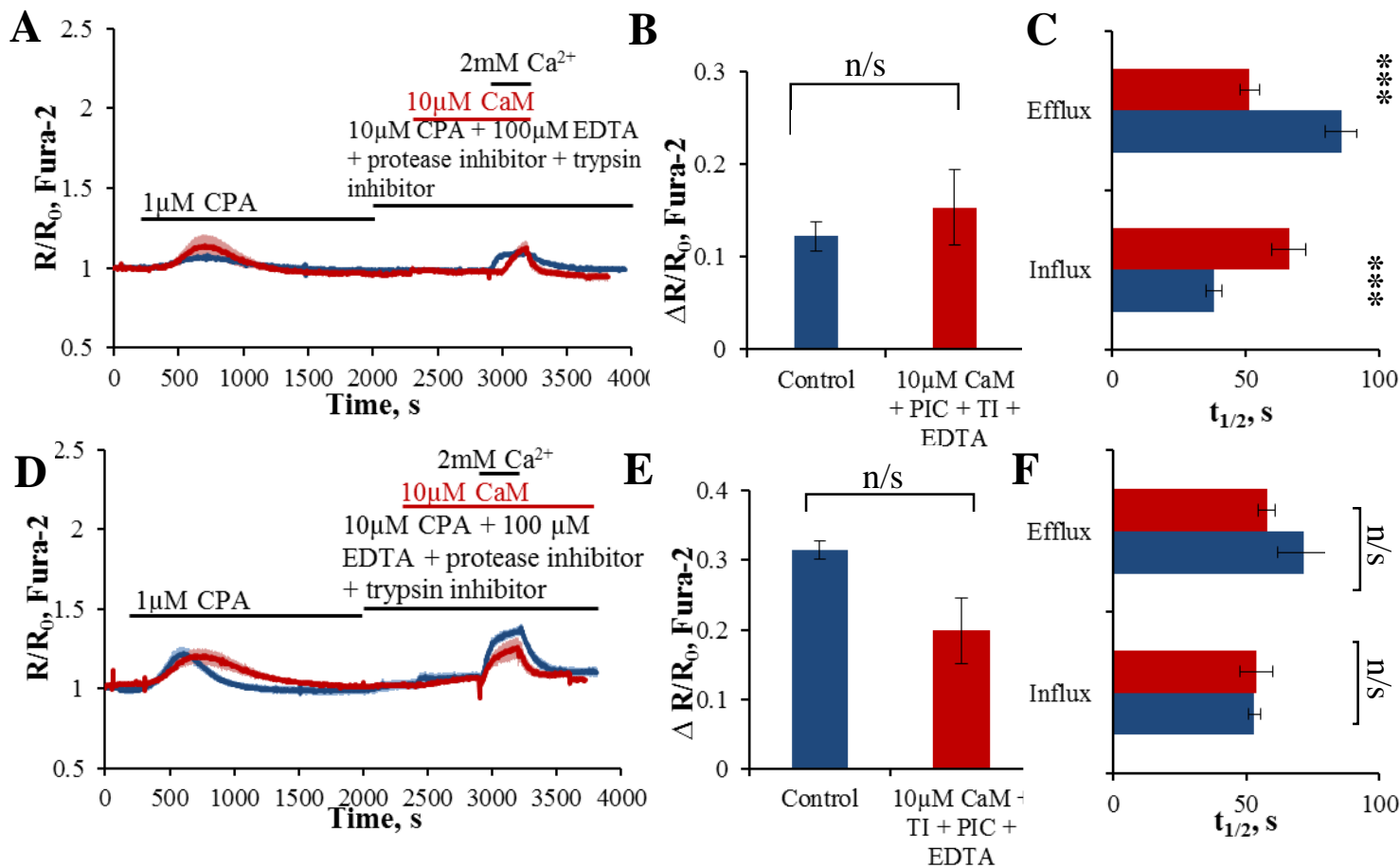
Average traces (±SEM) from Fura-2 loaded pancreatic acinar cells

A- ER stores were depleted according to the protocol in section 2.5.5, 10 µM Chymostatin, 0.01 % trypsin inhibitor and 100 µM EDTA were added to the extracellular solution during the second step of store depletion. After 400 seconds 10 µM calmodulin was introduced to the extracellular solution, by perfusion rather than hand addition, and pre-incubated with cells for 10 minutes before the re-introduction of 2 mM Ca^{2+} to the extracellular solution, blue trace – control (n = 8) and red trace – 10 µM Calmodulin (n = 4). **B-** Summary of the changes in ratio amplitude due to Ca^{2+} influx (from cells in Figure **A**) in control (blue bar) and calmodulin treated (red bar p = 0.3677), both in the presence of chymostatin, trypsin inhibitor and EDTA. **C-** Summary of the changes in half time of Ca^{2+} influx (lower bars p = 0.0485) control – blue, calmodulin treated – red. Half time of Ca^{2+} efflux (upper bars p = 0.2646) control - blue, calmodulin treated – red.

In figure 4.20 A the trypsin inhibitor was removed from the inhibitor solution, chymostatin and EDTA were utilised to inhibit chymotrypsin and metalloproteases. 10 μM chymostatin and 100 μM EDTA were introduced to the extracellular solution during the second stage of store depletion and were incubated with cells before calmodulin was introduced to the extracellular solution by perfusion. Cells were incubated with calmodulin in the continuous presence of the inhibitors for ten minutes before the re-introduction of 2 mM Ca^{2+} to the extracellular solution. The amplitude of Ca^{2+} influx in cells pre-incubated with calmodulin was not significantly different to the amplitude of Ca^{2+} influx in control cells (increased by 15.3 ± 21.7 %, figure 4.20 B). The time taken to reach half maximal Ca^{2+} influx was significantly prolonged in cells pre-incubated with calmodulin compared with control cells (26.3 ± 4.9 %, $p = 0.0122$) and the time taken to reach half maximal efflux in cells pre-incubated with calmodulin was significantly shorter compared with control cells ($35.9 \pm 6.5\%$, figure 4.20 C).

Some initial pilot experiments with small peptide fragments are shown in figure 2 and 3, in the appendix of the thesis. They demonstrate some preliminary data utilising fragments of calmodulin predicted by the protease cleavage computer models detailed in section 4.3.2. One peptide, designated CaM-A, resulted in a significant reduction in the amplitude of Ca^{2+} influx ($p = 0.0054$) but did not affect the rate of Ca^{2+} influx or efflux. The second peptide, designated CaM-B, did not significantly alter the amplitude or the half time of Ca^{2+} influx or efflux.
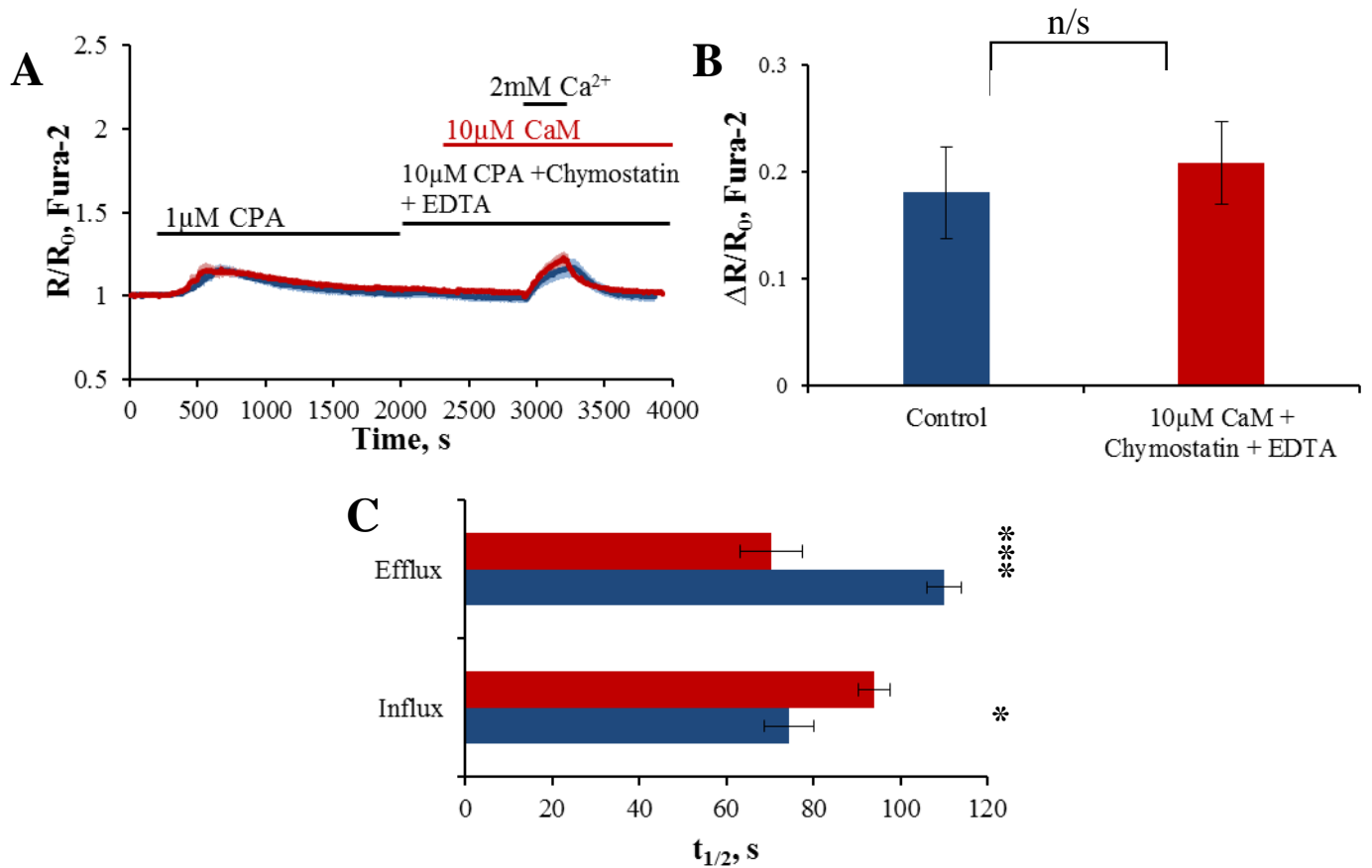
Figure 4.20 Combined inhibition of chymotrypsin and metalloproteases relieved the calmodulin-mediated inhibition on Ca^{2+} entry.

Average traces (±SEM) from Fura-2 loaded pancreatic acinar cells

A- ER stores were depleted according to the protocol in section 2.5.5, 10 µM Chymostatin and 100 µM EDTA were added to the extracellular solution during the second step of store. After 400 seconds 10 µM calmodulin was introduced to the extracellular solution, by perfusion rather than hand addition, and pre-incubated with cells for 10 minutes before the re-introduction of 2 mM Ca^{2+} to the extracellular solution, blue trace – control (n = 6) and red trace – 10 µM calmodulin (n = 7). **B-** Summary of the changes in ratio amplitude due to Ca^{2+} influx (from cells in Figure **A**) in control (blue bar) and cells pre-incubated with 10 µM calmodulin (red bar p = 0.3566), both in the presence of a chymostatin and EDTA. **C-** Summary of the changes in half time of Ca^{2+} influx (lower bars p = 0.0122) control – blue, calmodulin treated – red. Half time of Ca^{2+} efflux (upper bars p = 0.0006) control – blue, calmodulin treated – red.

4.3 Discussion.

Since the undertaking of the experiments in this chapter a paper has been published detailing recent evidence that indicates, in an overexpression model of Orai1/STIM-1 and calmodulin, the Ca^{2+}-dependent inactivation of the CRAC channel is calmodulin independent (380). Utilising the Ca^{2+} insensitive mutant form of calmodulin, researchers could find no difference in the fast Ca^{2+}-dependent inactivation of the CRAC channel current compared with cells expressing WT calmodulin. This contradicts previous evidence, not only from this research group utilising Orai1 mutants that were no longer able to bind calmodulin (159), but also evidence from other research groups, utilising the Ca^{2+} insensitive form of calmodulin, that demonstrated a small but significant reduction in the fast inactivation in cells expressing the mutant protein (177,366). A possible explanation for this apparent discrepancy is that the recent study was undertaken in overexpression systems of Orai1, STIM1 and Ca^{2+} insensitive calmodulin (380), whereas the other two studies were undertaken utilising RBL-1 cells and an immortalised liver cell line both of which express endogenous CRAC channels as opposed to overexpressed channels (177,366) and then overexpressing the Ca^{2+} insensitive mutant calmodulin. It could be that the overexpressed Orai1/STIM1 CRAC channel is gated somewhat differently and does not interact with overexpressed calmodulin in quite the same manner as the endogenous form of the channel does.

Although the CaM binding domain may (159,160,177) or may not (380) be necessary for Ca^{2+}-dependent inactivation of the CRAC channel; the inactivation domain of STIM1 is necessary(381). It is interesting to note that calmodulin has also been found to bind to the cytoplasmic domain of STIM2 (372). In the first instance a putative calmodulin binding domain was identified on the C-terminal domain of STIM1 (371) which was further supported by biochemical evidence of calmodulin binding to both STIM1 and STIM2 (176). There is evidence that cytosolic Ca^{2+} as well as ER luminal Ca^{2+} concentrations have a role in store operated Ca^{2+} entry via CRAC channels. A study found that Ca^{2+} bound-calmodulin had an inhibitory role in SOCE when it bound STIM1, but apo-calmodulin lacked such an effect. This was repeatable for STIM2 expressing cells (176,382).

4.3.1 CALP3

It was shown that the CALP peptides CALP1, designed to have inverse hydropathy for an ancestral Ca^{2+} binding site, CALP2 and CALP3, designed to have inverse hydropathy to the EF hand 4 of calmodulin, have a complementary surface to Ca^{2+} binding sites and can bind the calmodulin EF hand. CALP1 induced conformational changes and activated calmodulin

159

resulting in subsequent phosphodiesterase activation and cGMP hydrolysis (361), although it cannot be assumed that due to structural similarity that CALP3 will induce the same changes. Based on the hypothesis that Ca^{2+} bound-calmodulin can bind to STIM1 and act as the molecular switch for STIM1/Orai1 disassembly thus resulting in a cessation of Ca^{2+} influx, then it is plausible that CALP3 bound-calmodulin could also bind to STIM1 in the same way (176). This hypothesis would then provide an explanation for why the incubation of cells with CALP3 results in a decrease in cytosolic Ca^{2+} due to a reduction in SOCE, which is true for ten minute pre-incubation with CALP3 (figure 4.6 A & B), a much shorter pre-incubation with CALP3 (figure 4.7 A) and acute application of CALP3 (figure 4.7 E). CALP3/Calmodulin can bind to STIM1 and provide the molecular switch for disassemble of STIM1/Orai1. This hypothesis is yet to be tested.

In the paper where CALP3 was shown to be a protective agent for pancreatic acinar cells it was effective at 100 µM (359). However, whether due to experimental difficulty or not, 100 µM was ineffective at inhibiting Ca^{2+} influx only 200 µM demonstrated a significant inhibitory effect. It is highly possible that this is a non-specific effect of a supramaximal concentration of CALP3.

4.3.2   Calmodulin inhibitors and mutant calmodulin

Both calmidazolium and W-7 were found to potentiate SOCE, initiated by thapsigargin in pulmonary artery smooth muscle cells (368) and furthermore in HEK293 cells (369) and MDCK cells (352,353). Extracellular application of 10 µM calmidazolium, in smooth muscle cells with replete intracellular Ca^{2+} stores, elicited a significant elevation in cytosolic Ca^{2+} levels in the presence of extracellular Ca^{2+}. In the absence of extracellular Ca^{2+} calmidazolium did not elicit a significant increase in cytosolic Ca^{2+}, suggesting the elevated Ca^{2+} was due to an influx pathway that was store independent and not due to Ca^{2+} release from intracellular stores (368,374). In a somewhat conflicting report it has been demonstrated that calmidazolium has no effect on the development or the amplitude of the store-operated Ca^{2+} current (I_{soc}) compared with control cells in liver cells in the presence of 10 mM Ca^{2+} in the extracellular solution (366), potentially indicating no role for calmodulin in the activation of the store-operated Ca^{2+} current. These findings were not true for the effect of calmidazolium on SOCE in pancreatic acinar cells when 10 mM Ca^{2+} was also added to the extracellular solution (figure 4.1 A & B). At least when measured using fluorescent calcium imaging the application of 10 µM calmidazolium significantly inhibited the amplitude of Ca^{2+} entry. Furthermore the rate of Ca^{2+} influx, which more accurately represents the number

of CRAC channels open than the amplitude, was significantly slower compared with control cells. The difference in amplitude of Ca^{2+} influx between treated and untreated cells was not as remarkable as when a CRAC channel inhibitor was used (see chapter 3) but the difference indicates that calmodulin inhibition is effective in reducing Ca^{2+} influx. This difference between calmidazolium treated cells and control cells was more remarkable when the driving force for Ca^{2+} was decreased towards more representative physiological concentrations of extracellular Ca^{2+} such as 2 mM (figure 4.2 A & B), then pre-incubation with 10 µM calmidazolium resulted in a further reduction in amplitude of Ca^{2+} entry in pancreatic acinar cells compared with control cells and compared with figure 4.1 A. An older study found that in hepatocytes calmidazolium treatment inhibited store operated Ca^{2+} influx (370), although this was not repeatable in a later study in a liver cell line (383). This could be due to the difference between primary hepatocytes and hepatocyte cell line, data from primary hepatocytes (370) is in line with data generated in this chapter in primary pancreatic acinar cells (figure 4.1 A, D and figure 4.2 A). Inhibition of Ca^{2+} influx by calmidazolium has also been demonstrated in cardiac myocytes (356) although this is likely by affecting calmodulin associated with voltage gated Ca^{2+} channels.

The plateau in elevated cytosolic Ca^{2+} levels that is attained during Ca^{2+} influx in this type of protocol is an equilibrium between Ca^{2+} influx mechanisms into the cytosol and Ca^{2+} extrusion mechanisms from the cytosol. At all points during the SOCE protocol either thapsigargin or CPA the SERCA pump inhibitors are present, removing active Ca^{2+} uptake into the ER as an extrusion mechanism; Ca^{2+} extrusion is almost entirely mediated by the PMCA. A plateau in cytosolic Ca^{2+} is attained at the point that Ca^{2+} influx through CRAC channels is equal to Ca^{2+} extrusion by PMCA, resulting in no net change in cytosolic Ca^{2+} levels (234). It is well established that the PMCA pump is regulated by calmodulin (341), thereby inhibiting calmodulin ought to have a dual effect on the plateau in cytosolic Ca^{2+} levels attained. So rather than a direct action of calmidazolium on the CRAC channel, from which position it is hypothesised to be protected from pharmacological target, it is possible that the effect of calmidazolium is mediated through the interaction of calmodulin with PMCA. Although, inhibition of calmodulin has been demonstrated to slow the rate of Ca^{2+} removal from the cytosol via PMCA previously (177).

W-7 was also observed to potentiate store-operated Ca^{2+} entry in pulmonary artery smooth muscle cells (368) and MDCK cells (353); although the concentration used in MDCK cells was five times higher than used in this study which is a possible explanation for the

contrasting effects observed in pancreatic acinar cells. The amplitude of Ca^{2+} influx was qualitatively inhibited in pancreatic acinar cells, compared with control cells (figure 4.3). However, as previously mentioned the rate of Ca^{2+} influx is a more accurate measure of the number of CRAC channels that are open than the steady-state amplitude measurement, as it is less of a dynamic equilibrium between Ca^{2+} influx and Ca^{2+} efflux pathways and largely driven by Ca^{2+} influx into the cytosol. The rate of Ca^{2+} influx in cells pre-incubated with W-7 is significantly inhibited compared with control cells, in a similar manner to cells pre-incubated with calmidazolium. There are known instances where pharmacological agents are known to have biphasic effects on CRAC channels, 2-APB is well established to potentiate CRAC channel activity at low concentrations whilst acting in an inhibitory manner when applied at higher concentrations (192,295), this could provide one explanation. Another is that, like calmidazolium, W-7 too activates a store-independent Ca^{2+} influx pathway. When applied to RBL-1 cells W-7 was found to inhibit CRAC channel currents, in whole cell patch clamp experiments. The current was activated by depleting ER stores using EGTA. This finding is similar to data in figure 4.3. Furthermore, W-7 was found to inhibit store-operated Ca^{2+} influx induced by thapsigargin in primary liver cells (370) and also in a liver cell line (383), which are more similar to primary pancreatic acinar cells than MDCK cells.

The Ca^{2+} insensitive mutant form of calmodulin has been employed to more accurately determine the role of calmodulin in CRAC channel activation and inactivation in previous studies as the data from pharmacological interventions, such as calmidazolium, were difficult to interpret at times (384). RBL-1 cells expressing the mutant form of calmodulin exhibited a reduced amplitude and rate of store-operated Ca^{2+} entry compared with cells that were not transfected with the mutant protein, however the rate of Ca^{2+} efflux remained unaffected (384). For the most part, this is in line with data in this chapter (figure 4.4) in which there is a reduction in amplitude of a Ca^{2+} transient in cells expressing the Ca^{2+} insensitive mutant form of calmodulin, compared with cells expressing the WT form of calmodulin. The data from the overexpression of mutant calmodulin is similar to data obtained with calmidazolium and W-7, that is by inhibiting calmodulin there was a resultant reduction in cytosolic Ca^{2+} (figure 4.2, 4.3 and 4.4). Findings surrounding the effect of calmodulin inhibition on rate of efflux is somewhat different in this chapter compared with previous studies, in that rate of Ca^{2+} extrusion from the cytosol was prolonged in cells treated with calmidazolium (figure 4.1 C and figure 4.2 C), which is similar to findings in RBL-1 cells treated with calmidazolium (177), whereas it was unaffected in RBL1 cells expressing the mutant calmodulin. One

possibility for this is that the duration of expression of the mutant calmodulin was insufficient to turn-over all calmodulin in the cell (384).

The calmodulin pharmacological data in pancreatic acinar cells was very similar to RBL-1 cells, in which the rate of Ca^{2+} efflux is slowed in cells treated with calmidazolium (177). The effect of calmidazolium on the rate of Ca^{2+} efflux in RBL-1 cells was not as dramatic as the effect on efflux in pancreatic acinar cells (figure 4.1 and figure 4.2); this was due to the fact that researchers were reluctant to pre-incubate cells with calmidazolium due to its ability to cause Ca^{2+} influx independent of store depletion in smooth muscle cells (368,374). Either thapsigargin or CPA are used to induce store-depletion and activate CRAC channels in the experiments in this chapter, pre-incubating pancreatic acinar cells with calmidazolium did not activate any further Ca^{2+} influx, as it was applied in nominally Ca^{2+} free extracellular solution, even if calmidazolium activates a non-store operated Ca^{2+} influx pathway there was minimal extracellular Ca^{2+} and therefore no chemical gradient for Ca^{2+} influx (figure 4.1 and figure 4.2).

It is likely that a combination of therapeutic targets will be necessary to rapidly resolve severe cases of acute pancreatitis. Thus far it is evident that inhibiting CRAC channels directly utilising a CRAC channel blocker is efficient in dramatically reducing cytosolic Ca^{2+} overload driven by Ca^{2+} influx; furthermore evidence in this chapter indicates that indirectly targeting CRAC channels by interfering with the gating mechanisms i.e. targeting calmodulin is also a mechanism by which cytosolic Ca^{2+} overload can be dramatically reduced. SOCE experiments based on the hypothesis of targeting both the CRAC channel directly, with an inhibitor, and targeting calmodulin regulation of the channel are demonstrated in figure 4.9 A and figure 4.10 A. Pre-incubating cells with both calmidazolium and GSK-7975A resulted in a dramatic reduction in Ca^{2+} influx, compared with calmidazolium treatment alone (figure 4.1A) and also a dramatic reduction of unidirectional Ba^{2+} influx, which reflects only Ca^{2+} influx not efflux.

Previous experiments in pancreatic acinar cells demonstrated that in permeabilised cells the effect of ethanol on Ca^{2+} release from intracellular stores was dramatically greater than the effect of ethanol on intact cells. This exacerbation of the Ca^{2+} signal was attributed to the loss of calmodulin from cells upon permeabilisation (359). This effect was also seen in another study where calmodulin was lost from the cell to the patch pipette (382). Application of calmodulin in both instances resulted in the return of its protective effect and an inhibition in

the cytosolic Ca^{2+} signalling. This is an intriguing premise in pancreatic acinar cells, which are by their very nature highly proteolytic. In a freshly isolated pancreatic acinar cell preparation there is an unavoidable percentage of cellular necrosis, due to the use of collagenase to disperse cells from the tissue, to enable them to be studied using microscopy. This cellular necrosis will result in the release of the digestive pro-enzymes, much like during an acute pancreatitis attack. Subsequent activation of digestive enzymes results in the destruction of pancreatic tissue *in vivo*, in addition to the large scale proteolytic attack there is likely a smaller scale digestion of intracellular proteins that are also released during cellular necrosis; calmodulin would be one such protein.

Chymotrypsinogen and trypsinogen are the two major digestive proenzymes synthesised by pancreatic acinar cells, calmodulin possesses several trypsin and chymotrypsin cleavage sites in its amino acid sequence (figure 1, in appendix). These cleavage sites were utilised to determine the primary sequence of bovine brain calmodulin (385). In addition to chymotrypsin and trypsin cleavage sites. Figure 4.11 A depicts the inhibition of Ca^{2+} influx elicited by pre-incubation of pancreatic acinar cells with calmodulin, as calmodulin is 148 amino acids in length it is unlikely to permeate the cell and presently there is no known extracellular CRAC channel calmodulin binding domain, making these ideas unlikely mechanisms by which Ca^{2+} influx is inhibited by calmodulin. Data generated using CALP peptides led to the hypothesis that inhibition in store-operated Ca^{2+} entry could be mediated by smaller peptide fragments of calmodulin. Predictions about which peptide products could be made from protease cleavage of calmodulin were generated using protease cleavage predicting computer tools such as the peptide cutter (http://web.expasy.org/peptide_cutter/) and another free tool called PROSPER (https://prosper.erc.monash.edu.au/webserver.html) (386). The cleavage data from computer models and functional data in which chymotrypsin inhibitor, trypsin inhibitor, protease inhibitor cocktail and metalloprotease inhibitor were used demonstrated that when the majority of pancreatic proteases are inhibited the reduction in store operated Ca^{2+} influx induced by calmodulin pre-treatment was no longer observed. However, this functional data does not provide any insight into what peptide sequence was mediating the inhibitory effect or how long the peptide is, and furthermore, there is no mechanistic information as to how the peptide is inhibiting store-operated Ca^{2+} influx. It is possible that inhibition of Ca^{2+} influx is mediated by blocking of the Ca^{2+} influx channel pore, either CRAC channels or non-specific cation channels such as TRPC channels, which are also expressed by pancreatic acinar cells. Appendix figures 2 and 3 depict two small peptide

fragments derived from predictions made of protease cleavage of calmodulin. The peptides were designated CaM A and CaM B.

4.4   Further experiments

As there is evidence to indicate that Ca^{2+} bound calmodulin binds with STIM1, it should be determined if this is sufficient to trigger the disassembly of STIM1/Orai1 to prevent further Ca^{2+} influx (176,382). It should also be determined if CALP3 bound calmodulin is able to bind STIM1 to mediate this process. It is possible that rather than calmodulin binding to STIM1 it is the complex of CALP3 bound calmodulin binding to Orai1 (159,160) that mediates Ca^{2+} dependent inactivation of Orai1, as has long been thought the process (159,177,366).

There is evidence supporting the hypothesis that a cleavage product of calmodulin, due to action of activated digestive enzymes, could be used to inhibit SOCE in pancreatic acinar cells. However, in order to determine the peptides that are mediating the inhibitory effects on the channel in an efficient manner it may be necessary to attempt to mimic conditions *in vitro*. The first step would be to incubate a solution of chymotrypsin and trypsin with calmodulin to allow proteolytic cleavage of calmodulin. After the incubation, in order to determine the sequence of the peptides a high-pressure liquid chromatography (HPLC) linked to a mass spectrometer can be used. HPLC ionises the peptide and electrosprays peptide ions into the mass spectrometer which can determine the sequence of the amino acids in the peptide (387). Armed with peptide sequences, derived from the mass spectrometry one can compare these with computer model predictions, and select peptides to be synthesised and tested functionally for inhibitory properties for CRAC channels. A small molecule microarray can be used with the minimal functional domains of CRAC channels to determine where peptides bind to in order to modulate channel activity, as in (209).

Experiments in which calmidazolium and GSK7975-A were combined demonstrated significant inhibition of Ca^{2+} influx. CALP3, also demonstrated remarkable inhibition of store-operated Ca^{2+} entry alone, it would be interesting to see if when combined with GSK7975-A whether there would be a further inhibitory effect on Ca^{2+} influx compared to treatment of cells with either drug alone.

Pharmacological interventions are always problematic due to limited specificity of inhibitors for their targets. CRISPR/Cas9 mediated deletion of calmodulin in cells would be a more efficient way to determine the effects of calmodulin on cells. It may be possible to determine

the exact role calmodulin plays in CRAC channel activation and inactivation. However, this approach is limited by the ubiquitous nature of calmodulin and its plethora of intracellular functions. This makes it a somewhat complicated therapeutic target, as modulation of calmodulin activity is unlikely to result in just the therapeutically desired action but also a multitude of off-target effects. For further information about therapeutic targets in treating acute pancreatitis see chapter 5.

5 General discussion

5.1 Implications of modulating Ca^{2+} influx

The aim of this thesis was to find a means of reducing cytosolic Ca^{2+} overload, the primary trigger in a series of events that results in acute pancreatitis. Figure 5.1 demonstrates this chain of events, between the stages the figure details general interventions that can be undertaken in an attempt to prevent disease progression. The vast majority of drugs that have made their way to clinical trials to treat acute pancreatitis have been agents that were directed at preventing the latter stages of the disease; interventions such as administration of protease inhibitors, anti-secretory or anti-inflammatory agents (267,276). However, despite numerous clinical trials using a variety of different classes of agents there has been a distinct lack of success in finding a treatment for acute pancreatitis. It is thought that the lack of success is because the intervention strategies have not been targeting the trigger for the chain of events but rather are attempting to prevent the disease from progressing any further, in its latter stages (276), once there is already significant amount of pancreatic necrosis and inflammation.

Utilising inhibitors of the Ca^{2+} release channels, or even inhibitors of accessory proteins that regulate the Ca^{2+} release channels would serve to prevent the initial Ca^{2+} signal that leads to all future steps, including the activation of store-operated Ca^{2+} entry which drives the sustained phase of Ca^{2+} elevation leading to cytosolic Ca^{2+} overload and intracellular proenzyme activation. Further to inhibition of Ca^{2+} release from intracellular stores, inhibition of CRAC channel mediated Ca^{2+} influx can also be undertaken to prevent cytosolic Ca^{2+} overload. A clinical study sought to use an intracellular Ca^{2+} chelator, DP-b99, in the treatment of acute pancreatitis, in an attempt to inhibit the elevation of cytosolic Ca^{2+} associated with intracellular proenzyme activation; however, the study was terminated due to slow recruitment (276,388). Therefore, the field is no further forward in terms of clinical evidence that modulation of Ca^2 signalling, with a view to reduce cytosolic Ca^{2+} overload, is clinically beneficial and a viable therapeutic option for treating acute pancreatitis; However, the evidence generated using CRAC channel inhibitors to reduce cytosolic Ca^{2+} overload *in vitro* and in mouse models is highly promising (130,253,268). CRAC channel inhibitors are likely to be the most promising means of achieving this goal, with the attention of multiple different fields of enquiry converging on this one target (389,390), a clinically approved drug is highly likely to come to fruition. CM_128 is due to start phase I trials in the near future.
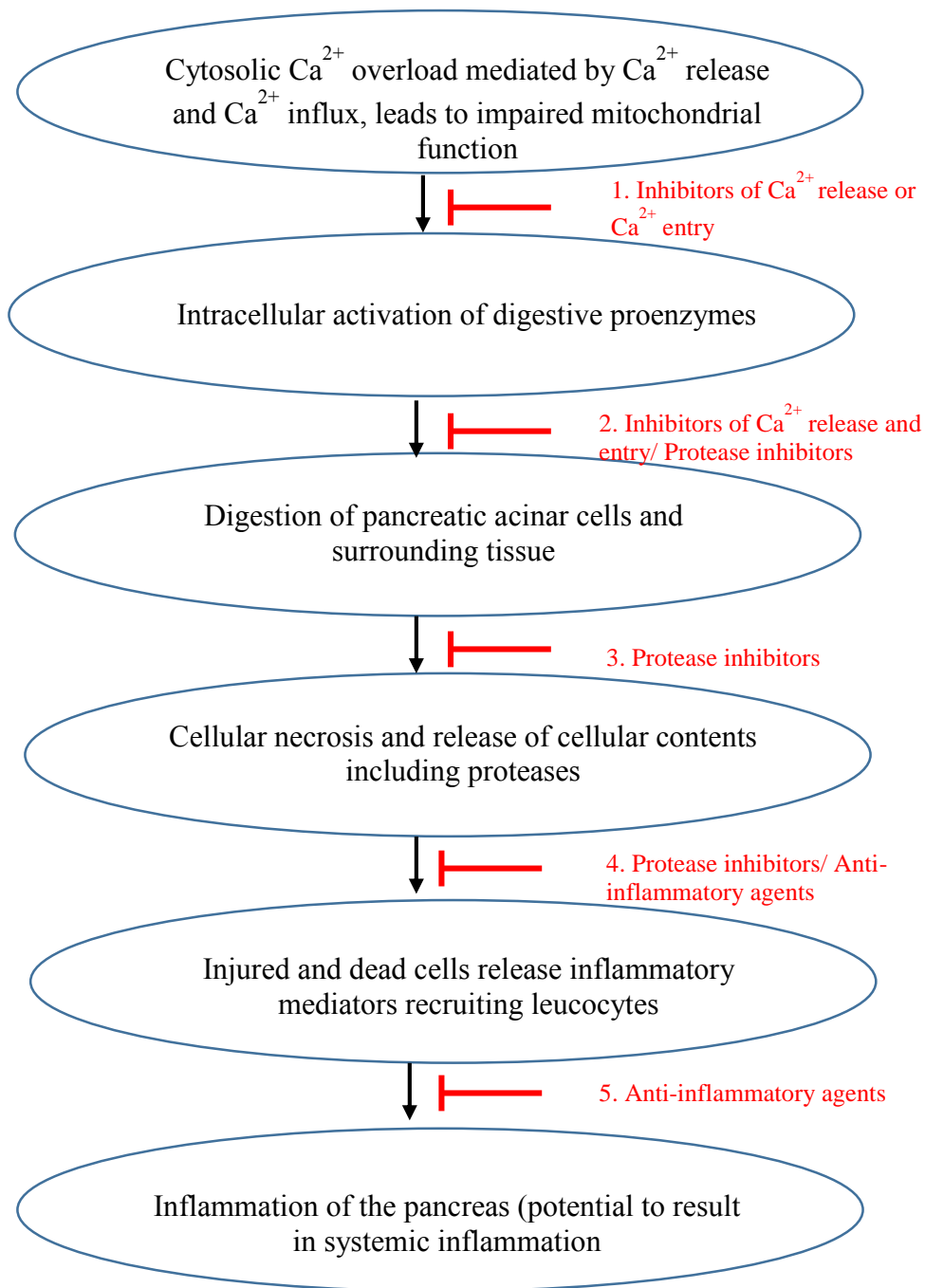
Figure 5.1 Flow diagram depicting the chain of events involved in the onset of acute pancreatitis

The major events in the onset of acute pancreatitis are detailed in the flow diagram, from the cytosolic Ca^{2+} overload to the digestion of pancreatic tissue and subsequent inflammatory response this mediates. At each step interventions (listed in red) are highlighted that might prevent the progression of the disease to the next stage.

1. Using inhibitors to prevent Ca^{2+} release from intracellular stores and inhibitors of Ca^{2+} entry channels to prevent cytosolic Ca^{2+} overload. Agents that prevent mitochondrial dysfunction 2. Using inhibitors of Ca^{2+} signalling and protease inhibitors to inactivate trypsin/chymotrypsin to prevent digestion. 3. Using protease inhibitors. 4. Using protease inhibitors and anti-inflammatory agents to prevent the inflammatory response. 5. Using anti-inflammatory agents to prevent both the local inflammatory response and potential systemic inflammatory response

Modulation of calmodulin as a potential therapy for acute pancreatitis is a possibility as both agonists (CALP1 and CALP3) and antagonists (trifluoperazine, calmidazolium and W-7) of calmodulin exist for use *in* v*itro* and trifluoperazine is used clinically already to treat schizophrenia (391). Calmodulin antagonists, such as trifluoperazine, have been demonstrated to sensitise pancreatic cancer cells to chemotherapy agent induced cell death (392) and inhibit cancer cell migration in lung cancer (393). Furthermore, a patent has been filed to use calmodulin inhibitors to treat ribosomal-related diseases known as ribosomapathies (394). In addition to direct inhibition of calmodulin, there are instances in which modulation of calmodulin dependent kinases has been used as therapies for heart disease such as calmodulin kinase II inhibitors and calmodulin dependent kinase IV inhibitors have been shown to have promise in the treatment of autoimmune diseases (395). This demonstrates that inhibitors of calmodulin are a viable treatment option for diseases. However, calmodulin is the primary cytosolic Ca^{2+} sensing protein and is found in almost all cell types where it is implicated in several different signal transduction pathways, calmodulin dependent kinase pathways, calcineurin/NFAT pathway (35,343). Calmodulin in particular has an important role in the regulation of cellular components involved in Ca^{2+} handling in cells, such as regulation of voltage gated Ca^2 channels in cardiac myocytes, RyR in both skeletal and cardiac muscle and SERCA via its regulation of phospholamban (396). Due to its vital role in the intracellular Ca^{2+} signal transduction using calmodulin modulators in order to treat acute pancreatitis is likely to affect lots of other cell types, including vital cells such as cardiac myocytes and skeletal muscle. Using calmodulin as a target to treat acute pancreatitis could be achieved if a pharmacological agent is used at submaximal concentration in combination with another inhibitor, such as a CRAC channel inhibitor at submaximal concentration, this strategy has proved effective as a potential therapy for nasal polyps (326). Extensive tests would be required on isolated pancreatic acinar cells before determining if the strategy is effective to translate initially to a mouse model of the disease.

CRAC channels are also ubiquitous cellular components (127,183). In the same way that targeting calmodulin as a therapeutic for acute pancreatitis is likely to be complex due to its ubiquitous expression, targeting of CRAC channels is also likely to not only affect the pancreatic acinar cells but also other cell types. Primarily, it is non-excitable cells that are dependent on the activity of CRAC channels to provide Ca^{2+} influx in response to store depletion. Immune cell functionality is largely dependent on cytosolic Ca^{2+} signals (314), patients suffering with SCID were found to have inactive Ca^{2+} influx due to a mutation in

Orai1 (152). One potential issue with inhibiting CRAC channels is the potential immunosuppression of patients. However, it has been demonstrated that excitable cells such as cardiac myocytes, including pacemaker cells (397), neurones (398) and skeletal myocytes (399,400) also possess functional CRAC channels that contribute to Ca^{2+} influx. CRAC channels are not the primary Ca^{2+} influx pathway in these cells. Excitable cells have a myriad of voltage gated Ca^{2+} channels (401) and also the NCX which in reverse mode and permit Ca^{2+} to enter the cells (20). It would seem that CRAC channel mediated Ca^{2+} influx plays more of a role in pathological remodelling in cardiac myocytes (402). As such, even though these channels are ubiquitous, targeting of CRAC channels as a therapeutic for acute pancreatitis should not have a significant impact on the functioning of excitable cells. Non-excitable cells, such as hepatocytes that are dependent on Ca^{2+} influx through CRAC channels to drive cellular processes such as exocytosis are likely to be affected by CRAC channel inhibition. However, it has been demonstrated, at least *in vitro* that hepatocytes are minimally affected by the CRAC channel inhibitor GSK-7975A (130). Another notable finding of the study was that GSK-7975A pre-treatment had only minor effects on the physiological Ca^{2+} signals induced by both ACh and CCK in pancreatic acinar cells. As the treatment of acute pancreatitis by its very nature will be an acute treatment, any undesired side effects of treatment, provided they do not impact on an individual's brain, heart or skeletal muscle (breathing) can more easily be tolerated as the treatment is not prolonged.

5.2 Limitations

Measuring intracellular Ca^{2+} in real time allows for monitoring of Ca^{2+} fluxes with a relatively good temporal resolution. As a fluorescent Ca^{2+} indicator Fura-2 allows for measurement of changes in intracellular Ca^{2+} signals in real time. Fura-2 is a dual excitation wavelength dye and as such is an ideal dye for quantitative Ca^{2+} measurements. When measuring smaller amplitude Ca^{2+} signals, such as Ca^{2+} oscillations that are restricted to the apical pole induced by physiological concentrations of either ACh or CCK, can be difficult when using Fura-2; because Fura-2 has a higher buffering capacity for free Ca^{2+} than other fluorescent Ca^{2+} indicators such as Fluo-4 (k_d of Fura-2 = 145 nM k_d of Fluo-4 = 345 nM). It has also been noted that Fura-2 is more resistant to photo-bleaching making it ideal for experiments in which Ca^{2+} signals are measured over extended periods of time (403). As this thesis was not particularly focused on the spatial aspects of Ca^{2+} signalling Fura-2 was suitable for measuring changes in cytosolic Ca^{2+} due to store-operated Ca^{2+} entry and was of particular use as experiments were often in excess of 30 minutes.

The modulation of calmodulin was the primary aim of chapter 4, as a role for calmodulin has been implicated in the regulation of CRAC channel function, due to its binding to both Orai1 (159,177) and STIM1 (176). The most notable aspect of store-operated Ca^{2+} hypothesised to be affected by calmodulin modulation is the Ca^{2+}-dependent inactivation of the CRAC channel. However, it is difficult to measure the inactivation of the CRAC channel using fluorescent microscopy, most investigators have measured inactivation of CRAC channels using electrophysiology (148,366,404). It is possible, using this technique, to observe the change in channel conductance, due to channel inactivation, in the sustained presence of extracellular Ca^{2+} in isolation from other factors that contribute to Ca^{2+} homeostasis in the cell.

In addition, using electrophysiological techniques, such as whole cell patch clamp, it is possible to monitor the current through the ion channel of interest, without interference from other ion channel fluxes. When measuring the effect of inhibitors of Ca^{2+} influx, using fluorescent Ca^{2+} indicators, increased cytosolic Ca^{2+} would be observed due to Ca^{2+}influx through non-selective cation channels, such as TRPC3, as well as through CRAC channels. TRPC3 is also speculated to be a STIM1 gated, store-regulated ion channel (222) and therefore would be activated by thapsigargin or CPA mediated store depletion. Using fluorescent Ca^{2+} indicators identification of Ca^{2+} influx through each channel is only possible by using inhibitors of the channels and therefore is limited by the specificity of said inhibitors, whereas CRAC channel currents and TRPC3 channel currents have distinct biophysical properties and so can be differentiated through electrophysiological experiments (127,405). It is possible to simultaneously measure channel conductance using whole cell patch clamp whilst monitoring intracellular Ca^{2+} flux using fluorescent indicators such as Fura-2 or Fluo-4 using microscopy. This method has been used effectively in the past to give a real time read out of channel currents and spatiotemporal aspects of Ca^{2+} signals, in pancreatic acinar cells (123).

Intracellular Ca^{2+} homeostasis is a dynamic equilibrium between Ca^{2+} influx mechanisms into the cytosol, across the plasma membrane and across the ER membrane; and Ca^{2+} efflux pathways from the cytosol, across the plasma membrane, across the ER membrane and into the mitochondria (as depicted in figure 1.1). In measuring global Ca^{2+} influx, using fluorescent microscopy, there is interference in the Ca^{2+} signal by the activation of Ca^{2+} efflux mechanisms, mostly due to activation of PMCA. It is possible to measure only Ca^{2+} influx activity using fluorescence microscopy, used in this thesis, Ca^{2+} ions in the

extracellular solution are substituted for Ba^{2+} ions. CRAC channels are more permeable to Ba^{2+} than Ca^{2+}, furthermore Ba^{2+} can bind to Fura-2 resulting in fluorescent changes associated with influx of Ba^{2+} into the cytosol of Fura-2 loaded cells. The dynamic equilibrium of Ca^{2+} homeostasis employed by cells is subverted as although Ba^{2+} can permeate the ion channels in the plasma membrane, the Ca^{2+} ATPases cannot pump Ba^{2+} either into the ER or across the plasma membrane (310–312). Such measurements allow for effects of pharmacological agents on CRAC channel activity to be observed without interference of their potential effects on Ca^{2+} extrusion mechanism; which would largely be PMCA as CRAC channel activity is measured in the presence of SERCA pump inhibitors, either CPA or thapsigargin. Measurement of the half time of Ca^{2+} influx can be problematic, as in some experiments a plateau in cytosolic Ca^{2+} levels after re-introduction of $Ca^{2=}$ to the extracellular solution was not attained. This was to ensure that all experiments were time-locked, but proved problematic for analysis. An alternative method of analysis would be to measure the initial rate of rate of influx.

Experiments in chapter 4 which assessed the effect of CALP3 on store-operated Ca^{2+} influx were undertaken in Fura-2 loaded cells in the presence of extracellular $Ca^{2=}$. If Ca^{2+} ions were substituted for Ba^{2+} ions the effect of CALP3 on Ca^{2+} influx could have been measured in isolation from Ca^{2+} efflux mechanisms. As CALP3 and other agents used in chapter 4 are modulators of calmodulin and it is known that calmodulin regulates PMCA as well as Orai1 and STIM1 measuring the effect of each agent on Ca^{2+} influx in isolation from Ca^{2+} efflux by using Ba^{2+} substitution would give a more accurate results on the effect of calmodulin modulation of Ca^{2+} influx. Using electrophysiology would provide more insight on the effect of calmodulin modulation on the Ca^{2+} dependent inactivation of the CRAC channel.

5.3 Future considerations

One of the biggest problems of clinical trials testing drugs with the potential to treat acute pancreatitis is primarily the time frame in which patients are required to receive treatment after onset of symptoms. In order to be successful most treatments need to be administered to patients as quickly as possible from the onset of the disease, to prevent extensive pancreatic necrosis and injury. It is difficult to determine the time of onset of the disease, it has been demonstrated that the onset of pancreatic necrosis in human pancreatitis can take up to four days to be detected (406), rather than approximately 6 hours in a mouse model (253). Any therapeutic intervention that is made, will be made after the onset of symptoms, but the earlier it is made the more likely it is to prevent the onset of necrosis and subsequent

inflammation. It is evident from all studies to date that the pre-treatment with any therapeutic agent offers maximal protection against Ca^{2+} overload and subsequent pancreatic necrosis (chapter 3 and 4), (130,359); as such steps are being taken by the field to determine biomarkers that precede the onset of acute pancreatitis. Detection of biomarkers in patients allows for early identification of the disease, allowing for earlier intervention and improved chances of survival. There are also indications that the earlier someone is treated the fewer days they spend in hospital, improving the burden placed on global healthcare systems. There are clinical trials underway in China, that are seeking to test for the presence of micro RNAs and long non-coding RNA in the blood, to see if it could be correlated with a diagnosis of acute pancreatitis that is likely to develop persistent organ failure (407,408)

5.4 Concluding remarks

Targeting the initial trigger of acute pancreatitis seems likely to be the most efficient means of treating this multi-faceted disease. Targeting individual cellular components that are responsible for contributing to cytosolic Ca^{2+} overload in isolation or by targeting multiple components simultaneously would remove the trigger for the premature activation of digestive enzymes. One such mechanism to achieve this is to utilise CRAC channel inhibition, using CRAC channel inhibitors and thereby preventing Ca^{2+} influx triggered by the emptying of intracellular Ca^{2+} stores. Stopping the disease in its earliest stages has been demonstrated in animal models of the disease, it is now to be determined if this is the case in the human disease.

References

1. Ringer S. Concerning the Influence exerted by each of the Constituents of the Blood on the Contraction of the Ventricle. J Physiol. 1882 Aug;3(5–6):380–93.

2. Ringer S. A further Contribution regarding the influence of the different Constituents of the Blood on the Contraction of the Heart. J Physiol. 1883 Jan;4(1):29–42.3.

3. Carafoli E. The calcium-signalling saga: tap water and protein crystals. Nat Rev Mol Cell Biol. 2003 Apr;4(4):326–32.

4. Scoote M, Williams AJ. Myocardial calcium signalling and arrhythmia pathogenesis. Biochem Biophys Res Commun. 2004 Oct 1;322(4):1286–309.

5. Berridge MJ. Calcium signalling and Alzheimer's disease. Neurochem Res. 2011 Jul;36(7):1149–56.

6. Stewart TA, Yapa KTDS, Monteith GR. Altered calcium signaling in cancer cells. Biochim Biophys Acta BBA - Biomembr. 2015 Oct;1848(10, Part B):2502–11.

7. Petersen OH, Gerasimenko OV, Gerasimenko JV. Pathobiology of acute pancreatitis: focus on intracellular calcium and calmodulin. F1000 Med Rep. 2011;3:15.

8. Chakrabarti R, Chakrabarti R. Calcium signaling in non-excitable cells: Ca2+ release and influx are independent events linked to two plasma membrane Ca2+ entry channels. J Cell Biochem. 2006 Dec 15;99(6):1503–16.

9. Zhivotovsky B, Orrenius S. Calcium and cell death mechanisms: a perspective from the cell death community. Cell Calcium. 2011 Sep;50(3):211–21.

10. Berridge MJ, Bootman MD, Roderick HL. Calcium signalling: dynamics, homeostasis and remodelling. Nat Rev Mol Cell Biol. 2003 Jul;4(7):517–29.

11. Petersen OH, Tepikin AV. Polarized calcium signaling in exocrine gland cells. Annu Rev Physiol. 2008;70:273–99.

12. Fearnley CJ, Roderick HL, Bootman MD. Calcium Signaling in Cardiac Myocytes. Cold Spring Harb Perspect Biol. 2011 3(11). a004242.

13. Berridge MJ. Inositol trisphosphate and calcium signalling. Nature. 1993 Jan 28;361(6410):315–25.

14. Clapham DE. Calcium Signaling. Cell. 2007 Dec 14;131(6):1047–58.

15. Mogami H, Tepikin AV, Petersen OH. Termination of cytosolic Ca2+ signals: Ca2+ reuptake into intracellular stores is regulated by the free Ca2+ concentration in the store lumen. EMBO J. 1998 Jan 15;17(2):435–42.

16. Ehrlich BE, Watras J. Inositol 1,4,5-trisphosphate activates a channel from smooth muscle sarcoplasmic reticulum. Nature. 1988 Dec 8;336(6199):583–6.

17. Taylor CW, Tovey SC. IP3 Receptors: Toward Understanding Their Activation. Cold Spring Harb Perspect Biol. 2010 Dec 1;2(12):a004010.

18. Gerasimenko JV, Charlesworth RM, Sherwood MW, Ferdek PE, Mikoshiba K, Parrington J, et al. Both RyRs and TPCs are required for NAADP-induced intracellular Ca^{2+} release. Cell Calcium. 2015 Sep;58(3):237–45.

19. Calcraft PJ, Ruas M, Pan Z, Cheng X, Arredouani A, Hao X, et al. NAADP mobilizes calcium from acidic organelles through two-pore channels. Nature. 2009 May 28;459(7246):596–600.

20. Bers DM. Calcium Fluxes Involved in Control of Cardiac Myocyte Contraction. Circ Res. 2000 Aug 18;87(4):275–81.

21. Futatsugi A, Nakamura T, Yamada MK, Ebisui E, Nakamura K, Uchida K, et al. IP3 Receptor Types 2 and 3 Mediate Exocrine Secretion Underlying Energy Metabolism. Science. 2005 Sep 30;309(5744):2232–4.

22. Fitzsimmons TJ, Gukovsky I, McRoberts JA, Rodriguez E, Lai FA, Pandol SJ. Multiple isoforms of the ryanodine receptor are expressed in rat pancreatic acinar cells. Biochem J. 2000 Oct 1;351(Pt 1):265–71.

23. Thorn P, Lawrie AM, Smith PM, Gallacher DV, Petersen OH. Local and global cytosolic Ca2+ oscillations in exocrine cells evoked by agonists and inositol trisphosphate. Cell. 1993 Aug 27;74(4):661–8.

24. Leite MF, Dranoff JA, Gao L, Nathanson MH. Expression and subcellular localization of the ryanodine receptor in rat pancreatic acinar cells. Biochem J. 1999 Jan 15;337 (Pt 2):305–9.

25. Straub SV, Giovannucci DR, Yule DI. Calcium wave propagation in pancreatic acinar cells: functional interaction of inositol 1,4,5-trisphosphate receptors, ryanodine receptors, and mitochondria. J Gen Physiol. 2000 Oct;116(4):547–60.

26. Carafoli E. Biogenesis: plasma membrane calcium ATPase: 15 years of work on the purified enzyme. FASEB J. 1994 Oct 1;8(13):993–1002.

27. Deluca HF, Engstrom GW. Calcium uptake by rat kidney mitochondria. Proc Natl Acad Sci U S A. 1961 Nov 15;47:1744–50.

28. Kirichok Y, Krapivinsky G, Clapham DE. The mitochondrial calcium uniporter is a highly selective ion channel. Nature. 2004 Jan 22;427(6972):360–4.

29. De Stefani D, Raffaello A, Teardo E, Szabò I, Rizzuto R. A 40 kDa protein of the inner membrane is the mitochondrial calcium uniporter. Nature. 2011 Jun 19;476(7360):336–40.

30. Szabadkai G, Simoni AM, Rizzuto R. Mitochondrial Ca2+ Uptake Requires Sustained Ca2+ Release from the Endoplasmic Reticulum. J Biol Chem. 2003 Apr 25;278(17):15153–61.

31. Jouaville LS, Pinton P, Bastianutto C, Rutter GA, Rizzuto R. Regulation of mitochondrial ATP synthesis by calcium: Evidence for a long-term metabolic priming. Proc Natl Acad Sci. 1999 Nov 23;96(24):13807–12.

32. Giorgi C, Agnoletto C, Bononi A, Bonora M, De Marchi E, Marchi S, et al. Mitochondrial calcium homeostasis as potential target for mitochondrial medicine. Mitochondrion. 2012 Jan;12(1):77–85.

33. Schwaller B. Cytosolic Ca2+ buffers. Cold Spring Harb Perspect Biol. 2010 Nov;2(11):a004051.

34. Carafoli E, Santella L, Branca D, Brini M. Generation, control, and processing of cellular calcium signals. Crit Rev Biochem Mol Biol. 2001 Apr;36(2):107–260.

35. Chin D, Means AR. Calmodulin: a prototypical calcium sensor. Trends Cell Biol. 2000 Aug 1;10(8):322–8.

36. Heizmann CW, Berchtold MW, Rowlerson AM. Correlation of parvalbumin concentration with relaxation speed in mammalian muscles. Proc Natl Acad Sci U S A. 1982 Dec;79(23):7243–7.

37. Schmidt H, Stiefel KM, Racay P, Schwaller B, Eilers J. Mutational analysis of dendritic Ca2+ kinetics in rodent Purkinje cells: role of parvalbumin and calbindin D28k. J Physiol. 2003 Aug 15;551(Pt 1):13–32.

38. Caillard O, Moreno H, Schwaller B, Llano I, Celio MR, Marty A. Role of the calcium-binding protein parvalbumin in short-term synaptic plasticity. Proc Natl Acad Sci U S A. 2000 Nov 21;97(24):13372–7.

39. Petersen OH. Stimulus-secretion coupling: cytoplasmic calcium signals and the control of ion channels in exocrine acinar cells. J Physiol. 1992 Mar;448:1–51.

40. Streb H, Irvine RF, Berridge MJ, Schulz I. Release of Ca2+ from a nonmitochondrial intracellular store in pancreatic acinar cells by inositol-1,4,5-trisphosphate. Nature. 1983 Nov 3;306(5938):67–9.

41. Putney JW, Bird GS. The inositol phosphate-calcium signaling system in nonexcitable cells. Endocr Rev. 1993 Oct;14(5):610–31.

42. Berridge MJ, Lipp P, Bootman MD. The versatility and universality of calcium signalling. Nat Rev Mol Cell Biol. 2000 Oct;1(1):11–21.

43. Furuichi T, Yoshikawa S, Miyawaki A, Wada K, Maeda N, Mikoshiba K. Primary structure and functional expression of the inositol 1,4,5-trisphosphate-binding protein P400. Nature. 1989 Nov 2;342(6245):32–8.

44. Finch EA, Turner TJ, Goldin SM. Calcium as a coagonist of inositol 1,4,5-trisphosphate-induced calcium release. Science. 1991 Apr 19;252(5004):443–6.

45. Sato C, Hamada K, Ogura T, Miyazawa A, Iwasaki K, Hiroaki Y, et al. Inositol 1,4,5-trisphosphate Receptor Contains Multiple Cavities and L-shaped Ligand-binding Domains. J Mol Biol. 2004 Feb 6;336(1):155–64.

46.   Taylor CW, Genazzani AA, Morris SA. Expression of inositol trisphosphate receptors. Cell Calcium. 1999 Dec;26(6):237–51.

47.   Mikoshiba K. IP3 receptor/Ca2+ channel: from discovery to new signaling concepts. J Neurochem. 2007 Sep;102(5):1426–46.

48.   Dufour JF, Arias IM, Turner TJ. Inositol 1,4,5-trisphosphate and calcium regulate the calcium channel function of the hepatic inositol 1,4,5-trisphosphate receptor. J Biol Chem. 1997 Jan 31;272(5):2675–81.

49.   Marchant JS, Taylor CW. Cooperative activation of IP3 receptors by sequential binding of IP3 and Ca2+ safeguards against spontaneous activity. Curr Biol. 1997 Jul 1;7(7):510–8.

50.   Boehning D, Joseph SK. Direct association of ligand-binding and pore domains in homo- and heterotetrameric inositol 1,4,5-trisphosphate receptors. EMBO J. 2000 Oct 16;19(20):5450–9.

51.   Changya L, Gallacher DV, Irvine RF, Petersen OH. Inositol 1,3,4,5-tetrakisphosphate and inositol 1,4,5-trisphosphate act by different mechanisms when controlling Ca2+ in mouse lacrimal acinar cells. FEBS Lett. 1989 Jul 17;251(1–2):43–8.

52.   Bird GS, Rossier MF, Hughes AR, Shears SB, Armstrong DL, Putney JW. Activation of Ca2+ entry into acinar cells by a non-phosphorylatable inositol trisphosphate. Nature. 1991 Jul 11;352(6331):162–5.

53.   Toescu EC, O'Neill SC, Petersen OH, Eisner DA. Caffeine inhibits the agonist-evoked cytosolic Ca2+ signal in mouse pancreatic acinar cells by blocking inositol trisphosphate production. J Biol Chem. 1992 Nov 25;267(33):23467–70.

54.   Mignery GA, Südhof TC, Takei K, De Camilli P. Putative receptor for inositol 1,4,5-trisphosphate similar to ryanodine receptor. Nature. 1989 Nov 9;342(6246):192–5.

55.   Amador FJ, Stathopulos PB, Enomoto M, Ikura M. Ryanodine receptor calcium release channels: lessons from structure–function studies. FEBS J. 2013 Nov 1;280(21):5456–70.

56.   Pessah IN, Waterhouse AL, Casida JE. The calcium-ryanodine receptor complex of skeletal and cardiac muscle. Biochem Biophys Res Commun. 1985 Apr 16;128(1):449–56.

57.   Campbell KP, Knudson CM, Imagawa T, Leung AT, Sutko JL, Kahl SD, et al. Identification and characterization of the high affinity [3H]ryanodine receptor of the junctional sarcoplasmic reticulum Ca2+ release channel. J Biol Chem. 1987 May 15;262(14):6460–3.

58.   Lai FA, Meissner G. The muscle ryanodine receptor and its intrinsic Ca2+ channel activity. J Bioenerg Biomembr. 1989 Apr;21(2):227–46.

59.   Sorrentino V, Volpe P. Ryanodine receptors: how many, where and why? Trends Pharmacol Sci. 1993 Mar 1;14(3):98–103.

60.   Shoshan-Barmatz V. High affinity ryanodine binding sites in rat liver endoplasmic reticulum. FEBS Lett. 1990 Apr 24;263(2):317–20.

61.   Sanchez-Bueno A, Cobbold PH. Agonist-specificity in the role of Ca2+-induced Ca2+ release in hepatocyte Ca2+ oscillations. Biochem J. 1993 Apr 1;291(1):169–72.

62.   Nathanson MH, Burgstahler AD, Fallon MB. Multistep mechanism of polarized Ca2+ wave patterns in hepatocytes. Am J Physiol. 1994 Sep;267(3 Pt 1):G338-349.

63.   Tunwell RE, Lai FA. Ryanodine receptor expression in the kidney and a non-excitable kidney epithelial cell. J Biol Chem. 1996 Nov 22;271(47):29583–8.

64.   DiJulio DH, Watson EL, Pessah IN, Jacobson KL, Ott SM, Buck ED, et al. Ryanodine receptor type III (Ry3R) identification in mouse parotid acini. Properties and modulation of [3H]ryanodine-binding sites. J Biol Chem. 1997 Jun 20;272(25):15687–96.

65.   Zhang X, Wen J, Bidasee KR, Besch HR, Wojcikiewicz RJ, Lee B, et al. Ryanodine and inositol trisphosphate receptors are differentially distributed and expressed in rat parotid gland. Biochem J. 1999 Jun 1;340 (Pt 2):519–27.

66.   Ozawa T. Ryanodine-sensitive Ca2+ release mechanism in non-excitable cells (Review). Int J Mol Med. 2001 Jan;7(1):21–5.

67.   Sims CE, Allbritton NL. Metabolism of Inositol 1,4,5-Trisphosphate and Inositol 1,3,4,5-Tetrakisphosphate by the Oocytes of Xenopus laevis. J Biol Chem. 1998 Feb 13;273(7):4052–8.

68.   Tepikin AV, Voronina SG, Gallacher DV, Petersen OH. Pulsatile Ca2+ extrusion from single pancreatic acinar cells during receptor-activated cytosolic Ca2+ spiking. J Biol Chem. 1992 Jul 15;267(20):14073–6.

69.   Zylińska L, Soszyński M. Plasma membrane Ca2+-ATPase in excitable and nonexcitable cells. Acta Biochim Pol. 2000;47(3):529–39.

70.   Savage AL, Biffen M, Martin BR. Vasopressin-stimulated Ca2+ influx in rat hepatocytes is inhibited in high-K+ medium. Biochem J. 1989 Jun 15;260(3):821–7.

71.   Mangialavori I, Ferreira-Gomes M, Pignataro MF, Strehler EE, Rossi JPFC. Determination of the dissociation constants for Ca2+ and calmodulin from the plasma membrane Ca2+ pump by a lipid probe that senses membrane domain changes. J Biol Chem. 2010 Jan 1;285(1):123–30.

72.   Brini M, Carafoli E. The Plasma Membrane Ca2+ ATPase and the Plasma Membrane Sodium Calcium Exchanger Cooperate in the Regulation of Cell Calcium. Cold Spring Harb Perspect Biol.2011;3(2). a004168

73.   Pott C, Goldhaber JI, Philipson KD. Genetic manipulation of cardiac Na+/Ca2+ exchange expression. Biochem Biophys Res Commun. 2004 Oct 1;322(4):1336–40.

74. Mogami H, Nakano K, Tepikin AV, Petersen OH. Ca2+ flow via tunnels in polarized cells: recharging of apical Ca2+ stores by focal Ca2+ entry through basal membrane patch. Cell. 1997 Jan 10;88(1):49–55.

75. Ashby MC, Tepikin AV. Polarized calcium and calmodulin signaling in secretory epithelia. Physiol Rev. 2002 Jul;82(3):701–34.

76. Ambudkar IS. Polarization of Calcium Signaling and Fluid Secretion in Salivary Gland Cells. Curr Med Chem. 2012;19(34):5774–81.

77. Nathanson MH, Fallon MB, Padfield PJ, Maranto AR. Localization of the type 3 inositol 1,4,5-trisphosphate receptor in the Ca2+ wave trigger zone of pancreatic acinar cells. J Biol Chem. 1994 Feb 18;269(7):4693–6.

78. Yule DI, Ernst SA, Ohnishi H, Wojcikiewicz RJ. Evidence that zymogen granules are not a physiologically relevant calcium pool. Defining the distribution of inositol 1,4,5-trisphosphate receptors in pancreatic acinar cells. J Biol Chem. 1997 Apr 4;272(14):9093–8.

79. Lee MG, Xu X, Zeng W, Diaz J, Wojcikiewicz RJ, Kuo TH, et al. Polarized expression of Ca2+ channels in pancreatic and salivary gland cells. Correlation with initiation and propagation of [Ca2+]i waves. J Biol Chem. 1997 Jun 20;272(25):15765–70.

80. Lur G, Sherwood MW, Ebisui E, Haynes L, Feske S, Sutton R, et al. InsP3 receptors and Orai channels in pancreatic acinar cells: co-localization and its consequences. Biochem J. 2011 Jun 1;436(2):231–9.

81. Gerasimenko OV, Gerasimenko JV, Rizzuto RR, Treiman M, Tepikin AV, Petersen OH. The distribution of the endoplasmic reticulum in living pancreatic acinar cells. Cell Calcium. 2002 Nov;32(5–6):261–8.

82. Amaya MJ, Nathanson MH. Calcium signaling in the liver. Compr Physiol. 2013 Jan;3(1):515–39.

83. Belan PV, Gerasimenko OV, Tepikin AV, Petersen OH. Localization of Ca2+ extrusion sites in pancreatic acinar cells. J Biol Chem. 1996 Mar 29;271(13):7615–9.

84. Leung PS, Ip SP. Pancreatic acinar cell: Its role in acute pancreatitis. Int J Biochem Cell Biol. 2006;38(7):1024–30.

85. Williams JA. Regulation of Acinar Cell Function in The Pancreas. Curr Opin Gastroenterol. 2010 Sep;26(5):478–83.

86. Anagnostides A, Chadwick VS, Selden AC, Maton PN. Sham feeding and pancreatic secretion. Evidence for direct vagal stimulation of enzyme output. Gastroenterology. 1984 Jul;87(1):109–14.

87. Pandol SJ. Regulation of Whole-Organ Pancreatic Secretion. 2010 [cited 2016 Feb 19]; Available from: http://www.ncbi.nlm.nih.gov/books/NBK54132/

88. Kreiss C, Schwizer W, Erlacher U, Borovicka J, Lochner-Kuery C, Muller R, et al. Role of antrum in regulation of pancreaticobiliary secretion in humans. Am J Physiol - Gastrointest Liver Physiol. 1996 May 1;270(5):G844–51.

89. Keller J, Layer P. Human pancreatic exocrine response to nutrients in health and disease. Gut. 2005 Jul;54(Suppl 6):1–28.

90. Palade G. Intracellular aspects of the process of protein synthesis. Science. 1975 Aug 1;189(4200):347–58.

91. Kitamoto Y, Yuan X, Wu Q, McCourt DW, Sadler JE. Enterokinase, the initiator of intestinal digestion, is a mosaic protease composed of a distinctive assortment of domains. Proc Natl Acad Sci U S A. 1994 Aug 2;91(16):7588–92.

92. Amsterdam A, Jamieson JD. Studies on dispersed pancreatic exocrine cells. I. Dissociation technique and morphologic characteristics of separated cells. J Cell Biol. 1974 Dec;63(3):1037–56.

93. Gerasimenko OV, Gerasimenko JV, Belan PV, Petersen OH. Inositol Trisphosphate and Cyclic ADP-Ribose–Mediated Release of Ca2+ from Single Isolated Pancreatic Zymogen Granules. Cell. 1996 Feb 9;84(3):473–80.

94. Nielsen SP, Petersen OH. Transport of calcium in the perfused submandibular gland of the cat. J Physiol. 1972 Jun 1;223(3):685–97.

95. Matthews EK, Petersen OH, Williams JA. Pancreatic acinar cells: acetylcholine-induced membrane depolarization, calcium efflux and amylase release. J Physiol. 1973 Nov 1;234(3):689–701.

96. Petersen OH, Ueda N. Pancreatic acinar cells: the role of calcium in stimulus-secretion coupling. J Physiol. 1976 Jan 1;254(3):583–606.

97. Ueda N, Petersen OH. The dependence of caerulein-evoked pancreatic fluid secretion on the extracellular calcium concentration. Pflüg Arch. 370(2):179–83.

98. Powers RE, Johnson PC, Houlihan MJ, Saluja AK, Steer ML. Intracellular Ca2+ levels and amylase secretion in Quin 2-loaded mouse pancreatic acini. Am J Physiol. 1985 May;248(5 Pt 1):C535-541.

99. Ochs DL, Korenbrot JI, Williams JA. Relation between free cytosolic calcium and amylase release by pancreatic acini. Am J Physiol - Gastrointest Liver Physiol. 1985 Sep 1;249(3):G389–98.

100. Maruyama Y, Inooka G, Li YX, Miyashita Y, Kasai H. Agonist-induced localized Ca2+ spikes directly triggering exocytotic secretion in exocrine pancreas. EMBO J. 1993 Aug;12(8):3017–22.

101. Lee M, Chung S, Uhm DY, Park MK. Regulation of zymogen granule exocytosis by Ca2+, cAMP, and PKC in pancreatic acinar cells. Biochem Biophys Res Commun. 2005 Sep 9;334(4):1241–7.

102.	Li Y, Hao Y, Owyang C. High-affinity CCK-A receptors on the vagus nerve mediate CCK-stimulated pancreatic secretion in rats. Am J Physiol. 1997 Sep;273(3 Pt 1):G679-685.

103.	Owyang C. Physiological mechanisms of cholecystokinin action on pancreatic secretion. Am J Physiol. 1996 Jul;271(1 Pt 1):G1-7.

104.	Katschinski M, Steinicke C, Reinshagen M, Dahmen G, Beglinger C, Arnold R, et al. Gastrointestinal motor and secretory responses to cholinergic stimulation in humans. Differential modulation by muscarinic and cholecystokinin receptor blockade. Eur J Clin Invest. 1995 Feb;25(2):113–22.

105.	Pandol SJ. Digestive Enzymes. 2010 [cited 2016 Feb 19]; Available from: http://www.ncbi.nlm.nih.gov/books/NBK54127/

106.	Schnefel S, Banfic H, Eckhardt L, Schultz G, Schulz I. Acetylcholine and cholecystokinin receptors functionally couple by different G-proteins to phospholipase C in pancreatic acinar cells. FEBS Lett. 1988 Mar 28;230(1):125–30.

107.	Bianchi BR, Miller TR, Witte DG, Lin CW. Novel CCK analogues and bombesin: a detailed analysis between phosphoinositide breakdown and high-dose inhibition of pancreatic enzyme secretion in three rodent species. J Pharmacol Exp Ther. 1994 Feb 1;268(2):996–1002.

108.	Kisfalvi K, Rácz G, Zsirka-Klein A, Pelosini I, Scarpignato C, Varga G. Different affinity states of CCK1 receptors on pancreatic acini and gastric smooth muscle in the rat. J Physiol-Paris. 2001 Jan;95(1–6):391–8.

109.	Sternfeld L, Krause E, Guse AH, Schulz I. Hormonal Control of ADP-ribosyl Cyclase Activity in Pancreatic Acinar Cells from Rats. J Biol Chem. 2003 Sep 5;278(36):33629–36.

110.	Cosker F, Cheviron N, Yamasaki M, Menteyne A, Lund FE, Moutin M-J, et al. The Ecto-enzyme CD38 Is a Nicotinic Acid Adenine Dinucleotide Phosphate (NAADP) Synthase That Couples Receptor Activation to Ca2+ Mobilization from Lysosomes in Pancreatic Acinar Cells. J Biol Chem. 2010 Dec 3;285(49):38251–9.

111.	Yamasaki M, Thomas JM, Churchill GC, Garnham C, Lewis AM, Cancela J-M, et al. Role of NAADP and cADPR in the Induction and Maintenance of Agonist-Evoked Ca2+ Spiking in Mouse Pancreatic Acinar Cells. Curr Biol. 2005 May 10;15(9):874–8.

112.	Lee HC, Aarhus R. A derivative of NADP mobilizes calcium stores insensitive to inositol trisphosphate and cyclic ADP-ribose. J Biol Chem. 1995 Feb 3;270(5):2152–7.

113.	Cancela JM, Churchill GC, Galione A. Coordination of agonist-induced Ca2+-signalling patterns by NAADP in pancreatic acinar cells. Nature. 1999 Mar 4;398(6722):74–6.

114.	Thorn P, Gerasimenko O, Petersen OH. Cyclic ADP-ribose regulation of ryanodine receptors involved in agonist evoked cytosolic Ca2+ oscillations in pancreatic acinar cells. EMBO J. 1994 May 1;13(9):2038–43.

115. Brailoiu E, Churamani D, Cai X, Schrlau MG, Brailoiu GC, Gao X, et al. Essential requirement for two-pore channel 1 in NAADP-mediated calcium signaling. J Cell Biol. 2009 Jul 27;186(2):201–9.

116. Kasai H, Li YX, Miyashita Y. Subcellular distribution of Ca2+ release channels underlying Ca2+ waves and oscillations in exocrine pancreas. Cell. 1993 Aug 27;74(4):669–77.

117. Ashby MC, Craske M, Park MK, Gerasimenko OV, Burgoyne RD, Petersen OH, et al. Localized Ca2+ uncaging reveals polarized distribution of Ca2+-sensitive Ca2+ release sites mechanism of unidirectional Ca2+ waves. J Cell Biol. 2002 Jul 22;158(2):283–92.

118. Maruyama Y, Petersen OH. Delay in granular fusion evoked by repetitive cytosolic Ca2+ spikes in mouse pancreatic acinar cells. Cell Calcium. 1994 Nov 1;16(5):419–30.

119. Ito K, Miyashita Y, Kasai H. Micromolar and submicromolar Ca2+ spikes regulating distinct cellular functions in pancreatic acinar cells. EMBO J. 1997 Jan 15;16(2):242–51.

120. Petersen CC, Toescu EC, Petersen OH. Different patterns of receptor-activated cytoplasmic Ca2+ oscillations in single pancreatic acinar cells: dependence on receptor type, agonist concentration and intracellular Ca2+ buffering. EMBO J. 1991 Mar;10(3):527–33.

121. Tinel H, Cancela JM, Mogami H, Gerasimenko JV, Gerasimenko OV, Tepikin AV, et al. Active mitochondria surrounding the pancreatic acinar granule region prevent spreading of inositol trisphosphate-evoked local cytosolic Ca(2+) signals. EMBO J. 1999 Sep 15;18(18):4999–5008.

122. Park MK, Ashby MC, Erdemli G, Petersen OH, Tepikin AV. Perinuclear, perigranular and sub-plasmalemmal mitochondria have distinct functions in the regulation of cellular calcium transport. EMBO J. 2001 Apr 17;20(8):1863–74.

123. Voronina S, Sukhomlin T, Johnson PR, Erdemli G, Petersen OH, Tepikin A. Correlation of NADH and Ca2+ signals in mouse pancreatic acinar cells. J Physiol. 2002 Feb 1;539(1):41–52.

124. Fogarty KE, Kidd JF, Tuft DA, Thorn P. Mechanisms underlying InsP3-evoked global Ca2+ signals in mouse pancreatic acinar cells. J Physiol. 2000 Aug 1;526 Pt 3:515–26.

125. Yule D i., Gallacher D v. Oscillations of cytosolic calcium in single pancreatic acinar cells stimulated by acetylcholine. FEBS Lett. 1988 Nov 7;239(2):358–62.

126. Wakui M, Potter BV, Petersen OH. Pulsatile intracellular calcium release does not depend on fluctuations in inositol trisphosphate concentration. Nature. 1989 May 25;339(6222):317–20.

127. Prakriya M, Lewis RS. Store-Operated Calcium Channels. Physiol Rev. 2015 Oct;95(4):1383–436.

128. Lur G, Haynes LP, Prior IA, Gerasimenko OV, Feske S, Petersen OH, et al. Ribosome-free terminals of rough ER allow formation of STIM1 puncta and segregation of STIM1 from IP(3) receptors. Curr Biol CB. 2009 Oct 13;19(19):1648–53.

129. Dingsdale H, Voronina S, Haynes L, Tepikin A, Lur G. Cellular geography of IP3 receptors, STIM and Orai: a lesson from secretory epithelial cells. Biochem Soc Trans. 2012 Feb;40(1):108–11.

130. Gerasimenko JV, Gryshchenko O, Ferdek PE, Stapleton E, Hébert TOG, Bychkova S, et al. Ca2+ release-activated Ca2+ channel blockade as a potential tool in antipancreatitis therapy. Proc Natl Acad Sci. 2013 Aug 6;110(32):13186–91.

131. Gerasimenko JV, Sherwood M, Tepikin AV, Petersen OH, Gerasimenko OV. NAADP, cADPR and IP3 all release Ca2+ from the endoplasmic reticulum and an acidic store in the secretory granule area. J Cell Sci. 2006 Jan 15;119(2):226–38.

132. Tepikin AV, Voronina SG, Gallacher DV, Petersen OH. Acetylcholine-evoked increase in the cytoplasmic Ca2+ concentration and Ca2+ extrusion measured simultaneously in single mouse pancreatic acinar cells. J Biol Chem. 1992 Feb 25;267(6):3569–72.

133. Zhang BX, Zhao H, Loessberg P, Muallem S. Activation of the plasma membrane Ca2+ pump during agonist stimulation of pancreatic acini. J Biol Chem. 1992 Aug 5;267(22):15419–25.

134. Lee MG, Xu X, Zeng W, Diaz J, Kuo TH, Wuytack F, et al. Polarized expression of Ca2+ pumps in pancreatic and salivary gland cells. Role in initiation and propagation of [Ca2+]i waves. J Biol Chem. 1997 Jun 20;272(25):15771–6.

135. Camello P, Gardner J, Petersen OH, Tepikin AV. Calcium dependence of calcium extrusion and calcium uptake in mouse pancreatic acinar cells. J Physiol. 1996 Feb 1;490 (Pt 3):585–93.

136. Wakasugi H, Kimura T, Haase W, Kribben A, Kaufmann R, Schulz I. Calcium uptake into acini from rat pancreas: evidence for intracellular ATP-dependent calcium sequestration. J Membr Biol. 1982;65(3):205–20.

137. Park MK, Petersen OH, Tepikin AV. The endoplasmic reticulum as one continuous Ca(2+) pool: visualization of rapid Ca(2+) movements and equilibration. EMBO J. 2000 Nov 1;19(21):5729–39.

138. Parekh AB, Putney JW Jr. Store-operated calcium channels. Physiol Rev. 2005 Apr;85(2):757–810.

139. Hogan PG, Chen L, Nardone J, Rao A. Transcriptional regulation by calcium, calcineurin, and NFAT. Genes Dev. 2003 Sep 15;17(18):2205–32.

140. Kar P, Nelson C, Parekh AB. CRAC Channels Drive Digital Activation and Provide Analog Control and Synergy to Ca2+-Dependent Gene Regulation. Curr Biol. 2012 Feb 7;22(3):242–7.

141. Casteels R, Droogmans G. Exchange characteristics of the noradrenaline-sensitive calcium store in vascular smooth muscle cells or rabbit ear artery. J Physiol. 1981 Aug 1;317(1):263–79.

142. Putney JW Jr. A model for receptor-regulated calcium entry. Cell Calcium. 1986 Feb;7(1):1–12.

143. Parod RJ, Putney JW. The role of calcium in the receptor mediated control of potassium permeability in the rat lacrimal gland. J Physiol. 1978 Aug 1;281(1):371–81.

144. Putney JW. Muscarinic, alpha-adrenergic and peptide receptors regulate the same calcium influx sites in the parotid gland. J Physiol. 1977 Jun;268(1):139–49.

145. Putney JW. Recent breakthroughs in the molecular mechanism of capacitative calcium entry (with thoughts on how we got here). Cell Calcium. 2007 Aug;42(2):103–10.

146. Takemura H, Hughes AR, Thastrup O, Putney JW. Activation of calcium entry by the tumor promoter thapsigargin in parotid acinar cells. Evidence that an intracellular calcium pool and not an inositol phosphate regulates calcium fluxes at the plasma membrane. J Biol Chem. 1989 Jul 25;264(21):12266–71.

147. Hoth M, Penner R. Depletion of intracellular calcium stores activates a calcium current in mast cells. Nature. 1992 Jan 23;355(6358):353–6.

148. Hoth M, Penner R. Calcium release-activated calcium current in rat mast cells. J Physiol. 1993 Jun;465:359–86.

149. Lepple-Wienhues A, Cahalan MD. Conductance and permeation of monovalent cations through depletion-activated Ca2+ channels (ICRAC) in Jurkat T cells. Biophys J. 1996 Aug 1;71(2):787–94.

150. Roos J, DiGregorio PJ, Yeromin AV, Ohlsen K, Lioudyno M, Zhang S, et al. STIM1, an essential and conserved component of store-operated Ca2+ channel function. J Cell Biol. 2005 May 9;169(3):435–45.

151. Liou J, Kim ML, Heo WD, Jones JT, Myers JW, Ferrell JE Jr, et al. STIM is a Ca2+ sensor essential for Ca2+-store-depletion-triggered Ca2+ influx. Curr Biol CB. 2005 Jul 12;15(13):1235–41.

152. Feske S, Gwack Y, Prakriya M, Srikanth S, Puppel S-H, Tanasa B, et al. A mutation in Orai1 causes immune deficiency by abrogating CRAC channel function. Nature. 2006 May 11;441(7090):179–85.

153. Zhang SL, Yeromin AV, Zhang XH-F, Yu Y, Safrina O, Penna A, et al. Genome-wide RNAi screen of Ca(2+) influx identifies genes that regulate Ca(2+) release-activated Ca(2+) channel activity. Proc Natl Acad Sci U S A. 2006 Jun 13;103(24):9357–62.

154. Vig M, Peinelt C, Beck A, Koomoa DL, Rabah D, Koblan-Huberson M, et al. CRACM1 is a plasma membrane protein essential for store-operated Ca2+ entry. Science. 2006 May 26;312(5777):1220–3.

155. Zhang SL, Yu Y, Roos J, Kozak JA, Deerinck TJ, Ellisman MH, et al. STIM1 is a Ca2+ sensor that activates CRAC channels and migrates from the Ca2+ store to the plasma membrane. Nature. 2005 Oct 6;437(7060):902–5.

156. Prakriya M, Feske S, Gwack Y, Srikanth S, Rao A, Hogan PG. Orai1 is an essential pore subunit of the CRAC channel. Nature. 2006 Sep 14;443(7108):230–3.

157. Sather WA, McCleskey EW. Permeation and Selectivity in Calcium Channels. Annu Rev Physiol. 2003;65(1):133–59.

158. Prakriya M, Lewis RS. Regulation of CRAC Channel Activity by Recruitment of Silent Channels to a High Open-probability Gating Mode. J Gen Physiol. 2006 Sep 1;128(3):373–86.

159. Mullins FM, Chan YP, Dolmetsch RE, Lewis RS. STIM1 and calmodulin interact with Orai1 to induce Ca2+-dependent inactivation of CRAC channels. Proc Natl Acad Sci U S A. 2009 Sep 8;106(36):15495–500.

160. Liu Y, Zheng X, Mueller GA, Sobhany M, DeRose EF, Zhang Y, et al. Crystal Structure of Calmodulin Binding Domain of Orai1 in Complex with Ca2+•Calmodulin Displays a Unique Binding Mode. J Biol Chem. 2012 Dec 14;287(51):43030–41.

161. Peterson BZ, DeMaria CD, Yue DT. Calmodulin Is the Ca2+ Sensor for Ca2+-Dependent Inactivation of L-Type Calcium Channels. Neuron. 1999 Mar 1;22(3):549–58.

162. Roberts-Thomson SJ, Peters AA, Grice DM, Monteith GR. ORAI-mediated calcium entry: mechanism and roles, diseases and pharmacology. Pharmacol Ther. 2010 Aug;127(2):121–30.

163. Luik RM, Wu MM, Buchanan J, Lewis RS. The elementary unit of store-operated Ca2+ entry: local activation of CRAC channels by STIM1 at ER-plasma membrane junctions. J Cell Biol. 2006 Sep 11;174(6):815–25.

164. Wu MM, Buchanan J, Luik RM, Lewis RS. Ca2+ store depletion causes STIM1 to accumulate in ER regions closely associated with the plasma membrane. J Cell Biol. 2006 Sep 11;174(6):803–13.

165. Muik M, Frischauf I, Derler I, Fahrner M, Bergsmann J, Eder P, et al. Dynamic coupling of the putative coiled-coil domain of ORAI1 with STIM1 mediates ORAI1 channel activation. J Biol Chem. 2008 Mar 21;283(12):8014–22.

166. Navarro-Borelly L, Somasundaram A, Yamashita M, Ren D, Miller RJ, Prakriya M. STIM1-Orai1 interactions and Orai1 conformational changes revealed by live-cell FRET microscopy. J Physiol. 2008 Nov 15;586(22):5383–401.

167. Luik RM, Wang B, Prakriya M, Wu MM, Lewis RS. Oligomerization of STIM1 couples ER calcium depletion to CRAC channel activation. Nature. 2008 Jul 24;454(7203):538–42.

168. Stathopulos PB, Li G-Y, Plevin MJ, Ames JB, Ikura M. Stored Ca2+ Depletion-induced Oligomerization of Stromal Interaction Molecule 1 (STIM1) via the EF-SAM

Region an Initiation Mechanism for Capacatitice Ca^{2+} entry. J Biol Chem. 2006 Nov 24;281(47):35855–62.

169.   Covington ED, Wu MM, Lewis RS. Essential role for the CRAC activation domain in store-dependent oligomerization of STIM1. Mol Biol Cell. 2010 Jun 1;21(11):1897–907.

170.   Park CY, Hoover PJ, Mullins FM, Bachhawat P, Covington ED, Raunser S, et al. STIM1 Clusters and Activates CRAC Channels via Direct Binding of a Cytosolic Domain to Orai1. Cell. 2009 Mar 6;136(5):876–90.

171.   Zhou Y, Meraner P, Kwon HT, Machnes D, Oh-hora M, Zimmer J, et al. STIM1 gates the store-operated calcium channel ORAI1 in vitro. Nat Struct Mol Biol. 2010 Jan;17(1):112–6.

172.   Liou J, Fivaz M, Inoue T, Meyer T. Live-cell imaging reveals sequential oligomerization and local plasma membrane targeting of stromal interaction molecule 1 after Ca2+ store depletion. Proc Natl Acad Sci U S A. 2007 May 29;104(22):9301–6.

173.   Soboloff J, Spassova MA, Tang XD, Hewavitharana T, Xu W, Gill DL. Orai1 and STIM Reconstitute Store-operated Calcium Channel Function. J Biol Chem. 2006 Jul 28;281(30):20661–5.

174.   Srikanth S, Jung H-J, Kim K-D, Souda P, Whitelegge J, Gwack Y. A novel EF-hand protein, CRACR2A, is a cytosolic Ca2+ sensor that stabilizes CRAC channels in T cells. Nat Cell Biol. 2010 May;12(5):436–46.

175.   Palty R, Raveh A, Kaminsky I, Meller R, Reuveny E. SARAF Inactivates the Store Operated Calcium Entry Machinery to Prevent Excess Calcium Refilling. Cell. 2012 Apr 13;149(2):425–38.

176.   Bauer MC, O'Connell D, Cahill DJ, Linse S. Calmodulin Binding to the Polybasic C-Termini of STIM Proteins Involved in Store-Operated Calcium Entry†. Biochemistry (Mosc). 2008 Jun 1;47(23):6089–91.

177.   Kar P, Samanta K, Kramer H, Morris O, Bakowski D, Parekh AB. Dynamic Assembly of a Membrane Signaling Complex Enables Selective Activation of NFAT by Orai1. Curr Biol. 2014 Jun 16;24(12):1361–8.

178.   Lewis RS. Store-operated calcium channels: new perspectives on mechanism and function. Cold Spring Harb Perspect Biol. 2011 Dec;3(12).

179.   Sun S, Zhang H, Liu J, Popugaeva E, Xu N-J, Feske S, et al. Reduced Synaptic STIM2 Expression and Impaired Store-Operated Calcium Entry Cause Destabilization of Mature Spines in Mutant Presenilin Mice. Neuron. 2014 Apr 2;82(1):79–93.

180.   Chen Y-F, Chiu W-T, Chen Y-T, Lin P-Y, Huang H-J, Chou C-Y, et al. Calcium store sensor stromal-interaction molecule 1-dependent signaling plays an important role in cervical cancer growth, migration, and angiogenesis. Proc Natl Acad Sci U S A. 2011 Sep 13;108(37):15225–30.

181. Kondratska K, Kondratskyi A, Yassine M, Lemonnier L, Lepage G, Morabito A, et al. Orai1 and STIM1 mediate SOCE and contribute to apoptotic resistance of pancreatic adenocarcinoma. Biochim Biophys Acta. 2014 Oct;1843(10):2263–9.

182. Raphaël M, Lehen'kyi V 'yacheslav, Vandenberghe M, Beck B, Khalimonchyk S, Vanden Abeele F, et al. TRPV6 calcium channel translocates to the plasma membrane via Orai1-mediated mechanism and controls cancer cell survival. Proc Natl Acad Sci U S A. 2014 Sep 16;111(37):E3870-3879.

183. Parekh AB. Store-operated CRAC channels: function in health and disease. Nat Rev Drug Discov. 2010 May;9(5):399–410.

184. Spinelli AM, González-Cobos JC, Zhang X, Motiani RK, Rowan S, Zhang W, et al. Airway smooth muscle STIM1 and Orai1 are upregulated in asthmatic mice and mediate PDGF-activated SOCE, CRAC currents, proliferation, and migration. Pflüg Arch Eur J Physiol. 2012 Nov;464(5):481–92.

185. Lacruz RS, Feske S. Diseases caused by mutations in ORAI1 and STIM1. Ann N Y Acad Sci. 2015 Nov;1356:45–79.

186. Kaufmann U, Shaw PJ, Kozhaya L, Subramanian R, Gaida K, Unutmaz D, et al. Selective ORAI1 Inhibition Ameliorates Autoimmune Central Nervous System Inflammation by Suppressing Effector but Not Regulatory T Cell Function. J Immunol Baltim Md 1950. 2016 Jan 15;196(2):573–85.

187. Raraty M, Ward J, Erdemli G, Vaillant C, Neoptolemos JP, Sutton R, et al. Calcium-dependent enzyme activation and vacuole formation in the apical granular region of pancreatic acinar cells. Proc Natl Acad Sci U S A. 2000 Nov 21;97(24):13126–31.

188. Lansman JB. Blockade of current through single calcium channels by trivalent lanthanide cations. Effect of ionic radius on the rates of ion entry and exit. J Gen Physiol. 1990 Apr 1;95(4):679–96.

189. Clapham DE, Runnels LW, Strübing C. The TRP ion channel family. Nat Rev Neurosci. 2001 Jun;2(6):387–96.

190. Herscher CJ, Rega AF. On the Mechanism of Inhibition of the PMCa2+ -ATPase by Lanthanum. Ann N Y Acad Sci. 1997 Nov 1;834(1):407–9.

191. Hou X, Pedi L, Diver MM, Long SB. Crystal Structure of the Calcium Release–Activated Calcium Channel Orai. Science. 2012 Dec 7;338(6112):1308–13.

192. Bootman MD, Collins TJ, Mackenzie L, Roderick HL, Berridge MJ, Peppiatt CM. 2-aminoethoxydiphenyl borate (2-APB) is a reliable blocker of store-operated Ca2+ entry but an inconsistent inhibitor of InsP3-induced Ca2+ release. FASEB J Off Publ Fed Am Soc Exp Biol. 2002 Aug;16(10):1145–50.

193. DeHaven WI, Smyth JT, Boyles RR, Bird GS, Putney JW. Complex actions of 2-aminoethyldiphenyl borate on store-operated calcium entry. J Biol Chem. 2008 Jul 11;283(28):19265–73.

194. Peinelt C, Lis A, Beck A, Fleig A, Penner R. 2-Aminoethoxydiphenyl borate directly facilitates and indirectly inhibits STIM1-dependent gating of CRAC channels. J Physiol. 2008 Jul 1;586(13):3061–73.

195. Schleifer H, Doleschal B, Lichtenegger M, Oppenrieder R, Derler I, Frischauf I, et al. Novel pyrazole compounds for pharmacological discrimination between receptor-operated and store-operated Ca2+ entry pathways. Br J Pharmacol. 2012 Dec;167(8):1712–22.

196. He L-P, Hewavitharana T, Soboloff J, Spassova MA, Gill DL. A Functional Link between Store-operated and TRPC Channels Revealed by the 3,5-Bis(trifluoromethyl)pyrazole Derivative, BTP2. J Biol Chem. 2005 Mar 25;280(12):10997–1006.

197. Trevillyan JM, Chiou XG, Chen YW, Ballaron SJ, Sheets MP, Smith ML, et al. Potent inhibition of NFAT activation and T cell cytokine production by novel low molecular weight pyrazole compounds. J Biol Chem. 2001 Dec 21;276(51):48118–26.

198. Ishikawa J, Ohga K, Yoshino T, Takezawa R, Ichikawa A, Kubota H, et al. A pyrazole derivative, YM-58483, potently inhibits store-operated sustained Ca2+ influx and IL-2 production in T lymphocytes. J Immunol Baltim Md 1950. 2003 May 1;170(9):4441–9.

199. Zitt C, Strauss B, Schwarz EC, Spaeth N, Rast G, Hatzelmann A, et al. Potent inhibition of Ca2+ release-activated Ca2+ channels and T-lymphocyte activation by the pyrazole derivative BTP2. J Biol Chem. 2004 Mar 26;279(13):12427–37.

200. Takezawa R, Cheng H, Beck A, Ishikawa J, Launay P, Kubota H, et al. A pyrazole derivative potently inhibits lymphocyte Ca2+ influx and cytokine production by facilitating transient receptor potential melastatin 4 channel activity. Mol Pharmacol. 2006 Apr;69(4):1413–20.

201. Ng SW, di Capite J, Singaravelu K, Parekh AB. Sustained activation of the tyrosine kinase Syk by antigen in mast cells requires local Ca2+ influx through Ca2+ release-activated Ca2+ channels. J Biol Chem. 2008 Nov 14;283(46):31348–55.

202. Di Sabatino A, Rovedatti L, Kaur R, Spencer JP, Brown JT, Morisset VD, et al. Targeting gut T cell Ca2+ release-activated Ca2+ channels inhibits T cell cytokine production and T-box transcription factor T-bet in inflammatory bowel disease. J Immunol Baltim Md 1950. 2009 Sep 1;183(5):3454–62.

203. Li J, McKeown L, Ojelabi O, Stacey M, Foster R, O'Regan D, et al. Nanomolar potency and selectivity of a Ca2+ release-activated Ca2+ channel inhibitor against store-operated Ca2+ entry and migration of vascular smooth muscle cells. Br J Pharmacol. 2011 Sep 1;164(2):382–93.

204. Ashmole I, Duffy SM, Leyland ML, Morrison VS, Begg M, Bradding P. CRACM/Orai ion channel expression and function in human lung mast cells. J Allergy Clin Immunol. 2012 Jun 1;129(6):1628–1635.e2.

205. Derler I, Schindl R, Fritsch R, Heftberger P, Riedl MC, Begg M, et al. The action of selective CRAC channel blockers is affected by the Orai pore geometry. Cell Calcium. 2013 Feb;53(2):139–51.

206. Rice LV, Bax HJ, Russell LJ, Barrett VJ, Walton SE, Deakin AM, et al. Characterization of selective Calcium-Release Activated Calcium channel blockers in mast cells and T-cells from human, rat, mouse and guinea-pig preparations. Eur J Pharmacol. 2013 Mar 15;704(1–3):49–57.

207. Chaudhari S, Wu P, Wang Y, Ding Y, Yuan J, Begg M, et al. High glucose and diabetes enhanced store-operated Ca2+ entry and increased expression of its signaling proteins in mesangial cells. Am J Physiol Renal Physiol. 2014 May;306(9):F1069-1080.

208. Vegas AJ, Fuller JH, Koehler AN. Small-molecule microarrays as tools in ligand discovery. Chem Soc Rev. 2008 Jul;37(7):1385–94.

209. Sadaghiani AM, Lee SM, Odegaard JI, Leveson-Gower DB, McPherson OM, Novick P, et al. Identification of Orai1 Channel Inhibitors by Using Minimal Functional Domains to Screen Small Molecule Microarrays. Chem Biol. 2014 Oct 23;21(10):1278–92.

210. Cui J, Bian J-S, Kagan A, McDonald TV. CaT1 Contributes to the Stores-operated Calcium Current in Jurkat T-lymphocytes. J Biol Chem. 2002 Dec 6;277(49):47175–83.

211. Philipp S, Strauss B, Hirnet D, Wissenbach U, Mery L, Flockerzi V, et al. TRPC3 mediates T-cell receptor-dependent calcium entry in human T-lymphocytes. J Biol Chem. 2003 Jul 18;278(29):26629–38.

212. Mori Y, Wakamori M, Miyakawa T, Hermosura M, Hara Y, Nishida M, et al. Transient receptor potential 1 regulates capacitative Ca(2+) entry and Ca(2+) release from endoplasmic reticulum in B lymphocytes. J Exp Med. 2002 Mar 18;195(6):673–81.

213. Worley PF, Zeng W, Huang GN, Yuan JP, Kim JY, Lee MG, et al. TRPC channels as STIM1-regulated store-operated channels. Cell Calcium. 2007 Aug;42(2):205–11.

214. Yuan JP, Zeng W, Huang GN, Worley PF, Muallem S. STIM1 heteromultimerizes TRPC channels to determine their function as store-operated channels. Nat Cell Biol. 2007 Jun;9(6):636–45.

215. Zeng W, Yuan JP, Kim MS, Choi YJ, Huang GN, Worley PF, et al. STIM1 Gates TRPC Channels, but Not Orai1, by Electrostatic Interaction. Mol Cell. 2008 Nov 7;32(3):439–48.

216. Zhu X, Jiang M, Peyton M, Boulay G, Hurst R, Stefani E, et al. trp, a novel mammalian gene family essential for agonist-activated capacitative Ca2+ entry. Cell. 1996 May 31;85(5):661–71.

217. Liu X, Wang W, Singh BB, Lockwich T, Jadlowiec J, O'Connell B, et al. Trp1, a candidate protein for the store-operated Ca(2+) influx mechanism in salivary gland cells. J Biol Chem. 2000 Feb 4;275(5):3403–11.

218. Liu X, Cheng KT, Bandyopadhyay BC, Pani B, Dietrich A, Paria BC, et al. Attenuation of store-operated Ca2+ current impairs salivary gland fluid secretion in TRPC1(-/-) mice. Proc Natl Acad Sci U S A. 2007 Oct 30;104(44):17542–7.

219. Kim JY, Zeng W, Kiselyov K, Yuan JP, Dehoff MH, Mikoshiba K, et al. Homer 1 Mediates Store- and Inositol 1,4,5-Trisphosphate Receptor-dependent Translocation and Retrieval of TRPC3 to the Plasma Membrane. J Biol Chem. 2006 Oct 27;281(43):32540–9.

220. Kim MS, Hong JH, Li Q, Shin DM, Abramowitz J, Birnbaumer L, et al. Deletion of TRPC3 in mice reduces Store-Operated Ca2+ influx and the severity of acute pancreatitis. Gastroenterology. 2009 Oct;137(4):1509–17.

221. Kim MS, Lee KP, Yang D, Shin DM, Abramowitz J, Kiyonaka S, et al. Genetic and Pharmacological Inhibition of the Ca2+ Influx Channel TRPC3 Protects Secretory Epithelia from Ca2+-Dependent Toxicity. Gastroenterology. 2011 Jun;140(7):2107–2115.e4.

222. Lee KP, Choi S, Hong JH, Ahuja M, Graham S, Ma R, et al. Molecular Determinants Mediating Gating of Transient Receptor Potential Canonical (TRPC) Channels by Stromal Interaction Molecule 1 (STIM1). J Biol Chem. 2014 Mar 7;289(10):6372–82.

223. Pandol SJ, Saluja AK, Imrie CW, Banks PA. Acute pancreatitis: bench to the bedside. Gastroenterology. 2007 Mar;132(3):1127–51.

224. Choices NHS. Acute pancreatitis - NHS Choices [Internet]. 2015 [cited 2016 Feb 22]. Available from: http://www.nhs.uk/conditions/Pancreatitis/Pages/Introduction.aspx

225. Peery AF, Dellon ES, Lund J, Crockett SD, McGowan CE, Bulsiewicz WJ, et al. Burden of Gastrointestinal Disease in the United States: 2012 Update. Gastroenterology. 2012 Nov;143(5):1179–1187.e3.

226. Wu BU, Banks PA. Clinical management of patients with acute pancreatitis. Gastroenterology. 2013 Jun;144(6):1272–81.

227. Lankisch PG, Apte M, Banks PA. Acute pancreatitis. The Lancet. 2015 Jul 10;386(9988):85–96.

228. Johnson CD, Besselink MG, Carter R. Acute pancreatitis. BMJ. 2014;349:g4859.

229. Raimondi S, Lowenfels AB, Morselli-Labate AM, Maisonneuve P, Pezzilli R. Pancreatic cancer in chronic pancreatitis; aetiology, incidence, and early detection. Best Pract Res Clin Gastroenterol. 2010 Jun;24(3):349–58.

230. Williams JA. Receptor-mediated signal transduction pathways and the regulation of pancreatic acinar cell function. Curr Opin Gastroenterol. 2008 Sep;24(5):573–9.

231. Petersen OH, Sutton R. Ca2+ signalling and pancreatitis: effects of alcohol, bile and coffee. Trends Pharmacol Sci. 2006 Feb;27(2):113–20.

232. Xue J, Sharma V, Habtezion A. Immune cells and immune-based therapy in pancreatitis. Immunol Res. 2014 May;58(2–3):378–86.

233. Gukovskaya AS, Gukovsky I, Zaninovic V, Song M, Sandoval D, Gukovsky S, et al. Pancreatic acinar cells produce, release, and respond to tumor necrosis factor-alpha. Role in regulating cell death and pancreatitis. J Clin Invest. 1997 Oct 1;100(7):1853–62.

234. Petersen OH. Ca2+ signaling in pancreatic acinar cells: physiology and pathophysiology. Braz J Med Biol Res Rev Bras Pesqui Médicas E Biológicas Soc Bras Biofísica Al. 2009 Jan;42(1):9–16.

235. Krüger B, Albrecht E, Lerch MM. The Role of Intracellular Calcium Signaling in Premature Protease Activation and the Onset of Pancreatitis. Am J Pathol. 2000 Jul;157(1):43–50.

236. Laposata EA, Lange LG. Presence of nonoxidative ethanol metabolism in human organs commonly damaged by ethanol abuse. Science. 1986 Jan 31;231(4737):497–9.

237. Criddle DN, Raraty MGT, Neoptolemos JP, Tepikin AV, Petersen OH, Sutton R. Ethanol toxicity in pancreatic acinar cells: mediation by nonoxidative fatty acid metabolites. Proc Natl Acad Sci U S A. 2004 Jul 20;101(29):10738–43.

238. Petersen OH, Tepikin AV, Gerasimenko JV, Gerasimenko OV, Sutton R, Criddle DN. Fatty acids, alcohol and fatty acid ethyl esters: Toxic Ca2+ signal generation and pancreatitis. Cell Calcium. 2009 Jun;45(6):634–42.

239. Roberts SE, Williams JG, Meddings D, Goldacre MJ. Incidence and case fatality for acute pancreatitis in England: geographical variation, social deprivation, alcohol consumption and aetiology – a record linkage study. Aliment Pharmacol Ther. 2008 Oct 1;28(7):931–41.

240. Irving HM, Samokhvalov AV, Rehm J. Alcohol as a risk factor for pancreatitis. A systematic review and meta-analysis. JOP J Pancreas. 2009;10(4):387–92.

241. Siech M, Heinrich P, Letko G. Development of acute pancreatitis in rats after single ethanol administration and induction of a pancreatic juice edema. Int J Pancreatol Off J Int Assoc Pancreatol. 1991 Feb;8(2):169–75.

242. Pandol SJ, Periskic S, Gukovsky I, Zaninovic V, Jung Y, Zong Y, et al. Ethanol diet increases the sensitivity of rats to pancreatitis induced by cholecystokinin octapeptide. Gastroenterology. 1999 Sep;117(3):706–16.

243. Zhan X, Wang F, Bi Y, Ji B. Animal Models of Acute and Chronic Pancreatitis. Am J Physiol Gastrointest Liver Physiol. 2016 Jul 14;ajpgi.00372.2015.

244. Schneider A, Whitcomb DC, Singer MV. Animal Models in Alcoholic Pancreatitis — What Can We Learn? Pancreatology. 2002 Jan 1;2(3):189–203.

245. Criddle DN. The role of fat and alcohol in acute pancreatitis: A dangerous liaison. Pancreatology. 2015 Jul;15(4):S6–12.

246. Laposata M, Hasaba A, Best CA, Yoerger DM, McQuillan BM, Salem RO, et al. Fatty acid ethyl esters: recent observations. Prostaglandins Leukot Essent Fatty Acids. 2002 Aug;67(2–3):193–6.

247. Gukovskaya AS, Mouria M, Gukovsky I, Reyes CN, Kasho VN, Faller LD, et al. Ethanol metabolism and transcription factor activation in pancreatic acinar cells in rats. Gastroenterology. 2002 Jan;122(1):106–18.

248. Nordback IH, MacGowan S, Potter JJ, Cameron JL. The role of acetaldehyde in the pathogenesis of acute alcoholic pancreatitis. Ann Surg. 1991 Dec;214(6):671–8.

249. Lombardo D. Bile salt-dependent lipase: its pathophysiological implications. Biochim Biophys Acta BBA - Mol Cell Biol Lipids. 2001 Aug 29;1533(1):1–28.

250. Huang W, Booth DM, Cane MC, Chvanov M, Javed MA, Elliott VL, et al. Fatty acid ethyl ester synthase inhibition ameliorates ethanol-induced Ca2+-dependent mitochondrial dysfunction and acute pancreatitis. Gut. 2014 Aug 1;63(8):1313–24.

251. Werner J, Laposata M, Fernandez-del Castillo C, Saghir M, Iozzo R, Lewandrowski K, et al. Pancreatic injury in rats induced by fatty acid ethyl ester, a nonoxidative metabolite of alcohol. Gastroenterology. 1997 Jul;113(1):286–94.

252. Criddle DN, Murphy J, Fistetto G, Barrow S, Tepikin AV, Neoptolemos JP, et al. Fatty Acid Ethyl Esters Cause Pancreatic Calcium Toxicity via Inositol Trisphosphate Receptors and Loss of ATP Synthesis. Gastroenterology. 2006 Mar;130(3):781–93.

253. Wen L, Voronina S, Javed MA, Awais M, Szatmary P, Latawiec D, et al. Inhibitors of ORAI1 Prevent Cytosolic Calcium-Associated Injury of Human Pancreatic Acinar Cells and Acute Pancreatitis in 3 Mouse Models. Gastroenterology. 2015 Aug;149(2):481–+.

254. Lange LG, Sobel BE. Mitochondrial dysfunction induced by fatty acid ethyl esters, myocardial metabolites of ethanol. J Clin Invest. 1983 Aug;72(2):724–31.

255. Shalbueva N, Mareninova OA, Gerloff A, Yuan J, Waldron RT, Pandol SJ, et al. Effects of oxidative alcohol metabolism on the mitochondrial permeability transition pore and necrosis in a mouse model of alcoholic pancreatitis. Gastroenterology. 2013 Feb;144(2):437–446.e6.

256. Opie EL. The etiology of acute hemorrhagic pancreatitis. Bull Johns Hopkins Hosp. 1901;12:182–8.

257. Perides G, van Acker GJD, Laukkarinen JM, Steer ML. Experimental acute biliary pancreatitis induced by retrograde infusion of bile acids into the mouse pancreatic duct. Nat Protoc. 2010 Feb;5(2):335–41.

258. Kim JY, Kim KH, Lee JA, Namkung W, Sun A, Ananthanarayanan M, et al. Transporter-mediated bile acid uptake causes Ca2+-dependent cell death in rat pancreatic acinar cells. Gastroenterology. 2002 Jun;122(7):1941–53.

259. Voronina S, Longbottom R, Sutton R, Petersen OH, Tepikin A. Bile acids induce calcium signals in mouse pancreatic acinar cells: implications for bile-induced pancreatic pathology. J Physiol. 2002 Apr 1;540(Pt 1):49–55.

260. Hallam TJ, Rink TJ. Agonists stimulate divalent cation channels in the plasma membrane of human platelets. FEBS Lett. 1985 Jul 8;186(2):175–9.

261. Xu X, Star RA, Tortorici G, Muallem S. Depletion of intracellular Ca2+ stores activates nitric-oxide synthase to generate cGMP and regulate Ca2+ influx. J Biol Chem. 1994 Apr 29;269(17):12645–53.

262. Hofmann AF. The continuing importance of bile acids in liver and intestinal disease. Arch Intern Med. 1999 Dec 13;159(22):2647–58.

263. Moody FG, Senninger N, Runkel N. Another challenge to the Opie myth. Gastroenterology. 1993 Mar 1;104(3):927–31.

264. Voronina SG, Gryshchenko OV, Gerasimenko OV, Green AK, Petersen OH, Tepikin AV. Bile Acids Induce a Cationic Current, Depolarizing Pancreatic Acinar Cells and Increasing the Intracellular Na+ Concentration. J Biol Chem. 2005 Jan 21;280(3):1764–70.

265. Laukkarinen JM, Acker GJDV, Weiss ER, Steer ML, Perides G. A mouse model of acute biliary pancreatitis induced by retrograde pancreatic duct infusion of Na-taurocholate. Gut. 2007 Nov 1;56(11):1590–8.

266. Voronina SG, Barrow SL, Gerasimenko OV, Petersen OH, Tepikin AV. Effects of Secretagogues and Bile Acids on Mitochondrial Membrane Potential of Pancreatic Acinar Cells Comparison of Differnet modes of Evaluating $\Delta\Psi$m. J Biol Chem. 2004 Jun 25;279(26):27327–38.

267. Kambhampati S, Park W, Habtezion A. Pharmacologic therapy for acute pancreatitis. World J Gastroenterol WJG. 2014 Dec 7;20(45):16868–80.

268. Voronina S, Collier D, Chvanov M, Middlehurst B, Beckett AJ, Prior IA, et al. The role of Ca2+ influx in endocytic vacuole formation in pancreatic acinar cells. Biochem J. 2015 Feb 1;465:405–12.

269. Michikawa T, Hirota J, Kawano S, Hiraoka M, Yamada M, Furuichi T, et al. Calmodulin Mediates Calcium-Dependent Inactivation of the Cerebellar Type 1 Inositol 1,4,5-Trisphosphate Receptor. Neuron. 1999 Aug 1;23(4):799–808.

270. Booth DM, Murphy JA, Mukherjee R, Awais M, Neoptolemos JP, Gerasimenko OV, et al. Reactive oxygen species induced by bile acid induce apoptosis and protect against necrosis in pancreatic acinar cells. Gastroenterology. 2011 Jun;140(7):2116–25.

271. Halestrap AP, Richardson AP. The mitochondrial permeability transition: a current perspective on its identity and role in ischaemia/reperfusion injury. J Mol Cell Cardiol. 2015 Jan;78:129–41.

272. Baines CP, Kaiser RA, Purcell NH, Blair NS, Osinska H, Hambleton MA, et al. Loss of cyclophilin D reveals a critical role for mitochondrial permeability transition in cell death. Nature. 2005 Mar 31;434(7033):658–62.

273. Nakagawa T, Shimizu S, Watanabe T, Yamaguchi O, Otsu K, Yamagata H, et al. Cyclophilin D-dependent mitochondrial permeability transition regulates some necrotic but not apoptotic cell death. Nature. 2005 Mar 31;434(7033):652–8.

274. Shore ER, Awais M, Kershaw NM, Gibson RR, Pandalaneni S, Latawiec D, et al. Small Molecule Inhibitors of Cyclophilin D To Protect Mitochondrial Function as a Potential Treatment for Acute Pancreatitis. J Med Chem. 2016 Mar 24;59(6):2596–611.

275. Huang W, Cane MC, Mukherjee R, Szatmary P, Zhang X, Elliott V, et al. Caffeine protects against experimental acute pancreatitis by inhibition of inositol 1,4,5-trisphosphate receptor-mediated Ca2+ release. Gut. 2015 Dec 7;gutjnl-2015-309363.

276. Singh VK, Moran RA, Afghani E, de-Madaria E. Treating acute pancreatitis: what's new? Expert Rev Gastroenterol Hepatol. 2015 Jul;9(7):901–11.

277. Takeda K, Yamauchi J, Shibuya K, Sunamura M, Mikami Y, Matsuno S. Benefit of continuous regional arterial infusion of protease inhibitor and antibiotic in the management of acute necrotizing pancreatitis. Pancreatology. 2001 Jan 1;1(6):668–73.

278. Piaścik M, Rydzewska G, Milewski J, Olszewski S, Furmanek M, Walecki J, et al. The results of severe acute pancreatitis treatment with continuous regional arterial infusion of protease inhibitor and antibiotic: a randomized controlled study. Pancreas. 2010 Aug;39(6):863–7.

279. Seta T, Noguchi Y, Shikata S, Nakayama T. Treatment of acute pancreatitis with protease inhibitors administered through intravenous infusion: an updated systematic review and meta-analysis. BMC Gastroenterol. 2014;14:102.

280. Gukovskaya AS, Vaquero E, Zaninovic V, Gorelick FS, Lusis AJ, Brennan M-L, et al. Neutrophils and NADPH oxidase mediate intrapancreatic trypsin activation in murine experimental acute pancreatitis. Gastroenterology. 2002 Apr 1;122(4):974–84.

281. Gea-Sorlí S, Closa D. Role of macrophages in the progression of acute pancreatitis. World J Gastrointest Pharmacol Ther. 2010 Oct 6;1(5):107–11.

282. Akinosoglou K, Gogos C. Immune-modulating therapy in acute pancreatitis: Fact or fiction. World J Gastroenterol WJG. 2014 Nov 7;20(41):15200–15.

283. Yang Z, Meng X, Xu P. Central role of neutrophil in the pathogenesis of severe acute pancreatitis. J Cell Mol Med. 2015 Nov;19(11):2513–20.

284. Sendler M, Dummer A, Weiss FU, Krüger B, Wartmann T, Scharffetter-Kochanek K, et al. Tumour necrosis factor α secretion induces protease activation and acinar cell necrosis in acute experimental pancreatitis in mice. Gut. 2013 Mar;62(3):430–9.

285. Talukdar R, Saikia N, Singal DK, Tandon R. Chronic pancreatitis: Evolving paradigms. Pancreatology. 2006 Oct;6(5):440–9.

286. Maruyama T, Kanaji T, Nakade S, Kanno T, Mikoshiba K. 2APB, 2-Aminoethoxydiphenyl Borate, a Membrane-Penetrable Modulator of Ins(1,4,5)P3-Induced Ca2+ Release. J Biochem (Tokyo). 1997 Sep 1;122(3):498–505.

287. Prakriya M, Lewis RS. Potentiation and inhibition of Ca2+ release-activated Ca2+ channels by 2-aminoethyldiphenyl borate (2-APB) occurs independently of IP3 receptors. J Physiol. 2001 Oct 1;536(1):3–19.

288. Peppiatt CM, Collins TJ, Mackenzie L, Conway SJ, Holmes AB, Bootman MD, et al. 2-Aminoethoxydiphenyl borate (2-APB) antagonises inositol 1,4,5-trisphosphate-induced calcium release, inhibits calcium pumps and has a use-dependent and slowly reversible action on store-operated calcium entry channels. Cell Calcium. 2003 Jul;34(1):97–108.

289. Braun F-J, Aziz O, Putney JW. 2-Aminoethoxydiphenyl Borane Activates a Novel Calcium-Permeable Cation Channel. Mol Pharmacol. 2003 Jun 1;63(6):1304–11.

290. Gregory RB, Rychkov G, Barritt GJ. Evidence that 2-aminoethyl diphenylborate is a novel inhibitor of store-operated Ca2+ channels in liver cells, and acts through a mechanism which does not involve inositol trisphosphate receptors. Biochem J. 2001 Mar 1;354(Pt 2):285–90.

291. Kukkonen JP, Lund P-E, Åkerman KEO. 2-aminoethoxydiphenyl borate reveals heterogeneity in receptor-activated Ca2+discharge and store-operated Ca2+influx. Cell Calcium. 2001 Aug;30(2):117–29.

292. Bilmen JG, Wootton LL, Godfrey RE, Smart OS, Michelangeli F. Inhibition of SERCA Ca2+ pumps by 2-aminoethoxydiphenyl borate (2-APB). Eur J Biochem. 2002 Aug 1;269(15):3678–87.

293. DeHaven WI, Smyth JT, Boyles RR, Bird GS, Putney JWJ. Complex actions of 2-aminoethyldiphenyl borate on store-operated calcium entry. J Biol Chem. 2008 Jul 11;283(28):19265–73.

294. Ozaki S, Suzuki AZ, Bauer PO, Ebisui E, Mikoshiba K. 2-Aminoethyl diphenylborinate (2-APB) analogues: regulation of Ca2+ signaling. Biochem Biophys Res Commun. 2013 Nov 15;441(2):286–90.

295. Goto J-I, Suzuki AZ, Ozaki S, Matsumoto N, Nakamura T, Ebisui E, et al. Two novel 2-aminoethyl diphenylborinate (2-APB) analogues differentially activate and inhibit store-operated Ca2+ entry via STIM proteins. Cell Calcium. 2010 Jan;47(1):1–10.

296. Jairaman A, Prakriya M. Molecular pharmacology of store-operated CRAC channels. Channels. 2013 Sep 1;7(5):402–14.

297. Pedersen SF, Owsianik G, Nilius B. TRP channels: An overview. Cell Calcium. 2005 Sep;38(3–4):233–52.

298. Venkatachalam K, Montell C. TRP Channels. Annu Rev Biochem. 2007;76(1):387–417.

299. Huang GN, Zeng W, Kim JY, Yuan JP, Han L, Muallem S, et al. STIM1 carboxyl-terminus activates native SOC, I(crac) and TRPC1 channels. Nat Cell Biol. 2006 Sep;8(9):1003–10.

300. Cheung K-K, Yeung SS, Au SW, Lam LS, Dai Z-Q, Li Y-H, et al. Expression and association of TRPC1 with TRPC3 during skeletal myogenesis. Muscle Nerve. 2011 Sep 1;44(3):358–65.

301. Wu X, Zagranichnaya TK, Gurda GT, Eves EM, Villereal ML. A TRPC1/TRPC3-mediated Increase in Store-operated Calcium Entry Is Required for Differentiation of H19-7 Hippocampal Neuronal Cells. J Biol Chem. 2004 Oct 15;279(42):43392–402.

302. Liu X, Bandyopadhyay BC, Singh BB, Groschner K, Ambudkar IS. Molecular Analysis of a Store-operated and 2-Acetyl-sn-glycerol-sensitive Non-selective Cation Channel Heteromeric Assembly of TRPC1-TRPC3. J Biol Chem. 2005 Jun 3;280(22):21600–6.

303. Zagranichnaya TK, Wu X, Villereal ML. Endogenous TRPC1, TRPC3, and TRPC7 Proteins Combine to Form Native Store-operated Channels in HEK-293 Cells. J Biol Chem. 2005 Aug 19;280(33):29559–69.

304. Birnbaumer L. The TRPC class of ion channels: a critical review of their roles in slow, sustained increases in intracellular Ca(2+) concentrations. Annu Rev Pharmacol Toxicol. 2009;49:395–426.

305. Chen G, Panicker S, Lau K-Y, Apparsundaram S, Patel VA, Chen S-L, et al. Characterization of a novel CRAC inhibitor that potently blocks human T cell activation and effector functions. Mol Immunol. 2013 Jul;54(3–4):355–67.

306. Han Z, Madara JJ, Herbert A, Prugar LI, Ruthel G, Lu J, et al. Calcium Regulation of Hemorrhagic Fever Virus Budding: Mechanistic Implications for Host-Oriented Therapeutic Intervention. PLoS Pathog. 2015;11(10).

307. Sweeney ZK, Minatti A, Button DC, Patrick S. Small-Molecule Inhibitors of Store-Operated Calcium Entry. ChemMedChem. 2009 May 11;4(5):706–18.

308. Yonetoku Y, Kubota H, Miyazaki Y, Okamoto Y, Funatsu M, Yoshimura-Ishikawa N, et al. Novel potent and selective Ca2+ release-activated Ca2+ (CRAC) channel inhibitors. Part 3: Synthesis and CRAC channel inhibitory activity of 4′-[(trifluoromethyl)pyrazol-1-yl]carboxanilides. Bioorg Med Chem. 2008 Nov 1;16(21):9457–66.

309. Kiyonaka S, Kato K, Nishida M, Mio K, Numaga T, Sawaguchi Y, et al. Selective and direct inhibition of TRPC3 channels underlies biological activities of a pyrazole compound. Proc Natl Acad Sci. 2009 Mar 31;106(13):5400–5.

310. Kwan CY, Putney JW. Uptake and intracellular sequestration of divalent cations in resting and methacholine-stimulated mouse lacrimal acinar cells. Dissociation by Sr2+ and Ba2+ of agonist-stimulated divalent cation entry from the refilling of the agonist-sensitive intracellular pool. J Biol Chem. 1990 Jan 15;265(2):678–84.

311. Zeiger W, Ito D, Swetlik C, Oh-hora M, Villereal ML, Thinakaran G. Stanniocalcin 2 Is a Negative Modulator of Store-Operated Calcium Entry. Mol Cell Biol. 2011 Sep 15;31(18):3710–22.

312. Hoth M. Calcium and barium permeation through calcium release-activated calcium (CRAC) channels. Pflüg Arch. 430(3):315–22.

313. Mikami Y, Takeda K, Shibuya K, Qiu-Feng H, Egawa S, Sunamura M, et al. Peritoneal inflammatory cells in acute pancreatitis: Relationship of infiltration dynamics and cytokine production with severity of illness. Surgery. 2002 Jul;132(1):86–92.

314. Vaeth M, Zee I, Concepcion AR, Maus M, Shaw P, Portal-Celhay C, et al. Ca2+ Signaling but Not Store-Operated Ca2+ Entry Is Required for the Function of Macrophages and Dendritic Cells. J Immunol Baltim Md 1950. 2015 Aug 1;195(3):1202–17.

315. Choi KJ, Kim KS, Kim SH, Kim DK, Park HS. Caffeine and 2-Aminoethoxydiphenyl Borate (2-APB) Have Different Ability to Inhibit Intracellular Calcium Mobilization in Pancreatic Acinar Cell. Korean J Physiol Pharmacol Off J Korean Physiol Soc Korean Soc Pharmacol. 2010 Apr;14(2):105–11.

316. McCarl C-A, Picard C, Khalil S, Kawasaki T, Röther J, Papolos A, et al. ORAI1 deficiency and lack of store-operated Ca2+ entry cause immunodeficiency, myopathy and ectodermal dysplasia. J Allergy Clin Immunol. 2009 Dec;124(6):1311–1318.e7.

317. Inayama M, Suzuki Y, Yamada S, Kurita T, Yamamura H, Ohya S, et al. Orai1–Orai2 complex is involved in store-operated calcium entry in chondrocyte cell lines. Cell Calcium. 2015 May;57(5–6):337–47.

318. Schindl R, Frischauf I, Bergsmann J, Muik M, Derler I, Lackner B, et al. Plasticity in Ca2+ selectivity of Orai1/Orai3 heteromeric channel. Proc Natl Acad Sci U S A. 2009 Nov 17;106(46):19623–8.

319. Lis A, Peinelt C, Beck A, Parvez S, Monteilh-Zoller M, Fleig A, et al. CRACM1, CRACM2, and CRACM3 are store-operated Ca2+ channels with distinct functional properties. Curr Biol CB. 2007 May 1;17(9):794–800.

320. Gukovskaya AS, Pandol SJ. Cell death pathways in pancreatitis and pancreatic cancer. Pancreatol Off J Int Assoc Pancreatol IAP Al. 2004;4(6):567–86.

321. Bhatia M. Apoptosis of pancreatic acinar cells in acute pancreatitis: is it good or bad? J Cell Mol Med. 2004 Sep;8(3):402–9.

322. Criddle DN, Gerasimenko JV, Baumgartner HK, Jaffar M, Voronina S, Sutton R, et al. Calcium signalling and pancreatic cell death: apoptosis or necrosis? Cell Death Differ. 2007 Jul;14(7):1285–94.

323. Horinouchi T, Higashi T, Higa T, Terada K, Mai Y, Aoyagi H, et al. Different binding property of STIM1 and its novel splice variant STIM1L to Orai1, TRPC3, and TRPC6 channels. Biochem Biophys Res Commun. 2012 Nov 16;428(2):252–8.

324. Ampem PT, Smedlund K, Vazquez G. Pharmacological evidence for a role of the transient receptor potential canonical 3 (TRPC3) channel in endoplasmic reticulum stress-induced apoptosis of human coronary artery endothelial cells. Vascul Pharmacol. 2015 Jul 26;

325. Alkhani H, Ase AR, Grant R, O'Donnell D, Groschner K, Séguéla P. Contribution of TRPC3 to store-operated calcium entry and inflammatory transductions in primary nociceptors. Mol Pain. 2014;10:43.

326. Di Capite J, Nelson C, Bates G, Parekh AB. Targeting Ca2+ release-activated Ca2+ channel channels and leukotriene receptors provides a novel combination strategy for treating nasal polyposis. J Allergy Clin Immunol. 2009 Nov;124(5):1014-1021-3.

327. Gout J, Pommier RM, Vincent DF, Kaniewski B, Martel S, Valcourt U, et al. Isolation and Culture of Mouse Primary Pancreatic Acinar Cells. J Vis Exp JoVE. 2013; (78).

328. Ferdek PE, Gerasimenko JV, Peng S, Tepikin AV, Petersen OH, Gerasimenko OV. A Novel Role for Bcl-2 in Regulation of Cellular Calcium Extrusion. Curr Biol. 2012 Jul 10;22(13):1241–6.

329. Logsdon CD, Moessner J, Williams JA, Goldfine ID. Glucocorticoids increase amylase mRNA levels, secretory organelles, and secretion in pancreatic acinar AR42J cells. J Cell Biol. 1985 Apr;100(4):1200–8.

330. Rinn C, Aroso M, Prüssing J, Islinger M, Schrader M. Modulating zymogen granule formation in pancreatic AR42J cells. Exp Cell Res. 2012 Sep 10;318(15):1855–66.

331. Logsdon CD. Glucocorticoids increase cholecystokinin receptors and amylase secretion in pancreatic acinar AR42J cells. J Biol Chem. 1986 Feb 15;261(5):2096–101.

332. Shapovalov G, Ritaine A, Skryma R, Prevarskaya N. Role of TRP ion channels in cancer and tumorigenesis. Semin Immunopathol. 2016 May;38(3):357–69.

333. Alavijeh MS, Chishty M, Qaiser MZ, Palmer AM. Drug Metabolism and Pharmacokinetics, the Blood-Brain Barrier, and Central Nervous System Drug Discovery. NeuroRx. 2005 Oct;2(4):554–71.

334. Ikura M, Ames JB. Genetic polymorphism and protein conformational plasticity in the calmodulin superfamily: two ways to promote multifunctionality. Proc Natl Acad Sci U S A. 2006 Jan 31;103(5):1159–64.

335. Means AR, Dedman JR. Calmodulin--an intracellular calcium receptor. Nature. 1980 May 8;285(5760):73–7.

336. Li CJ, Heim R, Lu P, Pu Y, Tsien RY, Chang DC. Dynamic redistribution of calmodulin in HeLa cells during cell division as revealed by a GFP-calmodulin fusion protein technique. J Cell Sci. 1999 May 15;112(10):1567–77.

337. Craske M, Takeo T, Gerasimenko O, Vaillant C, Török K, Petersen OH, et al. Hormone-induced secretory and nuclear translocation of calmodulin: oscillations of

calmodulin concentration with the nucleus as an integrator. Proc Natl Acad Sci U S A. 1999 Apr 13;96(8):4426–31.

338. Copley RR, Schultz J, Ponting CP, Bork P. Protein families in multicellular organisms. Curr Opin Struct Biol. 1999 Jun;9(3):408–15.

339. Swindells MB, Ikura M. Pre-formation of the semi-open conformation by the apo-calmodulin C-terminal domain and implications for binding IQ-motifs. Nat Struct Mol Biol. 1996 Jun;3(6):501–4.

340. Calmodulin Target Database [Internet]. [cited 2016 Jul 29]. Available from: http://calcium.uhnres.utoronto.ca/ctdb/ctdb/home.html

341. Di Leva F, Domi T, Fedrizzi L, Lim D, Carafoli E. The plasma membrane Ca2+ ATPase of animal cells: Structure, function and regulation. Arch Biochem Biophys. 2008 Aug 1;476(1):65–74.

342. Guerrini R, Menegazzi P, Anacardio R, Marastoni M, Tomatis R, Zorzato F, et al. Calmodulin binding sites of the skeletal, cardiac, and brain ryanodine receptor Ca2+ channels: modulation by the catalytic subunit of cAMP-dependent protein kinase? Biochemistry (Mosc). 1995 Apr 18;34(15):5120–9.

343. Marshall CB, Nishikawa T, Osawa M, Stathopulos PB, Ikura M. Calmodulin and STIM proteins: Two major calcium sensors in the cytoplasm and endoplasmic reticulum. Biochem Biophys Res Commun. 2015 Apr 24;460(1):5–21.

344. Van Belle H. R 24571, a new and very potent inhibitor of calmodulin activation of PDE. Biochem Soc Trans. 1981;9:133P (abstract).

345. Sunagawa M, Kosugi T, Nakamura M, Sperelakis N. Pharmacological Actions of Calmidazolium, a Calmodulin Antagonist, in Cardiovascular System. Cardiovasc Drug Rev. 2000 Sep 1;18(3):211–21.

346. Hidaka H, Sasaki Y, Tanaka T, Endo T, Ohno S, Fujii Y, et al. N-(6-aminohexyl)-5-chloro-1-naphthalenesulfonamide, a calmodulin antagonist, inhibits cell proliferation. Proc Natl Acad Sci U S A. 1981 Jul;78(7):4354–7.

347. Nishikawa M, Tanaka T, Hidaka H. Ca2+ -calmodulin-dependent phosphorylation and platelet secretion. 1980 Oct 30;287(5785):863–5.

348. Dagher R, Brière C, Fève M, Zeniou M, Pigault C, Mazars C, et al. Calcium fingerprints induced by Calmodulin interactors in eukaryotic cells. Biochim Biophys Acta BBA - Mol Cell Res. 2009 Jun;1793(6):1068–77.

349. Ishiguro H, Hayakawa T, Kondo T, Shibata T, Kitagawa M, Sakai Y, et al. Effects of calmodulin inhibitors on amylase secretion from rat pancreatic acini. Digestion. 1992;53(3–4):162–70.

350. Meyer-Alber A, Höcker M, Fetz I, Fornefeld H, Waschulewski IH, Fölsch UR, et al. Differential inhibitory effects of serine/threonine phosphatase inhibitors and a calmodulin antagonist on phosphoinositol/calcium- and cyclic adenosine

monophosphate-mediated pancreatic amylase secretion. Scand J Gastroenterol. 1995 Apr;30(4):384–91.

351. Hashimoto N, Maruyama T, Toda G, Ikeda Y, Sugiyama Y, Oka H. Effects of calmodulin antagonists on secretion of bile and bile acid. Gastroenterol Jpn. 22(2):194–202.

352. Jan CR, Tseng CJ. Calmidazolium-induced rises in cytosolic calcium concentrations in Madin Darby canine kidney cells. Toxicol Appl Pharmacol. 2000 Jan 15;162(2):142–50.

353. Jan C-R, Tseng C-J. W-7 Induces [Ca2+]i Increases in Madin-Darby Canine Kidney (MDCK) Cells. J Pharmacol Exp Ther. 2000 Jan 1;292(1):358–65.

354. Ansah TA, Molla A, Katz S. Ca2+-ATPase activity in pancreatic acinar plasma membranes. Regulation by calmodulin and acidic phospholipids. J Biol Chem. 1984 Nov 10;259(21):13442–50.

355. Mahey R, Allen BG, Bridges MA, Katz S. Regulation of calcium transport in pancreatic acinar plasma membranes from guinea pig. Mol Cell Biochem. 1992 Jun 26;112(2):155–62.

356. Klockner U, Isenberg G. Calmodulin antagonists depress calcium and potassium currents in ventricular and vascular myocytes. Am J Physiol - Heart Circ Physiol. 1987 Dec 1;253(6):H1601–11.

357. Nakazawa K, Higo K, Abe K, Tanaka Y, Saito H, Matsuki N. Blockade by calmodulin inhibitors of Ca2+ channels in smooth muscle from rat vas deferens. Br J Pharmacol. 1993 May;109(1):137–41.

358. Zühlke RD, Pitt GS, Deisseroth K, Tsien RW, Reuter H. Calmodulin supports both inactivation and facilitation of L-type calcium channels. Nature. 1999 May 13;399(6732):159–62.

359. Gerasimenko JV, Lur G, Ferdek P, Sherwood MW, Ebisui E, Tepikin AV, et al. Calmodulin protects against alcohol-induced pancreatic trypsinogen activation elicited via Ca2+ release through IP3 receptors. Proc Natl Acad Sci. 2011 Apr 5;108(14):5873–8.

360. Dillon J, Woods WT, Guarcello V, LeBoeuf RD, Blalock JE. A peptide mimetic of calcium. Proc Natl Acad Sci U S A. 1991 Nov 1;88(21):9726–9.

361. Villain M, Jackson PL, Manion MK, Dong W-J, Su Z, Fassina G, et al. De Novo Design of Peptides Targeted to the EF Hands of Calmodulin. J Biol Chem. 2000 Jan 28;275(4):2676–85.

362. Manion MK, Su Z, Villain M, Blalock JE. A new type of Ca(2+) channel blocker that targets Ca(2+) sensors and prevents Ca(2+)-mediated apoptosis. FASEB J Off Publ Fed Am Soc Exp Biol. 2000 Jul;14(10):1297–306.

363. Gerasimenko JV, Lur G, Sherwood MW, Ebisui E, Tepikin AV, Mikoshiba K, et al. Pancreatic protease activation by alcohol metabolite depends on Ca2+ release via acid store IP3 receptors. Proc Natl Acad Sci. 2009 Jun 30;106(26):10758–63.

364. Houtman R, Ten Broeke R, Blalock JE, Villain M, Koster AS, Nijkamp FP. Attenuation of very late antigen-5-mediated adhesion of bone marrow-derived mast cells to fibronectin by peptides with inverted hydropathy to EF-hands. J Immunol Baltim Md 1950. 2001 Jan 15;166(2):861–7.

365. O'Neil KT, DeGrado WF. How calmodulin binds its targets: sequence independent recognition of amphiphilic α-helices. Trends Biochem Sci. 1990 Feb 1;15(2):59–64.

366. Litjens T, Harland ML, Roberts ML, Barritt GJ, Rychkov GY. Fast Ca(2+)-dependent inactivation of the store-operated Ca2+ current (ISOC) in liver cells: a role for calmodulin. J Physiol. 2004 Jul 1;558(Pt 1):85–97.

367. Imredy JP, Yue DT. Mechanism of Ca2+-sensitive inactivation of L-type Ca2+ channels. Neuron. 1994 Jun;12(6):1301–18.

368. McElroy SP, Drummond RM, Gurney AM. Regulation of store-operated Ca2+ entry in pulmonary artery smooth muscle cells. Cell Calcium. 2009 Aug;46(2):99–106.

369. Galán C, Dionisio N, Smani T, Salido GM, Rosado JA. The cytoskeleton plays a modulatory role in the association between STIM1 and the Ca2+ channel subunits Orai1 and TRPC1. Biochem Pharmacol. 2011 Aug 15;82(4):400–10.

370. Cao Y, Chatton J-Y. Involvement of calmodulin in the activation of store-operated Ca2+ entry in rat hepatocytes. FEBS Lett. 1998 Mar 6;424(1–2):33–6.

371. Frischauf I, Schindl R, Derler I, Bergsmann J, Fahrner M, Romanin C. The STIM/Orai coupling machinery. Channels. 2008 Jul 4;2(4):261–8.

372. Bhardwaj R, Müller H-M, Nickel W, Seedorf M. Oligomerization and Ca2+/calmodulin control binding of the ER Ca2+-sensors STIM1 and STIM2 to plasma membrane lipids. Biosci Rep. 2013;33(5).e00077.

373. Peppiatt CM, Holmes AM, Seo JT, Bootman MD, Collins TJ, McDonald F, et al. Calmidazolium and arachidonate activate a calcium entry pathway that is distinct from store-operated calcium influx in HeLa cells. Biochem J. 2004 Aug 1;381(Pt 3):929–39.

374. Smani T, Zakharov SI, Csutora P, Leno E, Trepakova ES, Bolotina VM. A novel mechanism for the store-operated calcium influx pathway. Nat Cell Biol. 2004 Feb;6(2):113–20.

375. Masson M, Spezzatti B, Chapman J, Battisti C, Baumann N. Calmodulin antagonists chlorpromazine and W-7 inhibit exogenous cholesterol esterification and sphingomyelinase activity in human skin fibroblast cultures. Similarities between drug-induced and niemann-pick type C lipidoses. J Neurosci Res. 1992 Jan 1;31(1):84–8.

376. Blödow A, Ngezahayo A, Ernst A, Kolb H-A. Calmodulin antagonists suppress gap junction coupling in isolated Hensen cells of the guinea pig cochlea. Pflüg Arch. 2003 Feb 25;446(1):36–41.

377. Kasri NN, Bultynck G, Smyth J, Szlufcik K, Parys JB, Callewaert G, et al. The N-terminal Ca2+-independent calmodulin-binding site on the inositol 1,4,5-trisphosphate receptor is responsible for calmodulin inhibition, even though this inhibition requires Ca2+. Mol Pharmacol. 2004 Aug;66(2):276–84.

378. Kasri NN, Török K, Galione A, Garnham C, Callewaert G, Missiaen L, et al. Endogenously bound calmodulin is essential for the function of the inositol 1,4,5-trisphosphate receptor. J Biol Chem. 2006 Mar 31;281(13):8332–8.

379. Awla D, Abdulla A, Syk I, Jeppsson B, Regnér S, Thorlacius H. Neutrophil-derived matrix metalloproteinase-9 is a potent activator of trypsinogen in acinar cells in acute pancreatitis. J Leukoc Biol. 2012 May;91(5):711–9.

380. Mullins FM, Yen M, Lewis RS. Orai1 pore residues control CRAC channel inactivation independently of calmodulin. J Gen Physiol. 2016 Feb;147(2):137–52.

381. Mullins FM, Lewis RS. The inactivation domain of STIM1 is functionally coupled with the Orai1 pore to enable Ca2+-dependent inactivation. J Gen Physiol. 2016 Feb;147(2):153–64.

382. Parvez S, Beck A, Peinelt C, Soboloff J, Lis A, Monteilh-Zoller M, et al. STIM2 protein mediates distinct store-dependent and store-independent modes of CRAC channel activation. FASEB J Off Publ Fed Am Soc Exp Biol. 2008 Mar;22(3):752–61.

383. Rychkov G, Brereton HM, Harland ML, Barritt GJ. Plasma membrane Ca2+ release-activated Ca2+ channels with a high selectivity for Ca2+ identified by patch-clamp recording in rat liver cells. Hepatol Baltim Md. 2001 Apr;33(4):938–47.

384. Moreau B, Straube S, Fisher RJ, Putney JW, Parekh AB. Ca2+-calmodulin-dependent facilitation and Ca2+ inactivation of Ca2+ release-activated Ca2+ channels. J Biol Chem. 2005 Mar 11;280(10):8776–83.

385. Watterson DM, Sharief F, Vanaman TC. The complete amino acid sequence of the Ca2+-dependent modulator protein (calmodulin) of bovine brain. J Biol Chem. 1980 Feb 10;255(3):962–75.

386. Song J, Tan H, Perry AJ, Akutsu T, Webb GI, Whisstock JC, et al. PROSPER: An Integrated Feature-Based Tool for Predicting Protease Substrate Cleavage Sites. PLOS ONE. 2012 Nov 29;7(11):e50300.

387. Steen H, Mann M. The abc's (and xyz's) of peptide sequencing. Nat Rev Mol Cell Biol. 2004 Sep;5(9):699–711.

388. D-Pharm Ltd TUHB. Pilot Trial of Intravenous DP-b99 in the Treatment of First-ever Episode of Non-obstructive Acute High-risk Pancreatitis [Internet]. Vol. In: ClinicalTrial.gov [Internet]. Bethseda (MD): National Library of Medicine (US); 2013 [cited 2016 Sep 11]. Available from: https://clinicaltrials.gov/show/NCT02025049

389. Pevarello P, Cainarca S, Liberati C, Tarroni P, Piscitelli F, Severi E. Ca2+ release-activated Ca2+ channel inhibitors. Pharm Pat Anal. 2014 Mar 1;3(2):171–82.

390. Tian C, Du L, Zhou Y, Li M. Store-operated CRAC channel inhibitors: opportunities and challenges. Future Med Chem. 2016 May;8(7):817–32.

391. Marques LO, Lima MS, Soares BGO. Trifluoperazine for schizophrenia. Cochrane Database Syst Rev. 2004;(1):CD003545.

392. Yuan K, Yong S, Xu F, Zhou T, McDonald JM, Chen Y. Calmodulin antagonists promote TRA-8 therapy of resistant pancreatic cancer. Oncotarget. 2015 Sep 22;6(28):25308–19.

393. Linxweiler M, Schorr S, Schäuble N, Jung M, Linxweiler J, Langer F, et al. Targeting cell migration and the endoplasmic reticulum stress response with calmodulin antagonists: a clinically tested small molecule phenocopy of SEC62 gene silencing in human tumor cells. BMC Cancer. 2013;13:574.

394. Zon LI, TAYLOR AM. Calmodulin inhibitors for the treatment of ribosomal disorders and ribosomapathies [Internet]. EP2825173 A2, 2015 [cited 2016 Sep 11]. Available from: http://www.google.com/patents/EP2825173A2

395. Koga T, Mizui M, Yoshida N, Otomo K, Lieberman LA, Crispín JC, et al. KN-93, an inhibitor of calcium/calmodulin-dependent protein kinase IV, promotes generation and function of Foxp3$^+$ regulatory T cells in MRL/lpr mice. Autoimmunity. 2014 Nov;47(7):445–50.

396. Maier LS, Bers DM. Calcium, Calmodulin, and Calcium-Calmodulin Kinase II: Heartbeat to Heartbeat and Beyond. J Mol Cell Cardiol. 2002 Aug;34(8):919–39.

397. Liu J, Xin L, Benson VL, Allen DG, Ju Y-K. Store-operated calcium entry and the localization of STIM1 and Orai1 proteins in isolated mouse sinoatrial node cells. Front Physiol. 2015;6. 69.

398. Moccia F, Zuccolo E, Soda T, Tanzi F, Guerra G, Mapelli L, et al. Stim and Orai proteins in neuronal Ca2+ signaling and excitability. Front Cell Neurosci. 2015;9.153.

399. Stiber J, Hawkins A, Zhang Z-S, Wang S, Burch J, Graham V, et al. STIM1 signalling controls store-operated calcium entry required for development and contractile function in skeletal muscle. Nat Cell Biol. 2008 Jun;10(6):688–97.

400. Lyfenko AD, Dirksen RT. Differential dependence of store-operated and excitation-coupled Ca2+ entry in skeletal muscle on STIM1 and Orai1. J Physiol. 2008 Oct 15;586(20):4815–24.

401. Catterall WA. Voltage-Gated Calcium Channels. Cold Spring Harb Perspect Biol. 2011 Aug 1;3(8):a003947.

402. Horton JS, Buckley CL, Alvarez EM, Schorlemmer A, Stokes AJ. The calcium release-activated calcium channel Orai1 represents a crucial component in hypertrophic compensation and the development of dilated cardiomyopathy. Channels. 2014 Jan 1;8(1):35–43.

403. Bootman MD, Rietdorf K, Collins T, Walker S, Sanderson M. Ca2+-sensitive fluorescent dyes and intracellular Ca2+ imaging. Cold Spring Harb Protoc. 2013 Feb;2013(2):83–99.

404. Fierro L, Parekh AB. Fast Calcium-Dependent Inactivation of Calcium Release-Activated Calcium Current (CRAC) in RBL-1 Cells. J Membr Biol. 168(1):9–17.

405. Cheng KT, Ong HL, Liu X, Ambudkar IS. Contribution and Regulation of TRPC Channels in Store-Operated Ca2+ Entry. Curr Top Membr. 2013;71.

406. Spanier BWM, Nio Y, van der Hulst RWM, Tuynman H a. RE, Dijkgraaf MGW, Bruno MJ. Practice and yield of early CT scan in acute pancreatitis: a Dutch Observational Multicenter Study. Pancreatol Off J Int Assoc Pancreatol IAP Al. 2010;10(2–3):222–8.

407. Kuśnierz-Cabala B, Nowak E, Sporek M, Kowalik A, Kuźniewski M, Enguita FJ, et al. Serum levels of unique miR-551-5p and endothelial-specific miR-126a-5p allow discrimination of patients in the early phase of acute pancreatitis. Pancreatol Off J Int Assoc Pancreatol IAP Al. 2015 Aug;15(4):344–51.

408. Blenkiron C, Askelund KJ, Shanbhag ST, Chakraborty M, Petrov MS, Delahunt B, et al. MicroRNAs in mesenteric lymph and plasma during acute pancreatitis. Ann Surg. 2014 Aug;260(2):341–7.

M A D Q L T E E Q I A E F K E A F S L F
D K D G D G T I T T K E L G T V M R S L
G Q N P T E A E L Q D M I N E V D A D G
N G T I D F P E F L T M M A R K M K D T
D S E E E I R E A F R V F D K G N G Y I
S A A E L R H V M T N L G E K L T D E E
V D E M I R E A D I D G D G Q V N Y E E
F V Q M M T A K

Figure 1 Amino acid sequence of calmodulin with predicted protease cleavage sites

Light blue amino acids mark the site of chymotrypsin cleavage and bold/red amino acids mark trypsin cleavage sites. Red amino acids are multiple other serine protease cleavage sites
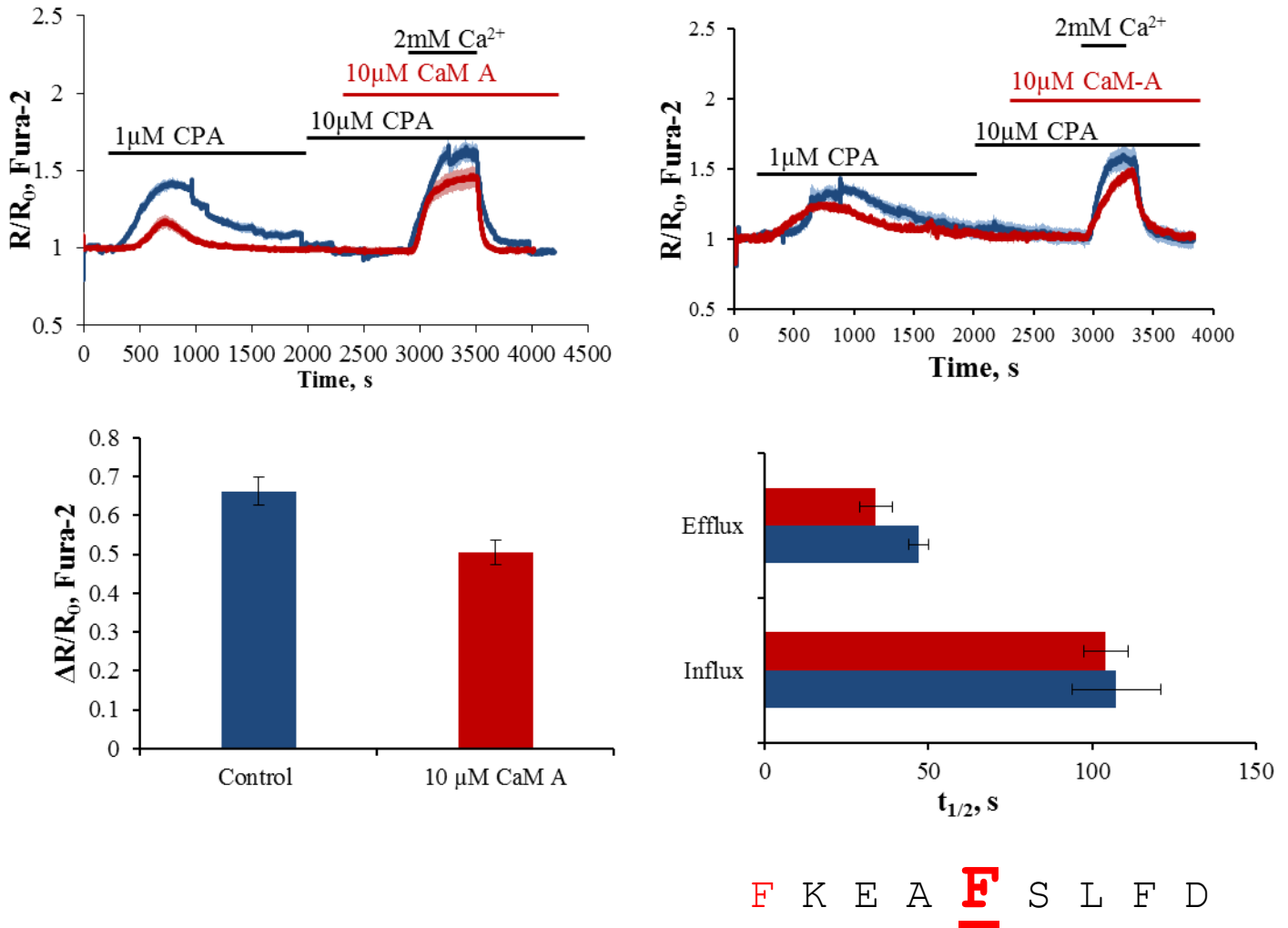
Figure 2 Pre-incubation with a peptide fragment predicted to be derived from proteolytic cleavage of calmodulin inhibited amplitude of Ca2+ influx but not rate

Average traces (± SEM) from Fura-2 loaded pancreatic acinar cells

A- ER stores were depleted according to the protocol in section 2.5.4 and then cells were pre-incubated with 10 µM CaM A for 10 minutes before the re-introduction of 2 mM Ca^{2+} to the extracellular solution. Blue trace – control (n = 12) and red trace – 10 µM CaM A (n = 8). **B-** Identical experiment to figure **A** with different time scale of Ca^{2+} addition to the extracellular solution, Blue trace – control (n = 4) and red trace – 10 µM CaM A (n = 6). **C-** Summary of the changes in ratio amplitude due to Ca^{2+} influx (from cells in Figure **A** and **B**) in control (blue bar) and CaM A treated (red bar). **D –** Summary of the changes in half time of Ca^{2+} influx (lower bars) control – blue, CAM A treated – red. Half time of Ca^{2+} efflux (upper bars) control – blue, calmodulin treated – red.

206
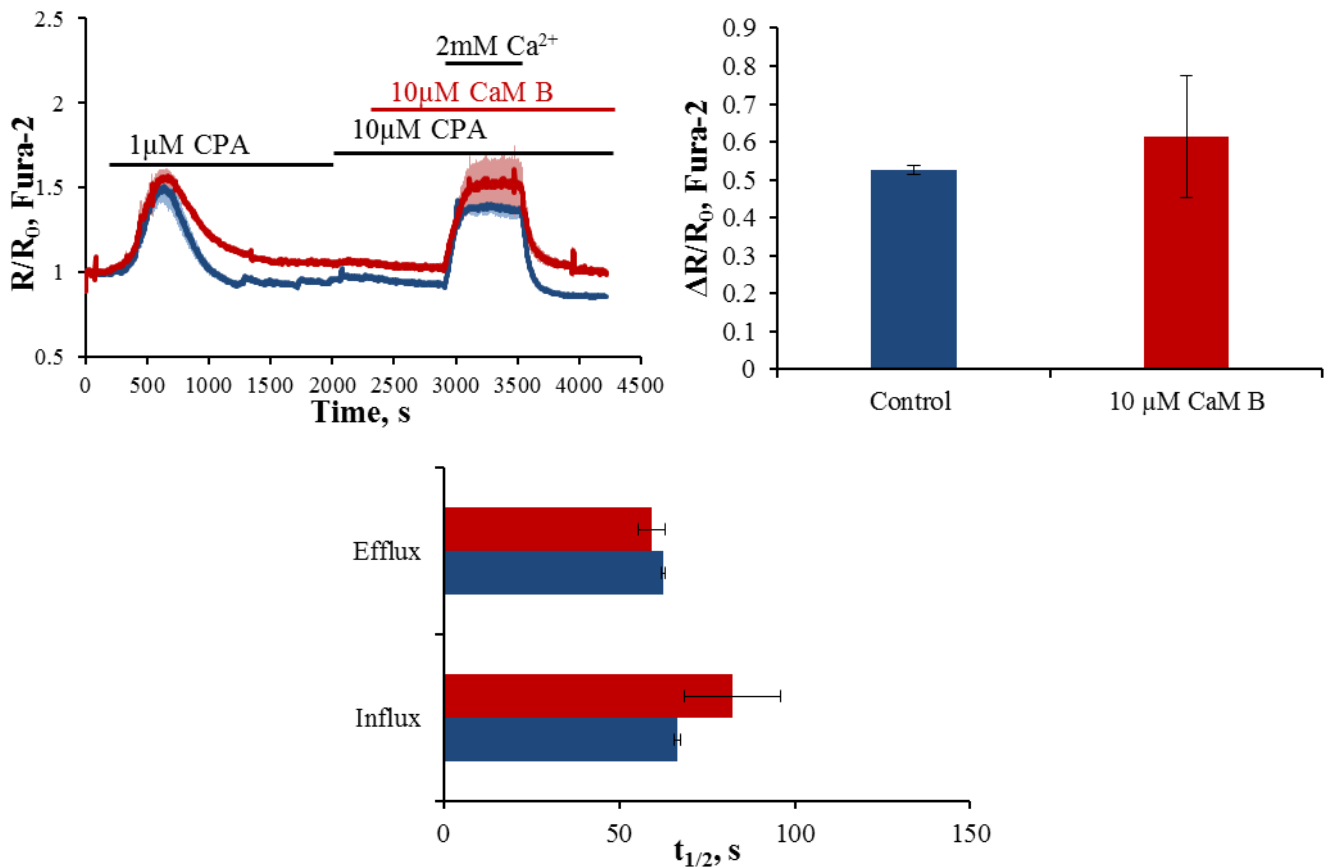
NYEEFVQMM

Figure 3 Pre-incubation with a second peptide fragment predicted to be derived from proteolytic cleavage of calmodulin did not affect the amplitude of Ca2+ influx nor the rate of Ca2+influx

Average traces (± SEM) from Fura-2 loaded pancreatic acinar cells

A- ER stores were depleted according to the protocol in section 2.5.4 and then cells were pre-incubated with 10 µM CaM B for 10 minutes before the re-introduction of 2 mM Ca^{2+} to the extracellular solution. Blue trace – control (n = 2) and red trace – 10 µM CaM A (n = 5). **B-** Summary of the changes in ratio amplitude due to Ca^{2+} influx (from cells in Figure **A)** in control (blue bar) and CaM A treated (red bar). **C –** Summary of the changes in half time of Ca^{2+} influx (lower bars) control – blue, CAM A treated – red. Half time of Ca^{2+} efflux (upper bars) control – blue, calmodulin treated – red.